

**Evaluation of a novel non-competitive antagonist as a
radioligand for the *N*-methyl-D-aspartate
receptor-channel complex *in vivo***

AILSA L. MCGREGOR

A thesis submitted for the Degree of Doctor of Philosophy
to the Faculty of Medicine, University of Glasgow

Wellcome Surgical Institute and Hugh Fraser Neuroscience Laboratories,
University of Glasgow,
Garscube Estate, Bearsden Road, Glasgow, G61 1QH

© A.L. McGregor, November 1997

ProQuest Number: 13818690

All rights reserved

INFORMATION TO ALL USERS

The quality of this reproduction is dependent upon the quality of the copy submitted.

In the unlikely event that the author did not send a complete manuscript and there are missing pages, these will be noted. Also, if material had to be removed, a note will indicate the deletion.



ProQuest 13818690

Published by ProQuest LLC (2018). Copyright of the Dissertation is held by the Author.

All rights reserved.

This work is protected against unauthorized copying under Title 17, United States Code
Microform Edition © ProQuest LLC.

ProQuest LLC.
789 East Eisenhower Parkway
P.O. Box 1346
Ann Arbor, MI 48106 – 1346



GLASGOW UNIVERSITY
LIBRARY

11144 (copy 1)

CONTENTS	PAGE
Contents	i
List of tables	vii
List of figures	viii
Acknowledgements	xi
Summary	xiii
Preface and declaration	xviii

CHAPTER I - INTRODUCTION

1.1	Excitatory amino acids as neurotransmitters in the CNS	1
1.2	Metabolism and release of glutamate	2
1.3	Glutamate receptor subtype classification	6
1.3.1	The NMDA receptor	6
1.3.2	The AMPA receptor	23
1.3.3	The Kainate receptor	25
1.3.4	The AP-4 receptor	26
1.3.5	The Metabotropic receptor	26
1.4	Excitotoxicity	29
1.4.1	NMDA-mediated neurotoxicity	29
1.4.2	Non-NMDA-mediated toxicity	31
1.4.3	The ischaemic penumbra	32
1.5	Therapeutic intervention in cerebral ischaemia	33
1.5.1	Strategies for improving perfusion	33
1.5.2	NMDA antagonists	34
1.6	NMDA antagonists as clinically useful drugs	36
1.6.1	Safety and tolerability	36
1.6.2	Animal studies	36
1.6.3	Human studies	37

	PAGE
1.7 Development of a novel NMDA antagonist	38
1.7.1 Basic concepts	38
1.7.2 Preclinical studies	38
1.7.3 Clinical studies	39
1.8 Receptor imaging in the central nervous system	41
1.8.1 Autoradiography	41
1.8.2 SPECT and PET	45
1.9 Synthesis of <i>N</i>-(1-naphthyl)-<i>N'</i>-(3-[¹²⁵I]iodo-phenyl)-<i>N'</i>methylguanidine	50

CHAPTER II - METHODS

2.1 Affinity and selectivity of CNS 1261	52
2.1.1 Whole crude synaptosomal membrane (WCSM) preparation	52
2.1.2 Assay procedure	53
2.1.3 Commercial screening of CNS 1261	53
2.2 Effect of CNS 1261 on local cerebral glucose utilisation	54
2.2.1 Surgical preparation of animals	55
2.2.2 The [¹⁴ C]2-deoxyglucose technique	55
2.2.3 Preparation of autoradiograms	55
2.2.4 Quantification of autoradiograms	56
2.2.5 Experimental protocol	57
2.2.6 Data analysis	57
2.2.7 <i>f</i> ranking	57
2.3 <i>In vivo</i> [¹²⁵I]MK801 autoradiography	58
2.3.1 Surgical preparation of animals	58
2.3.2 The [¹²⁵ I]MK801 technique	59
2.3.3 Preparation of autoradiograms	59
2.3.4 Quantification of autoradiograms	59

	PAGE
2.4 <i>In vivo</i> [^{125}I]CNS 1261 autoradiography	60
2.4.1 Surgical preparation of animals	60
2.4.2 The [^{125}I]CNS 1261 technique	60
2.4.3 Preparation of autoradiograms	60
2.4.4 Quantification of autoradiograms	61
2.5 Uptake and retention of [^{125}I]CNS 1261 and [^{125}I]MK801 in normal rat brain	61
2.5.1 Experimental design	61
2.5.2 Data analysis	62
2.6 Relative lipophilicity of [^{125}I]CNS 1261 and [^{125}I]MK801	62
2.6.1 Calculation of LogD values for CNS 1261 and MK801	62
2.6.2 Calculation of brain/aqueous partition ratios	62
2.6.3 Data analysis	63
2.7 Metabolism of [^{125}I]CNS 1261 and [^{125}I]MK801 in the rat	63
2.7.1 Determination of metabolites in rat plasma	63
2.7.2 Determination of metabolites in rat brain	64
2.7.3 Experimental analysis	64
2.8 Effect of MK801 on the uptake and retention of [^{125}I]CNS 1261 in normal rat brain	64
2.8.1 Experimental design	64
2.8.2 Data analysis	65
2.9 Uptake and retention of [^{125}I]MK801 and [^{125}I]CNS 1261 following changes in arterial CO₂ tension	65
2.9.1 [^{125}I]MK801 uptake following changes in arterial CO ₂ tension	65
2.9.2 Data analysis	66
2.9.3 [^{125}I]CNS 1261 uptake following changes in CO ₂ tension	66
2.9.4 Data analysis	66

	PAGE
2.10 Uptake and retention of [125I]CNS 1261 following intracortical injection of NMDA	67
2.10.1 Experimental design	67
2.10.2 Histological examination of the lesion	67
2.10.3 Data analysis	68
 CHAPTER III - RESULTS	
3.1 CNS 1261 binds to the NMDA receptor complex with high affinity and selectivity	69
3.1.1 Affinity of CNS 1261	69
3.1.2 Selectivity of CNS 1261	69
3.2 Effect of CNS 1261 on local cerebral glucose use	72
3.2.1 General observations	72
3.2.2 Local cerebral glucose utilisation	74
3.3 Uptake and retention of [125I]MK801 and [125I]CNS 1261 in normal rat brain	82
3.3.1 General observations	82
3.3.2 <i>In vivo</i> uptake and retention of [125 I]CNS 1261	82
3.3.3 Comparison of [125 I]CNS 1261 with [125 I]MK801	88
3.4 Relative lipophilicity of [125I]CNS 1261 and [125I]MK801	90
3.4.1 Lipophilicity of CNS 1261	90
3.4.2 Partition coefficients of [125 I]CNS 1261 and [125 I]MK801 in rat brain	90
3.4.3 Partition coefficients of [125 I]CNS 1261 and [125 I]MK801 in human brain	90
3.5 Metabolism of [125I]CNS 1261 in the rat	93
3.5.1 Stability of [125 I]CNS 1261 <i>in vitro</i>	93
3.5.2 Metabolism of [125 I]CNS 1261 in the rat	93
3.5.3 Metabolism of [125 I]MK801 in the rat	95

	PAGE
3.6 Effect of MK801 on the uptake and retention of [125I]CNS 1261 in the normal rat brain	97
3.6.1 General observations	97
3.6.2 Authenticity of MK801	97
3.6.3 Uptake and retention of [125I]CNS 1261	99
3.7 [125I]MK801 and [125I]CNS 1261 uptake following changes in arterial CO₂ tension	101
3.7.1 [125I]MK801 - general observations	101
3.7.2 Analysis of [125I]MK801 autoradiograms	101
3.7.3 [125I]CNS 1261 - general observations	105
3.7.4 Analysis of [125I]CNS 1261 autoradiograms	106
3.8 [125I]CNS 1261 uptake following intracortical injection of NMDA	109
3.8.1 Verification of dose	109
3.8.2 General observations	109
3.8.3 Histology	112
3.8.4 Uptake and retention of [125I]CNS 1261	112
 CHAPTER IV - DISCUSSION	
4.1 CNS 1261 acts as a non-competitive NMDA receptor antagonist	116
4.2 [125I]CNS 1261 uptake within the normal brain	120
4.3 [125I]CNS 1261 produces superior images to [125I]MK801 in normal brain	126
4.3.1 Kinetic modelling	128
4.4 Displacement of [125I]CNS 1261 from normal rat brain	131
4.5 Application of [125I]CNS 1261	133
4.6 SPECT imaging in man with [123I]CNS 1261	139

	PAGE
References	143
Appendix 1	168
Appendix 2	170
Published abstracts	173

List of Tables	PAGE
1. Excitatory amino acid receptors	7
2. Inhibition of radioligand binding by CNS 1261	70
3. CNS 1261 displayed no activity in a range of radioligand binding assays	71
4. Effect of CNS 1261 administration on physiological variables	73
5. Effect of CNS 1261 administration on glucose use in sensory and motor systems	75
6. Effect of CNS 1261 administration on glucose use in limbic system	76
7. Effect of CNS 1261 administration on glucose use in myelinated tracts	77
8. Hierarchy of regional responsiveness to CNS 1261	79
9. Hierarchy of regional responsiveness to MK801	80
10. Uptake and retention of [125 I]MK801 and [125 I]CNS 1261 - physiological variables	83
11. Comparison of [125 I]MK801 and [125 I]CNS 1261 uptake 30 minutes post-administration	84
12. Comparison of [125 I]MK801 and [125 I]CNS 1261 uptake 60 minutes post-administration	85
13. Comparison of [125 I]MK801 and [125 I]CNS 1261 uptake 120 minutes post-administration	86
14. LogD values for CNS 1261 and other non-competitive NMDA antagonists	91
15. Brain/aqueous partition ratios in rat and human brain	92
16. Species present in isotope solutions 6 hours after reconstitution	94
17. Physiological variables before and 60 minutes after initiation of MK801 infusion	98
18. Effect of MK801 on [125 I]CNS 1261 uptake	100
19. Physiological variables following changes in arterial CO ₂ tension	102
20. [125 I]MK801 uptake following changes in arterial CO ₂ tension	104
21. Physiological variables following changes in arterial CO ₂ tension	106
22. [125 I]CNS 1261 uptake following changes in arterial CO ₂ tension	107
23. Changes in glucose use following intracortical injection of NMDA	110
24. Physiological variables before and after intracortical injection of CSF or NMDA	111
25. Tracer uptake appears to reflect cerebral blood flow 5 minutes after administration	123

1. Pathways for glutamate utilisation and metabolism	2
2. Schematic illustration of the NMDA receptors	7
3. The modulatory actions of polyamines on the NMDA receptor	14
4. Phylogenic tree of ionotropic glutamate receptor subunits	20
5. Phylogenic tree of metabotropic glutamate receptor subunits	27
6. Chemical structures of NMDA and σ site ligands	38
7. Cambridge NeuroScience Inc. share prices from Oct.'96 to Sept.'97	40
8. Synthesis of [125 I]CNS 1261	50
9. The operational equation	56
10. Effect of CNS 1261 administration on mean arterial blood pressure	73
11. Changes in glucose utilisation following administration of CNS 1261	77
12. Effect of CNS 1261 administration on glucose use in the entorhinal cortex and inferior colliculus	77
13. Effect of CNS 1261 administration on glucose use in the limbic system	77
14. Frequency distribution profiles of f values for CNS 1261 and MK801	81
15. Correlation analysis of f values for glucose use after MK801 and CNS 1261 treatment	81
16. Comparison of [125 I]MK801 and [125 I]CNS 1261 uptake at 5 minutes	86
17. Comparison of [125 I]MK801 and [125 I]CNS 1261 uptake at 30 minutes	87
18. Comparison of [125 I]MK801 and [125 I]CNS 1261 uptake at 60 minutes	87
19. Comparison of [125 I]MK801 and [125 I]CNS 1261 uptake at 120 minutes	87
20. [125 I]CNS 1261 uptake is increased in cortical layer IV 5 minutes after administration	88
21. [125 I]CNS 1261 uptake is increased within the paraventricular hypothalamic nucleus	88
22. Uptake and retention of [125 I]CNS 1261 and [125 I]MK801 in white matter	89
23. Uptake and retention of [125 I]CNS 1261 and [125 I]MK801 in hippocampus	89
24. Metabolism of [125 I]CNS 1261 in the rat	94
25. Timecourse of [125 I]CNS 1261 metabolism in rat plasma	95
26. Metabolism of [125 I]MK801 in the rat	95
27. Timecourse of [125 I]MK801 metabolism in rat plasma	95
28. Comparison of plasma clearance of [125 I]CNS 1261 and [125 I]MK801	96

AFTER PAGE

29. NMRS trace from a sample of MK801 used in displacement studies	98
30. Effect of MK801 on [^{125}I]CNS 1261 uptake in normal rat brain	99
31. MK801 does not displace [^{125}I]CNS 1261 binding in normal brain	100
32. Effect of hypercapnic acidosis on [^{125}I]MK801 uptake	102
33. Effect of hypercapnic acidosis on [^{125}I]CNS 1261 uptake - graph	104
34. Effect of hypercapnic acidosis on [^{125}I]CNS 1261 uptake	108
35. Effect of hypercapnic acidosis on [^{125}I]CNS 1261 uptake - graph	108
36. Glucose use within parietal cortex is increased following injection of NMDA	111
37. Effect of NMDA (or CSF) injection on [^{125}I]CNS 1261 uptake 5 min. after administration	112
38. Effect of NMDA (or CSF) injection on [^{125}I]CNS 1261 uptake 60 min. after administration	112
39. Effect of NMDA (or CSF) injection on [^{125}I]CNS 1261 uptake 120 min. after administration	112
40. Comparison of the boundary zone between the area of pallor and histologically normal tissue at 120 min.	112
41. High power photomicrographs from the ipsilateral and contralateral cortex 5 minutes after injection of NMDA or CSF	112
42. High power photomicrographs from the ipsilateral and contralateral cortex 60 minutes after injection of NMDA or CSF	112
43. High power photomicrographs from the ipsilateral and contralateral cortex 120 minutes after injection of NMDA or CSF	112
44. Size and extent of lesions 60 minutes after injection of NMDA or CSF	113
45. Size and extent of lesions 120 minutes after injection of NMDA or CSF	114
46. [^{125}I]CNS 1261 uptake is increased in areas of damage	115
47. Washout rates of [^{125}I]MK801 and [^{125}I]CNS 1261 from regions of interest	125
48. 3 compartment model of tracer uptake into the brain	128
49. Hypothetical brain uptake following administration of a tracer with rapid or slow plasma clearance	130
50. Actual rates of tracer washout from the cerebellum	130
51. Relationship between pCO_2 and pH in plasma and brain	134
52. Effect of varying association rate on the hypothetical uptake and retention of a tracer with rapid plasma clearance	137
53. [^{123}I]CNS 1261 uptake and retention in a normal volunteer	139
54. Timecourse of [^{123}I]CNS 1261 clearance from plasma and occipital cortex in a normal volunteer	140

55. [¹²⁵ I]CNS 1261 uptake is increased in ischaemic areas	140
56. Timecourse of radioactivity in a stroke patient 6 hours after onset	140

Acknowledgements

I have enjoyed my time in Glasgow thanks to the kindness and generosity of everyone at the Wellcome Surgical Institute.

My greatest thanks go to Professor James McCulloch for his continual support and guidance which was a source of encouragement and served to increase my determination throughout this project. I feel confident that the experimental thoroughness he has instilled in me will serve me well in my future career. I feel my elbows are now sufficiently sharp!

I would also like to thank Dr Mhairi Macrae and Dr. Deborah Dewar for their continued interest in my research.

I owe a great debt of thanks to both Jonathan Owens and Andy Tebbutt for a (fairly!) constant supply of [^{125}I]CNS 1261 and for their contribution to the metabolite studies.

During my time at the Wellcome Surgical Institute I had the pleasure of working with Dr Kazuhiro Kodama. I thank him for his work on the [^{14}C]2-deoxyglucose experiments.

I would also like to thank Dr. Jim Patterson for his guidance with kinetic modelling.

A number of individuals contributed to the production of this thesis and thanks go to Alan May for his assistance with the photography, Douglas Armstrong for capturing the autoradiographic images onto CD and to Ian Dodd for all his help with printing and photocopying.

Many thanks to my colleagues Hilary Carswell, Manuela De Michele, Karen Horsburgh, Elaine Irving, Teresa Jover, Stephen Kelly, Amy Lam, Duncan MacGregor, Eileen McCracken, Iain Murdoch, David Paterson, Elaine Peters, Marc Soriano, Omar Touzani and Philippa Yam who have provided friendship and much scientific discussion throughout my time here.

I must also acknowledge the assistance of Margaret Stewart, Gordon Littlejohn and the technical staff (past and present) of the Wellcome Surgical Institute, in particular Michael Dunne, Joan Stewart and Lindsay Dover.

I would like to thank Allison, Michael and Ross for encouraging me when I lost my direction and Chris, for his constant support and unwavering faith in my ability.

Finally I would like to thank my parents whose support both emotional and financial has been overwhelming throughout my entire career, to thank them is not enough and I dedicate this thesis to them.

Summary

This thesis reports the synthesis and initial evaluation of the substituted guanidine N-(1-Naphthyl)-N'-(2-iodophenyl)-N'-methylguanidine (CNS 1261) as a potential agent to image N-methyl-D-aspartate (NMDA) receptor activation *in vivo*.

The pharmacology of unlabelled CNS 1261 was investigated *in vitro* using ligand binding assays and *in vivo* using autoradiographic procedures. Investigations were designed to examine the ability of CNS 1261 to inhibit radioligand binding to the NMDA receptor and to other neurotransmitter receptors. [^{14}C]2-deoxyglucose autoradiography was used to measure local rates of glucose utilisation following systemic administration of CNS 1261. The effects of CNS 1261 on glucose utilisation were compared to those obtained in a previous study carried out by Kurumaji *et al* (1989) using MK801. Secondly, in order to assess the ability of [^{125}I]CNS 1261 to measure levels of NMDA receptor activation in the brain, a modification of the [^{125}I]MK801 *in vivo* binding technique described by McCulloch *et al* (1992) was used to investigate the uptake and retention of [^{125}I]CNS 1261 in the normal rat brain. The pattern of [^{125}I]CNS 1261 uptake was compared to that of [^{125}I]MK801 in parallel experiments. Finally, autoradiographic techniques were used to assess the utility of [^{125}I]CNS 1261 in imaging changes in NMDA receptor activation *in vivo*. NMDA receptor activation was manipulated via proton blockade and microinjection of the excitatory amino acid agonist NMDA into the cortex

Pharmacology of CNS 1261

The ability of CNS 1261 to inhibit [^3H]MK801 binding was investigated in crude synaptic rat brain membranes (Cambridge NeuroScience Inc.). CNS 1261 (10nM) binds to the NMDA receptor *in vitro* with high affinity ($K_i = 25\text{nM}$ for displacing [^3H]MK801 binding). The effects of unlabelled CNS 1261 (10nM and $1\mu\text{M}$) on the binding of ligands to the NMDA receptor and to other neurotransmitter receptors was more extensively investigated by submitting the compound for commercial screening (Novascreen).

CNS 1261 (1 μ M) was extremely selective showing activity (99% inhibition) only in the [3 H]MK801 binding assay.

The effects of CNS 1261 (1, 3 and 10mg/kg) on local cerebral glucose use were examined in the conscious lightly restrained rat. The systemic administration of CNS 1261 resulted in overt behavioural responses and marked alterations in glucose use within the central nervous system. Administration of CNS 1261 produced highly circumscribed changes in glucose utilisation that could be readily visualised on autoradiograms. Decreases in glucose use (approximately 30%) were observed in layer IV of the frontal, sensory-motor and auditory cortices and in the inferior colliculus.

Distinct, significant elevations in glucose use were observed in the hippocampus molecular layer, dentate gyrus, limbic system (posterior cingulate cortex, caudal entorhinal cortex, mamillary body, anteroventral thalamus), retrosplenial cortex and the myelinated fiber tract of the fornix. Correlation analysis revealed that the overall pharmacological effects of CNS 1261 were extremely similar to the overall effects of MK801, correlation coefficient, $r = 0.87$. Subtle differences were observed in a number of regions. A greater number of regions displayed extreme sensitivity to CNS 1261 than to MK801, such as the anteroventral thalamus, mamillary body and inferior colliculus. In contrast, the entorhinal cortex was much less sensitive to CNS 1261 than to MK801

[125 I]CNS 1261 uptake in the normal rat brain

Radio-iodinated (125 I or 123 I)CNS 1261 was synthesised at high specific activity (>2000Ci/mmol) and chemical purity (>97%) at the West of Scotland Radionuclide Dispensary, Glasgow. Investigation of the *in vivo* uptake and retention of [125 I]CNS 1261 was carried out in halothane anaesthetised rats. The initial uptake of [125 I]CNS 1261 reflected cerebral blood flow. At time points beyond 30 minutes the uptake of [125 I]CNS 1261 reflected the classical pattern of NMDA receptor distribution with the highest levels of binding in the hippocampus and low levels in the hypothalamus and cerebellum. At 120 minutes, [125 I]CNS 1261 uptake within hippocampal regions relative

to that in the cerebellum (a measure of non-specific binding) was 70-140% greater than that observed with [^{125}I]MK801.

The mechanisms underlying the superior imaging capability of [^{125}I]CNS 1261 was addressed by investigation of the lipophilicity and metabolism of this tracer.

Calculation of LogD values (the octanol/buffer partition ratio at pH 7.4) showed that CNS 1261 was substantially less lipophilic than iodo-MK801 (2.19 and 3.3 respectively). Brain/aqueous partition coefficients calculated from the non-specific binding component of *in vitro* binding experiments showed that both [^{125}I]CNS 1261 and [^{125}I]MK801 were highly lipophilic compounds however, partition ratios for [^{125}I]CNS 1261 were approximately 40% lower than those for [^{125}I]MK801 in both rat and man, suggesting a lower non-specific binding component with this tracer.

High performance liquid chromatography analysis of plasma samples after administration of [^{125}I]CNS 1261 to halothane anaesthetised rats showed the presence of 2 species, identified as authentic CNS 1261 and free iodide. Almost all (95%) of the radioactivity in the brain at 120 minutes post-injection was authentic [^{125}I]CNS 1261. [^{125}I]CNS 1261 was metabolised much more rapidly than [^{125}I]MK801 such that five minutes after injection, 15% authentic [^{125}I]CNS 1261 remained in the plasma compared to 55% for [^{125}I]MK801. It is proposed that both the lower non-specific binding component observed with CNS 1261 and the rapid metabolism of this tracer confer significant advantage over MK801 as an imaging agent in the normal brain.

It was postulated that a reduction in [^{125}I]CNS 1261 uptake by administration of unlabelled MK801 would confirm that enhanced uptake in areas of high receptor density such as the hippocampus, represents increased binding of this tracer to the NMDA receptor ion channel. The results presented here show displacement of [^{125}I]CNS 1261 uptake from normal non-pathologic brain could not be demonstrated following administration of pharmacological doses of MK801. The precise mechanisms underlying this inability to demonstrate displacement are unknown, but it is recognised that this observation may impact on the future development of CNS 1261 as imaging agent in man.

CHAPTER I
INTRODUCTION

Imaging changes in NMDA receptor activation using [^{125}I]CNS 1261

The ability to image changes in NMDA receptor activation *in vivo* must be demonstrated for a tracer to be of any value in man. Varying the pH of the extracellular fluid has been shown to provide a mechanism of controlling the level of NMDA receptor activation without affecting agonist concentrations (through induction or relief of proton block of the ion channel). Hypercapnic acidosis was induced in halothane anaesthetised rats. Induction of hypercapnic acidosis (pH 6.9) caused a significant decrease in [^{125}I]CNS 1261 uptake within brain regions with a high density of NMDA receptors. [^{125}I]MK801 uptake within the same regions was not reduced by induction of hypercapnic acidosis. Demonstration of a reduction in [^{125}I]CNS 1261 uptake may be attributed to the improved signal to noise ratio of this tracer.

The utility of [^{125}I]CNS 1261 in measuring changes in NMDA receptor activation was further examined by measuring [^{125}I]CNS 1261 uptake at different time points after intracortical injection of NMDA in the rat. The pattern of [^{125}I]CNS 1261 distribution at the site of injection outlines a core area of reduced uptake (and hence receptor activation) surrounded by a narrow margin of increased uptake where isotope levels were 80% above contralateral values. Receptor activation was reduced within areas of decreased [^{125}I]CNS 1261 uptake (as confirmed by [^{14}C]2-deoxyglucose autoradiography). The increase in lesion size over time shows that [^{125}I]CNS 1261 is capable of imaging dynamic processes such as the evolution of excitotoxic damage. In a separate pilot study [^{125}I]CNS 1261 uptake and retention was also shown to be enhanced within the ischaemic caudate following permanent middle cerebral artery (MCA) occlusion in the rat. This region is generally accepted to be areas of excessive NMDA receptor activation. [^{125}I]CNS 1261 was also superior to [^{125}I]MK801 in labelling non-ischaemic NMDA binding sites in the hippocampus.

These results suggest that CNS 1261 acts as a high affinity, selective non-competitive antagonist at the NMDA receptor. The relative uptake of [^{125}I]CNS 1261 in regions with a high density of NMDA receptors was greater than that of [^{125}I]MK801 within the normal brain and, [^{125}I]CNS 1261 can image subtle changes in NMDA receptor

activation *in vivo* in the rat. [^{125}I]CNS 1261 uptake is determined by the activation state of the receptor and therefore appears to be a suitable candidate for evaluation as a SPECT agent to image excessive NMDA receptor activation in pathological situations in the living human patient.

Preface and Declaration

This thesis reports the synthesis and initial evaluation of the substituted guanidine N-(1-Naphthyl)-N'-(2-iodophenyl)-N'-methylguanidine (CNS 1261) as a potential agent to image N-methyl-D-aspartate (NMDA) receptor activation *in vivo*. Results are presented from investigations conducted in 3 broadly defined areas

1. Pharmacology of unlabelled CNS 1261
2. The uptake and retention of [125 I]CNS 1261 in normal rat brain and comparison with that of [125 I]MK801.
3. The ability of [125 I]CNS 1261 to image changes in NMDA receptor activation *in vivo*

The results of these investigations are presented and discussed separately.

The assistance of K. Kodama in [14 C]2-deoxyglucose studies is gratefully acknowledged. Hplc analysis of plasma samples in metabolite studies was carried out by J. Owens.

This thesis comprises my own original work and has not been presented previously as a thesis in any form.

1.1 Excitatory amino acids as neurotransmitters in the central nervous system

The successful treatment of petit mal seizures using orally administered glutamate was reported by Price and colleagues in 1943. This report was among the first to suggest that glutamate may have a function in the central nervous system and stimulated interest in the role of glutamate in brain metabolism. However, it was not until 1960 when a direct excitatory effect of glutamate was documented by Curtis and Watkins and this acidic amino acid received consideration as a neurotransmitter candidate. The high concentration (4-10mmol/kg wet weight) and even distribution relative to other transmitters (Meldrum, 1985, Greenamyre, 1986) contributed to the long delay between the observations of Price and Curtis and the acceptance of glutamate as a major neurotransmitter of several clinically important pathways, including cortical association fibres, corticofugal pathways such as the pyramidal tract and hippocampal, cerebellar and spinal cord pathways (Greenamyre, 1986). It is now believed that approximately 70% of fast excitatory neurotransmission within the central nervous system is mediated by amino acids such as glutamate, aspartate and possibly homocysteate (Danysz *et al*, 1995)

The most direct anatomical evidence that glutamate functions as a neurotransmitter was the demonstration of enrichment of this amino acid in nerve terminals by a combination of anterograde labelling of primary afferent terminals and immunocytochemistry (for review see Cooper *et al*, 1996).

Glutamate satisfies the four main criteria for the classification of a neurotransmitter, presynaptic localisation in specific neurons where it is stored and released from synaptic vesicles, Ca^{2+} -dependent release by physiological stimuli, identity of action with a naturally occurring transmitter and rapid termination of transmitter actions.

1.2 Metabolism and release of glutamate.

Glutamate is a nonessential amino acid and is ubiquitously distributed throughout the central nervous system. Glutamate has an important metabolic role in carbohydrate and nitrogen metabolism and is the major precursor for the inhibitory neurotransmitter γ -aminobutyric acid (GABA). In view of the many roles attributed to glutamate, the synthesis and metabolism of this compound are categorised in a complex way (Figure 1, for review see Fonnum, 1984, Fleck *et al*, 1993). A large compartment, localised to neuronal structures and nerve terminals, accounts for 85-98% of the total glutamate pool within the brain. A smaller compartment, containing mainly glutamine has been assigned to astroglial cells. The two compartments can be subdivided further into the 'transmitter' pool (20-45%) and 'precursor' glutamate for GABA synthesis. Double-label experiments have shown that the majority of released glutamate is derived from glutamine (Fonnum, 1984).

The ability of glutamate to function as a neurotransmitter is intrinsically linked to two transport systems, uptake carriers located in neurons and glia and a specific transporter capable of packaging glutamate into synaptic vesicles (Cooper *et al*, 1996). Glutamate transporters maintain low basal levels of extracellular glutamate and conserve released transmitter for reuse. The regional localisation and cellular distribution of different forms of these transporters may underlie the propensity of most diseases for specific brain areas (Torp *et al*, 1994). Under resting conditions glutamate concentrations are 1 μ M, 10mM and 100mM in the extracellular space, presynaptic cytoplasm and lumen of vesicles respectively.

The presence of a Na⁺-dependent uptake systems are common to the majority of transmitter amino acids such as GABA and glycine. The glutamate uptake systems terminate the post-synaptic action of the transmitter, recycle glutamate and maintain low extracellular glutamate concentrations. (Nicolls and Attwell, 1990).

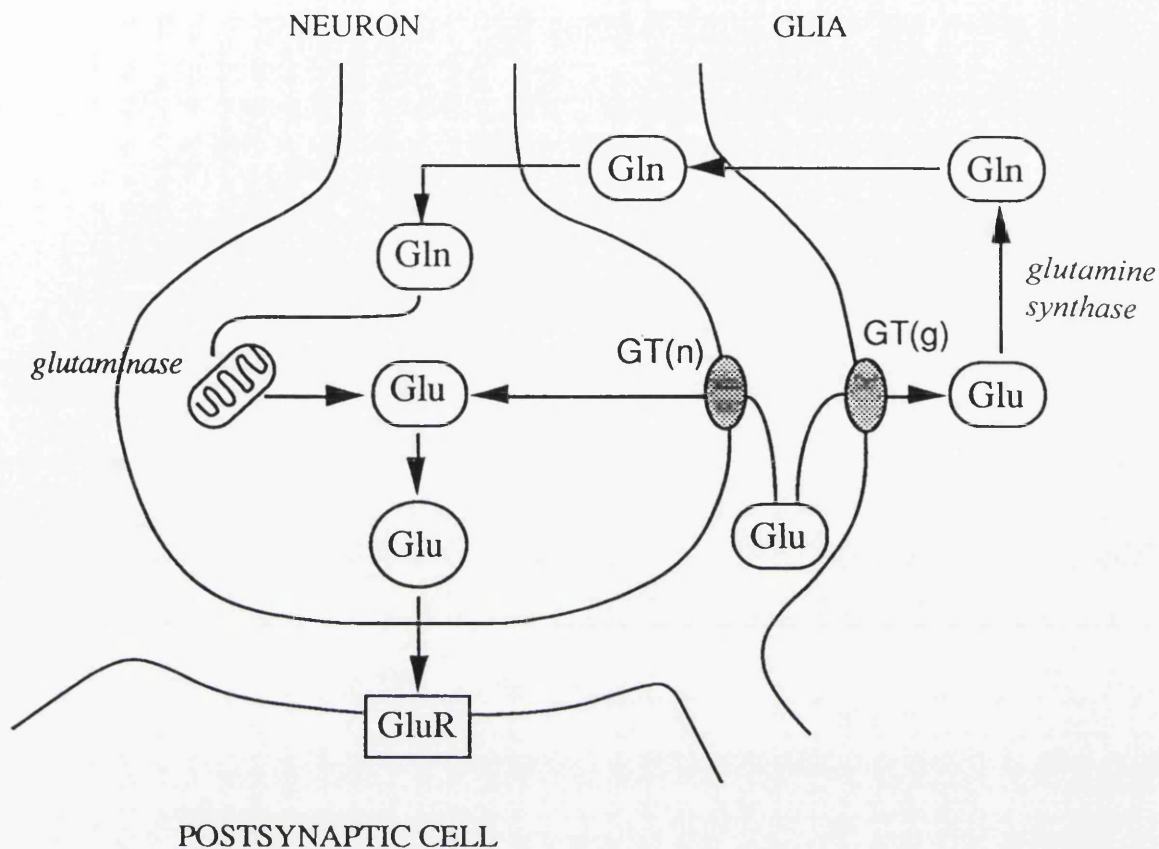


FIGURE 1 : Pathways for glutamate utilisation and metabolism

Glutamate (Glu) is released into the synaptic cleft and is recaptured by neuronal-type ($GT_{(n)}$) and glial-type ($GT_{(g)}$) Na^+ -coupled transporters. Glial glutamate is converted to glutamine (Gln) by the enzyme glutamine synthase. Gln is present in high concentrations in the CSF and can enter the neuron to help replenish glutamate after hydrolysis by mitochondrial glutaminase.

It is suggested that removal of glutamate from the synaptic cleft involves, to differing extents, a combination of uptake into the presynaptic neuron, uptake into glial cells and diffusion down the concentration gradient maintained by glial uptake (Nicolls and Attwell, 1990, Cooper *et al* , 1996).

Three glutamate genes have been identified and cloned, 2 of glial origin, GLT1 and GLAST (Torp *et al*, 1994) and a third found in neurons, EAAC1 (Cooper *et al*, 1996). These transporters display ~50% sequence identity and display different distribution patterns within the brain (Lehre *et al*, 1995). The uptake systems display high affinity (μM) and transport L-glutamate and D- or L-aspartate. The uptake process is accompanied by cotransport of 2 or 3 Na^+ ions and the counter transport of 1 K^+ ion and either the cotransport of 1 H^+ ion or the counter transport of 1 OH^- ion. Recently, Trotti and colleagues (1997) reported that glutamate uptake is regulated by the redox state of the reactive sulphydryl groups present on the glutamate transporters, with reduced or even abolished uptake capacity in their most oxidised form.

Naito and Ueda (1993) were among the first groups to demonstrate ATP-dependent uptake of glutamate into synaptic vesicles. The vesicular transporter is Na^+ -independent, has low affinity (mM) and is selective for glutamate. Calcium-dependent glutamate release from synaptosomes has been demonstrated by a number of different depolarisation methods, including electrical stimulation and high K^+ concentrations (Zhou *et al* 1995, Nicolls and Attwell, 1990). Approximately 15% of cortical/hippocampal synaptosomal glutamate release was found to be calcium-dependent. This glutamate release was also dependent on the maintenance of high energy levels. Vesicular glutamate release was triggered by localisation of high concentrations of free calcium in the cytoplasm near active release zones.

Calcium-dependent glutamate release was biphasic and shows an initial brief phase and a slower phase ($t_{1/2} = 70$ seconds) when the majority of the glutamate is released. This is thought to reflect the initial exocytosis of vesicles already docked with the

membrane and the detachment of the remaining vesicles from cytoskeletal elements (Wahl *et al*, 1994).

Glutamate release is regulated via the action of kainate and glutamate on presynaptic receptors controlling chloride channels. Glutamate and quisqualate inhibit neuronal calcium currents (through G-protein coupled mechanisms) providing a negative feedback control of glutamate release. The most established regulation is the inhibition of glutamate release by adenosine. Release is also inhibited by the GABA_A agonist baclofen (Burke and Nadler, 1988).

Glutamate levels in the extracellular space are markedly increased in pathological conditions such as focal cerebral ischaemia and epilepsy (Butcher *et al*, 1990). The increase in glutamate levels is biphasic and the majority of the glutamate released is of metabolic origin, originating from neurons and glia (Wahl *et al*, 1994). The elevation of extracellular glutamate has been attributed to several mechanisms, alone or in concert, including calcium-dependent release from neurotransmitter stores (Drejer *et al*, 1985), calcium-independent release from cytosolic stores by reversal of the Na⁺/glutamate transporter (Butcher *et al*, 1987) and ultimately cellular lysis.

Recent studies investigating the neuroprotective effect of the κ opioid agonist eliprodil (CI-977) in the cat showed that pretreatment prior to middle cerebral artery occlusion significantly attenuated the marked increase in extracellular glutamate, aspartate and GABA within the focal ischaemic penumbra. Eliprodil is thought to inhibit glutamate release via its action on κ opioid receptors specifically located on vesicular glutamate stores. This suggests that a proportion of the glutamate arises from calcium-dependent glutamate release (MacKay *et al*, 1996).

Under normal conditions the Na⁺/glutamate transporter is the primary mechanism for glutamate reuptake by neurons, however, during depolarisation or when Na⁺ is entering the cell, this carrier can export glutamate into the extracellular space (Graham *et al*, 1993). The resulting glutamate potentiates a positive feedback system by depolarising more neurons.

Exposure of astrocyte cultures to free radical generating systems has been shown to result in a marked decrease in high affinity glutamate transport. Long-lasting oxidation of protein sulphydryl groups has been proposed as the mechanism of inhibition of glutamate uptake. It is suggested therefore, that free radicals may induce accumulation of glutamate by reduction of glial uptake (Volterra *et al*, 1994). Regardless of the precise mechanisms involved, it is apparent that the overflow of excitatory amino acids into the extracellular space is an important step in genesis of neurotoxic damage.

1.3 Glutamate receptor subtype classification

The excitatory effects of glutamate and its congeners are mediated by several distinct receptor types. These receptors can be classified into two groups based on transduction mechanisms. Activation of ionotropic receptors leads to direct opening of ion channels characterised by their differing cation permeabilities. The activation of metabotropic receptors modifies phosphoinositide hydrolysis through a GTP-binding protein-dependent mechanism.

Four classes of ionotropic receptors have been defined by physiology and ligand binding techniques. The most common three are named according to the most specific agonist compound at each of these receptors, *N*-methyl-D-aspartate (NMDA), α -amino-3-hydroxy-5-methyl-4-isoxazolepropionate (AMPA) and kainate (Table 1). The fourth, L-2-amino-4-phosphonobutyrate (AP4) appears to represent an inhibitory autoreceptor.

Since the focus of this thesis is the NMDA receptor, this subclass will be discussed in greatest detail.

1.3.1 The NMDA receptor

The NMDA receptor is the most well characterised of all the ionotropic receptors, and plays a crucial role in many physiological, behavioural and pathological functions of the CNS including synaptic plasticity, information processing and memory. Like the GABA_A receptor, the NMDA receptor is now recognised as having several distinct binding and modulatory sites (Figure 2). This complexity raises the suggestion that different combinations of modulatory sites may imply the existence of pharmacologically distinguishable receptor sites.

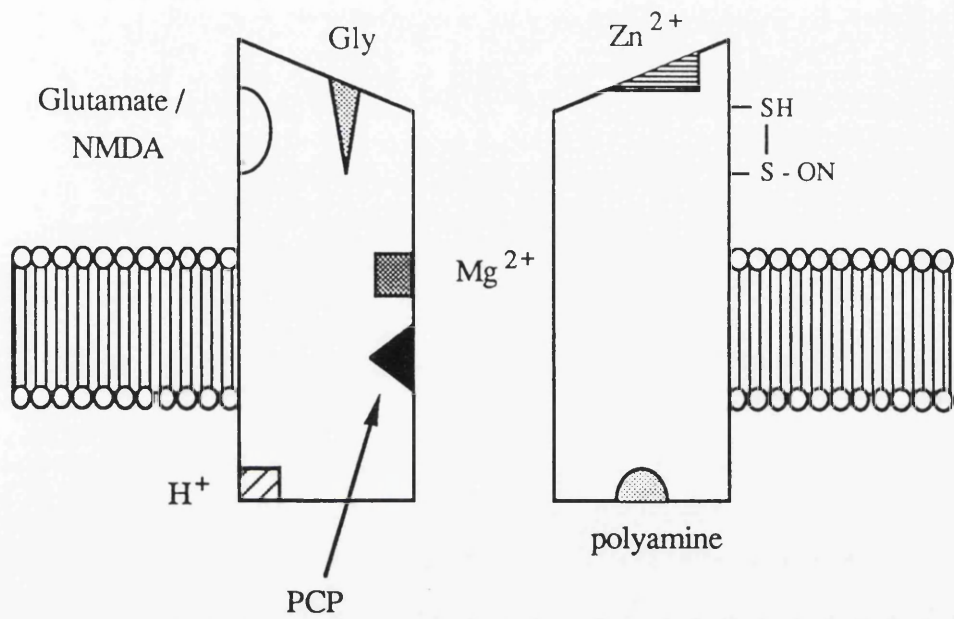
TABLE 1
Excitatory amino acid receptors

Receptor class	Agonist	Antagonist	Radioligand
NMDA <i>recognition site</i>	NMDA L-glutamate L-aspartate D,L(tetrazol-5-yl)glycine	D-AP5 CPP CGS 19755	L-[³ H]glutamate
<i>channel</i>		ketamine TCP MK801 CNS 1102	[³ H]MK801 [¹²⁵ I]MK801 [³ H]TCP
<i>glycine site</i>	glycine D-serine D-alanine D-cycloserine (P)	HA-966 (P) kynurenate 5,7-chlorokynurenate	[³ H]glycine
<i>polyamine site</i>	spermine spermidine	argiotoxin-636	
AMPA	AMPA L-glutamate quisqualate	NBQX CNQX LY-293558 GYKI-52466	[³ H]AMPA [³ H]quisqualate [³ H]glutamate
Kainate	kainate 4-methyl glutamic acid domoate quisqualate	NS102 CNQX	[³ H]kainate [³ H]glutamate
Metabotropic	trans-ACPD quisqualate ibotenate	L-AP4	

A summary of representative agonists, antagonists and radioligands for each of the excitatory amino acid receptor classes. Agents are not necessarily ranked in order of pharmacological potency. (P) partial agonist.

AMPA : (RS)- α -amino-3-hydroxy-5-methyl-4-isoxazolepropionic acid, L-AP4 : S-2-amino-4-phosphonobutyrate, D-AP5 : D(-)-2-amino-5-phosphonopentanoate, trans-ACPD : 1-aminocyclopentane-1S,3R-dicarboxylate, CGS 19755 : 4-phosphonomethyl-2-piperidinecarboxylic acid, CNS 1102 : N-(1-naphthyl)-N'-(3-ethylphenyl)-N'-methylguanidine hydrochloride, CNQX : 6-cyano-7-nitroquinoxaline-2,3-dione, CPP : (\pm)-(2-carboxypiperazine-4-yl)propyl-1-phosphonic acid, GYKI-53655 : 1-(4-aminophenyl)-4-methyl-7,8-methylenedioxy-5H-(3N-methylcarbamate)-2,3-benzodiazepine, HA966 : (R)-3-amino-1-hydroxypyrrolid-2-one, LY-293558 : 3S,4aR,6R,8aR-6[2(1H-tetrazol-5yl)ethyl]-decahydroisoquinoline-3-carboxylate, MK801 : (+)-5-methyl-10,11-dihydro-5H-dibenzo[a,d]cyclohepten-5,10-imine maleate, NMDA : N-methyl-D-aspartate, NBQX : 6-nitro-7-sulphamoyl-benz(f)quinoxaline-2,3-dione, NS102 : 5-nitro-6,7,8,9-tetrahydrobenzo-[γ]-inodole-2,3-dione-3-oxime, TCP : 1-[1-(2-thienyl)cyclohexyl]-piperidine

INACTIVE
(channel closed)



ACTIVE
(channel open)

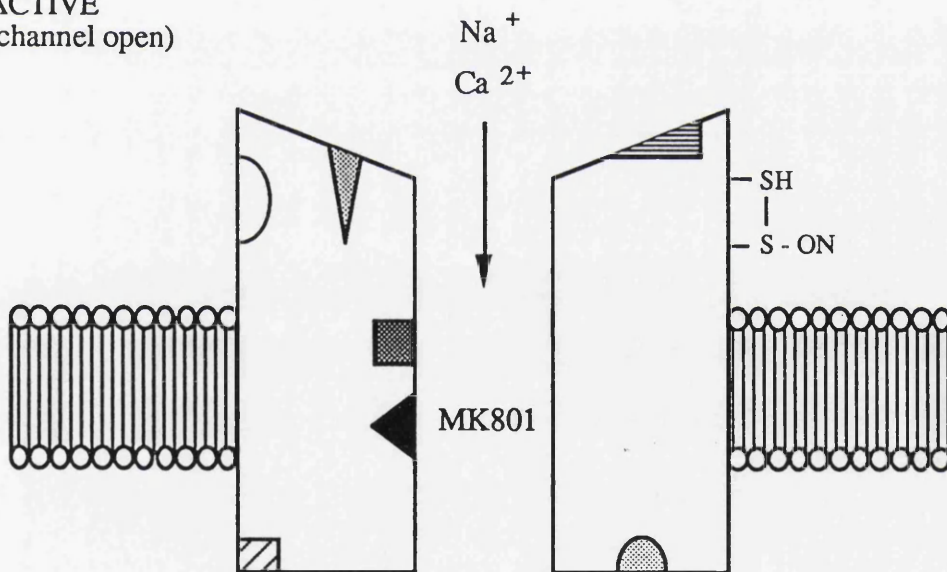


FIGURE 2 : Schematic illustration of the NMDA receptor

The transmitter binding site

The transmitter binding site binds L-glutamate (and L-aspartate) with high affinity promoting the opening of a high conductance channel permeable to Na^+ and Ca^{2+} . Two schemes have been suggested to describe channel responses to a brief pulse of L-glutamate.

1. Channel openings may occur with a moderately high probability ($\sim 10\text{ms}$) soon after agonist binding and repeatedly open and close until the agonist dissociates several hundred milliseconds later.
2. The majority of NMDA channels open after a considerable delay and after the initial burst, the likelihood of subsequent openings is reduced. Results from concentration jump and patch-clamp analysis support the short first latency scheme, where a significant number of channels exhibit long-lasting bursting (Dzubay and Jahr, 1996).

Two distinct binding sites are associated with the transmitter binding site, one which preferentially binds agonists and one which preferentially binds antagonists (Foster and Fagg 1987, Cooper *et al* 1996). Autoradiographic studies by Monaghan and colleagues (1988) examining [^3H]glutamate and [^3H]3-[(\pm)2-carboxypiperazine-4-yl]propyl-1-phosphonic acid ([^3H]CPP) binding suggested that these may represent 2 distinct receptors. More recently, ligand binding studies have identified pharmacologically distinct receptor subtypes which display differing preferences for agonists and antagonists (Bresink *et al* , 1995, Sucher *et al* , 1996).

A number of competitive antagonists exist for the transmitter binding site. The 'prototype' compounds are ω phosphono-substituted amino acids such as D-AP5 (2-amino-5-phosphonopentanoic acid) and D-AP7 (2-amino-7-phosphonopentanoic acid). The construction of conformationally restricted analogues of these compounds produced antagonists with increased affinity such as D-CPP (4-(3-phosphonopropyl)piperazine-2-carboxylic acid and its unsaturated analogue D-CPPene ((E)-4-(3-phosphono-prop-2-enyl)piperazine-2-carboxylic acid). A novel class of competitive antagonists have been characterised *in vitro* (Urwyler *et al*, 1996a) and *in*

vivo (Urwyler *et al*, 1996b). Structure-activity relationship of these biphenyl derivatives of 2-amino-7-phosphonoheptanoic acid have shown that the α -amino, α -carboxylate, and ω -acidic moiety are necessary for high affinity binding to the transmitter recognition site (Urwyler *et al*, 1996a).

The glycine modulatory site

The glycine recognition site has been proposed as a potentiator of NMDA evoked currents in a variety of preparations including cultured cortical neurons (Kemp and Priestly, 1991) and *Xenopus* oocytes (Kleckner and Dingledine, 1988). L-glutamate is virtually ineffective in activating NMDA receptor channels unless the glycine site is also occupied (Johnson and Ascher, 1987). This potentiation of glutamate responses is detected at glycine concentrations as low as 10nM and is not mediated by the inhibitory strychnine-sensitive glycine site (Johnson and Ascher, 1987). The very low concentration of glycine required for this effect, in relation to the concentration normally present in brain, suggest that glycine may serve as a constant enabling factor rather than a regulatory mechanism for NMDA-mediated effects .

An increasing amount of evidence suggests that the glutamate and glycine sites of the NMDA receptor are allosterically coupled. Patch clamp studies in hippocampal neurons showed that saturating concentrations of glycine prevented desensitisation of NMDA receptor currents and that glutamate increased the dissociation of glutamate from NMDA receptors (Lester *et al*, 1993). The interaction between glutamate and glycine sites had also been examined using ligand binding studies. Initial studies showed that glycine enhanced L-[³H]glutamate binding and inhibited binding of the glutamate antagonist, D-[³H]AP5 (2-amino-5-phosphonopentanoic acid) at concentrations consistent with action at the glycine recognition site (Monaghan *et al*, 1988). This observation suggests that glycine site agonists have opposite effects on the agonist or antagonist preferring states of the glutamate recognition site. More recent ligand binding studies propose a more complex interaction (Grimwood *et al*, 1993). Glycine, D-serine and D-cycloserine partially inhibited binding of the "C-5"

glutamate antagonist [^3H]CGS 19755 (*cis*-4-phosphonomethyl-2- ^3H piperidine carboxylate) and had little effect on [^3H]glutamate or the "C-7" glutamate antagonist [^3H]CPP. These effects can be explained by the proposal that glutamate, CPP and CGS 19755 bind to overlapping but nonidentical sites, and that glycine site ligands induce a conformational change that differentially affects the binding of these ligands. In the same study, in contrast to a lack of effect on [^3H]glycine binding, "C-7" antagonists partially inhibited binding of the glycine site antagonist [^3H]L-689,560 ((\pm)-4-*trans*-2-carboxy-5,7-dichloro-4- ^3H phenylaminocarbonylamino-1,2,3,4 tetrahydroquinoline). These inter-actions cannot be explained by an allosteric interaction and it has been suggested that a steric inhibition where glutamate site antagonists physically prevent access of [^3H]L-689,560 to its binding site may be responsible. Thus two mechanisms may operate in these interactions, depending on the size of the ligands involved, a true allosteric change of affinity and a steric inhibition.

Voltage-dependent Mg^{2+} block

A unique feature of the NMDA receptor is that it exhibits a voltage-dependent Mg^{2+} block (Nowak *et al*, 1984, Mayer *et al*, 1984). In the presence of Mg^{2+} , single channel currents measured at resting potential are chopped into bursts and the opening potential of the channel is reduced (Nowak *et al*, 1984). The channel current induced by a given amount of glutamate (or NMDA) is increased when the cell is depolarised and NMDA responses are also greatly potentiated by reducing the extracellular Mg^{2+} concentration below physiological levels ($\sim 1\text{mM}$). In addition to this site ~ 0.65 through the electric field of the ion channel (Johnson and Ascher, 1990) a superficial, high affinity divalent cation binding site ~ 0.2 through the electric field has also been identified (Premkumar and Auerbach, 1996). This external binding site is an important feature of the Ca^{2+} permeability of the NMDA receptor since it determines the fraction of NMDA receptor current carried by Ca^{2+} .

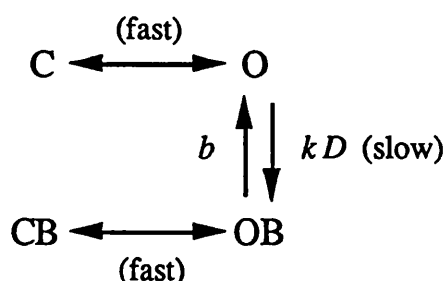
Recent studies by Wang and MacDonald (1995) have shown that, at positive potentials, Mg^{2+} can enhance NMDA responses in the presence of low glycine

concentrations. This potentiation was associated with a increase in the affinity of the NMDA receptor for glycine (Wang and MacDonald, 1995, Paoletti *et al*, 1995). It was suggested that Mg^{2+} may be acting as an agonist at the spermine site to produce these effects (Paoletti *et al*, 1995) since Mg^{2+} , like spermine relieved the inhibitory effect of protons on NMDA receptor responses (Traynelis *et al*, 1995).

Ion channel blockade

NMDA receptors are selectively blocked by a variety of dissociative anaesthetics such as ketamine, phencyclidine (PCP) and MK801 (Kemp *et al*, 1986). It is well established that this type of blockade is both voltage-dependent and dependent on the presence of agonist (use-dependent) (Javitt and Zukin, 1989, Rogawski, 1993). Therefore the state of the NMDA receptor determines the degree of antagonism in that binding is almost completely dependent on the activation of the receptor (Foster and Wong, 1987).

In the absence of channel blocking agent, the channel exists in one of two states, open (O) or closed (C). Presence of the channel blocker induces additional states, open-blocked (OB) and closed-blocked (CB). It is suggested that the blocking agent can only dissociate from the open form of the channel as detailed in the kinetic scheme below (MacDonald *et al*, 1991).



where k is the forward rate constant of blockade, D is the concentration of blocker and b is the reverse rate constant of blockade.

While a variety of binding studies have confirmed that dissociative anaesthetics interact most readily with the agonist-associated (open) state of the NMDA receptor (Huettnner and Bean, 1988, MacDonald and Nowak, 1990), it has been proposed that PCP-like agents may gain access to their binding site when the channel is closed. Drugs that interact exclusively with open channels should display single exponential association and dissociation kinetics. Javitt and Zukin (1989) reported that in the presence of L-glutamate (10 μ M), the kinetics of [³H]MK801 association were fit better by 2 exponentials. Under control conditions (absence of glutamate or glycine) or in the presence of AP5 99% of [³H]MK801 association could be accounted for by a single exponential thus, a degree of slow association of [³H]MK801 occurs under conditions when few NMDA receptors would be expected to be open. These results suggest that PCP-like agents can gain access to their binding site when the NMDA receptor channels is closed as well as via open channels. Bioexponential kinetics can be explained by agents gaining access to their recognition site by two pathways, each corresponding to one of the observed kinetic components. Channel blocking agents with pKa values close to physiological pH associate via a fast hydrophilic path representing access via open channels and a slow hydrophobic path representing binding via a path associated with closed channels. Closed channel access presumably requires transfer across lipid bilayer, or diffusion through hydrophobic domains (Javitt and Zukin, 1989, Chen *et al*, 1992).

Ketamine, PCP and MK801 display high affinity for the NMDA receptor channel and block 90-99% of agonist evoked NMDA currents at low concentrations (Foster and Wong, 1987). High affinity coupled with use-dependent blockade allows only minimal basal levels of glutamatergic activity within the brain. These agents display high neurobehavioural toxicity such as cognitive and sensory impairments (for review see McCulloch, 1992). Dissociative anaesthetics also produce transient and reversible histopathological changes in the cingulate cortex (McCulloch and Iversen, 1991).

More recently certain phenylcyclohexylamines (PCA's, primary amine analogues of

PCP), an analogue of MK801, ADCI and the anti-Parkinsonian, anti-viral agent memantine (1-amino-3,5-dimethyladamantane hydrochloride) were found to display affinity for the NMDA receptor channel in the low micromolar range and to demonstrate more advantageous behavioural effects than PCP or MK801. These low affinity blockers display rapid rates of block and unblock, memantine reaches steady-state within 1 second of application (Chen *et al*, 1992). The proportion of current blocked increases with agonist concentration while a basal level of agonist evoked responses remains. The relatively rapid kinetics of these low affinity compounds may underlie this favourable profile (Rogawski, 1993, Chen *et al*, 1992).

A novel high affinity channel blocking agent WIN 63480 ((\pm)-12,12-diethoxy-13,13-dimethyl-6,11-ethano-6,11-dihydrobenzo[b]-quinolizinium chloride) has recently been reported to lack observable behavioural effects at high concentrations. While WIN 63480 was an effective NMDA receptor channel blocker, it is strongly hydrophilic ($\log D = -4.1$) and was shown to have much less access to closed channels than MK801 ($\log D = +1.8$), Ault *et al*, 1995). Access to closed channels results in a non-competitive profile of antagonism for MK801 and PCP, compared to a more uncompetitive profile for WIN 63480.

Consequently WIN 63480 may produce less inhibition of physiological NMDA-mediated processes.

The polyamine modulatory site

The highly regulated nature of polyamine biosynthesis, retroconversion and biosynthesis verify the critical role of these ubiquitous aliphatic polycations in cell growth and differentiation (Scott *et al*, 1993). It is now established that these low molecular weight nitrogenous bases do not perform a single function and the known roles of polyamines can be divided in to those dependent on their chemical or biological properties. Spermine and spermidine interact with negatively charged molecules such as nucleic acids or phospholipids, stabilising these highly charged structures (Wallace *et al*, 1987). Polyamines also have effects on voltage-gated cation currents, spermine and spermidine

allosterically inhibit the binding of calcium channel ligands, and can modulate voltage-activated K^+ current (for review see Scott *et al*, 1993, Johnson, 1996). Multiple recognition sites for polyamines have been reported to account for the complex actions ranging from antagonism to enhancement of glutamate responses mediated NMDA receptors (Johnson, 1996). Polyamines appear to exert dual effects with low concentrations enhancing and high concentrations inhibiting responses (Scott *et al*, 1993). The potentiating effects of polyamines (Munir *et al*, 1993, Fahey *et al*, 1993) can be subdivided into 'glycine-independent' stimulation where spermine increases NMDA currents in the presence of saturating glycine, and 'glycine -dependent' stimulation which increases the affinity of the receptor for glycine (Johnson, 1996). The inhibitory effect can also be further divided into voltage-dependent inhibition and a decreased affinity for glutamate (Figure 3). Ransom and Stec (1988) identified another polyamine binding site allosterically linked to the MK801 binding site, where low spermine concentrations enhance MK801 binding. In addition to endogenous polyamines, these compounds are also major constituents of venoms produced by a number of vertebrates. The receptor-specific toxin sensitivity can be correlated with individual receptor subtype (see subunit-specific blockade).

Proton block

The strict regulation of pH within the brain is well established. It is of interest therefore that despite the wealth of homeostatic mechanism, neuronal activity gives rise to changes in intracellular and extracellular pH (Chesler and Kaila, 1992). These shifts occur rapidly in either the acid or alkaline direction. Alkaline and acid shifts typically lead to a respective increase or decrease in neuronal excitability and are of a large enough magnitude to influence the function of receptors.

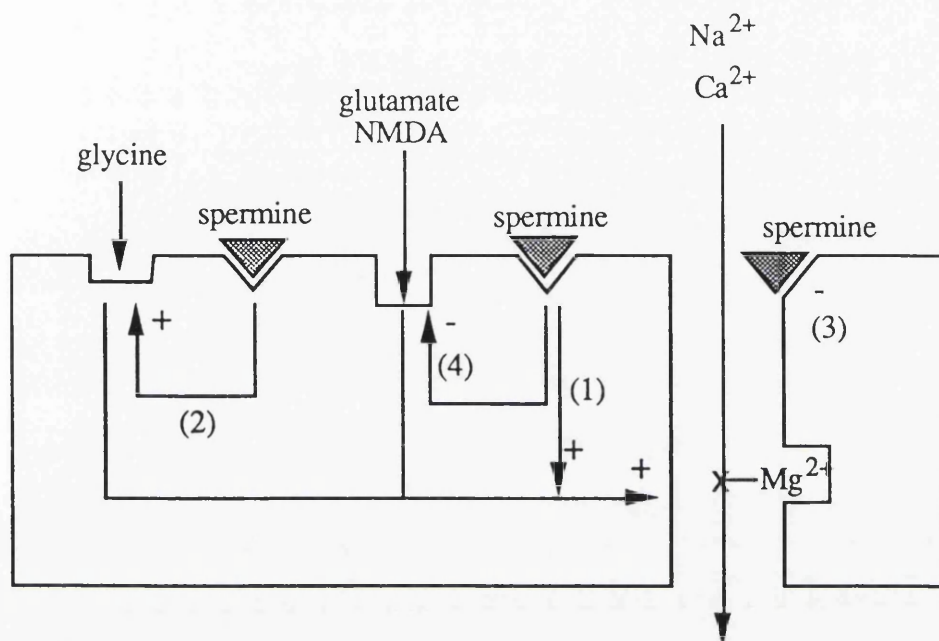


FIGURE 3 : The modulatory actions of polyamines on the NMDA receptor

(1) Glycine-independent stimulation : occurs at saturating glycine concentrations and involves an allosteric effect on the conformation of the channel protein to increase the frequency of channel opening. (2) Glycine-dependent stimulation : occurs at subsaturating glycine concentrations and increased NMDA receptor affinity for glycine. (3) Voltage-dependent inhibition : decreases channel conductance as a result of charge screening at the mouth of the channel, fast-open channel block at a site within the channel, possibly involving Mg^{2+} . (4) Decreases affinity for agonist : occurs at sub-saturating concentrations of NMDA or glutamate

NMDA receptor responses were selectively inhibited by protons (H^+) in cerebellar neurons. 50% inhibition of responses occurred at pH 7.3 implying that NMDA receptors are not fully activated under normal conditions (Traynelis and Cull-Candy, 1990). Non-competitive interactions at the agonist binding site, glycine site and Mg^{2+} site suggested that protons act at a specific site on or near the face of the NMDA receptor channel to decrease the frequency of channel opening. Strikingly similar results were obtained in cultured hippocampal neurons (Tang *et al*, 1990).

More recently, supporting evidence for the negative modulation by protons of NMDA receptors was provided by ligand binding studies. Increasing extracellular pH from 6.5-8.0 increased the association and dissociation rate of [3H]MK801 binding (Rajdev and Reynolds, 1993). Yoneda and colleagues (1994) also showed that glutamate-dependent [3H]MK801 binding to synaptic membranes increased with decreasing proton concentration over the pH range 6.0-9.0. These observations suggest that [3H]MK801 binding is controlled by the level of NMDA receptor activation.

Mild acidosis (pH 6.8-7.4) has been shown to inhibit the rise in intracellular Ca^{2+} (Takadera *et al*, 1992, Ebine *et al*, 1994) and to delay spreading depression and improve neuronal recovery following hypoxia in hippocampal slices (Tombaugh, 1994). This beneficial effect may be dependent on the severity of the acidosis since Ca^{2+} influx in hippocampal slices at pH 6.2 was twice that measured at pH 7.3 (O'Donnell and Bickler, 1994).

Acidosis has also been shown to be neuroprotective in ischaemia. Simon *et al* (1993) reported that mild acidosis (pH 6.8) induced by increasing the CO_2 tension in inspired air, attenuates ischaemic injury in the rat. However, this reduction in infarct volume was biphasic and the beneficial effect of acidosis was lost at pH 6.5. This is in agreement with the observation that a more severe acidosis (pH 6.3) induced by hypercapnia, exaggerated ischaemic damage in the rat (Katsura *et al*, 1994). It is suggested that inhibition of glial glutamate uptake is likely a major factor in attenuating the neuroprotective effect of acidosis. A toxic effect of acidosis on glia

was described by Giffard *et al* (1990), with a 9 hour exposure at pH 6.4 resulting in death of a third of the glial population.

It is noted that induction of hypercapnia has wider reaching effects within the central nervous system beyond those on NMDA receptors. An increase in cerebral blood flow occurs in all brain region following induction of hypercapnia (Simon *et al*, 1993) however, this vasoreactivity is lost in ischaemic areas (Dettmers *et al*, 1993).

In summary, modulation of the divalent ion-carrying NMDA current by protons may serve as a negative feedback mechanism controlling neuronal excitability under normal conditions and, as an intrinsic protective mechanism by which Ca^{2+} entry into neurons is regulated in pathological conditions. In situations where acidosis worsens the overall outcome of ischaemic damage, it may decrease the specific component of neuronal injury mediated by NMDA receptors.

The redox modulatory site

NMDA-evoked currents have been shown to be enhanced by disulphide-reducing agents (DTT, dithiothreitol) and inhibited (but not completely) by thiol-oxidising agents (DTNB, 5,5'-dithiobis-2-nitrobenzoic acid). Both reducing and oxidising agents modify the native receptor implying that the NMDA receptors are in equilibrium between a fully oxidised (disulphide) and fully oxidised (thiol) form (for review see Gozlan and Ben-Ari, 1995). DTT reacts at sites on the extracellular domain of the receptor to increase the frequency of single channel openings, the potentiation of NMDA-evoked currents correlates with an influx of Ca^{2+} through the NMDA channel (Aizenman and Harnett, 1992).

The variation in reports of the existence and variation in proportion of the 2 redox states in different preparations suggests the presence of endogenous compounds which interact at these sites. Potential candidates are thiol reagents such as cysteine, homocysteine which are released during depolarisation (Zangerle *et al*, 1992), and dihydrolipoic acid which increase NMDA responses. Disulphide reagents like lipoic acid and methoxalin react with free sulphhydryl (SH) groups to inhibit responses. The

endogenous reducing agent ascorbic acid has also been shown to inhibit NMDA-induced currents. Free radicals are also known to interact with thiol groups. Free radicals generated by xanthine oxidase inhibit NMDA responses. Particular attention has focused on nitric oxide which displays a direct action on SH groups of the redox site (Lei *et al*, 1992). Dynorphin, an endogenous opioid reduces NMDA-activated currents without involving opioid receptors. Dynorphin interacts with a site conformationally linked with the redox site(s) on the NMDA receptor altering the gating properties of the channel (Chen *et al*, 1995).

Fully oxidised receptors are functional, indicating redox modulation is not a switch turning NMDA receptors on or off, but is rather a buffer of NMDA receptor overactivity (Gozlan and Ben-Ari, 1995). This redox system can buffer small changes in redox potential that occur in relation to electrical activity thus maintaining activity within a controlled range. However, the buffering capacity probably plays a limited role in pathological conditions since it cannot overcome large changes in redox potential .

Modulation by zinc

The presence in high concentrations of zinc in the synaptic vesicles of mossy fibres within the hippocampus and its release into the extracellular space during neuronal excitation lead to the proposal that zinc could modulate neuronal excitability (Assaf *et al*, 1984). The demonstration of preferential uptake and Ca^{2+} -dependent release of zinc within hippocampal slices added weight to the hypothesis that zinc was involved in synaptic transmission (Howell *et al*, 1984). Studies by Westbrook and Mayer (1987) in hippocampal neurons confirmed that zinc ($50\mu\text{M}$) produced an almost complete inhibition of NMDA activated current via a direct effect on the receptor channel complex in a voltage-insensitive manner. At this concentration zinc was found to potentiate kainate and quisqualate mediated currents. More recently zinc has also been shown to modulate the binding of antagonists at the NMDA receptor (Terse and Komiskey, 1997). Zinc ($12.5\mu\text{M}$) significantly inhibited [^3H]CGP 39653

binding to rat brain homogenate by increasing the K_d of this compound. It was suggested from these results that the zinc concentration of the brain may influence the therapeutic effects of competitive NMDA receptor antagonists.

μ opioid interactions

μ opioid receptor activation had been reported to increase NMDA receptor currents postsynaptically (Martin *et al*, 1997). The mechanism of potentiation is unclear however, the effects of μ opioid receptor agonists on NMDA responses have been proposed to be linked to this voltage-dependent Mg^{2+} blockade (Cheng and Huang, 1992). μ opioid agonists cause sustained increases in NMDA-induced currents by activating protein kinase C (PKC). In this study PKC was found to potentiate NMDA receptor responses by increasing the open probability of the channel by reducing the voltage-dependent Mg^{2+} block.

Modulation by phosphorylation

Phosphorylation of glutamate receptors has been postulated as an important mechanism for modulating excitatory transmission (Ben-Ari *et al*, 1992), however the precise phosphatases involved were unknown. More recently Wang *et al* (1994) demonstrated that NMDA receptors were regulated by endogenous serine/threonine protein phosphatases in cultured hippocampal neurons. Protein phosphatases 1 and 2A decreased the open probability of the NMDA receptor and phosphatase inhibitors were shown to enhance NMDA-induced currents. These observations were supported by the demonstration that activation of calcineurin (Ca^{2+} /calmodulin-dependent phosphatase) by calcium entry through NMDA receptor channels shortens the duration of channel opening in rat dentate gyrus granule cells (Lieberman and Mody, 1994). It is apparent therefore that a negative feedback mechanism exists *in vitro* where phosphorylation of the NMDA receptor channel modulates neuronal excitability.

Two families of NMDA receptor subunits have been cloned and sequenced in the rat, consisting of 5 receptor subunits NMDAR1 (NR1) and 4 NMDAR2 subunits (NR2A-D, Nakanishi, 1992, for review see Sucher *et al*, 1996). An NMDA receptor-like subunit has also been cloned (NRL) which is closely related to NMDAR1 (Sucher *et al*, 1996). Isolated cDNA encoding a full length NMDA receptor subunit from human brain (nNR1) shares high sequence homology (99%) with rat brain NR1 and murine $\zeta 1$ (Nakanishi, 1992), suggesting that the cDNA clone of hNR1 which codes for a human brain NMDA receptor subunit is descendent from rodent and murine brain NR1 subunits (Planells-Cases *et al*, 1993). Alternative splicing of the single gene can generate at least 8 NR1 isoforms with distinct functional properties. One of these splice variants coded by exon 5, exists in 2 different forms with the presence (NR1b) or absence (NR1a) of a 21 amino acid N-terminal insert sequence, which is predicted to form a loop on the extracellular surface of the NR1 protein (Traynelis *et al*, 1995, Johnson, 1996). The human NR1 subunit, NMDAR1 or the murine homolog form homo-oligomers and exhibit electrophysiological and pharmacological properties characteristic of NMDA receptors when expressed in *Xenopus* oocytes (Seeburg, 1993, Planells-Cases *et al*, 1993) but not in mammalian cells (Sucher *et al*, 1996). It is suggested that the *in vivo* biological activity of the NMDA receptor is dependent on this essential subunit, since mice carrying a disrupted allele of NMDAR1 (Grin 1) possessed no NMDA responses and die when neonates (Forrest, 1994). NR1 subunits require co-assembly with NR2 subunits to yield currents of the magnitude found in neurons (for review see Seeburg, 1993, Sucher, 1996).

NR2 subunits therefore appear to have a modulatory role, with each recombinantly expressed, heteromeric NR1-NR2 receptor combination possessing distinct biophysical and pharmacological signatures. Subunit dependent properties include the strength of the Mg^{2+} block (Kuner and Schoeper, 1996), sensitivity to modulation by glycine (Monaghan *et al*, 1988), and affinities for agonists and antagonists (Marti *et al*, 1993, Lynch *et al*, 1995). Heterogeneity within the NR2 subunit family results

from expression of 4 closely related genes, NR2 subunits share 15% homology with NR1 subunits (Figure 4).

Natively expressed receptors are thought to comprise NR1 and at least one other member of the NR2 class but the exact stoichiometry remains unknown. It has been suggested that NMDA receptors may form pentamers like nicotinic acetylcholine receptors or follow the tetrameric structure of ion channels with pore loops. It has been reported that NR2A and NR2B can be immunoprecipitated with NR1 suggesting a portion of NMDA receptors form heterooligomers with at least 3 subunits (Sheng *et al* 1994) however it remains unknown if these subunits represent functional receptors.

Previously, ideas on the transmembrane topology of ligand-gated ion channels was based on data from nicotinic acetylcholine receptors and the majority of glutamate receptor sequences were interpreted on this framework. The NR1 primary amino acid sequence was originally interpreted to indicate 4 transmembrane domains (TMI-TMIV). A long N terminal extracellular segment before TMI has been postulated to contain the agonist binding site. Site directed mutagenesis had highlighted three charged residues within this region which are critical for glutamate binding (Planells-Cases *et al*, 1993). The putative TMII was designated the channel forming region, with highly conserved asparagine residue in the N position (also found in NMDAR2 subunits) mediating Ca^{2+} permeability and the voltage sensitivity of the Mg^{2+} block (Seeburg, 1993, Kuner and Schoepfer, 1996). The extensive C terminal sequence is currently modelled to be intracellular. An interaction has recently been reported between the C terminus of NR2A and NR2B subunits and the domains of PSD-95/SAP90, an abundant synaptic protein associated with the cytoskeleton (Niethammer *et al*, 1996).

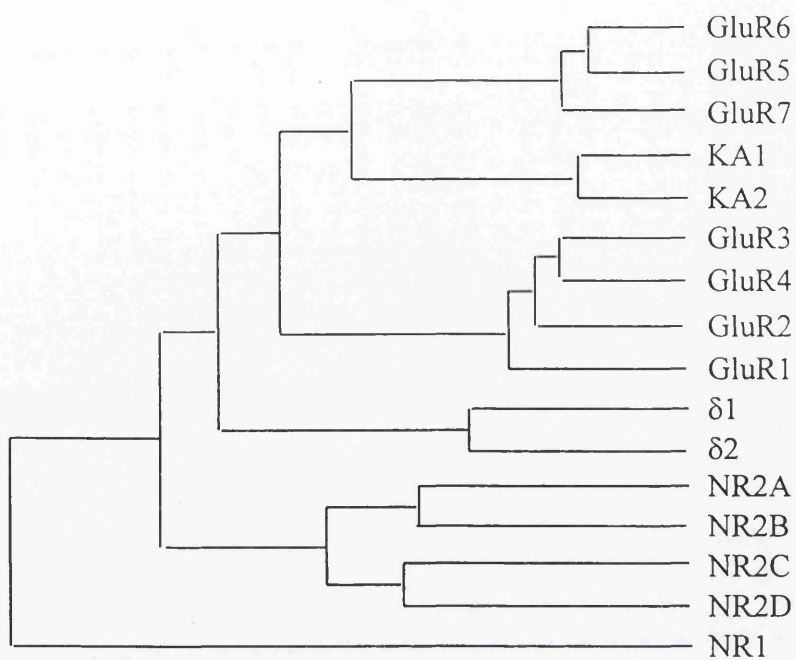


FIGURE 4 : Phylogenetic tree of ionotropic glutamate receptor subunits in the rat

NR1 and NR2A-D are NMDA receptor subunits. GluRA-GluRD are AMPA subunits. KA1, KA2 and GluR5-GluR7 are subunits of kainate receptors. The d subunits have yet to be assigned. The line length separating any pair of subunits represents the distance between their sequences.

It is proposed that the PSD-95 family of guanylate kinases may anchor NMDA receptor subunits to the cytoskeleton and assist in the assembly of receptor complexes. Recently several groups have put forward indirect evidence, inferred from the structure of the non-NMDA receptor subunit GluR1 that the NR1 subunit has 3 transmembrane domains with TMII forming a loop in the membrane to participate in the formation of a channel pore (Sucher *et al*, 1996).

Subunit specific block

Radioligand binding and electrophysiology studies have described 4 distinct populations of native NMDA receptors. Discrete populations are found within the cerebellum (Perkins and Stone, 1983, Widdowson *et al*, 1995) and the midline thalamic nuclei, while the remaining 2 differ in their affinities for agonists and antagonists (Monaghan *et al*, 1988). The anatomical distribution of each of the subtypes show striking parallels to the distribution of individual NR2 subunit mRNA. NR2A mRNA is localised in the cortex and hippocampus and distribution was similar to that of 'antagonist preferring' NMDA receptors, as defined by [³H]CPP binding (correlation coefficient 0.88). 'Agonist preferring' NMDA receptors were localised to forebrain regions expressing NR2B and NR1 mRNA. NR2C mRNA is almost exclusively localised within the cerebellum and NR2D to midline thalamic nuclei. The marked anatomical correspondence between distribution of mRNA and expression of NMDA receptors with different pharmacological profiles implies that a molecular basis underlies the heterogeneity in NMDA receptor properties and that the distinct properties of these subtypes are determined by NR2 subunits (Buller *et al*, 1994).

Kutsuwada and colleagues (1992) demonstrated that different subunits are distinct with respect to affinities for agonists and competitive antagonists and this was confirmed by autoradiographic studies (Yoneda and Ogita, 1991, Bresink *et al*, 1995). [³H]MK801 binds with lower affinity in the cerebellum compared to the cortex.

This observation was explained by preferential binding to distinct NMDA receptor subunits, [³H]MK801 may have a decreased affinity for NMDA receptors containing NR2C or NR2D subunits which are abundant within the cerebellum (Nakanishi, 1992).

It has also been suggested that the observation that low affinity NMDA channel blockers like amantadine and memantine bind with similar affinity to cortical and cerebellar binding sites may also be attributable to preferential binding to certain receptor subtypes (Porter and Greenamyre, 1995).

In addition to their uneven distribution throughout the brain, distinct NMDA receptor subtypes may be differentially involved in neurological disorders. Proton inhibition of NMDA receptors is determined by the presence or absence of exon 5 in the NR1 subunit (Traynelis *et al*, 1995). Brain regions that express exon 5 (brainstem, thalamus, cerebellum, hippocampus) may be uniquely vulnerable to glutamate induced neuronal damage inasmuch as the attenuation of proton inhibition by NR1 exon 5 enhances neuronal excitability and reduces the negative feedback of extracellular acidification occurring after excessive NMDA receptor activation (Traynelis *et al*, 1995). The development of subtype-specific antagonists has thus gained considerable interest.

A number of compounds have been identified that appear to discriminate between NMDA receptors composed of different subunit combinations, the best characterised is ifenprodil. Ifenprodil is an atypical, non-competitive NMDA antagonist which displays 400-fold higher affinity for NR1-NR2B than NR1-NR2A receptors (Williams, 1993). This agent was originally proposed to act at the polyamine site however, the interaction between ifenprodil and polyamines is non-competitive. Ifenprodil, in the presence of saturating concentrations of glycine, can potentiate the effect of NMDA receptor activation by low concentrations of agonist. Little effect on NMDA responses is detected at intermediate agonist concentrations, and profound block is observed at high agonist concentrations (Kew *et al*, 1996).

Ifenprodil inhibition of recombinant NR1-NR2B receptors in *Xenopus* oocytes was found to be pH sensitive, with less inhibition occurring at alkaline pH. The pH sensitivity of ifenprodil block occurs at NR1b-NR2B as well as NR1a-NR2B receptors suggesting that it is not influenced by the presence or absence of exon 5.

The attractive pharmacological profile of ifenprodil which lacks the side effects exhibited by other NMDA antagonists is attributable in part to both subunit selectivity and, the ability of this compound to block channels during periods of high activity while leaving resting channels relatively unaffected. Investigation of the mechanisms of action of such subunit specific compounds not only provides attractive therapeutic strategies with minimal side effects, but helps to refine our understanding of the complex interactions between various modulators of the NMDA receptor.

1.3.2 The AMPA receptor

AMPA receptors are found in the majority of excitatory synapses, with a similar distribution to NMDA receptors however AMPA receptors predominate in the molecular layer of the cerebellum whereas NMDA receptors are localised within the granule cell layer (for review see Farooqui and Horrocks, 1991). Investigation of AMPA binding kinetics revealed the presence of a high affinity and a low affinity binding site. The AMPA antagonist [³H]CNQX labels both sites with the same affinity. Due to the low calcium permeability of these receptors they do not carry sufficient ions to initiate biochemical and biological processes triggered by an increase in calcium levels. These receptors mediate fast excitatory transmission and are voltage-independent. Treatment of rat brain membranes with phospholipase A₂ has been shown to cause a significant increase in the affinity of the receptor for AMPA, without changing the number of binding sites (Farooqui and Horrocks, 1991).

Three selective AMPA antagonists exist DNQX (6,7-dinitroquinoxaline-2,3-dione), CNQX (6-cyano-7-nitroquinoxaline-2,3-dione) and the most selective NBQX (6-nitro-7-sulphamoylbenzo[f]quinoxaline-2,3-dione). The large body of neuroprotective data from studies using NBQX shows that AMPA receptors play an important role in the neuropathological effects of glutamate in cerebral ischaemia (Nellgard and Wieloch, 1992). More recently a selective AMPA antagonist LY 215490 (decahydroisoquinoline) has also been shown to be neuroprotective (Gill and Lodge, 1994)

Molecular biology

AMPA receptors can be reconstituted *in vivo* by expressing 1 or coexpressing 2 of 4 subunits, GluR1-GluR4 (Nakanishi, 1992). AMPA receptors are proposed to consist of pentameric assemblies. The GluR subunits are widely but differentially distributed throughout the CNS. The type of subunits expressed determines both the biophysical and pharmacological properties of the receptors. There is considerable sequence conservation across the 4 TM regions and subunits differ mainly in extracellular regions (Sheardown, 1993). All AMPA receptors are permeable to Na^+ and K^+ however only those receptors lacking a GluR2 subunit are permeable to Ca^{2+} (Danysz *et al*, 1995). The Ca^{2+} permeability can be linked to a single amino acid residue in the putative channel forming subunit TMII (McEntee and Crook, 1993). In GluR2 subunits the glutamine residue is replaced by arginine (Seeburg, 1993)

GluR subunits are 900 amino acids in length and can occur in two forms with respect to an alternatively spliced exonic sequence of 38 residues, 'flip' and 'flop' (for review see Seeburg, 1993). The prenatal brain expresses mostly 'flip' and this expression persists throughout life. 'Flop' forms appears from postnatal stages onwards and are coexpressed with 'flip' forms in many cells. These developmental changes are proposed to have functional significance. Adults receptors display currents with a fast desensitising component and a steady-state component. Receptors with a 'flip' module display slower desensitising kinetics than adult receptors (Seeburg, 1993).

1.3.3 The Kainate receptor

The distribution of kainate receptors is complementary to that of NMDA and AMPA receptors with a high density of kainate sites present in the stratum lucidum of the hippocampus (mossy fibre system), striatum, thalamus and the inner and outer layers of the cortex (Farooqui and Horrocks, 1991).

Despite the presence of functional kainate receptors in neuronal cultures, synaptic responses were completely blocked by the 2,3-benzodiazepine GYKI 1536559, a selective AMPA antagonist. This evidence and the observation that kainate-elicited responses undergo rapid and total desensitisation (Seeburg, 1993) suggests that kainate receptors do not participate in conventional synaptic transmission in cultured cells, or in adult neuronal populations (Lerma *et al*, 1997). Thus, the significance for the CNS of receptors exhibiting high affinity kainate sites is unclear. Studies by Chittajallu *et al* (1996) showed that kainate elicits a dose-dependent decrease in L-glutamate release from hippocampal synaptosome and also depressed glutamatergic synaptic transmission.

Molecular biology

Kainate receptors can be generated *in vitro* from GluR5, 6, 7 and KA1 or 2 subunits (Seeburg, 1993). The 5 subunits form a complex mosaic of expression in rat brain and the combined pattern of distribution approximates the pattern of high affinity [³H]kainate binding sites. KA1 or 2 expression alone does not generate functional channels. Combined with GluR5/6, receptor properties are different from homomeric channels, GluR5-KA2 channels show rapid desensitisation and display a different current/voltage relationship compared to GluR5 channels.

1.3.4 The AP4 receptor

AP4 receptors are characterised by the antagonistic action of AP4 on certain glutamate-using synapses. It has been suggested that AP4 may act at both pre- and post synaptic sites. Very little is known about the molecular biology of the AP4 receptor.

1.3.5 The Metabotropic receptor

Metabotropic glutamate receptors (mGluRs) are a novel family of recently cloned G protein-coupled receptors. These receptors are coupled to multiple second messenger systems including phosphoinositide hydrolysis and changes in cAMP formation (for review see Schoepp and Conn, 1993, Pin and Duvoisin, 1995). mGluRs can be classified into three groups (see molecular biology) which display different pharmacology. The rank order of agonist potency for group I receptors is quisqualate > glutamate > ibotenate > ACPD (1-amino-cyclopentane-1,3-dicarboxylate). The relative order of potency of group II receptors is reversed compared to group I. Group II receptors are distinctive in their sensitivity to L-AP4 and their insensitivity to ACPD. mGluRs have recently been considered as a putative target for neuroprotective strategies because their activation affects multiple intracellular events contributing to both the induction and progression of neuronal damage. Activation of group II and group III mGluRs protects neurons against excitotoxic damage (Bruno *et al*, 1995). This effect is partly ascribed to neuronal mGluR2 receptors which are located presynaptically and inhibit glutamate release (Pin and Duvoisin, 1995). It appears that new protein synthesis and neuronal-glial signalling are also required for this neuroprotective activity (Bruno *et al*, 1997)

At least 6 subtypes of mGluRs exist termed, mGluR1-mGluR6. These receptors are larger than any other G protein-coupled receptors and possess a common structural architecture. mGluRs possess a large extracellular NH₂ terminal domain and seven putative transmembrane spanning domains. A number of cysteine residues are highly conserved in the NH₂ terminal and may play a structural role (Nakanishi, 1992). Despite interactions being mediated through the same G protein molecules, mGluR's show no sequence homology with any other G protein linked receptors. mGluRs can be classified into three groups according to sequence similarities (Nakanishi, 1992, Figure 5). This classification is supported by the respective transduction mechanisms (Schoepp and Conn, 1993). Group I (mGluR1, mGluR5) stimulate phospholipase C resulting in increased IP₃ formation and mobilisation of Ca²⁺ from intracellular stores. These responses are only partly sensitive to pertussis toxin (PTX) implying the G_i-G_o family of G proteins is involved. Group II (mGluR2, mGluR3) and Group III (mGluR4, mGluR6, mGluR7, mGluR8) are coupled to the inhibition of adenylate cyclase. Group II receptors show a strong inhibition of forskolin stimulated cAMP production however, group II receptors show less than 50% inhibition, implying inappropriate coupling to the G protein. mGluRs of the same group show 70% sequence identity whereas identity between groups is around 45% (Pin and Duvoisin, 1995).

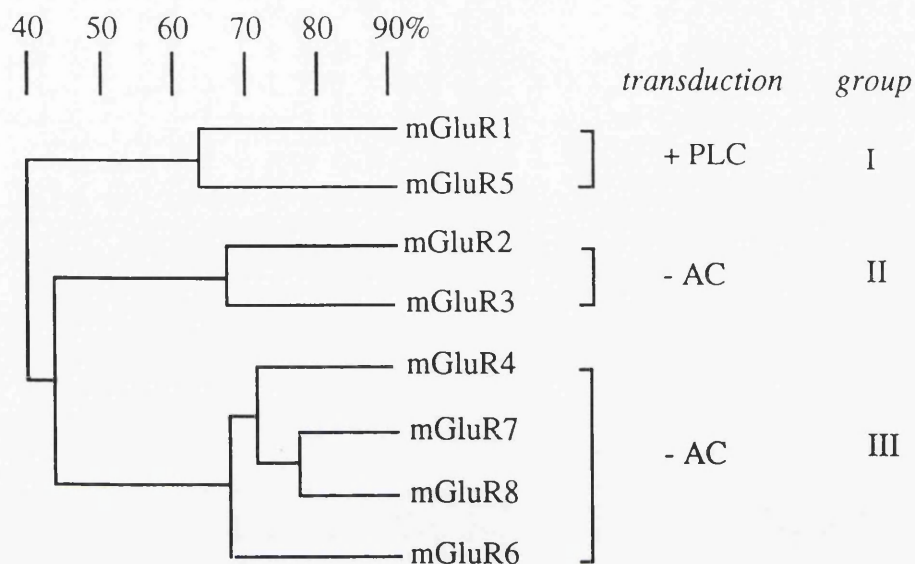


FIGURE 5 : Phylogenic tree of Metabotropic glutamate receptor subunits

The division of the metabotropic subunits into three groups is underpinned by structural homology and transduction mechanism. The sequence homology of subunits within and between groups is shown by the scale bar at the top of the diagram (%).

It is suggested that mGluRs perform regulatory functions throughout the brain (Nakanishi, 1992). Quisqualate stimulation of Group I mGluRs has been shown to inhibit voltage sensitive Ca^{2+} channels in cultured neurons while ACPD inhibits GABA_A receptor mediated currents and potentiates AMPA and NMDA currents (Pin and Duvoisin, 1995). It is therefore proposed that mGluRs have two opposing effects on excitotoxic cell death. A potentiating effect arises due to neuronal excitation and potentiation of NMDA receptor responses and a protective effect exists due to presynaptic inhibition of glutamate release (Pin and Duvoisin, 1995).

1.4 Excitotoxicity

1.4.1 NMDA-mediated neurotoxicity

Central nervous system neurons degenerate when exposed to abnormally high concentrations of excitatory amino acids such as L-glutamate and L-aspartate (Olney *et al*, 1971). This effect appears not to be direct, and depends on excitation of glutamate-releasing neurons (Meldrum and Garthwaite, 1990). Excitatory amino acid induced lesions have a characteristic cytopathology where postsynaptic structures are destroyed and axons and presynaptic terminals are spared (Foster *et al*, 1988, Meldrum and Garthwaite, 1990). Structure-activity studies revealed a strong correlation between the excitatory potency and toxic actions of these excitatory amino acids (Olney *et al*, 1971) suggesting that 'excitotoxicity' is a consequence of excessive activation of excitatory amino acid receptors (for review see Choi, 1987 and Meldrum and Garthwaite, 1990). The intrinsic potency of glutamate (at NMDA receptors) is high, however the effective potency *in vivo* is reduced by the presence of uptake mechanisms (Torp *et al*, 1994). Impairment of this uptake by energy depletion is probably a major cause of the increase in glutamate found in ischaemia. It is well documented that different neuronal populations display marked variations in vulnerability to glutamate (Swan *et al*, 1988, Swan and Meldrum, 1990). Different excitatory amino acid receptor agonists also selectively kill different populations of neurons. It appears that this variability reflects the differences in glutamate receptor expression throughout the brain, rat cerebellar Purkinje cells *in vivo* and *in vitro* are resistant to NMDA toxicity and express few NMDA receptors, however kainate preferentially destroys hippocampal CA3 neurons which are rich in high affinity kainate binding sites (Meldrum and Garthwaite, 1990). The effect of different toxins on the same neuronal type can also be distinguished histopathologically. NMDA induces a rapid progression into typical necrotic profile, with swelling and vacuolisation. AMPA and quisqualate produce a more gradual 'dark-cell degeneration'. Both types of histopathology are observed in acute degeneration *in vivo*, status epilepticus and cerebral ischaemia (for review see Meldrum and Garthwaite, 1990).

Two processes are thought to be involved in excitotoxic cell death, however the final common pathway underlying these processes is likely to be excessive Ca^{2+} influx. NMDA toxicity towards all vulnerable neurons in cerebellar and hippocampal slices was abolished in Ca^{2+} -free medium, or when Ca^{2+} buffering is increased. Ca^{2+} accumulation in neurons also parallels the cytopathological changes in both time course and the sites involved, from swelling of the Golgi apparatus, chromatin clumping within the nucleus, mitochondrial swelling and changes in the cytoplasm. The main piece of evidence for the role of Ca^{2+} in excitotoxicity is that NMDA antagonists like MK801 provide dramatic protection against damage (Foster *et al*, 1988).

The initial phase of glutamate neurotoxicity is dependent on both Na^+ and Cl^- . Continuous exposure of neurons to toxic concentrations of glutamate opens membrane cation channels to an excessive influx of Na^+ and a secondary passive influx of Cl^- and water, resulting in acute neuronal swelling (Rothman, 1985). Acute neuronal swelling was absent in cultures when Na^+ was removed from the medium (Choi, 1987, Goldberg and Choi, 1993).

The second phase of neurotoxicity is not dependent on the continued presence of the NMDA agonist and this delayed toxicity is markedly reduced in the absence of Ca^{2+} (Garthwaite and Garthwaite, 1986, Murphy *et al*, 1988). Delayed neurotoxicity is triggered primarily by the entry of Ca^{2+} through NMDA receptors. The activation of glutamate receptors is associated with the initiation of a number of secondary processes facilitated by the physical colocalisation of NMDA receptors with Ca^{2+} dependent rate-limiting substrates and enzymes (Tymianski *et al*, 1993). The secondary rise which precedes cell death is due to the loss of Ca^{2+} homeostasis. These secondary processes include the formation of free radicals and the activation of lipases and proteases. The activation of lipolytic enzymes such as phospholipase A leads to formation of arachidonic acid from neuronal membrane phospholipids which can be metabolised to form free radicals and lipid hydroperoxides (Farooqui and Horrocks, 1991).

The activation of proteases may lead to cellular damage. Intense stimulation of NMDA receptors has been shown to activate Ca^{2+} -activated neural proteases (calpains) in

hippocampal cultures (del Cerro *et al*, 1994). The two isoforms, calpain I and II are activated by micromolar and millimolar Ca^{2+} respectively (for review see Saido *et al*, 1994, Bartus *et al*, 1995). Calpains degrade spectrin, microtubules, and neurofilaments and may be involved in breakdown of the cytoskeleton (Saatman *et al*, 1996). Calpains also convert xanthine dehydrogenase to xanthine oxidase generating free radicals (Werns and Lucchesi, 1990). Other targets of Ca^{2+} -induced injury may be Ca^{2+} -calmodulin-dependent protein kinases and protein kinase which cause enhanced glutamate release and prolonged Ca^{2+} influx respectively (Nichols *et al*, 1990). Nitric oxide synthesis can also lead to free radical formation. Reactions with superoxide ions produces highly toxic hydroxyl radicals which cause lipid peroxidation of plasma membranes (Pellegrini-Giampietro *et al*, 1990). Ca^{2+} also activate endonucleases which cause fragmentation of DNA and may have a role in programmed cell death (Orrenius *et al*, 1989).

1.4.2 Non-NMDA mediated excitotoxicity

Two types of AMPA excitotoxicity are proposed to exist, a direct effect resulting from long exposures at low concentrations and, a delayed effect resulting from short exposures (Meldrum and Garthwaite, 1990). Application of the antagonist CNQX (6-cyano-7-dinitroquinoxaline-2,3-dione) during exposure to AMPA in cerebellar slices had no effect on neurodegeneration. However, after a 90 minute recovery period, CNQX was highly effective in preventing AMPA induced neuronal degeneration (Garthwaite and Garthwaite, 1991). It is suggested that receptor desensitisation prevents an immediate toxic effect. AMPA induced degeneration can be inhibited by nifedipine, implying that Ca^{2+} entry through voltage operated Ca^{2+} channels may be involved (Weiss *et al*, 1990). Kainate-induced excitotoxicity is similar to NMDA toxicity in that it is Ca^{2+} dependent and Cl^- independent. In contrast to AMPA-induced degeneration, CNQX inhibits kainate induced toxicity during the exposure period (Garthwaite and Garthwaite, 1990).

1.4.3 The ischaemic penumbra

Occlusion of a major intracerebral artery causes a decrease in cerebral blood flow, the density of which is dependent on collateral circulation and local perfusion pressure. Complete arrest of the cerebral circulation leads to cessation of neuronal activity and subsequently to deterioration of ion homeostasis. If this situation persists for more than 5-10 minutes, irreversible cell damage is likely. The classical concept of ischaemic thresholds states that cell death occurs when the cerebral blood flow is less than 15-20% of control values (Astrup *et al*, 1977). That is, a threshold flow rate is required to supply the minimum amount of oxygen and substrates to prevent complete cell membrane depolarisation. The concept of the 'ischaemic penumbra' was introduced to define brain tissue perfused at a level of blood flow below that needed to sustain electrical activity but above that required to maintain ionic gradients. A more recent concept defines 'penumbra' as viable tissue with an undetermined fate which may lead to necrosis, but has the capacity to recover if perfusion is improved (Heiss and Graf, 1994). The progression from penumbra to infarction is a function of the intensity and the duration of ischaemia (Jones *et al*, 1981). Simultaneous measurement of cerebral blood flow, protein synthesis and ATP concentrations following MCA occlusion showed that the limiting factor for cell survival within the ischaemic penumbra is the persistence of suppressed protein synthesis (Mies *et al*, 1991). A number of biochemical alterations contribute to ischaemic cell damage and several of these features are characteristic of the ischaemic penumbra (for review see Obrenovitch, 1995). PET studies in both humans and animals have shown that increased oxygen extraction is a reliable feature for the early identification of viable tissue surrounding the ischaemic core. Tissue acidosis is also a well established feature of ischaemic tissue. In the ischaemic core, tissue depolarises permanently within a few minutes while spreading depression-like waves of transient neuronal depression are consistently observed in peri-infarct areas. Spreading depression has been shown to contribute to ischaemic damage (Gill *et al*, 1992). High extracellular K^+ is the driving force for SD propagation and Ca^{2+} entry through NMDA channels is also required for propagation (Obrenovitch, 1995).

1.5 Therapeutic intervention in cerebral ischaemia

The adult central nervous system has minimal capacity for regeneration following damage. Cells at risk do not die immediately and damage can take hours or days to occur. Tissue damage progresses from regions most metabolically compromised to regions less compromised. The concept of the ischaemic penumbra therefore offers a window for therapeutic intervention.

1.5.1 Strategies for improving perfusion

The target of therapeutic strategies in acute CNS damage is to prevent irreversible damage or at least to limit its extent by therapeutic intervention. Stroke therapy can be directed at a wide range of pathophysiological mechanisms and there has been a great deal of interest in strategies improving blood flow to the ischaemic tissue. Drugs which improve blood flow e.g. nimodipine, are of benefit to subarachnoid haemorrhage patients at risk of delayed ischaemia due to vasospasm. The Intravenous Nimodipine West European Stroke Trial (INWEST) was abandoned due to hypotension associated worsening of the outcome in the nimodipine treated group (Muir and Lees, 1995). A second general approach applies to a subset of stroke patients. Where cerebral blood vessels are blocked by blood clots, it is possible to restore blood supply to ischaemic tissue using thrombolytic enzymes. Success has been reported following treatment with recombinant human tissue plasminogen activator (rt-PA). Restricting patients to those which could be treated within three hours from the onset of the stroke was probably an important determinant in the positive outcome of this trial. Other trials administering thrombolytic agents later than three hours (urokinase, streptokinase, rt-PA) failed to show any beneficial effect (Muir and Lees, 1995, McBurney, 1997). It has now been deemed unethical to withhold this treatment from suitable patients and all other clinical trials of neuroprotective agents in the United States must be carried out in tandem with rt-PA.

Tirilizad mesylate (U74006F), a lipid peroxidation inhibitor has been shown to reduce cortical infarct size in transient ischaemia. This effect is related to an improvement in

regional blood flow. This agent has been suggested as a useful adjunct to thrombolysis in the treatment of acute stroke patients (Xue *et al*, 1992).

1.5.2 NMDA antagonists

A third approach, not dependent on an improvement of blood flow (McCulloch *et al*, 1992) is to limit Ca^{2+} overload by shutting down the main pathways through which it enters the cell. The predominant pathway is through NMDA receptors. From the mid to late 80's a large number of drug candidates which demonstrated the ability to limit the extent of brain damage in animal models of stroke became available. The common feature of these agents was blockade of the NMDA receptor (for review see McCulloch, 1992, 1994a, 1994b). Neuroprotective effects have been demonstrated in all species studied (mouse, rat, cat, baboon) and the magnitude of reduction in infarct is similar regardless of the site targeted (approximately 50%).

Competitive antagonists

Conceptually, the simplest site to block is the neurotransmitter recognition site. Pre-treatment with competitive antagonists such as DCPPE have shown anti-ischaemic efficacy in models of intracranial haemorrhage (Chen *et al*, 1991) and are neuroprotective against ischaemic brain damage and swelling following focal ischaemia in the rat (Park *et al*, 1994). NCP 17747 (2R,4R,5S-2-amino-4,5-(1,2-cyclohexyl)-7-phosphonoheptanoic acid) also afforded protection when administered before transient focal ischaemia and during reperfusion in the cat (Nishikawa *et al*, 1994).

Non-competitive antagonists

Non-competitive antagonists acting at the NMDA channel have also been widely investigated. A number of studies have reported that pre and post treatment with MK801 is protective against ischaemic damage in focal ischaemia (Park *et al*, 1988, Gill *et al*, 1991). Some controversy existed regarding the effects of non-competitive antagonists in global ischaemia. MK801 pretreatment prevented hippocampal

neurodegeneration following unilateral carotid occlusion in the hands of Gill *et al*, (1987), but no protection was observed by Buchan and colleagues against CA1 damage following transient forebrain ischaemia (1991). More recently Yao *et al* (1994) demonstrated that the volume of infarction was decreased in MK801 treated groups following incomplete but not complete ischaemia. It appears therefore that the efficacy of these agents is not due to the focality, but the severity of the insult. This suggests a minimum level of blood flow is required for anti-ischaemic efficacy and supports the ability to salvage tissue in regions of moderately severe ischaemia (penumbra) and, the lack of efficacy in densely ischaemic core regions (McCulloch *et al*, 1994).

1.6 NMDA antagonists as clinically useful drugs

1.6.1 Safety and tolerability

Anti-ischaemic efficacy is only one element in the selection of drugs for clinical evaluation. Safety and adverse effects are also of paramount importance. While NMDA antagonists are the furthest advanced agents in clinical development for stroke treatment, the number of compounds advancing towards definitive proof of efficacy in the clinic has decreased. Clinical development of MK801, the agent with highest affinity for NMDA ion channels and the first consistently shown to be neuroprotective *in vivo*, was abandoned after safety concerns over changes in brain histology in the rat (Muir and Lees, 1995, see below).

1.6.2 Animal studies

Administration of NMDA antagonists produces a number of effects on physiological parameters (for review see McCulloch *et al*, 1992). Competitive and non-competitive NMDA antagonists decrease respiration and induce hypercapnia (Kurumaji *et al*, 1989). Non-competitive antagonists produce disparate effects on blood pressure, MK801 administration increases blood pressure in conscious animals and decreases blood pressure in halothane anaesthetised animals. At high doses, competitive antagonists induce hypotension. Administration of NMDA antagonists also produces profound behavioural effects. Non-competitive antagonists produce disruption of learning and memory, ataxia, sedation and ultimately anaesthesia (Kurumaji *et al*, 1991). These effects are apparent at concentrations required for anti-ischaemic effects. Competitive antagonists produce similar behavioural effects but at concentrations 3-10 times greater than neuroprotective doses (Kurumaji *et al*, 1989).

Autoradiographic studies mapping changes in local cerebral glucose utilisation following administration of NMDA antagonists describe markedly dissimilar alterations in function-related glucose use for non-competitive and competitive agents (Kurumaji *et al*, 1989, 1991). Non-competitive agents like MK801 produce dose-related increases in glucose

utilisation throughout the limbic system and widespread decreases in the neocortex. Competitive antagonists (like DCPene) induce small and anatomically circumscribed alterations in glucose utilisation in areas such as the hippocampus, olfactory areas, cerebellar nucleus and superior olives. These functional changes are thought to be predictive of morphological alterations, since the occurrence of transient neuronal vacuolation coincides with areas showing hypermetabolism. This dose-dependent, reversible swelling and vacuolisation in medium and large sized neurones within the cingulate and retrosplenial cortex following administration of non-competitive NMDA antagonists was first described by Olney and colleagues (1989). Similar effects were observed with competitive antagonists (CGS 19755) but at a much higher dose relative to the neuroprotective dose, compared to MK801 (Hargreaves *et al*, 1994).

1.6.3 Human studies

All competitive and non-competitive agents cause similar symptoms and signs in humans regardless of the pharmacology of action, if used in large enough doses. Selfotel (CGS 19755) has been extensively investigated in normal subjects and patients with stroke (Grotta *et al*, 1995). While a single intravenous dose was well tolerated, higher doses produced agitation, hallucinations, confusion and paranoia. Low doses of non-competitive antagonist cause altered sensory perception, dysphoria, hypertension, nystagmus and disorientation leading to agitation, paranoia, hallucinations, severe motor retardation and catatonia at higher doses (Muir and Lees, 1995).

1.7 Development of a novel NMDA antagonist

1.7.1 Basic concepts

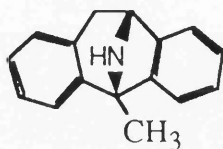
Molecules which are cation channel blockers generally possess 2 chemical characteristics, a cationic region, centered on a protonatable nitrogen and a hydrophobic region. Such agents need to possess a high enough affinity to be selective for the ion channel, but not so high that its effects cannot be reversed. A relatively short half life combined with good blood brain barrier permeability are also desirable (McBurney, 1997).

An extensive cross-reactivity exists between σ receptor ligands and ligands acting at the NMDA receptor ion channel and vice-versa. It was reasoned that chemical alterations to the chemical structure of N,N'-di-*o*-tolylguanidine (DTG), a potent σ site ligand, might generate compounds that were selective for the NMDA receptor ion channel over the σ site (Reddy *et al*, 1994). More than 50 diarylguanidines were synthesised in an effort to find high affinity ligands for the NMDA ion channel. It was found that tri- and tetrasubstituted versions of N,N-dinaphthyl- and N-naphthyl-N'-(3-substitutedphenyl)-guanidines exhibited remarkably high affinity and selectivity for the NMDA receptor ion channel site. One of these compounds N-1-naphthyl-N'(3-ethylphenyl)-N''N-methylguanidine (aptiganel hydro-chloride, CNS 1102, Cerestat[®]) was selected as a candidate for development as a treatment to limit ischaemic brain damage (Figure 6).

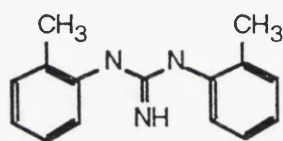
1.7.2 Preclinical studies

The efficacy of aptiganel has been demonstrated *in vitro* and *in vivo*. Aptiganel protects cultured neurons against exposure to glutamate ($ED_{50} = 0.38\mu M$) at a concentration consistent with its affinity ($K_i = 28nm$) for the NMDA receptor. Aptiganel is also effective in reducing the volume of ischaemic damage (by 40-70%) produced by permanent MCA occlusion (Minematsu *et al*, 1993a, Cohen *et al*, 1994)) and reduces early postischaemic injury and improves perfusion in reversible ischaemia (Minematsu *et al*, 1993b).

(a)



(b)



(c)

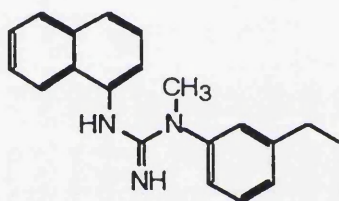


FIGURE 6 : Chemical structures of NMDA and σ site ligands

(a) MK801 (dizocilpine) : (+)-5-methyl-10,11-dihydro-5*H*-dibenzo[*a,d*]cyclohepten-5,10-imine and (c) CNS 1102 (Aptiganel, CERESTAT®): *N*-(1-naphthyl)-*N'*-(3-ethylphenyl)methyl guanidine are ligands at the NMDA receptor ion channel.

(b) DTG : *N,N'*-di-*o*-tolylguanidine is a σ site ligand

The pharmacokinetics of Aptiganel have been examined in a number of species (McBurney, 1997). Aptiganel distributes rapidly into a large volume of distribution. The plasma half-life of aptiganel is approximately 60 minutes in rat and 90 minutes in non-human primates. Six minutes after administration of [^{14}C]Aptiganel hydrochloride, the level of radioactivity within the brain was approximately 12-fold higher than in plasma. All the radioactivity within the brain could be attributed to the parent compound.

1.7.3 Clinical studies

The safety and tolerability of Aptiganel in normal volunteers has been examined clinically. The most common side effects reported were dizziness, numbness and increased heart rate and blood pressure at higher doses. All effects subsided without medical intervention (Muir *et al*, 1994).

It appeared from these results that Aptiganel was well positioned to advance to a definitive test of the hypothesis that NMDA antagonists can limit the extent of brain damage. A statistically significant beneficial effect on the outcome of drug-treated patients would provide support for the concept of neuroprotection.

The international stroke trial was initiated in July 1996 and was designed to examine efficacy. However, the acquisition of new patients into this Phase III trial was stopped in June 1997, when concerns were raised during an interim analysis of data over the benefit to risk ratio of the drug treatment (Reuters, June 1997). In September, 1997, Cambridge Neuroscience Inc. announced the discontinuation of their 500 patient Phase III traumatic brain injury clinical trial. While interim analysis of the data showed the drug was safe and well tolerated on a number of safety parameters, there was insufficient evidence of its clinical efficacy. Despite the forward looking statements included in the press release such as the continuation of data analysis for possible future clinical development and to "explore the viability of other clinical applications" the effect of these announcements on the value of the company stock was undeniable (Reuters, PR Newswire, September 1997).

The NASDAQ forecast from recent months (Figure 7) shows a marked drop in share prices and a consequent increase in the volume of shares available on the market corresponding to the stroke trial press release at the end of June and the discontinuation of the TBI trial in September, culminating in an overall 6-fold decrease in share prices. The impact of the failure of Aptiganel highlights both the profound financial interest in the development of an effective neuroprotective therapy and, the clinical requirement for such an agent .

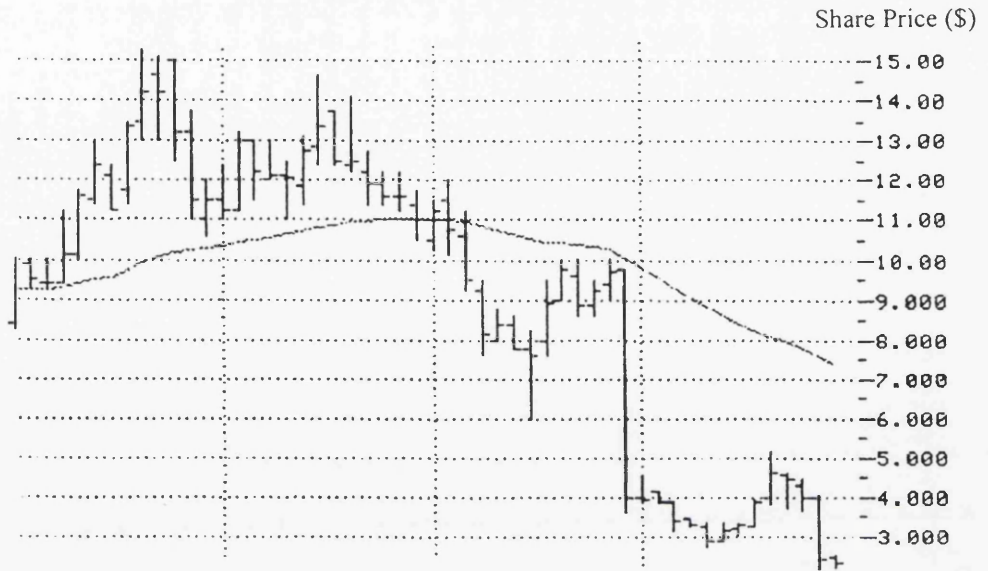


FIGURE 7 : Cambridge NeuroScience Inc share prices from Oct '96 to Sept '97

The solid line shows the change in Cambridge NeuroScience Inc. share prices (\$) in relation to the average stock price on the NASDAQ market index (broken line). Marked decreases in value were observed in July 1997 and in September 1997, which correspond to announcements of the termination of the traumatic brain injury and stroke clinical trials of Cerestat (CNS 1102)

1.8 Receptor imaging in the central nervous system

No other factor has influenced the study of receptors more than the development of tritiated and radioiodinated ligands with high affinity and specific activity for target sites. This ability to localise radioactivity labelled compounds in thin sections of tissue by autoradiography offers the opportunity to study drug receptors with good spatial resolution. Localising neurotransmitter receptors by autoradiographic techniques has several important applications. It allows a unique view of the biochemical organisation of the brain and it provides an adjunct to histochemical methods for the study of neurotransmitters *per se*. Autoradiography can also be used as a neuropathological tool, since receptors are primarily localised to neurons and receptor changes may reflect underlying pathological processes (Kuhar, 1986).

1.8.1 Autoradiography

The NMDA receptor subtype of glutamate receptors has been subject to intense investigation due to its key role in a variety of physiological and pathophysiological processes. Radioligand binding studies have contributed to the understanding of ligand interactions at a number of ligand binding sites on the NMDA receptor complex. The most potent and selective ligands for NMDA receptors are those which bind non-competitively to a site within the associated ion channel e.g. [^3H]1-[1-(2-thienyl)cyclohexyl]piperidine ([^3H]TCP) and [^3H]MK801. The utility of these ligands is partly dependent on their use-dependency and sensitivity to the state of activation of the receptor (Hosford *et al*, 1990, MacDonald and Nowak, 1990).

Quantitative localisation of [^3H]TCP binding to rat brain sections (Sircar and Zukin, 1985) showed a distribution pattern of binding sites that was similar to that observed with [^3H]phencyclidine (PCP), but more sharply defined. Highest levels were observed within the hippocampus and intermediate levels in the frontal cortex, striatum, amygdala and cerebellum. No specific binding was observed within the corpus callosum.

The application of autoradiography to map the distribution of drug receptors in target tissues depends on the ability to demonstrate specific receptor binding. Further studies confirmed a striking similarity between the relative density of [^3H]TCP and NMDA receptor binding sites labelled with L-[^3H]glutamate ($r = 0.95$, $p < 0.001$, Maragos *et al*, 1986), while Jarvis and colleagues (1987) showed a significant relationship existed between binding sites labelled by the competitive NMDA antagonist [^3H]CPP and [^3H]TCP ($r = 0.88$, $p < 0.01$).

The underlying aim of these studies was to develop a radioligand which could ultimately be used to investigate the role of NMDA receptors in a number of neurological diseases in man and, the majority of attention focused on MK801, the most potent compound at the channel binding site. Early studies with [^3H]MK801 in rat brain sections confirmed that this ligand produced a map of binding sites which corresponded to the map of NMDA-type glutamate receptors obtained with L-[^3H]glutamate (Bowery *et al*, 1988). Specific [^3H]MK801 binding was prevented by PCP and ketamine. The distribution of [^3H]MK801 binding sites was similar to that previously described for [^3H]TCP, with highest levels in the hippocampal formation, cerebral cortex, olfactory bulb and thalamus and low levels in the cerebellum and hypothalamus. This data was supported by the uneven distribution of [^3H]MK801 binding sites observed in rat brain membranes (Wong *et al*, 1988). A decrease in the density of [^3H]MK801 binding sites within CA1 region of the hippocampus after unilateral carotid artery occlusion indicated that their presence was vulnerable to ischaemia (Bowery *et al*, 1988). More recently, [^3H]dextrorphan recognition sites have been characterised in rat brain. [^3H]dextrorphan binding is localised to the same site as MK801 and TCP and is both glutamate and glycine dependent (Franklin and Murray, 1992). The distribution of [^3H]dextrorphan binding sites is similar to that reported for [^3H]MK801, with the greatest levels of binding within the hippocampus and intermediate levels within the cortex, thalamus and striatum (Roth *et al*, 1996).

The criteria for receptor binding in *in vivo* imaging studies is similar to those for *in vitro* homogenate binding studies. The receptor site should be saturable by the radioligand of

interest and, increasing doses of unlabelled ligand should reduce the binding of the radiolabelled ligand in a dose-dependent fashion. Appropriate competition by various receptor ligands known to bind to the receptor of interest should be demonstrated. The regional distribution of the radioligand should be consistent with the known pattern of receptors.

Wallace *et al* (1992) used quantitative autoradiography to assess the *in vivo* uptake of [³H]MK801 and to compare it with *in vitro* [³H]MK801 binding after focal ischaemia. These investigations showed that *in vitro* binding does not determine the *in vivo* uptake of [³H]MK801. Fifteen minutes post-ischaemia, *in vivo* uptake of [³H]MK801 was similar to cerebral blood flow autoradiograms obtained with [¹⁴C]iodoantipyrine, with uptake in regions of middle cerebral artery territory approximately 75% lower than contralateral regions. At 60 minutes, [³H]MK801 uptake was 60% greater in middle cerebral artery territory than in contralateral region. The increased levels of [³H]MK801 in ischaemic areas is consistent with the effect of glutamate on [³H]MK801 binding to the NMDA receptor complex in synaptosomes (Foster and Wong, 1987). Uptake was therefore determined by both the regional density of receptors (little uptake was observed within white matter) and, local extracellular glutamate concentrations. [³H]MK801 uptake in areas outwith the middle cerebral artery territory was different from *in vitro* autoradiograms, no laminar heterogeneity in [³H]MK801 uptake was observed within the contralateral cortex.

In vitro, the concentrations of glutamate and glycine are relatively constant, therefore autoradiograms reflect the regional heterogeneity of NMDA receptors. These observations suggest that *in vivo*, at constant glutamate levels, factors other than the number of receptors (lipophilicity) influence local radioisotope levels and uptake reflects receptor activation. An increase in extracellular pH has been shown to increase the rate of association and dissociation of [³H]MK801. This supports the hypothesis that the rates of [³H]MK801 binding are controlled by the level of activation of the NMDA receptor (Rajdev and Reynolds, 1993)

A number of problems have been described using tritiated ligands in autoradiography. Significant tissue quenching or absorption occurs due to the low energy of the β emissions produced by tritium. The amount of energy reaching the film emulsion is dependent on the density of material from which the β particle is emitted. White matter has a higher density than grey and therefore produces more quenching (Kuhar and Unnerstall, 1985). A long exposure time (4-8 weeks) is also required due to the low energy β emissions. In addition to these problems, [^3H]MK801 binding has been reported to be differentially modulated by the presence of divalent cations, implying this ligand is unsuitable for the study of NMDA receptors in intact cellular systems (Enomoto *et al*, 1992). Iodinated analogues of MK801 have preferential properties over [^3H]MK801. The higher energy of some emissions from ^{125}I overcome the problems of quenching and, the extremely high specific activity of iodinated ligand allows visualisation of autoradiograms with high anatomical resolution following 24-48 hours of exposure (Jacobson and Cottrell, 1993). Iodo-MK801 is also relatively insensitive to the inhibitory actions of divalent cations (Rajdev and Reynolds, 1992).

The use of (+)-3-[^{125}I]iodo-MK801 ([^{125}I]MK801) to study *in vivo* labelling of the NMDA receptor complex in the normal rat brain was described by Gibson *et al* (1992). At 15 minutes, the pattern of [^{125}I]MK801 uptake was essentially the same as that obtained using a blood flow tracer. Blockade of [^{125}I]MK801 uptake by unlabeled MK801 was demonstrable when examined 4 hours post-injection. No blockade was observed at times before 4 hours. While *in vitro* autoradiography was consistent with previous reports on NMDA receptor distribution this study provided no systematic validation of the [^{125}I]MK801 binding site as a true receptor. Jacobson and Cottrell (1993) showed that [^{125}I]MK801 binding to thin sections could be displaced by (+)MK801 but not by (-)MK801. Binding was also displaced by PCP but not by naloxone, GABA or kainic acid. [^{125}I]MK801 binding was completely eliminated by heat treatment, providing further evidence of binding to a traditional receptor.

The utility of [^{125}I]MK801 in pathological situations was examined by McCulloch *et al* (1992). In the presence of increased glutamate concentrations [^{125}I]MK801 binding to normal and ischaemic tissue is increased. Following MCA occlusion, the initial uptake of [^{125}I]MK801 reflects cerebral blood flow. At later time points the retention of the tracer is increased within the MCA territory, reflecting the elevated concentrations of glutamate in ischaemia and the glutamate dependence of MK801 binding (McCulloch *et al*, 1992). Coadministration of MK801 significantly reduced [^{125}I]MK801 in ischaemic areas and only slightly in non-ischaemic areas. It was concluded from these results that highly lipophilic agents such as MK801 are not suitable *in vivo* ligands in the normal brain, due to high non-specific binding and a failure to reliably demonstrate displacement. The enhanced uptake in ischaemic areas appears to map the extent of NMDA receptor activation (increased uptake in areas of increased extracellular glutamate) implying [^{125}I]MK801 autoradiography can be used to map dynamic processes, providing a strategy for defining the localisation of areas of NMDA receptor activation.

1.8.2 SPECT and PET

Postmortem autoradiographic studies of human brain receptors are flawed by methodological limitations such as small population samples, conditions of death, premortem effects of drugs, and postmortem or age-related non-specific receptor changes. *In vivo* characterisation of receptor density and functional state would preclude most of these limitations.

Two main categories of functional imaging exist PET (Positron Emission Tomography) and SPECT (Single Photon Emission Computed Tomography), based on the properties of the radionuclides used. Positron emitting radionuclides decay releasing a positively charged particle (β^+). This positron interacts rapidly with a neighbouring electron and emits two 511KeV photons 180° apart. A single photon is a γ radiation usually emitted in random directions. The imaging devices, positron scanners and single photon cameras, measure the location and density of different γ rays emitted by PET and SPECT ligands respectively. While PET imaging has higher sensitivity and a better quantification

capacity, SPECT imaging is more readily available and does not require a local cyclotron to manufacture radioligands.

The majority of routine imaging procedures are performed using single photon radionuclides in conjunction with gamma cameras or single photon emission computed tomography (SPECT). Technetium (^{99m}Tc) is the most widely used, in over 85% of imaging procedures (for review see Kung, 1993, Masdeu *et al*, 1994), however Iodine-123 with a half life of 13 hours and 159KeV γ rays is also well suited for SPECT imaging.

The most widely used radiopharmaceuticals targeted to the brain generally measure perfusion and are detailed below (Gibson *et al*, 1993). A less common application of [^{123}I]iodoamphetamine has been to image patients with systemic lupus erythematosus. Scans from patients with psychiatric manifestations of the disease showed areas of hypoperfusion (Kodama *et al*, 1995)

Target	Radiopharmaceutical	Parameter measured
Brain	[^{99m}Tc]HMPAO	relative cerebral blood flow
	[^{99m}Tc]ECD	relative cerebral blood flow
	[^{123}I]iodoamphetamine	relative cerebral blood flow
	[^{99m}Tc]DTPA	lesions (stroke, tumours)

In addition to their use in determining perfusion, the non-invasive imaging techniques of nuclear medicine provide a powerful tool to map biochemical interactions in man with high sensitivity and can be used in the discovery and development of new drugs. An important application of these imaging techniques is to monitor the occupancy of receptors by therapeutic drugs and to relate the findings to clinical status, providing a better adjustment of drug dosage and an indication of therapeutic efficacy. So far the measurement of receptor occupancy has been most extensively applied to the study of anti-psychotic drug binding (Farde, 1996).

Baron *et al* (1985) were among the first to demonstrate the feasibility of studying specific receptors in the human brain with PET, using [^{11}C]pimozide to label dopamine receptors. More recently, clinical studies have been carried out using iodinated benzamide

derivatives to image D₂ dopamine receptors, especially [¹²³I]iodobenzamide (IBZM, Kung *et al*, 1990). [¹²³I]IBZM SPECT images have been useful in relating antipsychotic drug D₂ receptor occupancy with the administered dose in schizophrenic patients, showing qualitatively diminished activity in the basal ganglia following haloperidol treatment (Vallabhajosula *et al*, 1997).

The number of radioligands for imaging neuroreceptors systems is increasing and it is now possible to image GABA_A receptors using [¹²³I]Iomazenil (Busatto *et al*, 1994) and muscarinic cholinergic receptors, among others. [¹²³I]quinuclidinylbenzilate (QNB) has been employed to image muscarinic receptors. Kinetic modelling indicated that this ligand take a long time (approximately 18 hours) to reach optimal specific to non-specific binding ratios. Clinical studies in Alzheimer patients have shown that deficit regions could be visualised by RS-QNB. Much effort has been applied to the development of other stereoisomers of QNB with lower affinity for the receptor which may produce imaging agents which are more readily displaced by endogenous transmitter. More recently [¹²³I]Iododexetamine has been reported as a potential SPECT ligand to image muscarinic receptors (Boundy *et al*, 1995)

Much interest has been devoted to the development of radiotracers with the ability to trace NMDA receptor activation and ongoing neurodegenerative processes. The whole understanding of excitotoxicity in man is largely based on extrapolation from rodent data, so clarification of the mechanisms involved in man would help assess neuroprotective agents in clinical trials.

The first PET studies, TCP and a number of analogues were fluorinated to provide potential *in vivo* radioligands for the NMDA receptor. 1-(1-[5-(2'-[¹⁸F]fluoroethyl)-2-thienyl]-cyclohexyl)piperidine ([¹⁸F]FE-TCP) showed heterogeneous distribution in the brain following intravenous administration in the rat which was similar to the known distribution of PCP-labelled sites (Blin *et al*, 1989). Brain regions were normalised to the cerebellum and ratios for CA1, striatum and cortex were 2.08, 1.7 and 1.5 respectively 15 minutes after administration. This localised regional cerebral distribution was blocked by coinjection of unlabelled FE-TCP with largest reductions observed within the hippocampus followed by the striatum and cortex. It was suggested that the

low affinity for the NMDA receptor and the high non-specific binding (due to lipophilicity) may make this an unsuitable radioigand for PET investigations of the NMDA receptor complex. Fluorinated analogues of TCP such as 1-[1-2-thienyl]-4-([^{18}F]fluoro)-cyclohexyl]-1, 2, 5, 6, tetrahydropyridine showed good uptake into rat brain following intravenous injection (Ouyang *et al*, 1996). However specific uptake improved only marginally with time compared to the cerebellum. Preliminary PET studies in the Rhesus monkey showed good uptake but little retention in receptor rich areas. (1S*,2R*)-2-(hydroxymethyl)- and (1S*,2R*)-2-(methoxymethoxymethyl)-1-(N-piperidyl) -1-[2-(2'-[^{18}F]fluoroethyl)thiophenyl]cyclohexane also showed no selective accumulation of radioactivity (Shibayama *et al*, 1996).

Other studies investigated analogues of MK801 to image the NMDA receptor complex, Orita *et al* (1993) used 5b-fluoroethyl-MK801 ([^{18}F]FE-MK801), labelled with ^{18}F . The *in vitro* affinity of this ligand was similar to that of MK801, IC_{50} for displacing [^3H]TCP binding to homogenates was 20nM. Fifteen minutes after intravenous injection uptake ratios (relative to the cerebellum) for cortex and striatum were 1.1 and 1.6 respectively. The uptake of [^{18}F]FE-MK801 was also examined in non-basal conditions. Pretreatment with PCP did not measurably decrease specific binding. Transient arterial hypoxia was used to induce acute glutamate release in an attempt to increase specific binding to open receptors, however no clear cut increase in specific binding was observed.

The synthesis of (+)-3-[^{123}I]MK801 with high purity and good yield provided the potential to imaging of NMDA receptor activation in man by SPECT (Owens *et al*, 1997). Clinical assessment of [^{123}I]MK801 was carried out in 5 patients, 4 with subarachnoid haemorrhage and 1 with intracranial haemorrhage. All patients had clinical indications of ischaemia and images were taken at post-ictus times between 1 and 5 days. Initial uptake of [^{123}I]MK801 into the ipsilateral hemisphere was decreased which was consistent with reduced blood flow. In 2 patients increased retention of [^{123}I]MK801 was observed at later time points in cortical areas adjacent to the site of the haematoma, consistent with receptor activation. The remaining three patients displayed no evidence of increased

retention. These results propose that it may be possible to image excessive NMDA receptor activation following an ischaemic episode. The utility of this tracer is limited by the high lipophilicity and reported non-specific accumulation in white matter areas. [¹²³I]MK801 is therefore not a suitable agent for imaging in the normal brain, or to image moderate alterations in NMDA receptor activation. An agent with lower lipophilicity is therefore necessary to pursue further investigation of glutamate NMDA receptor mediated processes in the human brain

1.9 Synthesis of *N*-(1-Naphthyl)-*N'*-(3-[¹²⁵I]iodophenyl)-*N'*-methylguanidine ([¹²⁵I]CNS 1261)

Development of a suitable radioiodinated agents for use as NMDA radiotracers in SPECT would provide a valuable tool to investigate mechanisms of excitotoxicity in man and to evaluate neuroprotective therapies. To this end, an analogue of *N*-(1-naphthyl)-*N'*-(3-ethylphenyl)-*N'*-methylguanidine (Cerestat, CNS 1102), *N*-(1-naphthyl)-*N'*-(3-[¹²⁵I]iodophenyl)-*N'*-methylguanidine ([¹²⁵I]CNS 1261), was synthesised by J. Owens and A. Tebbutt at the West of Scotland Radioisotope Dispensary, Glasgow, Scotland, as a potential radioligand to image NMDA receptor activation *in vivo*. Radioiodination of the iodine moiety on the phenyl ring of CNS 1261 produced a radioligand with high specific activity which is suitable for *in vivo* autoradiography.

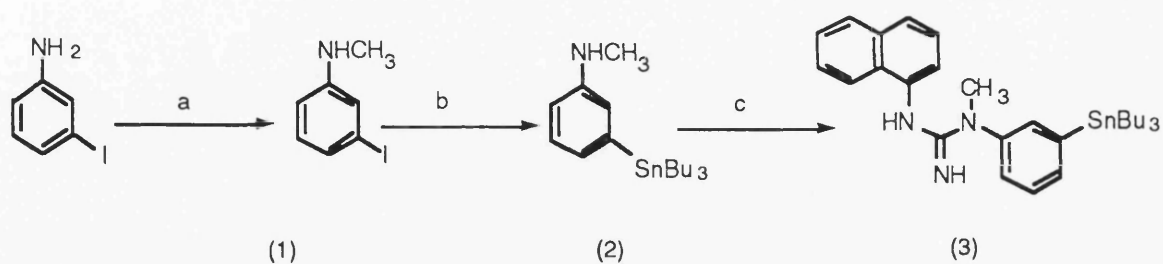
Precursor synthesis

The synthetic route to *N*-(1-naphthyl)-*N'*-(3-tributylstannylphenyl)-*N'*-methylguanidine (3) is summarised in Figure 8, scheme 1.

3-Iodo-*N*-methylaniline (1) was prepared in a 79% overall yield by protection with formic acid followed by a borane reduction. *N*-methyl-3-tributylstannylaniline (2) was synthesised in 71% yield using a palladium catalysed substitution with hexabutylditin. It was found necessary to use the free base of *N*-methyl-3-Iodo-aniline (1) to ensure reasonable yields (> 70 %), if the hydrochloride salt was used the product yield decreased substantially. Synthesis of *N*-(1-naphthyl)-*N'*-(3-tributylstannylphenyl)-*N'*-methyl guanidine (3) was achieved by the acid catalysed addition of *N*-methyl-3-tributylstannylaniline (2) to 1-naphthylcyanamide (5). A low yield (20 %) was recorded due to competing protodestannylation.

Chemistry

Scheme 1



(a) i. formic acid, toluene ii. $\text{BH}_3\cdot\text{THF}$

(b) $\text{Pd}(\text{PPh}_3)_4$, $(\text{SnBu}_3)_2$

(c) H^+ , 1-naphthylcyanamide

Radiochemistry

Scheme 2

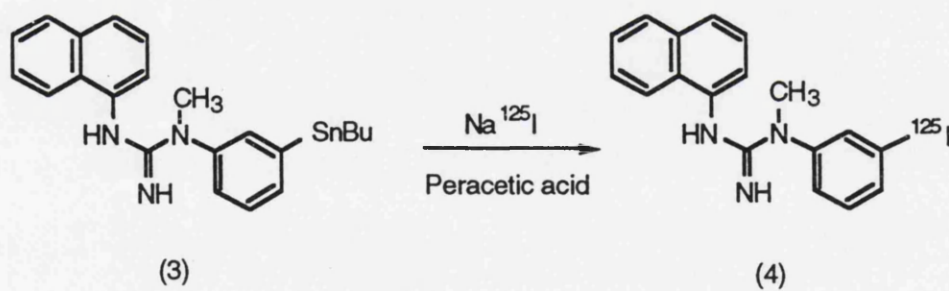


FIGURE 8 : Synthesis of [^{125}I]CNS 1261

Radiochemistry

Electrophilic iododestannylation and iododesilylation provide an effective method for the introduction of iodine into complex organic molecules with high specific activities. Various oxidants have been used including Chloramine-T, N-chlorosuccinimide, iodogen, and peracetic acid.

Radioiodinated [^{125}I]CNS 1261 (4) was prepared by iododestannylation of N-(1-naphthyl)-N'-(3-tributylstannylphenyl)-N'-methylguanidine (3). Peracetic acid as the oxidant consistently gave the best results, with a 59 % isolated radiochemical yield and > 99 % radiochemical purity after semi-preparative HPLC purification, with a synthesis time of 1 h (Figure 8, scheme 2). Aliquots of the [^{125}I]CNS 1261 were dried under a stream of nitrogen and reconstituted in physiological buffer as required.

CHAPTER II

METHODS

2.1 Affinity and selectivity of CNS 1261

2.1.1 Whole crude synaptosomal membrane (WCSM) preparation

Frozen whole rat brains were thawed on ice, cerebella and brain stems were removed and the forebrains placed in ice cold 0.32M sucrose and weighed. 2-3 forebrains were transferred to 40ml fresh 0.32M sucrose then homogenised with a teflon-glass homogeniser (Thomas C) for 8 strokes on setting 3.

The homogenate was centrifuged in a J6-B Beckmann centrifuge at 1,000 x g for 10 minutes at 4°C. The supernatant was decanted and centrifuged in the J2-21M Beckmann centrifuge at 20,000 x g for 20 minutes at 4°C.

The pellet was pooled and resuspended in 40ml ice-cold Milli-Q purified H₂O and homogenised (Brinkmanm polytron) for 30s. The homogenate was then centrifuged at 8,000 x g for 20 minutes at 4°C. The upper third layer of supernatant and the upper buffy coat (upper tannish layer of pellet) were pooled and homogenised for 30s, then decanted into 40ml tubes for centrifugation at 48,000 x g for 10 minutes at 4°C.

The pellet was resuspended in 20ml of ice-cold 50mm Tris acetate, pH 7.4 and homogenised for 10s. Another 20ml of Tris acetate was added to the homogenate, mixed, then centrifuged at 48,000 x g for 10 minutes at 4°C. The pellet was resuspended in 20ml 50mm Tris acetate, homogenised for 10s and diluted 1:10 with artificial cerebrospinal fluid (ACSF) assay buffer (final composition : 147mm NaCl, 2.5mm KCl, 2.5mM CaCl₂, 1.3mm MgCl₂, and 10mm HEPES, brought to pH, 6.4, 7.4 or 8.4 at room temperature with NaOH). 1% Triton X-100 was added to a final concentration of 0.01% and the tubes were vortexed then incubated at 37°C for 15 minutes.

An additional 20ml of ACSF assay buffer was added and the homogenate allowed to cool on ice for 10-15 minutes before it was centrifuged at 48,000 x g for 10 minutes at 4°C. The resulting pellet was resuspended in 20ml ACSF assay buffer, homogenised for 5s, then a further 20ml ACSF assay buffer added. The homogenate was centrifuged at 48,000 x g for 10 minutes at 4°C. The protein content of the pellet was determined after a further two further cycles of washing.

2.1.2 Assay procedure

The binding assay was performed in triplicate in a total volume of 500µl. Glutamate and glycine were added at a concentration of 1µM each in 5mM Tris acetate and at 10µM each in ACSF assay buffer to maximally stimulate [³H]MK801 binding. [³H]MK801 was added at a final concentration 1nM in Tris acetate buffer and at 12nM in ACSF buffer in the presence or absence of various concentrations of CNS 1261. The binding reaction was initiated by adding 100µg of WCSM preparation to each tube, vortexing the tubes and incubating for 4 hours at room temperature.

The incubation was terminated by rapid filtration under vacuum through glass fibre filters (presoaked in 0.05% PEI for 45 minutes), followed by three 4ml washes, using a Brandel 48-well cell harvester. Filters were transferred to vials and 5ml of Cytoscint ES scintillation cocktail added. Vials were shaken for 15 minutes prior to counting.

Non-specific binding was defined as binding measured in the presence of glutamate, glycine and 10µM PCP. This value was subtracted from all other conditions to yield specific binding.

IC₅₀ values and Hill coefficients were calculated in RS-1 (BBN Software products) by fitting displacement curves using non-linear least squares regression analysis. The association affinity constant (K_i) was calculated using the Cheng-Prusoff equation :

$$K_i = IC_{50} / 1 + ([^3H]MK801) / K_d$$

where the [³H]MK801 concentration = 1nM in Tris acetate, 12nM in ACSF assay buffer.

2.1.3 Commercial screening of CNS 1261

The effect of CNS 1261 on the binding of ligands to the NMDA receptor, and to other neurotransmitter receptors was further investigated by submitting the compound for commercial screening (NovaScreen, Maryland, USA). The effect of two doses of CNS 1261 (10nM and 1µM) were examined in a total of 42 radioligand binding assays.

The individual protocols for each of the 42 binding assay are not detailed here, however a brief outline of the basic assay procedure is detailed below.

Binding assays were performed in duplicate under conditions known to maximally stimulate binding of the radioligand of interest. Radioligands were added in a final concentration of 0.5-20nM in the appropriate buffer in the presence or absence of various concentrations of CNS 1261. In the absence of CNS 1261 all radioligands displayed between 60 and 90% specific binding. The binding reaction was initiated by adding an aliquot of receptor preparation (generally rat forebrain membranes) to the assay mix. Reactions were terminated by rapid filtration onto glass fibre filters. Radioactivity trapped onto the filters was determined and compared to control values in order to ascertain any interactions of CNS 1261 with the binding site in question. 'Activity' was defined as $\geq 50\%$ inhibition of radioligand binding. Assays in which activity was detected were repeated twice to confirm findings.

2.2 Effect of CNS 1261 on local cerebral glucose utilisation

2.2.1 Surgical preparation of animals

Rats were initially anaesthetised with 5% halothane in a nitrous oxide and oxygen gas mixture (70%:30%). Anaesthesia was subsequently maintained by administration of 0.5-1% halothane via a face mask. The femoral vessels were exposed bilaterally by blunt dissection. Polyethylene cannulae (Portex, external diameter 0.96mm, internal 0.58mm, 15cm long) were inserted approximately 2cm into the femoral arteries and veins and secured by silk threads. Incision sites were infiltrated with local anaesthetic gel (Xylocaine, 2%), sutured and covered with gauze pads. Animals were covered using a surgical stocking and a plaster of Paris bandage (Gypsona, Smith and Nephew Medical Ltd.) applied to the pelvis and lower abdomen to immobilise the animal. Care was taken to avoid restriction of thoracic movements. The plaster was taped to a lead brick for support. At this point the halothane was discontinued and the animals allowed to recover for at least 2 hours before any further manipulations were performed. A pressure transducer was connected to one femoral artery in order to measure arterial blood

pressure. Animals were maintained normothermic by means of a rectal thermometer and an external heating lamp.

2.2.2 The [^{14}C]2-deoxyglucose technique

Local rates of cerebral glucose use were measured in conscious rats using the method developed by Sokoloff (1977). The procedure was initiated by an intravenous injection of [^{14}C]2-deoxyglucose (specific activity 55mCi/mmol, 50 μCi in 0.7ml) at a constant rate over 30 seconds. Fourteen timed arterial blood samples (100 μl) were taken over the subsequent 45 minutes and immediately centrifuged. Plasma aliquots were assayed to determine ^{14}C and glucose concentrations by means of scintillation analysis and semi-automated glucose oxidase enzyme assay (Beckman, Glucose Analyzer 2) respectively. Further arterial blood samples were taken at predetermined intervals before and after tracer administration for analysis of pCO_2 , pO_2 and pH using a blood gas analyser (Ciba Corning, Blood gas system 288). Forty-five minutes post-tracer administration, animals were killed by decapitation. Brains were removed, frozen in isopentane at -42°C and processed for quantitative autoradiography.

2.2.3 Preparation of autoradiograms

At the end of the 45 minute experimental period, rats were decapitated and the brains removed. Brains were frozen in isopentane chilled to -42°C for ten minutes. Frozen brains were mounted onto microtome chucks using embedding matrix (Gurr) and covered in cryoprotectant (Lipshaw). The entire procedure was performed within 5 minutes of decapitation. Brains were stored at -20°C (for no longer than 3 days) prior to being cut into 20 μm coronal cryostat sections. Triplicate sections were collected at 200 μm intervals throughout the brain. Sections were thaw-mounted onto heated glass cover slips and dried rapidly on a hot plate at 60°C . The coverslips were then glued onto card. Autoradiograms were generated by exposing the sections together with precalibrated epoxy resin ^{14}C standards (11 standards with concentration range 44-1886nCi/g tissue equivalents) to Biomax film (Kodak) in light tight cassettes for 7-14 days. At the end of

the exposure time film were developed manually in LX-24 X-ray developer (Kodak) for 5 minutes. Development was stopped by a 30 second rinse in Indicator stop-bath (85% acetic acid, Kodak). After fixing for 10 minutes (FX-40 fixative, HX-40 hardener, Kodak), films were washed for 30 minutes in filtered running water. Films were briefly rinsed in Photo-flo glaze (Kodak) and suspended in a drying cabinet.

2.2.4 Quantification of autoradiograms

Autoradiograms were analysed using a computer based image analysis system (M4 MCID, Imaging Research Inc.). The optical densities of images produced by precalibrated epoxy resin ¹⁴C standards were measured providing a calibration curve of optical density against isotope concentration and allowing subsequent quantification of tissue isotope concentration for 36 regions of interest in nCi/g. In general six bilateral readings were taken from sections where structures could be identified from the rat brain atlas of Paxinos and Watson (1986).

Sokoloff and colleagues (1977) described a theoretical model based on an operational equation (Figure 9) where the rate of glucose utilisation can be calculated from (1) the levels of glucose and [¹⁴C]2-deoxyglucose in the plasma during the experimental period and (2) the total concentration of ¹⁴C within a given region at the end of the experiment, provided the values of predetermined constants are known.

Standard values for the rate constants k_1^* , k_2^* , k_3^* and K are detailed below

	grey matter	white matter
k_1^*	0.189	0.079
k_2^*	0.245	0.133
k_3^*	0.052	0.020
Lumped constant (K)	0.483	

$$R_i = \frac{C_i^* (T) - k_1^* e^{-(k_2^* + k_3^*) T} \int_0^T C_p^* e^{-(k_2^* + k_3^*) t} dt}{K \left[\int_0^T (C_p^*/C_p) dt - e^{-(k_2^* + k_3^*) T} \int_0^T (C_p^*/C_p) e^{-(k_2^* + k_3^*) t} dt \right]}$$

FIGURE 9 : The Operational Equation

The rate of glucose utilisation (R_i) in any region of cerebral tissue is calculated from C_i^* , the total tissue concentration of ^{14}C in that region measured by densitometry at the end of the experiment (T).

C_p^* and C_p , the concentrations of [^{14}C]2-deoxyglucose and glucose in the plasma at given times throughout the experiment (t).

k_1^* , k_2^* and k_3^* , the rate constants for deoxyglucose transport to and from the plasma and tissue precursor pools and for the phosphorylation of deoxyglucose by hexokinase.

K , the lumped constant (Sokoloff *et al*, 1977)

2.2.5 Experimental protocol

Prior to drug administration animals were prepared for [^{14}C]2-deoxyglucose autoradiography as described in section 2.2.1. The 2-deoxyglucose procedure was performed according to protocol outlined in section 2.2.2 after the injection of the following compound. CNS 1261 (1, 3 and 10mg/kg) was administered by intravenous injection at a constant rate over 1 minute, 15 minutes prior to the administration of 2-deoxyglucose. Control animals received an intravenous injection of saline 15 minutes prior to tracer injection.

2.2.6 Data analysis

LCGU values measured in 36 regions of interest following intravenous injection of CNS 1261 (1, 3 and 10mg/kg) were compared with LCGU values of corresponding regions on control animals for multiple comparisons. One-way analysis of variance (ANOVA) was used initially to identify the anatomical regions in which significant alterations in glucose use occurred, followed by independent Student's t-tests to identify the drug groups producing significant changes relative to control values.

A Bonferroni correction factor was applied to probability values from the t-tests, to take into consideration the multiple comparisons between treated and control groups.

2.2.7 *f* ranking

Alterations in glucose utilisation produced by CNS 1261 administration were compared to those of MK801 (from an experiment performed by Kurumaji *et al*, 1989) by examination of "*f*" ranking function values generated in each region independently for the effects of CNS 1261 (1, 3 and 10mg/kg) or MK801 (0.05, 0.5 and 5mg/kg).

"f" is an arithmetic function which provides an index of the degree of responsiveness of each CNS region to each of the 2 drugs, taking into consideration the entire dose-response data available following administration of multiple drug doses (Ford *et al*, 1985)

$$f = \sum (x_c - x_{Ti})^2$$

x_c is the mean of \log_e (glucose use) for control group members

x_{Ti} is the mean of \log_e (glucose use) for the i th dose of the treatment group in question

T is either CNS 1261 (1, 3 and 10mg/kg) or MK801 (0.1, 1 and 10mg/kg)

2.3 *In vivo* [125 I]MK801 autoradiography

2.3.1 Surgical preparation of animals

Rats were initially anaesthetised in a perspex chamber with 5% halothane in a nitrous oxide and oxygen gas mixture (70%:30%). A tracheotomy was performed and animals were artificially ventilated. Anaesthesia was subsequently maintained by administration of 0.5-1% halothane. The femoral vessels were exposed bilaterally by blunt dissection. Polyethylene cannulae (Portex, external diameter 0.96mm, internal 0.58mm, 15cm long) were inserted approximately 2cm into the femoral arteries and veins and secured by silk threads.

2.3.2 The [125 I]MK801 technique

The amount of radioactivity in discrete brain regions after intravenous injection of [125 I]MK801 was measured in halothane anaesthetised rats by a modification of the technique described by McCulloch (1992).

The procedure was initiated by intravenous injection of [125 I]MK801, specific activity 2200Ci/mmol, at a constant rate over 30 seconds (200 μ Ci in 0.8ml). Fourteen timed arterial samples (100 μ l) were taken over the subsequent 120 minutes and immediately centrifuged. Plasma aliquots were assayed to determine 125 I and glucose concentrations by means of liquid scintillation analysis and semi-automated glucose oxidase enzyme

assay (Beckman, Glucose Analyzer 2) respectively. Further arterial blood samples were taken at predetermined intervals before and after tracer administration for analysis of pCO₂, pO₂ and pH using a blood gas analyser (Ciba Corning, Blood Gas System 288). Blood pressure was monitored throughout the experimental period and animals were maintained normothermic by means of a rectal thermometer and external heating lamp. Animals were killed by decapitation 120 minutes after tracer administration and the brain removed and processed for quantitative autoradiography as described below in section 2.3.3.

2.3.3 Preparation of autoradiograms

Brains were removed and frozen in isopentane chilled to -42°C for ten minutes. Frozen brains were mounted onto microtome chucks using embedding matrix (Gurr) and covered in cryoprotectant (Lipshaw). The entire procedure was performed within 5 minutes of decapitation. Brains were stored at -20°C (for no longer than 3 days) prior to being cut into 20µm coronal cryostat sections. Triplicate serial sections were taken at 200µm intervals throughout the brain. Triplicate sections were thaw-mounted onto heated glass coverslips and dried rapidly on a hot plate at 60°C. The coverslips were then glued onto card. Autoradiograms were generated by exposing the sections together with ¹²⁵I microscales (10 standards in the concentration range 660-31300nCi/g tissue equivalents) to SB-5 or Biomax MR film (Kodak) in light tight cassettes for 7-21 days. At the end of the exposure time films were developed manually in LX-24 X-ray developer (Kodak) for 5 minutes. Development was stopped by a 30 second rinse in Indicator stop-bath (85% acetic acid, Kodak). After fixing for 10 minutes (FX-40 fixative, HX-40 hardener, Kodak), films were washed for 30 minutes in filtered running water. Films were briefly rinsed in Photo-flo glaze (Kodak) and suspended in a drying cabinet.

2.3.4 Quantification of autoradiograms

Autoradiograms were analysed using a computer based image analysis system (M4 MCID, Imaging Research Inc.). The optical density of images produced by precalibrated

[¹²⁵I] microscales were measured providing a calibration curve of optical density against isotope concentration in nCi/g, allowing subsequent quantification of tissue isotope concentration for the regions of interest in nCi/g. Six bilateral readings were taken from sections where structures could be identified from the rat brain atlas of Paxinos and Watson (1986).

Regional ¹²⁵I concentrations (nCi/g) were corrected for isotope decay (60 day half-life) allowing direct comparison between non-contemporaneous experiments.

2.4 *In vivo* [¹²⁵I]CNS 1261 autoradiography

2.4.1 Surgical preparation of animals

Animals were prepared for [¹²⁵I]CNS 1261 autoradiography according to the method described in section 2.3.1.

2.4.2 The [¹²⁵I]CNS 1261 technique

The amount of radioactivity in discrete brain regions after intravenous injection of [¹²⁵I]CNS 1261 was measured in halothane anaesthetised rats according to the technique described in section 2.3.2. for the [¹²⁵I]MK801 procedure. However in this case, the procedure was initiated by intravenous injection of [¹²⁵I]CNS 1261 (specific activity \geq 2200Ci/mmol, 200 μ Ci in 0.8ml) over 30s.

2.4.3 Preparation of autoradiograms

Brains were removed and frozen in isopentane chilled to -42°C for ten minutes. Frozen brains were mounted onto microtome chucks using embedding matrix (Gurr) and covered in cryoprotectant (Lipshaw). The entire procedure was performed within 5 minutes of decapitation. Brains were stored at -20°C (for no longer than 3 days) prior to being cut into 20 μ m coronal cryostat sections. Triplicate sections were collected at 200 μ m intervals throughout the brain. Section were thaw-mounted onto heated glass coverslips and dried rapidly on a hot plate at 60°C. The coverslips were then glued onto card.

Autoradiograms were generated by exposing the sections together with ^{125}I microscales (10 standards, concentration range 660-31300nCi/g tissue equivalents) to Biomax MR film (Kodak) in light tight cassettes for 5-9 days. At the end of the exposure time films were developed manually in LX-24 X-ray developer (Kodak) for 5 minutes. Development was stopped by a 30 second rinse in Indicator stop-bath (85% acetic acid, Kodak). After fixing for 10 minutes (FX-40 fixative, HX-40 hardener, Kodak), films were washed for 30 minutes in filtered running water. Films were briefly rinsed in Photo-flo glaze (Kodak) and suspended in a drying cabinet.

2.4.4 Quantification of autoradiograms

Autoradiograms were analysed using a computer based image analysis system (M4 MCID, Imaging Research Inc.). The optical density of images produced by precalibrated [^{125}I] microscales were measured providing a calibration curve of optical density against isotope concentration in nCi/g, allowing subsequent quantification of tissue isotope concentration within regions of interest. Six bilateral readings were taken from sections where structures could be identified from the rat brain atlas of Paxinos and Watson (1986). Regional ^{125}I concentrations (nCi/g) were corrected for isotope decay (60 day half-life) allowing direct comparison between non-contemporaneous experiments.

2.5 Uptake and retention of [^{125}I]CNS 1261 and [^{125}I]MK801 in normal rat brain

2.5.1 Experimental design

Animals were surgically prepared for *in vivo* autoradiography as described in sections 2.3.1. and 2.4.1. [^{125}I]CNS 1261 or [^{125}I]MK801 (200 μCi , 0.8ml) was administered at time 0 and autoradiographic techniques were carried out as described in sections 2.3.2. and 2.4.2. Animals were killed 5, 30, 60 and 120 minutes after administration of the tracers and the brains removed and processed as detailed in section 2.4.3.

2.5.2 Data analysis

[¹²⁵I]CNS 1261 uptake (strictly the amount of radioactivity following intravenous injection of [¹²⁵I]CNS 1261, in nCi/g) was measured in 37 discrete brain regions for each time point and corrected for isotope decay. The corrected values were expressed as a ratio of [¹²⁵I]CNS 1261 uptake in regions of interest relative to [¹²⁵I]CNS 1261 uptake within the cerebellum. Region of interest/cerebellar ratios for [¹²⁵I]CNS 1261 were compared to corresponding ratios from animals receiving [¹²⁵I]MK801 by Student's unpaired t-test.

2.6 Relative lipophilicity of [¹²⁵I]CNS 1261 and [¹²⁵I]MK801

2.6.1 Calculation of LogD values for [¹²⁵I]CNS 1261 and [¹²⁵I]MK801

Calculation of LogD values was carried out at Cambridge NeuroScience Inc. Precise experimental details were unavailable.

2.6.2. Calculation of brain/aqueous partition ratios

Male Sprague-Dawley rats were killed by an overdose of halothane and the brains removed and frozen in isopentane at -42°C for 10 minutes. Brains were stored, mounted on swivel-headed chucks at -20°C until required. Serial coronal sections (20µm) were cut at the level of the caudate nucleus and thaw mounted onto microscope slides.

Serial sections (20µm) were cut from a block of cortex from a human control brain. Sections were thaw-mounted onto microscope slides. White matter was removed from the sections by dissecting with a scalpel blade. Both rat and human sections were stored at -20°C until required.

Sections from rat and human brain were washed for 1 hour in 50mm Tris HCl buffer, pH7.4 at 4°C. Total binding was assayed by applying 0.5nM [¹²⁵I]CNS 1261 or [¹²⁵I]MK801 in a volume of 0.2ml to each rat brain section (0.4ml for human sections). Non-specific binding was determined in adjacent sections using a solution containing 0.5nM radiolabelled ligand and 0.5µM unlabelled MK801. Aliquots of the incubation

solutions were taken for liquid scintillation analysis. Triplicate sections were incubated with their respective solutions for 2, 5, 10, 20, 30 or 60 minutes. Excess solution was poured off and the sections dipped in fresh buffer at 4°C. Sections were wiped from the slides using glass filter disks. The filters were placed in glass scintillation vials and allowed to dry overnight. Scintillation fluid was added to the vials and the amount of radioactivity bound assayed by liquid scintillation analysis

2.6.3 Data analysis

The amount of non-specifically bound radioactivity on each filter was expressed as nCi/g of brain tissue. The average weight of a brain section was obtained from the volume of the section (average area of the section, measured by MCID image analysis system, multiplied by the thickness of the section) assuming that the specific gravity of brain is 1. The brain/aqueous partition ratio (g/ml) at each time point was calculated by dividing the radioactivity bound per g of brain tissue by the amount of radioactivity present per ml of incubation solution at each time point.

2.7 Metabolism of [¹²⁵I]CNS 1261 and [¹²⁵I]MK801 in the rat

2.7.1 Determination of metabolites in rat plasma

Male Sprague-Dawley rats were anaesthetised with halothane and the left femoral artery and vein cannulated. Blood samples (1ml) were taken 5, 15, 60, 120 minutes after administration of 7.4MBq (200µCi) of tracer. The volume of blood removed at each time point was replaced by a slow intravenous injection of saline. Samples were immediately centrifuged and the plasma removed and stored on ice.

A 20µl aliquot of plasma was removed from each sample for gamma counting. 300µl of acetonitrile was added to 300µl of plasma from each time point. Acetonitrile removes tracer which is weakly bound to protein ('bioavailable tracer'). The mixture was vortexed then centrifuged at 2000 x g for 10min and the supernatant removed. 300µl of the supernatant was injected on to a 250 X 4.6mm Genesis C18 column (Jones

Chromatography). The column was eluted with the following solvent system : 0.1% Trifluoroacetic acid in water; 0.1% trifluoroacetic acid in acetonitrile (50 / 50); flow rate 1ml / min., UV detection at 230nm, radionuclide detection set for ^{125}I .

2.7.2 Determination of metabolites in rat brain

Animals were decapitated 120 minutes post intravenous injection of radioiodinated tracer and the brain removed and homogenised in 1ml of 0.9% saline using a small hand-held glass homogeniser. Equal volumes of homogenate and acetonitrile were mixed and centrifuged at $2000 \times g$ for 10 minutes to give a clear supernatant. The supernatant was injected directly onto the hplc column and processed in the same way as the plasma samples.

2.7.3 Experimental analysis

All chromatographic data was analysed using Packard FLO-ONE software. The background signal was subtracted from each trace and the start and end times of each peak assigned manually.

2.8 Effect of pharmacological doses of MK801 on the uptake and retention of [^{125}I]CNS 1261 in the normal rat brain

2.8.1 Experimental design

Animals were surgically prepared for [^{125}I]CNS 1261 autoradiography as detailed in section 2.4.1. MK801 was administered as an intravenous bolus dose followed by an infusion (0.4mg/kg + 6 $\mu\text{g/kg/min}$ or 1.2mg/kg + 16 $\mu\text{g/kg/min}$.) at a rate of 7.9 $\mu\text{l/min}$. [^{125}I]CNS 1261 (200 μCi) was administered 30 minutes after the start of the infusion. Animals were killed 120 minutes post-injection of tracer and their brains removed and processed as detailed in section 2.4.3.

2.8.2 Data analysis

[¹²⁵I]CNS 1261 uptake was measured in 37 discrete brain areas in each treatment group and the values compared to [¹²⁵I]CNS 1261 uptake in corresponding regions of animals killed 120 minutes after administration of the tracer (controls). As described previously values were expressed as a ratio of the concentration of radioactivity (nCi/g) uptake in each region of interest relative to concentration of radioactivity within the cerebellar cortex. Ratios from treated groups were compared to control values by ANOVA followed by Student's unpaired t-test with a Bonferroni correction to take into account simultaneous multiple comparisons.

2.9 Uptake and retention of [¹²⁵I]MK801 and [¹²⁵I]CNS 1261 following changes in arterial CO₂ tension

2.9.1 [¹²⁵I]MK801 uptake following changes in arterial CO₂ tension

Prior to manipulations, animals were surgically prepared as described in section 2.3.1. Hypercapnic acidosis or hypocapnic alkalosis was induced via adjustment of the respiratory status of the animals, since brain extracellular fluid is not buffered against changes in CO₂ tension. Hypercapnic acidosis was induced by increasing the concentration of CO₂ in the inspired air to approximately 20% (p_aCO₂ = 180mmHg, pH = 6.9). Hypocapnia was induced in a second group of animals via hyperventilation to give a p_aCO₂ of 20mmHg. Changes were induced 15 minutes prior to intravenous administration of [¹²⁵I]MK801 (200μCi) and were maintained throughout the experimental period. The [¹²⁵I]MK801 autoradiographic procedure was then carried out as described in section 2.3.3. however in these experiments, fifteen serial sections were collected from 3 predetermined planes, at the level of the striatum, dorsal hippocampus and cerebellum.

2.9.2 Data analysis

[¹²⁵I]MK801 uptake (strictly the amount of radioactivity following intravenous injection of [¹²⁵I]MK801 in nCi/g) was measured in 9 discrete brain areas in each treatment group and corrected for isotope decay. The corrected values were expressed as a ratio of [¹²⁵I]MK801 uptake in regions of interest relative to uptake within the cerebellum. Region of interest/cerebellar ratios were compared to corresponding values from normocapnic animals (ANOVA and subsequent Student's unpaired t-test with Bonferroni correction applied for simultaneous multiple comparisons).

2.9.3 [¹²⁵I]CNS 1261 uptake following changes in arterial CO₂ tension

Prior to manipulations, animals were surgically prepared as described in section 2.4.1. Hypercapnic acidosis was induced via adjustment of the respiratory status of the animals. Hypercapnic acidosis was induced by increasing the concentration of CO₂ in inspired air to approximately 20% ($p_a\text{CO}_2 = 180\text{mmHg}$, $\text{pH} = 6.9$). Changes were induced 15 minutes prior to intravenous administration of [¹²⁵I]CNS 1261 (200 μCi) and were maintained for the remainder of the experimental period. The [¹²⁵I]CNS 1261 autoradiographic technique was then carried out as detailed in section 2.4.2.

2.9.4 Data analysis

[¹²⁵I]CNS 1261 uptake (strictly the amount of radioactivity following intravenous injection of [¹²⁵I]CNS 1261 in nCi/g) was measured in discrete brain areas in each treatment group and corrected for isotope decay. The corrected values were expressed as a ratio of [¹²⁵I]CNS 1261 uptake in regions of interest relative to uptake within the cerebellum.

2.10 Uptake and retention of [125 I]CNS 1261 following intracortical injection of NMDA

2.10.1 Experimental design

Animals were surgically prepared as detailed in section 2.4.1. Animals were then turned prone and the head fixed in a stereotaxic frame. A burr hole was drilled in the skull 4mm lateral to Bregma (co-ordinates taken from Paxinos and Watson, 1996). A fine needle was used to make a small hole in the dura without damaging any underlying vessels. A needle (20 gauge) attached to a Hamilton syringe was inserted into the left parietal cortex. Coordinates for injection (relative to Bregma) were: anterior posterior +0.0mm; lateral +4.0mm. The needle was lowered to a depth of 1.5mm (below the dura) over 2 minutes to minimise mechanical damage. NMDA (27 nmoles, volume = 3 μ l) was injected at a constant rate over 2 minutes. Solutions for injection were made up in CSF (composition: NaCl 124mm; NaHCO₃ 25.5mM; KCl 1.2mM; KH₂PO₄ 1.2mM; CaCl₂ 2.5mM; MgCl₂ 1.0mM; 0.01% Evan's Blue dye. A second group of animals received an injection of CSF only. In both cases the needle was left in position for the remainder of the experiment. Fifteen minutes after injection of NMDA (or CSF), [125 I]CNS 1261 (200 μ Ci) was administered intravenously to initiate the [125 I]CNS 1261 technique. Animals were killed 5, 60 or 120 minutes after injection of tracer and the brains processed for autoradiography as detailed in section 2.6.3.

2.10.2 Histological examination of lesion

Sections adjacent to those taken for autoradiography were stained with haematoxylin and eosin. Briefly, sections were dehydrated in alcohol, stained in haematoxylin for 5 minutes, washed and stained in eosin for 30 seconds. Sections were examined by light microscopy to determine the anatomical extent of cell loss following injection of CSF or NMDA. The size of the lesion, identified by an area of pallor, was compared to the lesion size delineated by alterations in [125 I]CNS 1261 uptake.

2.10.3 Data analysis

The lesions evident on autoradiograms were initially described by their appearance. The size and extent of each lesion was also measured. The area of the lesion (mm^2) was measured in triplicate at the level of its first appearance by area analysis using an M4 image analyser and precalibrated area standards. This was repeated at $400\mu\text{m}$ intervals throughout the extent of the lesion. A stereotaxic atlas was used to designate stereotaxic coordinates (relative to bregma) to the brain levels to produce 2-D maps which could be used to compare the lesions

$[^{125}\text{I}]\text{CNS } 1261$ uptake was measured in 37 discrete brain areas following injection of NMDA or CSF. As described previously values were expressed as a ratio of the concentration of radioactivity (nCi/g) uptake in each region of interest relative to concentration of radioactivity within the cerebellar cortex.

CHAPTER III

RESULTS

3.1 CNS 1261 binds to the NMDA receptor complex with high affinity and selectivity

3.1.1 Affinity of CNS 1261

CNS 1261 was found to displace [^3H]MK801 binding to homogenates with $K_i = 25\text{nM}$ in tris buffer and 44nM in CSF (Cambridge Neuroscience in house data).

3.1.2 Selectivity of CNS 1261

The effect of CNS 1261 on the binding of ligands to the NMDA receptor, and to other neurotransmitter receptors was more extensively investigated by submitting the compound for commercial screening (NovaScreen, Maryland, USA).

CNS 1261 (10nM) inhibited [^3H]MK801 binding by $26.7 \pm 2.2\%$, which was consistent with the reported K_i for this compound. At this concentration, CNS 1261 did not produce any biologically significant effects in any of the other assays investigated.

CNS 1261 ($1\mu\text{M}$) was extremely selective and only showed activity ($>50\%$ inhibition of binding) in the MK801 binding site assay (Table 2). CNS 1261 ($1\mu\text{M}$) produced a 99% inhibition of [^3H]MK801 binding. The effect of CNS 1261 on [^3H]MK801 binding was confirmed by repeating the assay a further 2 times. The results from these assays were consistent with the initial results (10nM : $27 \pm 2\%$, $1\mu\text{M}$: $99 \pm 1\%$). At this concentration ($1\mu\text{M}$), some 40 times in excess of its affinity for the MK801 binding site on the NMDA receptor, CNS 1261 displayed marginal effects ($\geq 20\%$ inhibition) in three assays (Table 2). CNS 1261 had no effect ($< 20\%$) on the remaining 38 radioligand binding assays examined (Table 3).

In an extensive commercial screen at the concentrations examined, CNS 1261 binding appears to be selective for the MK801 binding site on the NMDA receptor.

TABLE 2
Inhibition of ligand binding by CNS 1261

ASSAY	RADIOLIGAND	% inhibition of binding	
		10nM	1μM
MK801 binding site	[³H]MK801	27 ± 2	99 ± 1
Na ⁺ channel 2	[³ H]batrachotoxin	-1 ± 3	38 ± 1
α-1 adrenoceptor	[³ H]prazosin	20 ± 1	33 ± 1
GABA uptake	[³ H]GABA	16 ± 8	21 ± 2

CNS 1261 (1μM) was extremely selective and only demonstrated activity (≥ 50% inhibition) in the MK801 binding site assay. Marginal effects (≥ 20% inhibition) were observed at three of the other 41 assays examined. Data are expressed as mean ± S.E.M., n = 2. Negative values indicate stimulation of binding. Data taken from commercial screen carried out by NovaScreen, Maryland, USA.

TABLE 3

CNS 1261 displayed no activity in a range of radioligand binding assays

ASSAY	RADIOLIGAND	% inhibition	
		10nM	1μM
AMPA	[³ H]AMPA	-2 ± 5	3 ± 5
Adenosine (ns)	[³ H]NECA	-9 ± 3	-4 ± 4
α-2 adrenoceptor	[³ H]RX 821002	4 ± 4	13 ± 4
β-adrenoceptor	[³ H]DHA	-2 ± 2	8 ± 2
Dopamine 1	[³ H]SCH 23390	7 ± 3	1 ± 4
Dopamine 2	[³ H]sulpiride	1 ± 0	9 ± 1
GABA _A	[³ H]GABA	0 ± 7	9 ± 4
GABA _B	[³ H]GABA (+ isoguavacine)	20 ± 1	9 ± 4
Glycine (strychnine sensitive)	[³ H]strychnine	4 ± 3	2 ± 1
Histamine 1	[³ H]pyrilamine	3 ± 0	17 ± 2
Histamine 2	[³ H]tiotidine	10 ± 8	14 ± 3
Histamine 3	[³ H]N ^a -methylhistamine	12 ± 4	8 ± 6
Angiotensin II	[¹²⁵ I]Sar ¹ , Ile ⁸ -angiotensin II	-10 ± 1	-11 ± 2
Noradrenaline uptake	[³ H]desmethylinipramine	-2 ± 0	11 ± 3
Serotonin uptake	[³ H]citalopram	1 ± 0	6 ± 1
Choline uptake	[³ H]choline chloride	6 ± 6	1 ± 1
Dopamine uptake	[³ H]WIN 35,428	-10 ± 5	10 ± 1
Adenosine uptake	[³ H]nitrobenzylthioinosine	1 ± 6	-1 ± 1
Glutamate uptake	[³ H]glutamate	6 ± 2	12 ± 3
Chloride channel	[³ H]TBOB	2 ± 0	1 ± 0
Ca ²⁺ channel (type T & L)	[³ H]nitrendipine	2 ± 0	2 ± 1
Ca ²⁺ channel (type N)	[¹²⁵ I]ω-conotoxin	0 ± 2	2 ± 1
K ⁺ (low conductance)	[¹²⁵ I]apamin	-11 ± 3	-2 ± 1
K ⁺ channel (ATP)	[³ H]glibenclamide	7 ± 1	8 ± 2
Kainic acid	[³ H]kainic acid	-1 ± 4	5 ± 0
Muscarinic (c)	[³ H]quinuclidinylbenzilate	1 ± 4	6 ± 2
Muscarinic (p)	[³ H]quinuclidinylbenzilate	-22 ± 1	-22 ± 12
Nicotinic (neuronal)	[³ H]N-methylcarbamylcholine	19 ± 0	16 ± 1
NMDA	[³ H]CGP 39653	-13 ± 0	-15 ± 1
Serotonin (5-HT ₁)	[³ H]hydroxyltryptamine binoxylate	9 ± 3	8 ± 0
Serotonin (5-HT ₂)	[³ H]ketanserin	9 ± 3	8 ± 0
Serotonin (5-HT ₃)	[³ H]GR65630	2 ± 1	16 ± 2
Glycine (strychnine insensitive)	[³ H]glycine	-4 ± 2	1 ± 2
Benzodiazepine (c)	[³ H]flunitrazepam	9 ± 1	15 ± 3
Opiate (ns)	[³ H]naloxone	0 ± 2	5 ± 2
Vasopressin-1	[³ H]phenylalanyl-3,4,5-vasopressin	-19 ± 3	-2 ± 3
K ⁺ channel (voltage dependent)	[¹²⁵ I]charybdotoxin	-10 ± 5	13 ± 1
Na ⁺ channel 1	[³ H]saxitoxin	3 ± 1	-12 ± 3

Table 3 shows the % inhibition of radioligand binding by CNS 1261 (10nM and 1μM) in 38 radioligand binding assays. 'Activity' was defined as >50% inhibition. Data are displayed as mean ± S.E.M., n=2. Negative values indicate a stimulation of radio-ligand binding. ns = non-specific, c = central and p = peripheral (NovaScreen)

3.2. Effect of CNS 1261 on local cerebral glucose utilisation

The effect of three doses of CNS 1261 (1, 3 and 10mg/kg) on local cerebral glucose utilisation were examined in the conscious lightly restrained rat. The pattern of alterations in glucose utilisation produced by CNS 1261 were compared to those obtained in a previous study using MK801 carried out by Kurumaji *et al* (1989).

3.2.1. General observations

Administration of CNS 1261 produced changes in overt behaviour of the animals at all of the doses examined. A degree of sedation and a reduced response to external stimuli was observed in all animals however, animals remained conscious throughout the experimental period. These effects appeared at around 5 minutes post-injection of CNS 1261 and lasted for the duration of the experiment. The normal grooming, sniffing and exploratory behaviour (displayed by all control rats) was absent in animals treated with CNS 1261. CNS 1261-treated animals exhibited stereotypical behaviour consisting of neck stretching and repetitive side-to-side and cyclical head movements. The severity of these effects was dose related and was most pronounced in the group receiving the highest dose of CNS 1261.

Administration of CNS 1261 (1mg/kg) had no significant effects on any of the cardiovascular and respiratory variables measured (Table 4). Treatment with CNS 1261 (10mg/kg) induced a modest, significant increase in arterial carbon dioxide tension. CNS 1261 administration produced an immediate, transient hypotension. However at each dose examined CNS 1261 ultimately effected a sustained increase in mean arterial blood pressure relative to control values at times beyond 10 minutes (Figure 10). Arterial plasma glucose concentration was unaffected by administration of CNS 1261.

TABLE 4

Effect of CNS 1261 administration on physiological variables

PARAMETER	VEHICLE	CNS 1261		
		1mg/kg	3mg/kg	10mg/kg
paCO ₂ (mmHg)	34 ± 1	37 ± 1	38 ± 1	41 ± 1*
arterial pH	7.43 ± 0.01	7.41 ± 0.01	7.41 ± 0.01	7.3 ± 0.01
paO ₂ (mmHg)	94 ± 3	98 ± 2	95 ± 2	88 ± 2
MABP (mmHg)	136 ± 4	142 ± 5	151 ± 3*	157 ± 3**
temperature (°C)	36.4 ± 0.3	36.2 ± 0.5	36.1 ± 0.4	36.0 ± 0.4
glucose (mM)	9.6 ± 0.7	8.6 ± 0.7	9.9 ± 0.2	10 ± 1
weight (g)	347 ± 16	323 ± 11	345 ± 12	366 ± 14
n	8	6	6	6

Arterial plasma glucose concentration was measured immediately prior to administration of [¹⁴C]2-deoxyglucose. Other physiological variables were assessed 30 minutes after radioisotope administration. *p<0.05, **p<0.01 for statistical comparison between each drug treated group and saline-treated controls (ANOVA, Student's t-test with Bonferroni correction). Data are derived from 26 animals and are expressed as mean ± S.E.M. (n = 6-8).

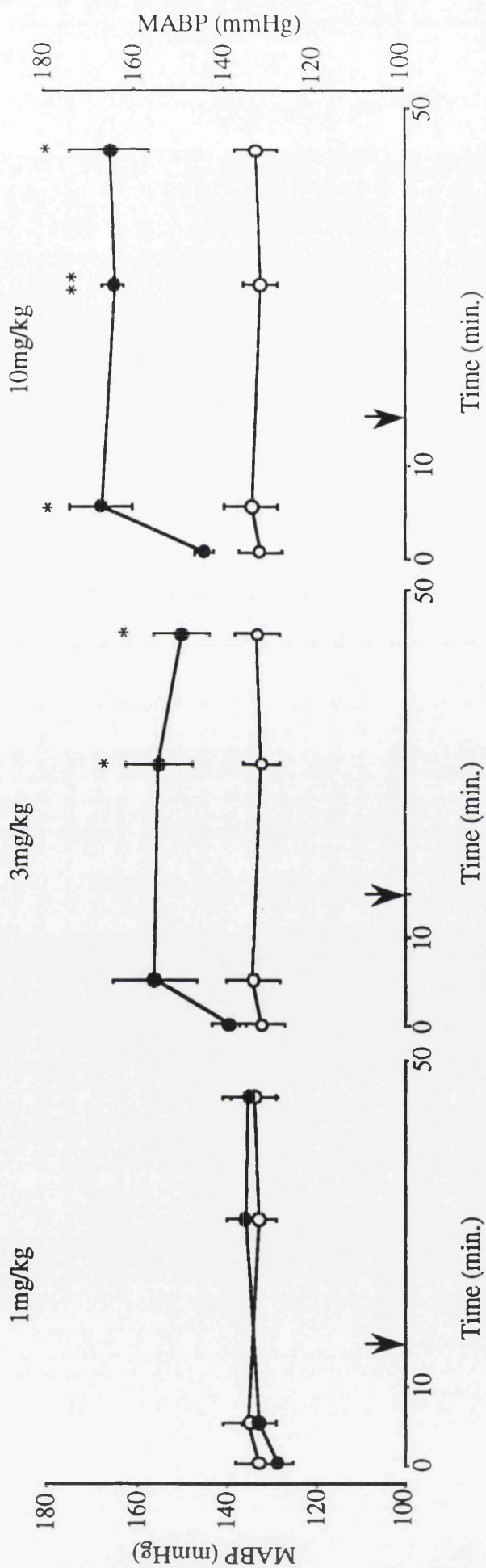


FIGURE 10 : Effect of CNS 1261 on mean arterial blood pressure

Administration of CNS 1261 produced a sustained, dose-dependent increase in mean arterial blood pressure. * $p < 0.05$, ** $p < 0.01$, significantly different from vehicle-treated animals (ANOVA, with subsequent Student's t-test with appropriate Bonferroni correction). Data are expressed as mean \pm S.E.M.

3.2.2. Local cerebral glucose utilisation

Administration of CNS 1261 produced highly circumscribed changes in glucose utilisation. The glucose use alterations associated with systemic administration of CNS 1261 (1, 3 and 10mg/kg) in 36 regions of interest are presented in Tables 5-7 (see Figures 11-13).

Following intravenous administration of CNS 1261 (1mg/kg) 6 of the regions examined displayed significant alterations in glucose use. Moderate decreases were observed in the auditory cortex, posterior cingulate cortex, retrosplenial cortex and inferior colliculus. Glucose use was elevated in entorhinal cortex (caudal) and within the fornix.

Administration of CNS 1261 (3mg/kg) caused significant alterations in glucose use in 11 of the 36 regions examined. Glucose use was decreased in layer IV of the auditory cortex and the inferior colliculus. Prominent increases in glucose use were observed in layer IV of the visual cortex, anteroventral thalamus, hippocampus molecular layer, dentate gyrus, entorhinal cortex (caudal), mamillary body, posterior cingulate cortex, retrosplenial cortex and fornix.

At the highest dose examined (10mg/kg) CNS 1261 administration produced alterations in glucose use that could be readily visualised on autoradiograms (Figure 11). Moderate decreases in glucose utilisation (approximately 30%) were observed in layer IV of the frontal, sensory-motor and auditory cortices and in the inferior colliculus (Figure 12). Distinct, significant elevations in glucose use were observed in a number of structures within the limbic system (Figure 13), namely, the entorhinal cortex (caudal), hippocampus molecular layer, dentate gyrus, anteroventral thalamus, mamillary body, posterior cingulate cortex, retrosplenial cortex and also within the fornix. There were no significant alterations in glucose use in the other four regions of white matter examined. The magnitude of these changes was generally in the region of 80%. however, extremely large magnitude changes were observed within the entorhinal cortex and mamillary body, where glucose use was increased by 238% and 125% respectively.

TABLE 5

Effect of CNS 1261 administration on glucose use in sensory and motor systems

STRUCTURE	Glucose Utilisation (μ moles/100g/min.)				<i>f</i> value	
	Vehicle	1mg/kg	3mg/kg	10mg/kg	CNS 1261	MK801
Visual cortex (IV)	75 \pm 3	81 \pm 4	95 \pm 5**	71 \pm 4	0.11	0.086
Auditory cortex (IV)	113 \pm 4	87 \pm 4**	87 \pm 8	69 \pm 4**	0.42	0.26
Medial geniculate body	93 \pm 6	74 \pm 6	94 \pm 11	90 \pm 5	0.047	0.042
Inferior colliculus	133 \pm 7	85 \pm 3**	79 \pm 1**	66 \pm 5**	1.02	0.4
Superior olivary nucleus	107 \pm 6	99 \pm 6	105 \pm 10	94 \pm 9	0.033	0.024
sensory-motor cortex (IV)	92 \pm 6	83 \pm 4	76 \pm 4	56 \pm 3**	0.27	0.47
Parietal cortex (IV)	80 \pm 4	97 \pm 5	95 \pm 8	66 \pm 4	0.11	0.062
Frontal cortex (IV)	93 \pm 6	88 \pm 6	80 \pm 2	63 \pm 3**	0.16	0.12
Thalamus mediodorsal	96 \pm 6	104 \pm 7	124 \pm 9	112 \pm 5	0.12	0.25
Thalamus ventrolateral	64 \pm 6	64 \pm 5	69 \pm 4	63 \pm 5	0.014	0.024
Caudate nucleus	86 \pm 7	107 \pm 8	112 \pm 8	96 \pm 5	0.17	0.026
Globus pallidus	46 \pm 4	57 \pm 5	63 \pm 7	53 \pm 2	0.21	0.13
Substantia nigra pars compacta	62 \pm 5	67 \pm 7	72 \pm 6	58 \pm 3	0.038	0.0091
Substantia nigra pars reticulata	39 \pm 3	43 \pm 3	48 \pm 2	41 \pm 1	0.069	0.091
Cerebellar hemisphere	42 \pm 2	43 \pm 2	43 \pm 2	41 \pm 3	0.0087	0.0089

Administration of CNS 1261 produced significant decreases in glucose use within the inferior colliculus and neocortex. Data are presented as mean \pm S.E.M., * $p < 0.01$, ANOVA. *f* values for regional responsiveness to CNS 1261 and to MK801 are also shown. *f* values show that the level of responsiveness in these areas was broadly similar for both CNS 1261 and MK801.

TABLE 6

Effect of CNS 1261 administration on glucose use in the limbic system

STRUCTURE	Glucose Utilisation (μ moles/100g/min.)				<i>f</i> value	
	Vehicle	1mg/kg	3mg/kg	10mg/kg	CNS 1261	MK801
Entorhinal cortex caudal	50 \pm 3	110 \pm 15**	167 \pm 5**	169 \pm 18**	3.45	1.85
Entorhinal cortex rostral	45 \pm 3	43 \pm 2	51 \pm 6	45 \pm 3	0.024	0.79
Hippocampal molecular layer	67 \pm 4	90 \pm 8	114 \pm 11**	109 \pm 1**	0.61	0.5
Dentate gyrus	52 \pm 4	64 \pm 7	97 \pm 12**	81 \pm 2**	0.64	0.34
Hippocampal CA1	44 \pm 4	37 \pm 3	39 \pm 4	36 \pm 2	0.081	0.017
Hippocampus CA3	51 \pm 4	47 \pm 4	52 \pm 5	55 \pm 3	0.013	0.035
Nucleus accumbens	63 \pm 6	77 \pm 7	86 \pm 7	76 \pm 4	0.21	0.11
Lateral habenular nucleus	91 \pm 5	99 \pm 7	100 \pm 7	85 \pm 3	0.028	0.012
Thalamus anteroventral	99 \pm 6	122 \pm 11	175 \pm 14**	162 \pm 9**	0.87	0.37
Medial amygdaloid nucleus	37 \pm 4	38 \pm 4	46 \pm 5	31 \pm 2	0.081	0.082
Mamillary body	86 \pm 5	122 \pm 11	191 \pm 15**	180 \pm 8**	1.22	0.45
Hypothalamus	36 \pm 4	31 \pm 3	39 \pm 4	30 \pm 2	0.064	0.0034
Posterior cingulate cortex	86 \pm 4	113 \pm 8*	132 \pm 9**	139 \pm 8**	0.48	0.69
Anterior cingulate cortex	94 \pm 7	105 \pm 10	120 \pm 9	81 \pm 3	0.12	0.013
Retrosplial cortex	69 \pm 3	102 \pm 10*	147 \pm 6**	136 \pm 4**		
Pons	47 \pm 4	42 \pm 3	47 \pm 1	43 \pm 3	0.016	0.011

Administration of CNS 1261 produced significant increases in glucose use within the entorhinal cortex (caudal), hippocampus molecular layer, mamillary body, posterior cingulate cortex and retrosplial cortex. Data are presented as mean \pm S.E.M., * $p < 0.05$, ** $p < 0.01$, ANOVA. *f* values for regional responsiveness are also shown. The level of regional responsiveness in these areas was broadly similar for both CNS 1261 and MK801.

TABLE 7

Effect of CNS 1261 administration on glucose use in myelinated tracts

STRUCTURE	Glucose Utilisation (μ moles/100g/min.)				<i>f</i> value	
	Vehicle	1mg/kg	3mg/kg	10mg/kg	CNS 1261	MK801
Corpus callosum	31 \pm 3	29 \pm 3	40 \pm 4	34 \pm 1	0.14	0.018
Genu of corpus callosum	28 \pm 4	25 \pm 3	35 \pm 4	27 \pm 2	0.066	0.0071
Internal capsule	30 \pm 3	29 \pm 2	35 \pm 3	27 \pm 2	0.11	0.041
Cerebellar white matter	26 \pm 3	23 \pm 1	23 \pm 2	25 \pm 2	0.015	0.035
Fornix	47 \pm 3	75 \pm 6**	114 \pm 10**	98 \pm 6**	1.57	0.54

Administration of CNS 1261 produced significant increases in glucose use within the fornix. CNS 1261 administration had no effect on any of the other white matter areas examined. Data are presented as mean \pm S.E.M., * $p < 0.01$, ANOVA. *f* values for regional responsiveness to CNS 1261 and to MK801 are also shown. *f* values show that the level of responsiveness in these areas was broadly similar for both CNS 1261 and MK801.

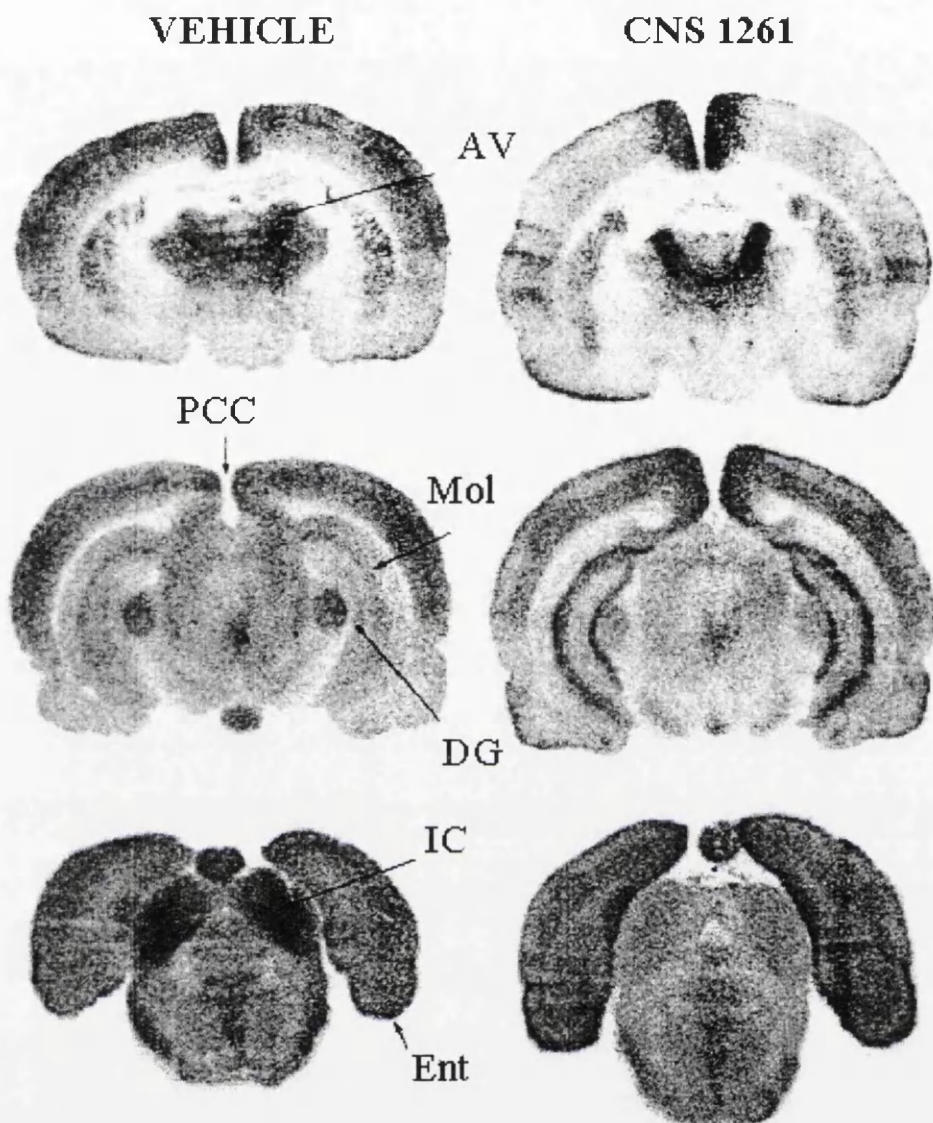


FIGURE 11 : Changes in glucose utilisation following administration of CNS 1261

Representative [^{14}C]2-deoxyglucose autoradiograms of coronal rat brain sections at the level of the anteroventral thalamic nucleus (upper), hippocampus molecular layer (middle) and inferior colliculus (lower). Administration of CNS 1261 (10mg/kg) produced marked increases in glucose use in a number of regions of the limbic system, including the anteroventral thalamus (AV), hippocampus molecular layer (Mol), dentate gyrus (DG), posterior cingulate cortex (PCC) and entorhinal cortex (Ent). Profound reductions in glucose use were observed within the inferior colliculus

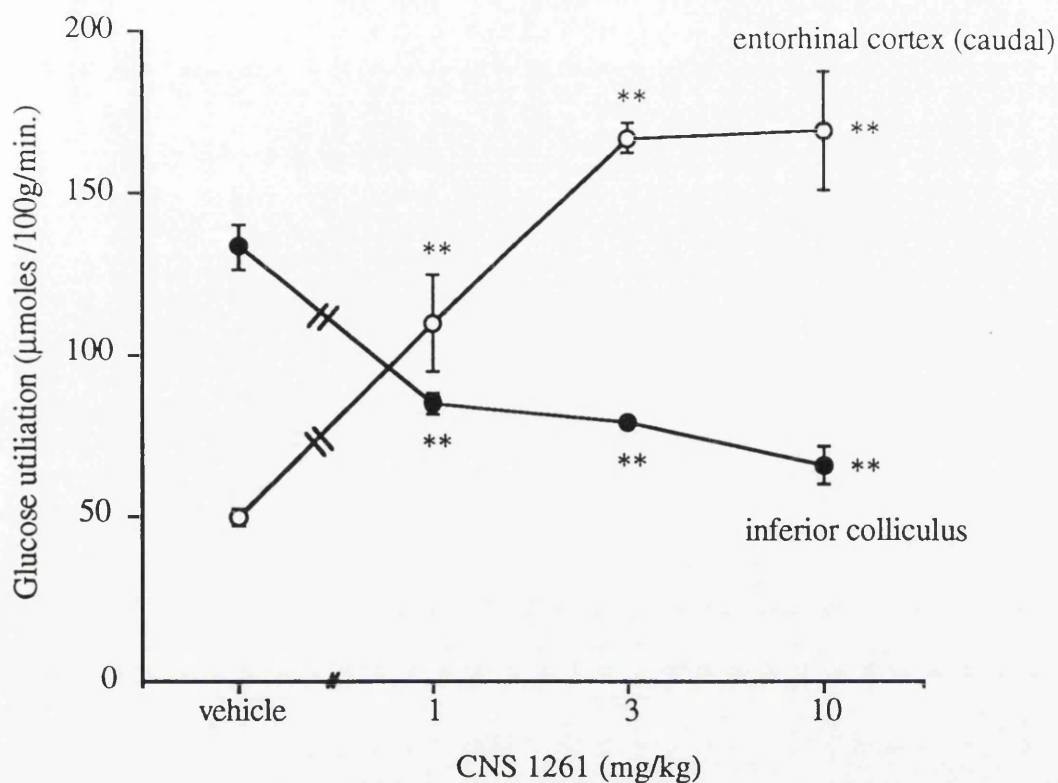


FIGURE 12 : Effect of CNS 1261 on glucose use in the entorhinal cortex and inferior colliculus.

Local cerebral glucose utilisation in the entorhinal cortex (caudal) and the inferior colliculus following intravenous administration of CNS 1261. Data are expressed as mean \pm S.E.M (n= 6-8). Significant elevations in glucose utilisation were observed in the entorhinal cortex (caudal) following administration of CNS 1261. CNS 1261 administration markedly reduced glucose utilisation in the inferior colliculus

**p< 0.01 ANOVA followed by Student's t-test with appropriate Bonferroni correction.

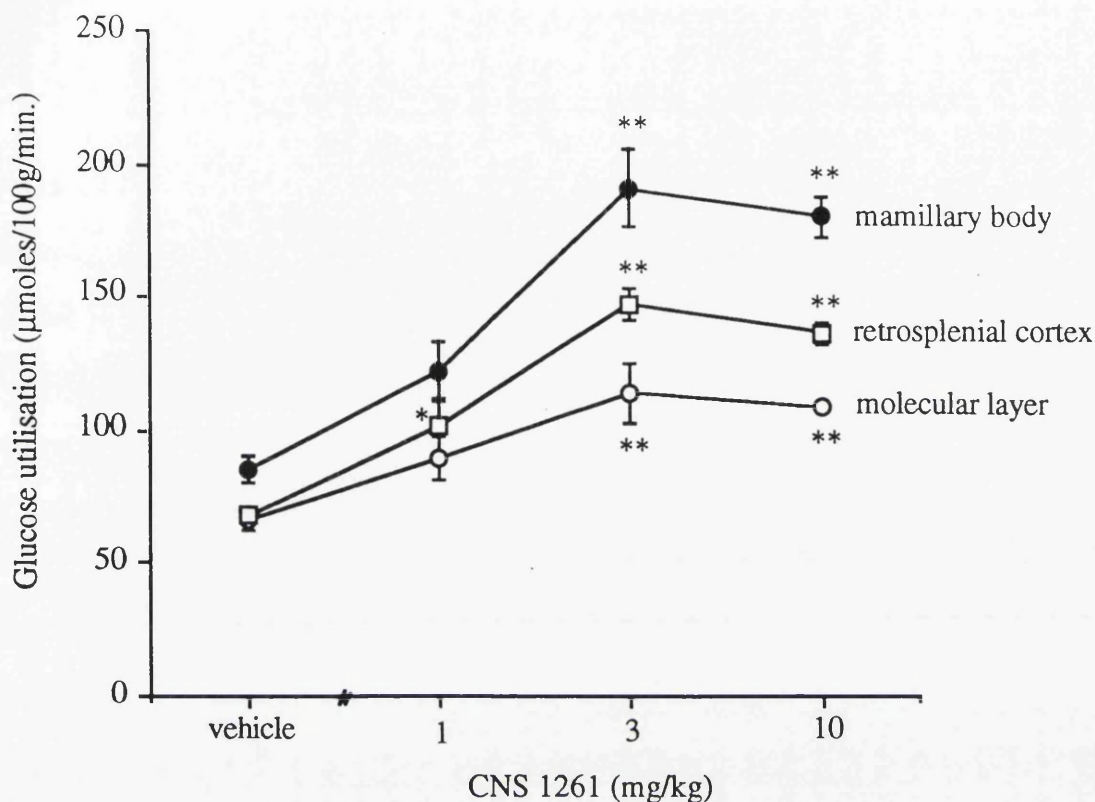


FIGURE 13: Effect of CNS 1261 on limbic structures

Glucose utilisation in selected structures within the limbic system following administration of CNS 1261. Data are expressed as mean \pm S.E.M (n=6-8). CNS 1261 produced dose-dependent elevations in glucose utilisation in the mamillary body, retrosplenial cortex and hippocampus molecular layer (posterior).

Note the similarity of the effects induced by administration of CNS 1261 in these three regions. In each region the greatest increase in glucose utilisation compared to control values was observed at 3mg/kg

The degree of responsiveness of each of the 36 regions to CNS 1261 was assessed by application of an arithmetic function which encompasses the entire dose-response data available for each region. A rank ordering of these regional responses was obtained from the function f .

$$f = \sum (x_c - x_{Ti})^2$$

x_c is the mean of loge (glucose use) for control group members, x_{Ti} is the mean of loge (glucose use) for the i th dose of the treatment group in question, T either CNS 1261 (1, 3 and 10mg/kg) or MK801 (0.05, 0.5 and 5mg/kg).

Calculated f values for regional responsiveness to CNS 1261 treatment were compared to corresponding values for MK801 (Kurumaji *et al*, 1989) and are shown in Tables 5-7.

f values were classified into groups where regions with $f > 0.8$ were described as "extremely sensitive". These regions generally displayed greater than 55% reductions or increases in glucose use after administration of the highest dose.

Regions with $0.5 < f < 0.8$ were described as "sensitive". Regions described as "moderately sensitive" generally displayed 30-50% increases or decreases in glucose use and $0.3 < f < 0.5$. "Minially sensitive" regions displayed f values < 0.3 , within this group the magnitude of change in glucose use was less than 30%.

Examination of the frequency hierarchies showed that regions which were particularly sensitive to CNS 1261 (Table 8) such as the entorhinal cortex (caudal), hippocampus molecular layer, dentate gyrus and fornix, were also in general, sensitive to MK801 (Table 9). Those areas least affected by CNS 1261 were also least affected by MK801, including most cortical areas and regions of white matter.

TABLE 8
Hierarchy of regional responsiveness to CNS 1261

Extremely sensitive $f > 0.8$	Sensitive $0.5 < f < 0.8$	Moderately sensitive $0.3 < f < 0.5$	Minimally sensitive $f < 0.3$
entorhinal cortex (caudal) thalamus anteroventral mamillary body inferior colliculus fornix	hippocampus molecular layer dentate gyrus	posterior cingulate gyrus auditory cortex (IV)	entorhinal cortex (rostral) hippocampus CA1 hippocampus CA3 nucleus accumbens lateral habenular nucleus medial amygdaloid nucleus hypothalamus anterior cingulate cortex pons visual cortex (IV) medial geniculate body superior olivary nucleus sensory-motor cortex (IV) parietal cortex (IV) frontal cortex (IV) thalamus mediodorsal thalamus ventrolateral caudate nucleus globus pallidus substantia nigra pars compacta substantia nigra pars reticulata cerebellar hemisphere corpus callosum genu of the corpus callosum internal capsule cerebellar white matter

TABLE 9
Hierarchy of regional responsiveness to MK801

Extremely sensitive $f > 0.8$	Sensitive $0.5 < f < 0.8$	Moderately sensitive $0.3 < f < 0.5$	Minimally sensitive $f < 0.3$
entorhinal cortex (caudal)	entorhinal cortex (rostral) hippocampus molecular layer posterior cingulate cortex fornix	dentate gyrus thalamus anteroventral mamillary body medial geniculate body inferior colliculus sensory-motor cortex (IV)	hippocampus CA1 hippocampus CA3 nucleus accumbens lateral habenular nucleus medial amygdaloid nucleus hypothalamus anterior cingulate cortex pons visual cortex (IV) auditory cortex (IV) superior olivary nucleus sensory-motor cortex (IV) parietal cortex (IV) frontal cortex (IV) thalamus mediodorsal thalamus ventrolateral caudate nucleus globus pallidus substantia nigra pars compacta substantia nigra pars reticulata cerebellar hemisphere corpus callosum genu of the corpus callosum internal capsule cerebellar white matter

Examination of frequency distribution profiles of f values for CNS 1261 and MK801 (Figure 14) show that both compounds were broadly similar, displaying a wide range of f values and a skewed distribution, with the majority of regions being minimally sensitive ($f < 0.3$). Differences in glucose use responses to the two agents occurred in a small number of regions, a greater number of regions displayed extreme sensitivity ($f > 0.8$) to CNS 1261 in contrast to MK801, such as the anteroventral thalamus, mamillary body and the inferior colliculus.

Correlation analysis of f values (Figure 15) showed that a significant relationship exists between the alterations in glucose use produced by CNS 1261 administration and those produced by MK801 (correlation coefficient, $r = 0.87$). The entorhinal cortex (rostral) was much less sensitive to CNS 1261 than to MK801.

These results confirm that the overall pharmacological effects of CNS 1261 were extremely similar to the overall effects of MK801

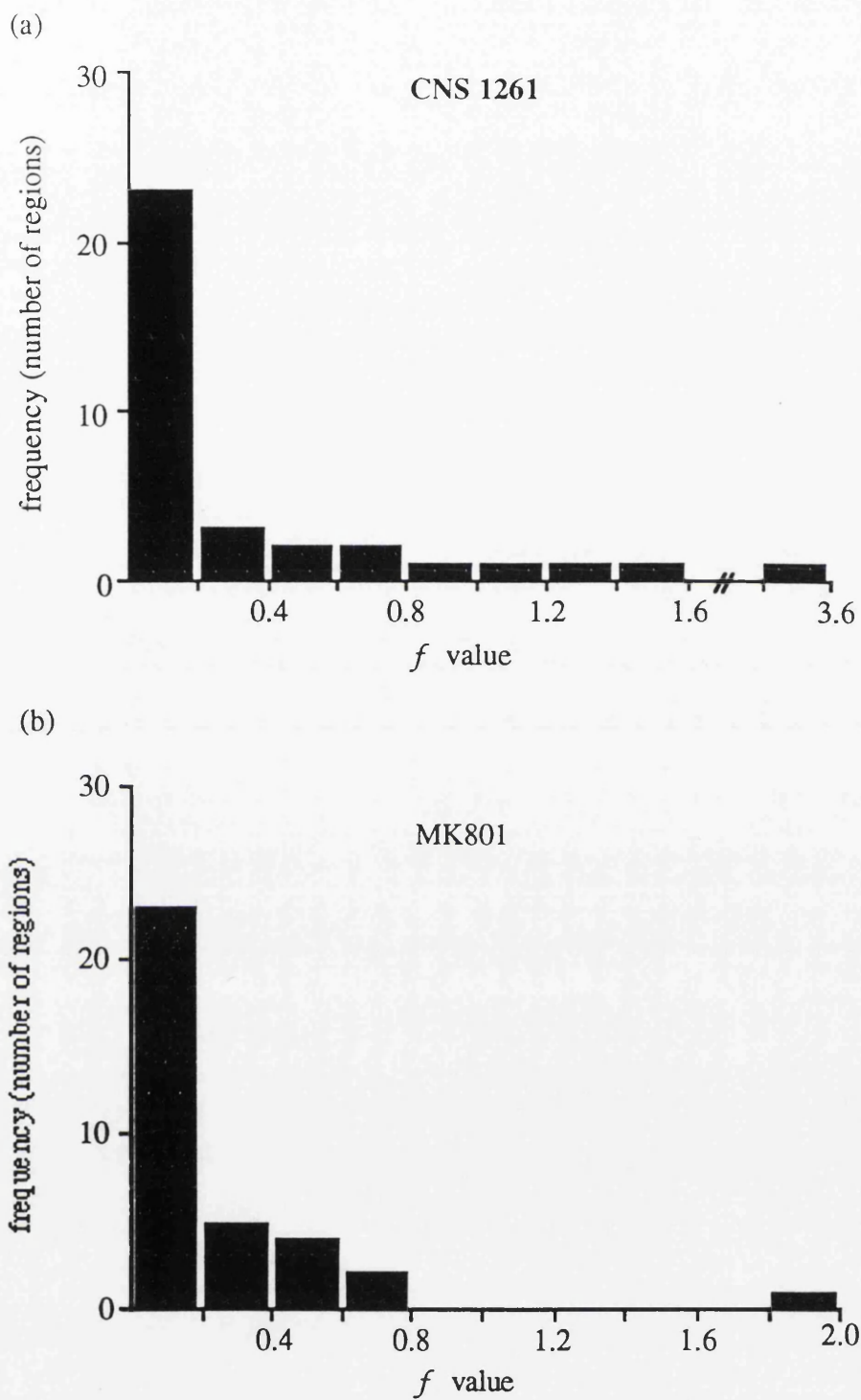


FIGURE 14 : Frequency distribution profiles of f values for (a) CNS 1261 and (b) MK801

f function values represent the sensitivity of individual regions to drug treatment following administration of CNS 1261 and MK801. f values for both compounds were broadly similar with a wide range of f values and a skewed distribution.

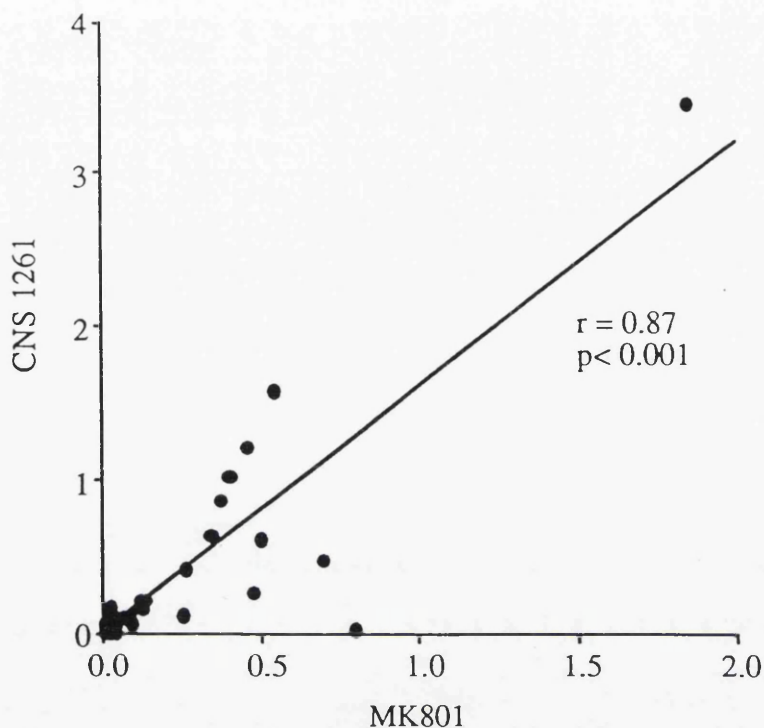


FIGURE 15 : Correlation analysis of f values for glucose use after MK801 and CNS 1261 treatment

Each data point represents the f value generated from analysis of the entire dose-response curve of a single structure in response to MK801 and CNS 1261.

Overall correlation coefficient, r , for all regions investigated was 0.87, indicating a high degree of association between regional effects of MK801 and CNS 1216. The entorhinal cortex (caudal) was much less sensitive CNS 1261 than to MK801

3.3 Uptake and retention of [125 I]MK801 and [125 I]CNS 1261 in normal rat brain

The uptake and retention of [125 I]CNS 1261 was examined under conditions of normal NMDA receptor activation and was compared to that of [125 I]MK801 under identical conditions.

3.3.1 General observations

Physiological variables were measured prior to, and 15 after administration of [125 I]MK801 or [125 I]CNS 1261 and are presented in Table 10. Administration of [125 I]MK801 or [125 I]CNS 1261 had no effect on any of the variables examined. There were no significant differences in any of the parameters between the two groups at any time point.

3.3.2 *In vivo* uptake and retention of [125 I]CNS 1261

The *in vivo* uptake and retention of [125 I]CNS 1261 was examined in 36 anatomically discrete regions at multiple time points in halothane anaesthetised rats. [125 I]CNS 1261 was administered and the animals sacrificed 5, 30, 60 and 120 minutes thereafter. The uptake of each tracer in individual regions of interest was expressed as a ratio relative to uptake within the cerebellar hemisphere (a within animal measure of non-specific binding), Tables 11-13 .

[125 I]CNS 1261 uptake 5 minutes after intravenous injection was greatest within areas of high cerebral blood flow such as the anterior thalamic nucleus and the majority of cortical areas examined. Intermediate levels of uptake were observed within the thalamus and lowest levels of uptake in the hippocampus and hypothalamus. [125 I]CNS 1261 uptake was also low in all areas of white matter examined (Figure 16, see also Figures 20-21).

TABLE 10
Uptake and retention of [¹²⁵I]MK801 and [¹²⁵I]CNS 1261
Physiological Variables

	sample time (min.)	30 min.		60 min.		120 min.	
		[¹²⁵ I]MK801	[¹²⁵ I]CNS 1261	[¹²⁵ I]MK801	[¹²⁵ I]CNS 1261	[¹²⁵ I]MK801	[¹²⁵ I]CNS 1261
PaCO ₂ (mmHg)	0	39 ± 2	39 ± 1	45 ± 1	42 ± 1	39 ± 3	38 ± 1
	15	40 ± 4	41 ± 3	40 ± 3	39 ± 1	42 ± 2	39 ± 1
Arterial pH	0	7.44 ± 0.03	7.41 ± 0.04	7.39 ± 0.01	7.42 ± 0.01	7.44 ± 0.01	7.45 ± 0.02
	15	7.40 ± 0.05	7.44 ± 0.00	7.37 ± 0.05	7.44 ± 0.00	7.41 ± 0.02	7.46 ± 0.04
PaO ₂ (mmHg)	0	156 ± 6	190 ± 12	149 ± 9	159 ± 14	150 ± 10	178 ± 6
	15	161 ± 2	188 ± 5	150 ± 7	175 ± 8	148 ± 9	175 ± 27
MABP (mmHg)	0	88 ± 18	89 ± 2	78 ± 3	87 ± 7	87 ± 5	85 ± 4
	15	88 ± 8	99 ± 12	78 ± 4	86 ± 3	84 ± 3	85 ± 8
Temp. (°C)	0	37.2 ± 0.1	37.4 ± 0.1	37.4 ± 0.2	37.3 ± 0.1	36.9 ± 0.1	36.9 ± 0.2
	15	36.9 ± 0.1	36.9 ± 0.8	37.2 ± 0.0	37.1 ± 0.3	37.1 ± 0.1	37.1 ± 0.2
n	-	2	2	3	3	4	4

Samples were taken immediately prior to (t = 0) and 15 minutes after (t = 15) administration of [¹²⁵I]MK801 or [¹²⁵I]CNS 1261. Brains were removed and processed for autoradiography 30, 60 and 120 minutes post-administration of radiolabelled tracer. Data are presented as mean ± S.E.M. There were no significant differences in any variable examined between groups receiving [¹²⁵I]MK801 or [¹²⁵I]CNS 1261 at 60 or 120 min. (Unpaired t-test).

TABLE 11
Comparison of [125 I]MK801 and [125 I]CNS 1261 uptake
30 minutes post-administration

STRUCTURE	[125 I]MK801	[125 I]CNS 1261
anterior cingulate cortex	1.24 ± 0.15	1.90 ± 0.16
genu	0.88 ± 0.02	0.73 ± 0.03
caudate nucleus	1.13 ± 0.05	1.30 ± 0.02
sensory-motor cortex		
layers I-III	1.12 ± 0.06	1.28 ± 0.01
IV	1.16 ± 0.06	1.30 ± 0.03
V-VI	1.18 ± 0.10	1.32 ± 0.04
corpus callosum	0.90 ± 0.02	0.80 ± 0.02
anterior thalamus	1.29 ± 0.13	1.62 ± 0.12
hippocampus CA1	1.38 ± 0.16	1.17 ± 0.01
hippocampus CA3	1.42 ± 0.11	1.19 ± 0.01
lateral habenular nucleus	1.01 ± 0.07	1.18 ± 0.05
mediodorsal thalamus	1.40 ± 0.22	1.55 ± 0.16
ventrolateral thalamus	1.32 ± 0.09	1.30 ± 0.02
internal capsule	0.91 ± 0.04	0.70 ± 0.03
parietal cortex		
layers I-III	1.16 ± 0.09	1.32 ± 0.04
IV	1.19 ± 0.10	1.35 ± 0.01
V-VI	1.20 ± 0.10	1.32 ± 0.05
hypothalamus	1.00 ± 0.10	1.04 ± 0.01
posterior cingulate cortex	1.14 ± 0.16	1.53 ± 0.06
hippocampus molecular layer	1.45 ± 0.22	1.48 ± 0.07
dentate gyrus	1.39 ± 0.15	1.39 ± 0.03
auditory cortex		
I-III	1.20 ± 0.08	1.54 ± 0.09
IV	1.21 ± 0.08	1.53 ± 0.07
V-VI	1.21 ± 0.14	1.48 ± 0.03
substantia nigra pars compacta	1.00 ± 0.07	1.13 ± 0.10
substantia nigra pars reticulata	0.97 ± 0.05	1.11 ± 0.12
medial geniculate body	1.23 ± 0.09	1.39 ± 0.08
visual cortex		
layers I-III	1.27 ± 0.09	1.55 ± 0.05
IV	1.24 ± 0.06	1.49 ± 0.02
V-VI	1.23 ± 0.02	1.50 ± 0.01
entorhinal cortex	1.16 ± 0.13	1.54 ± 0.13
inferior colliculus	1.04 ± 0.06	1.16 ± 0.04
pons	0.98 ± 0.01	1.30 ± 0.05
cerebellar hemisphere	1.00 ± 0.00	1.00 ± 0.00
cerebellar white matter	0.84 ± 0.05	0.68 ± 0.03
superior olivary nucleus	0.93 ± 0.03	1.14 ± 0.05

Uptake of [125 I]MK801 or [125 I]CNS 1261 in individual regions of interest were expressed as a ratio relative to uptake within the cerebellum. Roman numerals (I-VI) indicate the cortical layer examined. Data are presented as mean \pm S.E.M., $n = 2$.

TABLE 12
Comparison of [125 I]MK801 and [125 I]CNS 1261 uptake
60 minutes post-administration

STRUCTURE	[125 I]MK801	[125 I]CNS 1261
anterior cingulate cortex	1.34 \pm 0.08	1.77 \pm 0.18
genu	1.16 \pm 0.03	1.00 \pm 0.03*
caudate nucleus	1.11 \pm 0.05	1.27 \pm 0.02*
sensory-motor cortex		
layers I-III	1.14 \pm 0.08	1.41 \pm 0.04*
IV	1.18 \pm 0.07	1.59 \pm 0.11*
V-VI	1.20 \pm 0.08	1.52 \pm 0.11
corpus callosum	1.23 \pm 0.07	1.18 \pm 0.06
anterior thalamus	1.52 \pm 0.09	1.62 \pm 0.10
hippocampus CA1	1.87 \pm 0.11	1.85 \pm 0.09
hippocampus CA3	1.91 \pm 0.11	1.84 \pm 0.11
lateral habenular nucleus	1.04 \pm 0.03	1.21 \pm 0.03*
mediodorsal thalamus	1.51 \pm 0.03	1.54 \pm 0.09
ventrolateral thalamus	1.46 \pm 0.04	1.48 \pm 0.08
internal capsule	1.04 \pm 0.04	1.01 \pm 0.05
parietal cortex		
layers I-III	1.21 \pm 0.05	1.48 \pm 0.06*
IV	1.23 \pm 0.03	1.54 \pm 0.10*
V-VI	1.30 \pm 0.03	1.53 \pm 0.08*
hypothalamus	0.99 \pm 0.01	1.09 \pm 0.03*
posterior cingulate cortex	1.31 \pm 0.04	1.45 \pm 0.15
hippocampus molecular layer	2.03 \pm 0.15	2.09 \pm 0.13
dentate gyrus	1.85 \pm 0.07	1.88 \pm 0.12
auditory cortex		
layers I-III	1.25 \pm 0.05	1.60 \pm 0.09*
IV	1.28 \pm 0.06	1.62 \pm 0.12
V-VI	1.40 \pm 0.05	1.62 \pm 0.09
substantia nigra pars compacta	1.09 \pm 0.06	1.13 \pm 0.07
substantia nigra pars reticulata	1.05 \pm 0.05	1.05 \pm 0.05
medial geniculate body	1.35 \pm 0.05	1.39 \pm 0.06
visual cortex		
layers I-III	1.33 \pm 0.06	1.74 \pm 0.10*
IV	1.31 \pm 0.04	1.70 \pm 0.04*
V-VI	1.32 \pm 0.07	1.75 \pm 0.04*
entorhinal cortex	1.21 \pm 0.13	1.85 \pm 0.11*
inferior colliculus	1.02 \pm 0.05	1.13 \pm 0.03
pons	1.10 \pm 0.03	1.22 \pm 0.09
cerebellar hemisphere	1.00 \pm 0.00	1.00 \pm 0.00
cerebellar white matter	0.96 \pm 0.05	1.15 \pm 0.03*
superior olivary nucleus	1.03 \pm 0.06	1.22 \pm 0.03

Uptake of [125 I]MK801 or [125 I]CNS 1261 in individual regions of interest were expressed as a ratio relative to uptake within the cerebellum. Roman numerals (I-VI) indicate the cortical layer examined. Data are presented as mean \pm S.E.M, n=3.

*p<0.05, unpaired t-test.

TABLE 13
Comparison of [^{125}I]MK801 and [^{125}I]CNS 1261 uptake
120 minutes post-administration

STRUCTURE	[^{125}I]MK801	[^{125}I]CNS 1261
anterior cingulate cortex	1.32 ± 0.10	$1.69 \pm 0.10^*$
genu	1.01 ± 0.07	1.42 ± 0.16
caudate nucleus	1.16 ± 0.08	1.38 ± 0.05
sensory-motor cortex		
layers I-III	1.20 ± 0.11	1.40 ± 0.05
IV	1.22 ± 0.10	1.39 ± 0.07
V-VI	1.22 ± 0.10	1.51 ± 0.09
corpus callosum	1.07 ± 0.07	$1.47 \pm 0.08^*$
anterior thalamus	1.35 ± 0.12	1.58 ± 0.04
hippocampus CA1	1.71 ± 0.10	$2.44 \pm 0.21^*$
hippocampus CA3	1.63 ± 0.10	$2.43 \pm 0.19^*$
lateral habenular nucleus	1.18 ± 0.07	1.20 ± 0.03
mediodorsal thalamus	1.44 ± 0.09	1.61 ± 0.09
ventrolateral thalamus	1.36 ± 0.12	1.56 ± 0.09
internal capsule	1.07 ± 0.07	1.11 ± 0.04
parietal cortex		
layers I-III	1.32 ± 0.07	1.55 ± 0.08
IV	1.32 ± 0.07	1.49 ± 0.05
V-VI	1.29 ± 0.07	$1.68 \pm 0.10^*$
hypothalamus	0.98 ± 0.07	1.05 ± 0.04
posterior cingulate cortex	1.25 ± 0.11	1.51 ± 0.06
hippocampus molecular layer	1.72 ± 0.15	$2.91 \pm 0.22^*$
dentate gyrus	1.57 ± 0.12	$2.50 \pm 0.15^*$
auditory cortex		
layers I-III	1.31 ± 0.11	$1.63 \pm 0.06^*$
IV	1.30 ± 0.10	$1.64 \pm 0.05^*$
V-VI	1.36 ± 0.11	$1.77 \pm 0.05^*$
substantia nigra pars compacta	1.05 ± 0.09	1.24 ± 0.04
substantia nigra pars reticulata	1.08 ± 0.07	1.17 ± 0.05
medial geniculate	1.29 ± 0.07	1.49 ± 0.05
visual cortex		
layers I-III	1.33 ± 0.14	1.73 ± 0.09
IV	1.32 ± 0.13	1.64 ± 0.09
V-VI	1.31 ± 0.12	$1.67 \pm 0.04^*$
entorhinal cortex	1.24 ± 0.14	$1.91 \pm 0.11^*$
inferior colliculus	1.13 ± 0.09	1.08 ± 0.01
pons	1.08 ± 0.10	1.31 ± 0.06
cerebellar hemisphere	1.00 ± 0.00	1.00 ± 0.00
cerebellar white matter	0.95 ± 0.03	1.25 ± 0.14
superior olivary nucleus	1.04 ± 0.05	1.19 ± 0.07

Uptake of [^{125}I]MK801 or [^{125}I]CNS 1261 in individual regions of interest were expressed as a ratio relative to uptake within the cerebellum. Roman numerals (I-VI) indicate the cortical layer examined. Data are presented as mean \pm S.E.M, $n=3$. * $p<0.05$, unpaired t-test.

[¹²⁵I]MK801

[¹²⁵I]CNS 1261

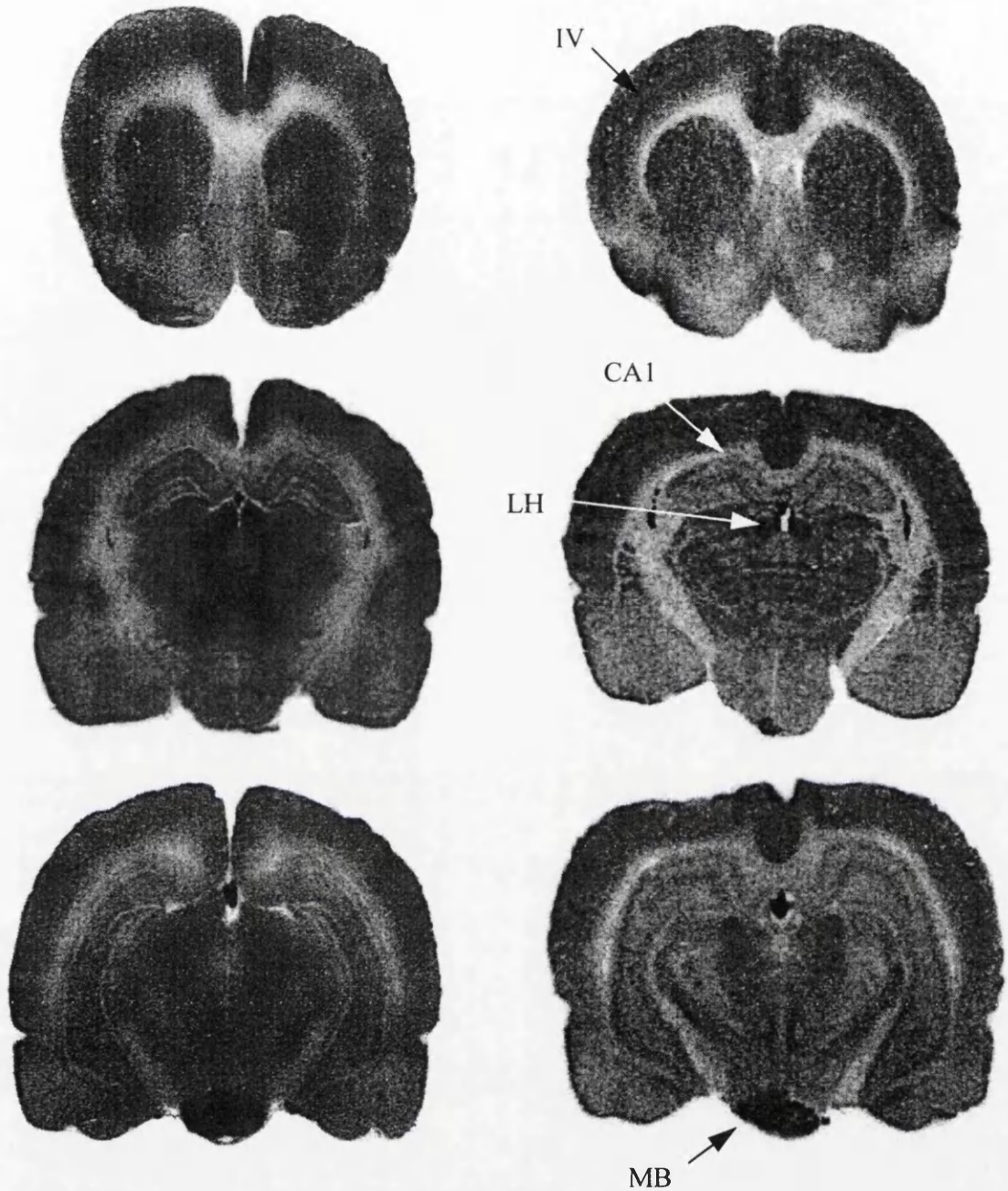


FIGURE 16 : Comparison of [¹²⁵I]MK801 and [¹²⁵I]CNS 1261 uptake at 5 minutes

Representative autoradiograms illustrate [¹²⁵I]MK801 (left) and [¹²⁵I]CNS 1261 (right) uptake 5 minutes after administration at the level of the caudate nucleus (upper), dorsal hippocampus (middle) and hippocampus molecular layer (lower). For both tracers, uptake was greatest in areas known to have high levels of blood flow such as cortical areas and within the mamillary body. Note that [¹²⁵I]CNS 1261 images possess a greater degree of clarity relative to [¹²⁵I]MK801 images. (IV : cortical layer IV, CA1 : hippocampus CA1, L : lateral habenula, MB : mamillary body).

Thirty minutes after administration, [^{125}I]CNS 1261 uptake was greatest within the anterior cingulate cortex (90% greater than that observed within the cerebellum). High levels of [^{125}I]CNS 1261 uptake were observed within the auditory and visual cortices where levels were approximately 50% above cerebellar values (Figure 17). Little variation in [^{125}I]CNS 1261 uptake could be observed between cortical layers. Lowest levels of [^{125}I]CNS 1261 uptake were observed within white matter areas. Uptake within genu, corpus callosum and internal capsule was generally 30% lower than that within the cerebellar hemisphere.

At times beyond 30 minutes, the highest levels of uptake of [^{125}I]CNS 1261 were observed within the hippocampus (notably CA1 and the molecular layer), with intermediate levels in the cortex and caudate nucleus and lowest levels in the hypothalamus and cerebellum (reflecting the known distribution of NMDA receptors). 60 minutes after injection [^{125}I]CNS 1261 uptake within hippocampal areas and within the entorhinal cortex was 80-100% greater than that within the cerebellum. Uptake in cortical areas was 50-70% above cerebellar values (Figure 18).

The relative uptake of [^{125}I]CNS 1261 within hippocampal areas continued to increase between 60 and 120 minutes. [^{125}I]CNS 1261 uptake within CA1, CA3, molecular layer and dentate gyrus was 150-200% greater than that observed within the cerebellum. Intermediate levels, 50-70% above that in the cerebellum were observed within anterior cingulate cortex, thalamus, and auditory, parietal and visual cortices. [^{125}I]CNS 1261 uptake was greatest within the deepest layers (V-VI) of the cortex. Lowest levels of uptake were present in areas of white matter, hypothalamus and pons (Figure 19).

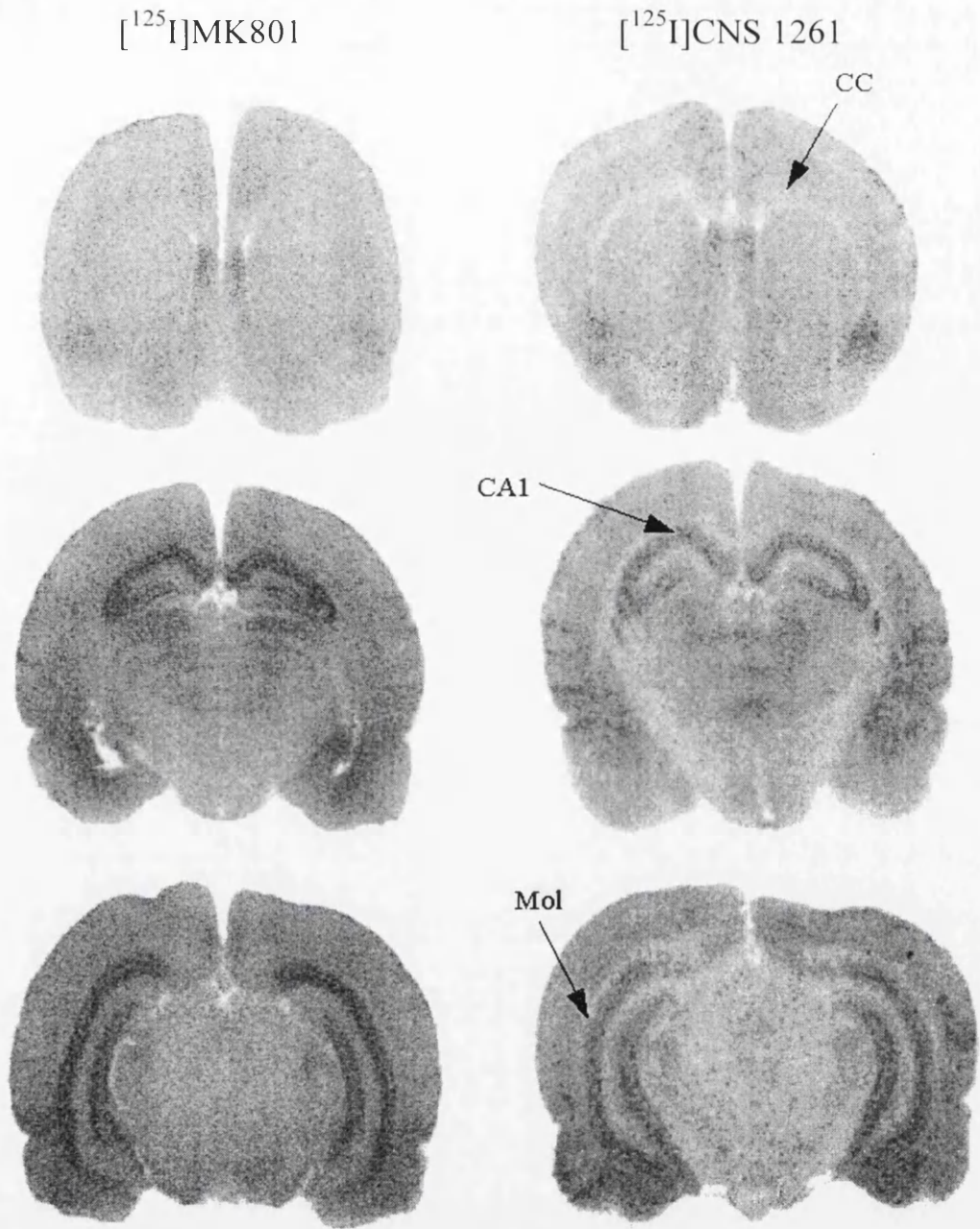


FIGURE 18: Comparison of [^{125}I]MK801 and [^{125}I]CNS 1261 uptake at 60 minutes

Representative autoradiograms illustrate [^{125}I]MK801 (left) and [^{125}I]CNS 1261 (right) uptake 60 minutes after administration at the level of the caudate nucleus (upper), dorsal hippocampus (middle) and hippocampus molecular layer (lower). Greatest levels of uptake for both tracers were observed within cortical areas and hippocampal structures. Note that [^{125}I]CNS 1261 uptake is lower than that of [^{125}I]MK801 in white matter areas. (CC : corpus callosum, CA1 : hippocampus CA1, Mol : molecular layer).

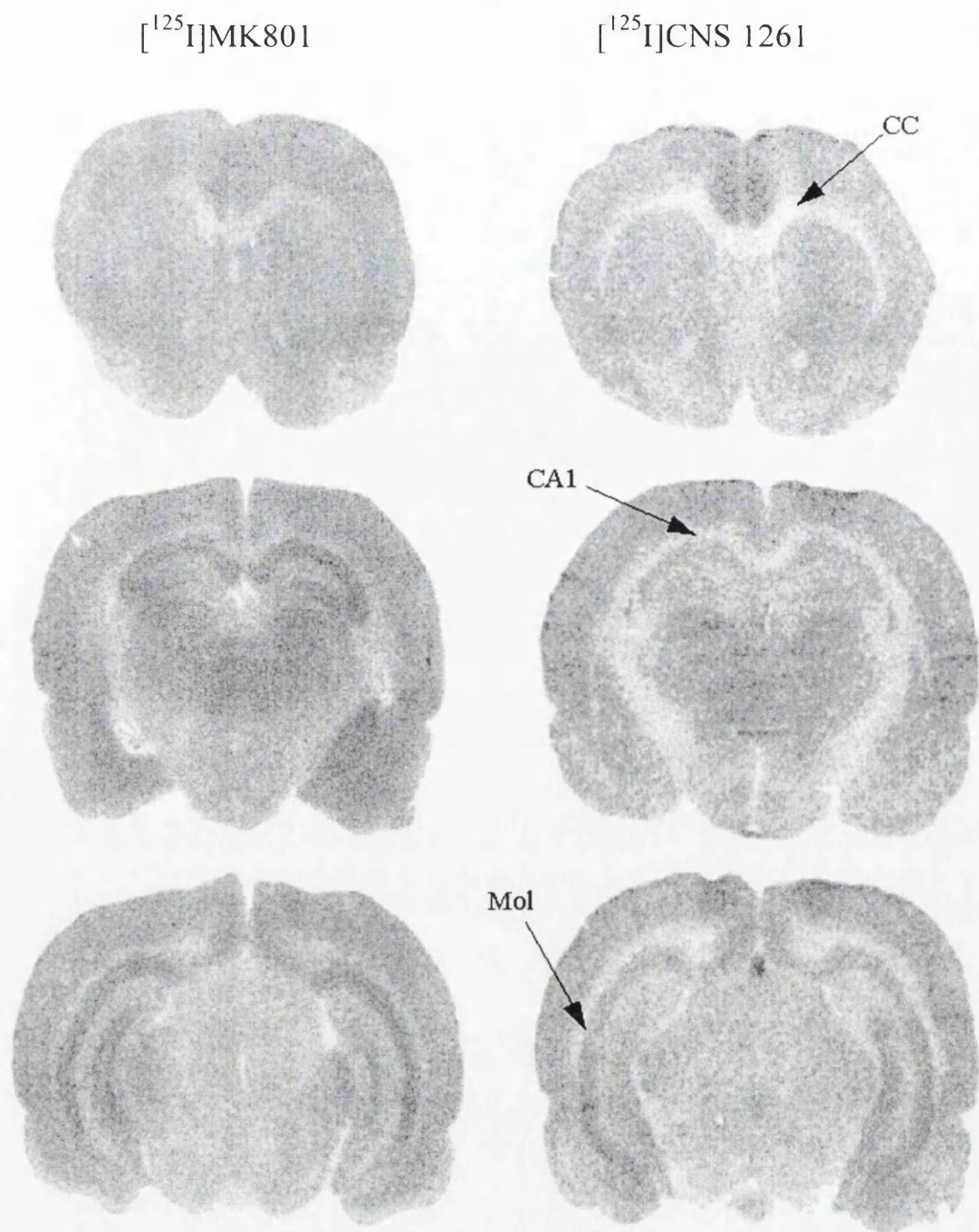


FIGURE 17 : Comparison of [^{125}I]MK801 and [^{125}I]CNS 1261 uptake at 30 minutes

Representative autoradiograms illustrate [^{125}I]MK801 (left) and [^{125}I]CNS 1261 (right) uptake 30 minutes after administration at the level of the caudate nucleus (upper), dorsal hippocampus (middle) and hippocampus molecular layer (lower). Greatest levels of uptake for both tracers were observed within cortical areas and hippocampal structures. Note that [^{125}I]CNS 1261 uptake is lower than that of [^{125}I]MK801 in white matter areas. (CC : corpus callosum, CA1 : hippocampus CA1, Mol : molecular layer).

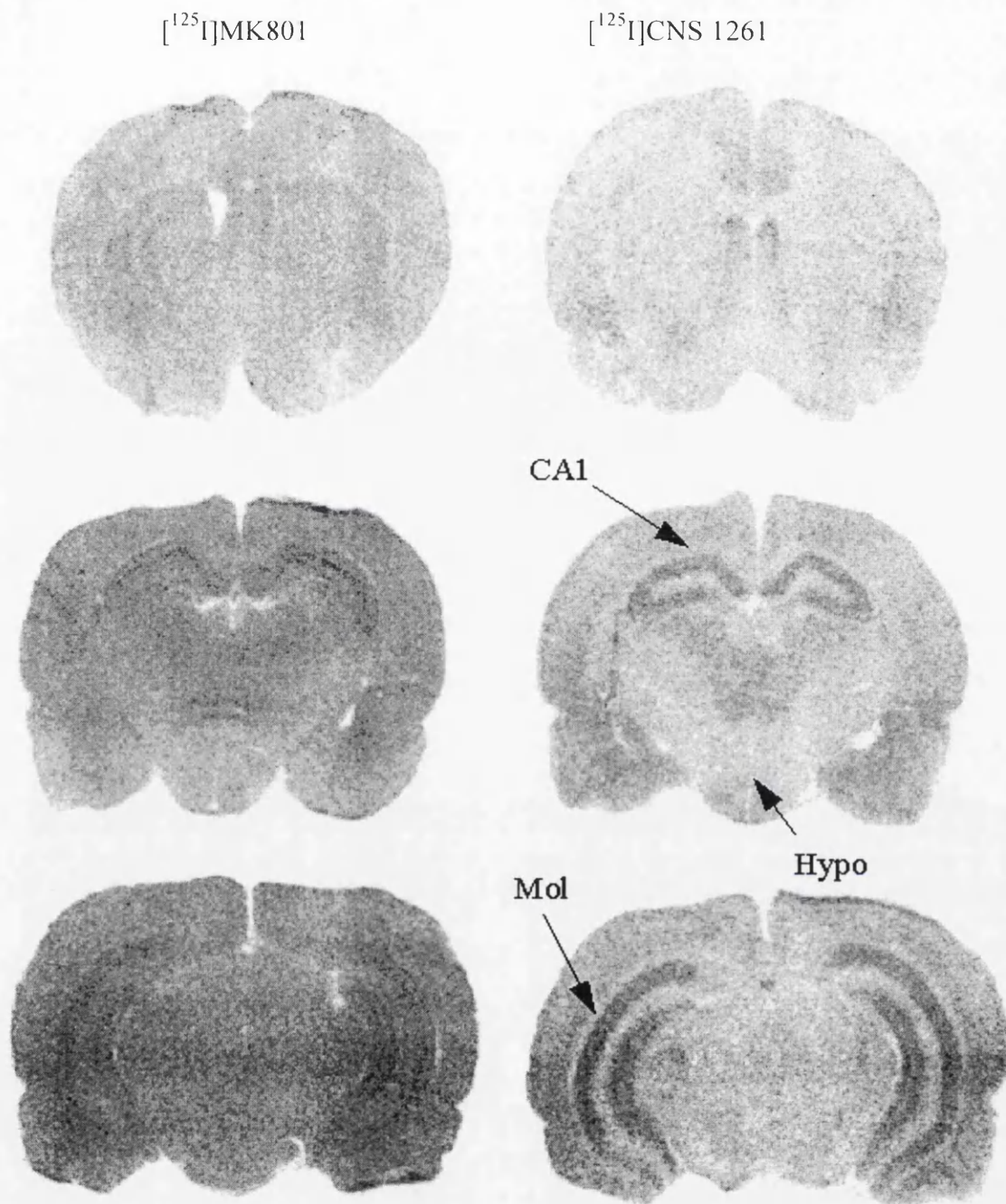


FIGURE 19 : Comparison of $[^{125}\text{I}]\text{MK801}$ and $[^{125}\text{I}]\text{CNS 1261}$ uptake at 120 minutes

Representative autoradiograms illustrate $[^{125}\text{I}]\text{MK801}$ (left) and $[^{125}\text{I}]\text{CNS 1261}$ (right) uptake 120 minutes after administration at the level of the caudate nucleus (upper), dorsal hippocampus (middle) and hippocampus molecular layer (lower). For both tracers uptake was greatest within hippocampal structures with lower levels observed within the hypothalamus (CA1 : hippocampus CA1, Mol, molecular layer, Hypo : hypothalamus).

3.3.3 Comparison of [^{125}I]CNS 1261 uptake with [^{125}I]MK801

[^{125}I]MK801 uptake and retention was examined in contemporaneous experiments and compared to that of [^{125}I]CNS 1261 at each time point (Figures 16-19)

Despite general similarities in the pattern of uptake of both tracers at 5 minutes, the appearance of the images differed markedly. The resolution of [^{125}I]MK801 images was poor and the overall appearance was similar to images produced with the blood flow tracer $^{99\text{m}}\text{Tc}$ -HMPAO (Gartshore, 1996). In comparison, [^{125}I]CNS 1261 images possessed a greater degree of clarity with cortical layer IV clearly visible on autoradiograms (Figure 20). Increased [^{125}I]CNS 1261 uptake was observed in the supraoptic and paraventricular hypothalamic nuclei. These regions were not evident in [^{125}I]MK801 autoradiograms at 5 minutes (Figure 21).

At 30 minutes, [^{125}I]MK801 uptake was greatest within hippocampal structures (approximately 40% greater than cerebellar levels) with intermediate levels in cortical areas (20% above cerebellum).

The relative uptake of [^{125}I]CNS 1261 at this time point was generally 20% higher than that of [^{125}I]MK801 within the caudate nucleus and cortical areas and approximately 40% greater within the entorhinal cortex and the pons. Relative [^{125}I]CNS 1261 uptake was not markedly different from that of [^{125}I]MK801 in any of the other regions examined at this time point.

Sixty minutes after administration of the tracers, the overall pattern of [^{125}I]CNS 1261 uptake was similar to that of [^{125}I]MK801 however, the relative uptake of [^{125}I]CNS 1261 was greater than that of [^{125}I]MK801 in 14 of the 36 regions examined. [^{125}I]CNS 1261 uptake was significantly greater in the caudate nucleus, sensory-motor, parietal, auditory, visual and entorhinal cortices compared to [^{125}I]MK801. Within the hippocampus (a region with high levels of NMDA receptors) tracer uptake relative to the cerebellum was similar for both ligands 60 minutes after injection.

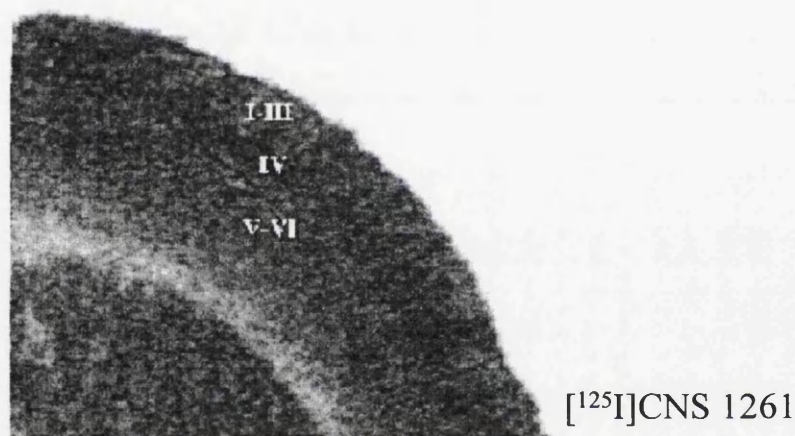


FIGURE 20 : [¹²⁵I]CNS 1261 uptake is increased in cortical layer IV 5 minutes after administration

Representative autoradiograms of [¹²⁵I]MK801 (upper) and [¹²⁵I]CNS 1261 (lower) uptake in the sensory-motor cortex 5 minutes after intravenous administration. [¹²⁵I]CNS 1261 uptake was increased within cortical layer IV, while [¹²⁵I]MK801 uptake was homogeneous throughout the cortex.

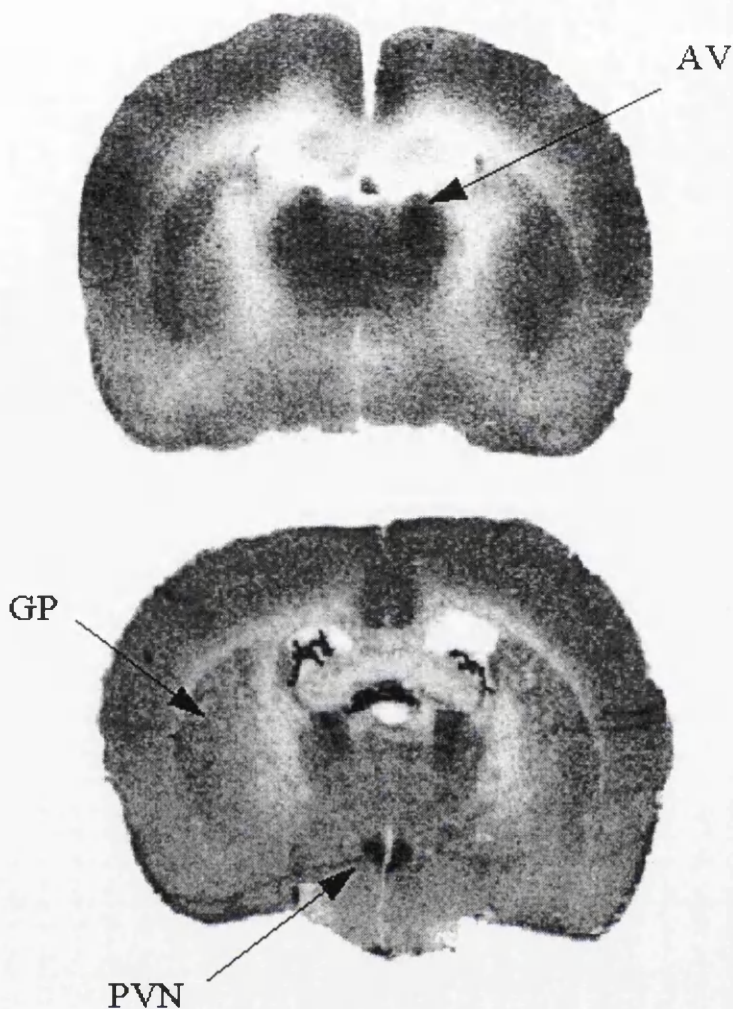


FIGURE 21 : [^{125}I]CNS 1261 uptake is increased within the paraventricular hypothalamic nucleus

Representative autoradiograms from the level of the globus pallidus comparing [^{125}I]MK801 (upper) and [^{125}I]CNS 1261 (lower) uptake in the normal brain 5 minutes after administration. High levels of both tracers are observed within the cerebral cortex and anteroventral thalamus. Only [^{125}I]CNS 1261 uptake is increased within the paraventricular hypothalamic nucleus. Note the greater degree of clarity within the [^{125}I]CNS 1261 autoradiogram. (AV : anteroventral thalamus, GP : globus pallidus, PVN : paraventricular hypothalamic nucleus).

120 minutes after intravenous injection uptake of [^{125}I]CNS 1261 was significantly greater than that of [^{125}I]MK801 in 12 of the 36 regions examined (anterior cingulate cortex, corpus callosum, hippocampus CA1 and CA3, superior layers of the parietal cortex, hippocampus molecular layer, dentate gyrus, auditory cortex, deep layers of the visual cortex and entorhinal cortex). The relative levels of [^{125}I]CNS 1261 were 40-70% greater than that of [^{125}I]MK801 in the majority of cortical areas examined (parietal, auditory, visual and entorhinal) and 40% greater than that of [^{125}I]MK801 in most white matter areas (Figure 22). A degree of laminar heterogeneity in the radioisotope concentrations in the cerebral cortex was observed with [^{125}I]CNS 1261, deep layers had higher isotope levels than superficial layers. Isotope levels were homogeneous within the cerebral cortex of [^{125}I]MK801 autoradiograms. The most striking observation was that the relative uptake of [^{125}I]CNS 1261 in hippocampal structures was approximately twice that of [^{125}I]MK801, (140% and 70% greater than cerebellar binding respectively) (Figure 23).

Under conditions of normal activation at the premium time point established for imaging [^{125}I]MK801 uptake (120 minutes), the relative uptake of [^{125}I]CNS 1261 was thus found to be superior to that of [^{125}I]MK801 in areas with a high density of NMDA receptors and hence a high level of NMDA receptor activation.

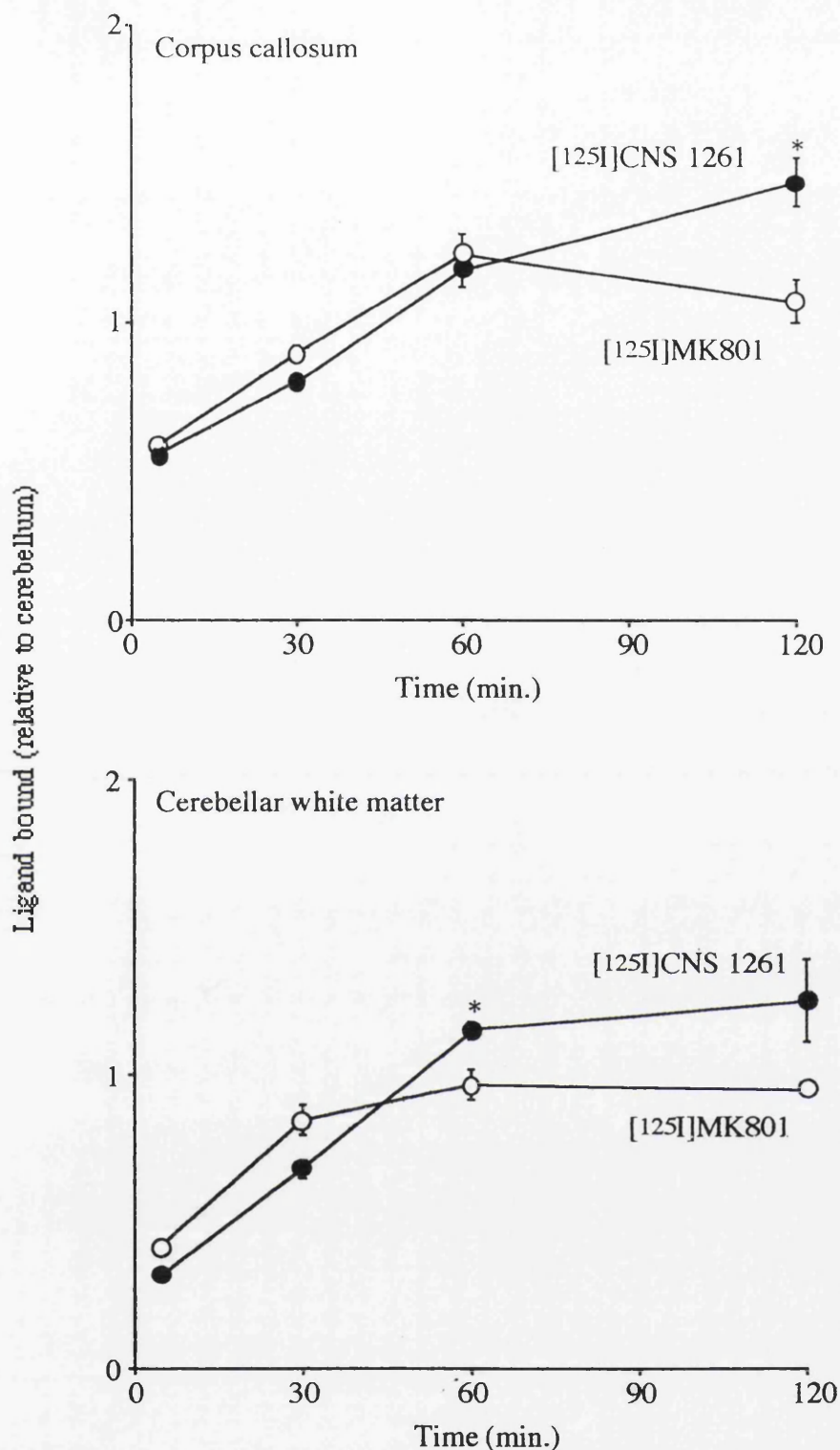


FIGURE 22 : Uptake and retention of [¹²⁵I]CNS 1261 and [¹²⁵I]MK801 in white matter

The uptake and retention of [¹²⁵I]CNS 1261 and [¹²⁵I]MK801 (relative to the cerebellum) was examined at different time points in normal brain. Uptake over the first 60 min. was similar for both ligands. At 120 min. relative levels of [¹²⁵I]CNS 1261 were approximately 40% above that of [¹²⁵I]MK801. Data are mean \pm S.E.M. (n = 2-4). *p<0.05, significantly different from [¹²⁵I]MK801 (unpaired t-test).

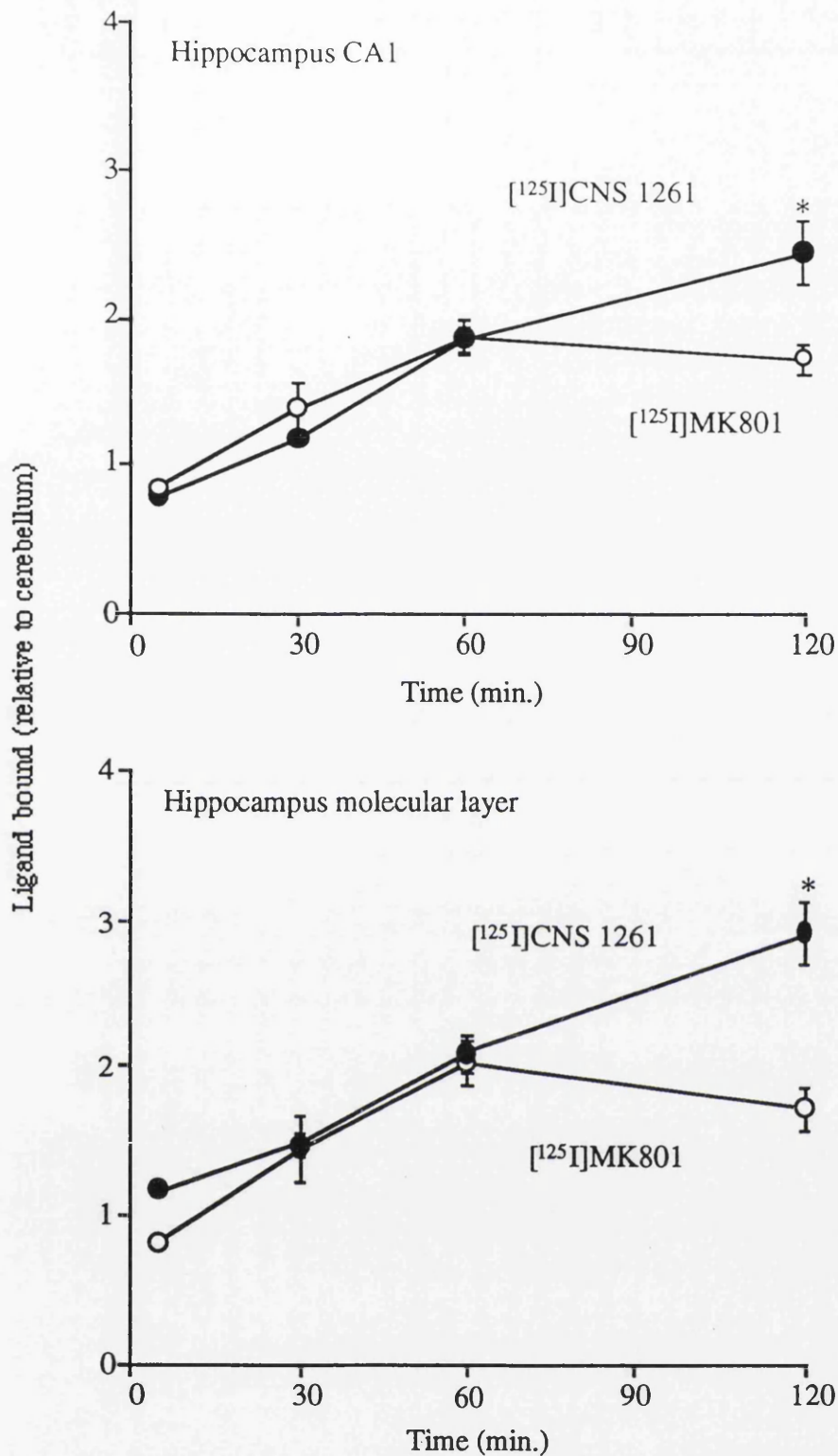


FIGURE 23 : Uptake and retention of [¹²⁵I]CNS 1261 and [¹²⁵I]MK801 in hippocampus

The uptake and retention of [¹²⁵I]CNS 1261 and [¹²⁵I]MK801 (relative to the cerebellum) was examined at different time points in normal brain. Uptake over the first 60 min. was similar for both ligands. At 120 min. relative levels of [¹²⁵I]CNS 1261 were approximately twice that of [¹²⁵I]MK801. Data are mean \pm S.E.M. (n = 2-4). *p<0.05, significantly different from [¹²⁵I]MK801 (unpaired t-test).

3.4 Relative lipophilicity of [125 I]CNS 1261 and [125 I]MK801

3.4.1 Lipophilicity of CNS 1261

The calculated LogD value for CNS 1261 at physiological pH is shown in Table 14. The logD values for structurally related (CNS 1102) and unrelated (MK801 and iodo-MK801) non-competitive NMDA receptor antagonists are shown for comparison. CNS 1261 has a higher LogD value and hence is more lipophilic than CNS 1102. CNS 1261 is more lipophilic than the structurally unrelated compound MK801, but has a lower LogD value and is therefore less lipophilic than iodo-MK801.

3.4.2 Partition coefficient of [125 I]CNS 1261 and [125 I]MK801 in rat brain

Brain/aqueous partition ratios were calculated for [125 I]CNS 1261 and [125 I]MK801 in rat brain and are presented in Table 15. The brain/aqueous partition ratios for [3 H]MK801 are shown for comparison.

The brain/aqueous partition ratios for [125 I]CNS 1261 and [125 I]MK801 show a higher accumulation in brain tissue relative to aqueous solution. The partition ratio for [3 H]MK801 was markedly lower than [125 I]MK801 in rat brain sections.

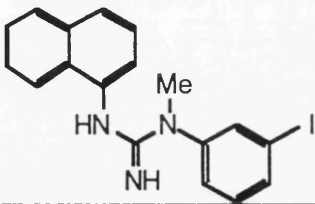
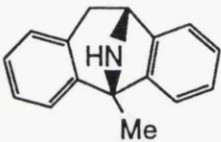
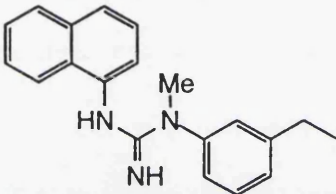
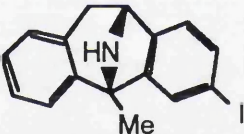
The brain/aqueous partition ratio for [125 I]CNS 1261 in rat brain was approximately 40% lower than that of [125 I]MK801, 20.6 ± 13 g/ml compared to 35.5 ± 4.6 g/ml.

3.4.3 Partition coefficient of [125 I]CNS 1261 and [125 I]MK801 in human brain

The brain/aqueous partition ratio of [125 I]CNS 1261 was also 40% lower than that of [125 I]MK801 (14.8 ± 0.8 g/ml relative to 25.5 ± 1.5 g/ml) in human grey matter (Table 15). The partition coefficient may be indicative of the degree of non-specific binding.

TABLE 14

LogD values for CNS 1261 and other non-competitive NMDA antagonists

Compound	Structure	LogD _{7.4}
CNS 1261		2.19
MK801		1.80
CNS 1102		1.72
I-MK801		3.30

LogD_{7.4} values, the partition coefficient between organic solvent (octanol) and aqueous buffer (15mM HEPES buffer / 0.135M NaCl) at physiological pH, are shown for CNS 1261, the related compound CNS 1102, MK801 and iodo-MK801.

Note that while CNS 1261 is more lipophilic than MK801 and CNS 1102, it is less lipophilic than iodo-MK801. Data supplied by Cambridge NeuroScience Inc.

TABLE 15

Brain/ aqueous partiton ratios in rat and human brain

LIGAND	BRAIN/AQUEOUS RATIO (g/ml)	
	Rat	Human (grey)
[¹²⁵ I]CNS 1261	20.6 ± 1.3	14.8 ± 0.8
[¹²⁵ I]MK801	35.5 ± 4.6	25.5 ± 1.5
[³ H]MK801	4.5 ± 0.3	9.7 ± 0.4

Brain/aqueous partition ratios for [¹²⁵I]CNS 1261, [¹²⁵I]MK801 and [³H]MK801 were calculated from the non-specific binding component of *in vitro* binding experiments. Ratios were calculated from the amount of non-specifically bound radioligand (dpm/g) and the amount of free radioligand present in the solution applied to the section (dpm/ml). Data are presented as mean ± S.E.M., n=6.

Note that [¹²⁵I]CNS 1261 has a lower brain/aqueous partition ratio than [¹²⁵I]MK801 in both rat and human sections.

3.5 Metabolism of [^{125}I]CNS 1261 in the rat

3.5.1 Stability of [^{125}I]CNS 1261 *in vitro*

Prior to investigation of the metabolism of [^{125}I]CNS 1261 *in vivo*, the stability of the compound under routine storage conditions was examined by determination of the amount of deiodination which occurred. [^{125}I]CNS 1261 was reconstituted in a 0.7% physiological saline solution identical to that used for intravenous injection of the tracer *in vivo*. The reconstituted tracer solution was stored at 4°C for approximately 4 weeks. High performance liquid chromatography (hplc) analysis of samples from the solution showed that little deiodination of [^{125}I]CNS 1261 occurred under the storage conditions described moreover, no significant deiodination of [^{125}I]CNS 1261 was observed following incubation of the aqueous solution in rat plasma at 37°C for 2 hours.

The amount of authentic tracer and degradation products present in [^{125}I]CNS 1261 injectate solutions from actual *in vivo* experiments was also examined (Table 16) and compared to that from experiments using [^{125}I]MK801.

[^{125}I]CNS 1261 injectate solutions, reconstituted up to 6 hours prior to hplc analysis (and stored at room temperature), were found to contain approximately 90% authentic tracer. [^{125}I]MK801 injectate solutions did not contain a significantly different amount of authentic material

3.5.2 Metabolism of [^{125}I]CNS 1261 in the rat

Representative hplc traces from plasma samples taken at 5, 15, 60 and 120 minutes following intravenous administration of [^{125}I]CNS 1261 are shown in Figure 24. The traces show the presence of two species in the plasma samples. The first species eluted with a retention time of 2.9 min and corresponds to iodide, the second species had a retention time of 7.6 min and was identified as authentic [^{125}I]CNS 1261.

TABLE 16
Species present in isotope solutions 6 hours after reconstitution

SPECIES	[¹²⁵ I]CNS 1261	[¹²⁵ I]MK801
authentic tracer	91.2 ± 5.9	95.7 ± 2.18
iodide	8.8 ± 5.9	4.3 ± 2.18
other	-	2.0 ± 0.0

Data are presented as mean ± S.E.M. (n = 3). Injectate solutions were reconstituted approximately 6 hours prior to hplc analysis. The amount of authentic material present in the injectate solutions was not different for the two tracers. The identity of the third species, present in only one of the [¹²⁵I]MK801 animals was not determined.

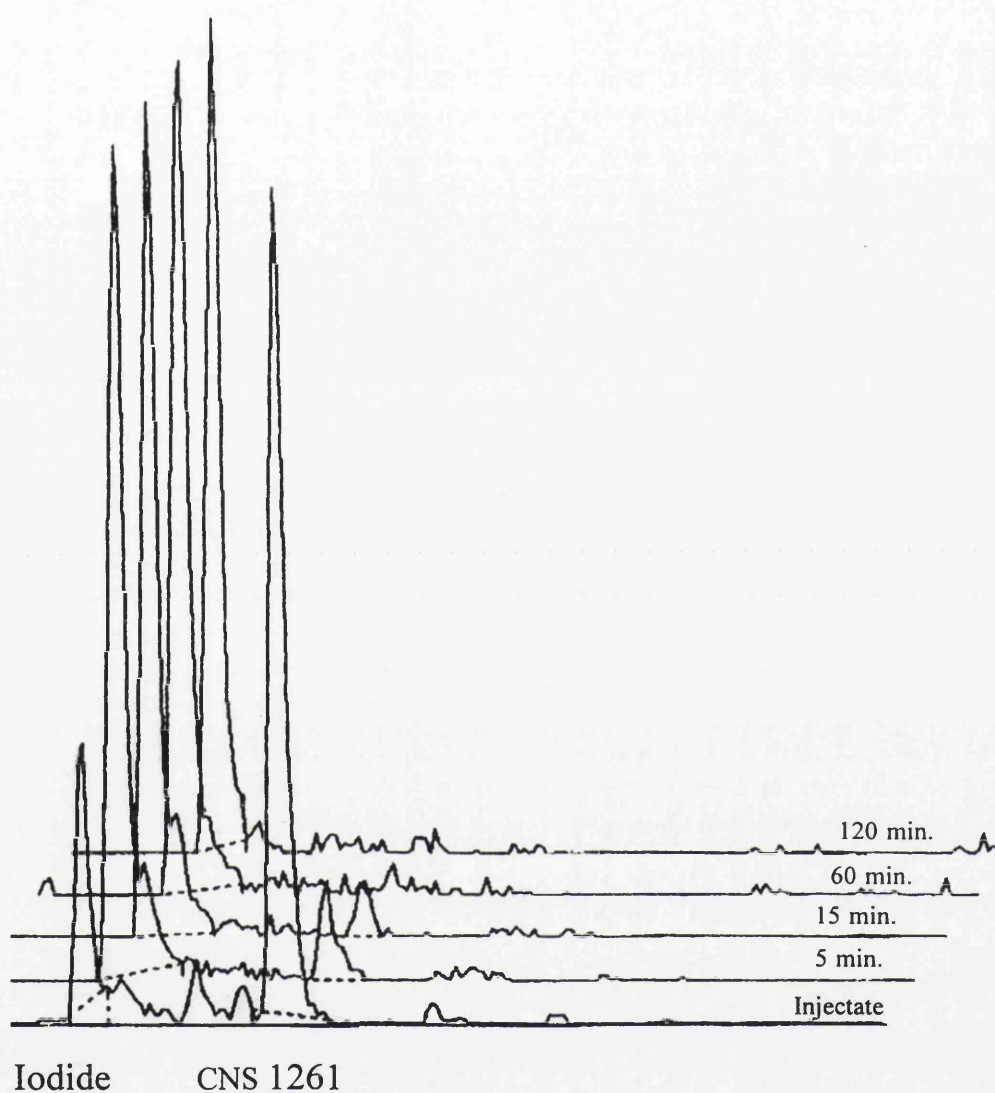


FIGURE 24 : Metabolism of [^{125}I]CNS 1261 in the rat

Representative hplc traces from plasma samples taken at 5, 15, 60 and 120 minutes after administration of the tracer show the presence of 2 species which were identified as free iodide and authentic CNS 1261. The amount of [^{125}I]CNS 1261 decreased rapidly over time while the amount of free iodide increased.

These traces show that the amount of authentic tracer decreased and the amount of free iodide increased with time.

[¹²⁵I]CNS 1261A was metabolised extremely rapidly, such that only 15% authentic material remained in the plasma at 5 minutes and no authentic [¹²⁵I]CNS 1261 could be detected in the plasma at 60 or 120 minutes (Figure 25).

Hplc analysis of all species present within the brain homogenate at 120 minutes confirmed that almost all the radioactivity within the brain could be attributed to authentic [¹²⁵I]CNS 1261 ($95.4 \pm 2.3\%$). In some instances, a small fast moving peak ($4.6 \pm 2.3\%$) could also be identified in brain extracts from animals killed at 120 minutes.

3.5.3 Metabolism of [¹²⁵I]MK801 in the rat

Plasma samples were also taken from a second group of animals at 5, 15, 60 and 120 min following intravenous injection of [¹²⁵I]MK801. Hplc traces are shown in Figure 26. The majority of traces showed the presence of only two species, with retention times of 2.9 min. and 8.3 min. which were identified as iodide and authentic [¹²⁵I]MK801 respectively. The amount of authentic [¹²⁵I]MK801 was found to decrease and the amount of iodide to increase with time. In a single animal, the amount of a third (unidentified) species was also found to increase with time. This retention time of this species was approximately 4.5 minutes.

[¹²⁵I]MK801 was metabolised slowly, with approximately 55% authentic tracer present in the plasma at 5 minutes and approximately 20% [¹²⁵I]MK801 could be detected at 120 minutes (Figure 27). Hplc analysis of all species present within the brain homogenate at 120 minutes confirmed that almost all (95%) of the radioactivity within the brain could be attributed to authentic [¹²⁵I]MK801.

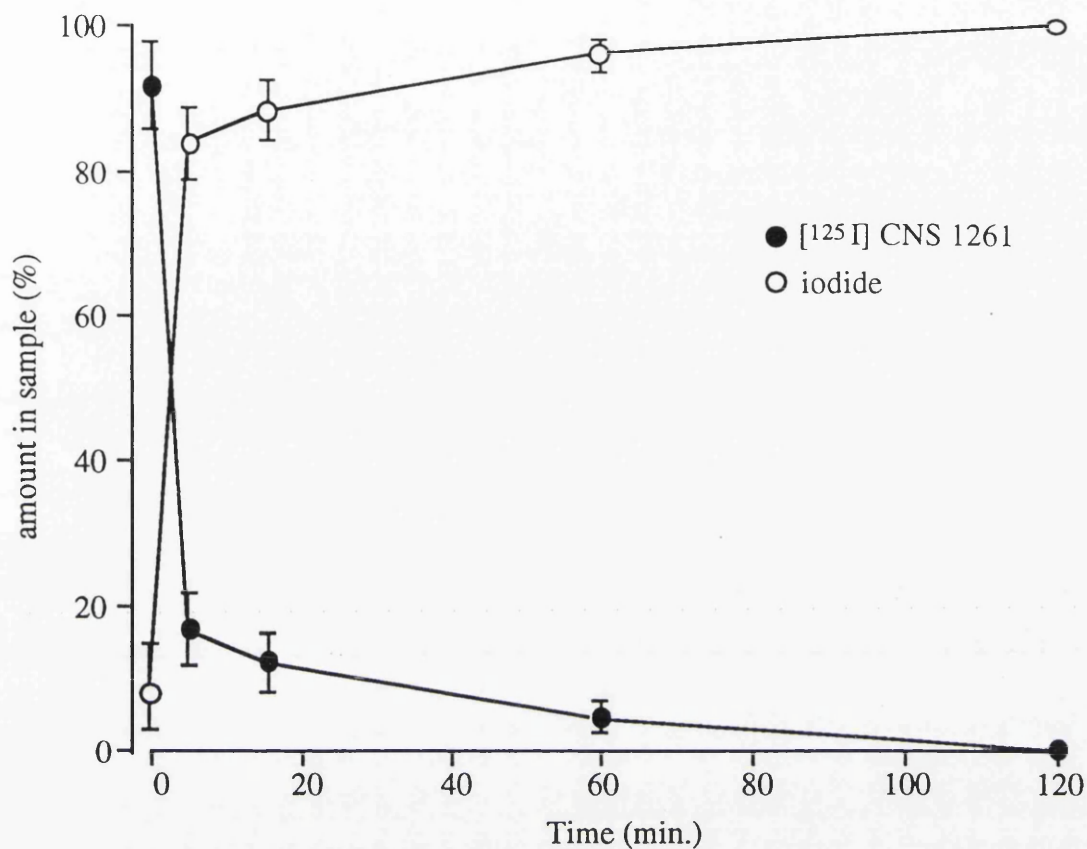


FIGURE 25 : Timecourse of [¹²⁵I]CNS 1261 metabolism in rat plasma.

Data represents levels of authentic [¹²⁵I]CNS 1261 and iodide detected by hplc analysis of rat plasma samples at different time points following intravenous injection of [¹²⁵I]CNS 1261. Data are expressed as means ± S.E.M., n=3.

Note the rapid clearance of authentic [¹²⁵I]CNS 1261 from the plasma within the first 5 minutes after injection.

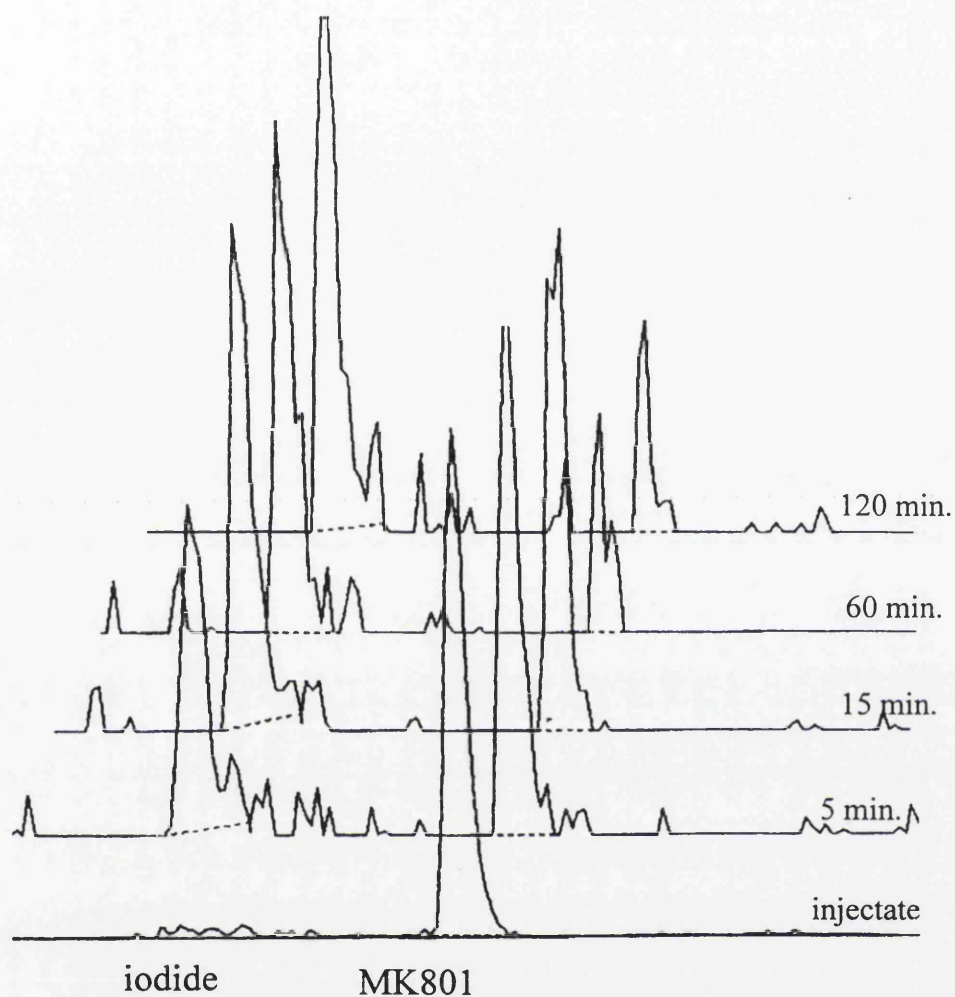


FIGURE 26 : Metabolism of [^{125}I]MK801 in the rat

Representative hplc traces from plasma samples taken at 5, 15, 60 and 120 minutes after administration of the tracer show the presence of 2 species which were identified as free iodide and authentic MK801. The amount of [^{125}I]MK801 decreased over the experiemntal period while the amount of free iodide increased

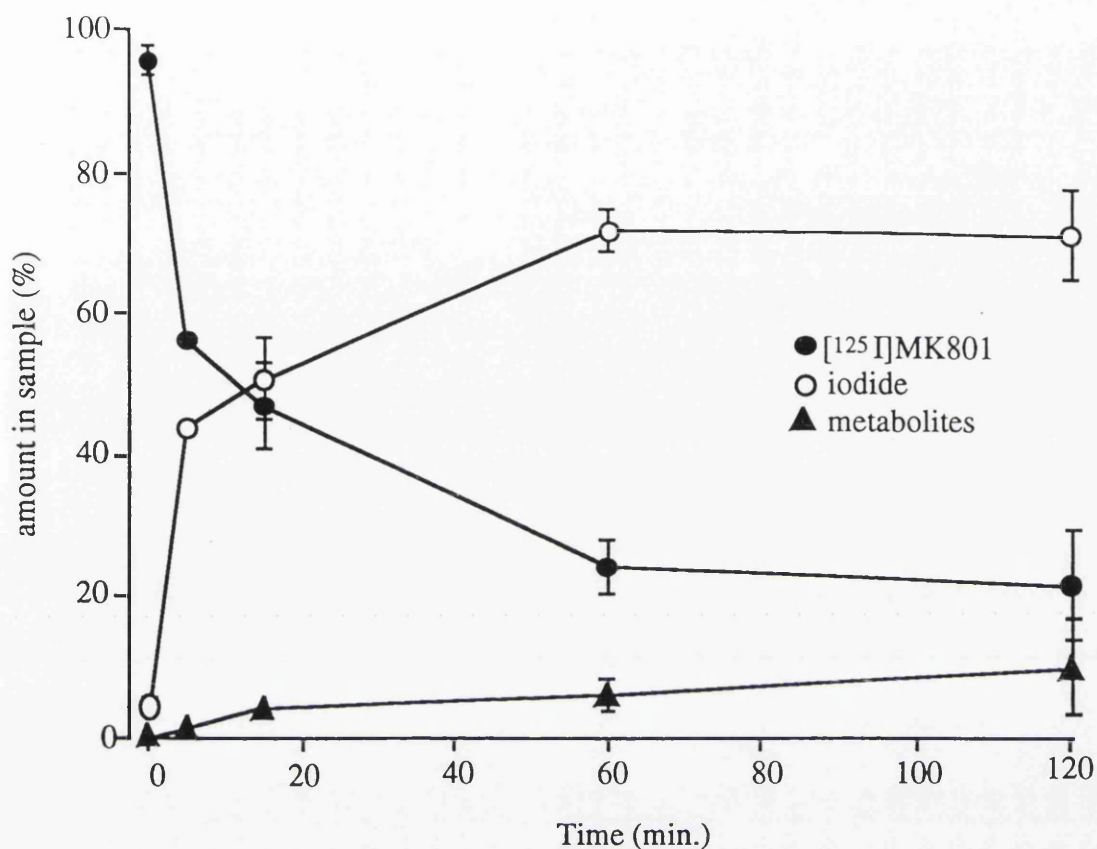


FIGURE 27 : Timecourse of $[^{125}\text{I}]\text{MK801}$ metabolism in rat plasma.

Data represents levels of authentic $[^{125}\text{I}]\text{MK801}$, iodide and metabolites detected by hplc analysis of rat plasma samples at different time points following intravenous injection of $[^{125}\text{I}]\text{MK801}$. Data are expressed as means \pm S.E.M., $n=3$.

Too few data points were available to calculate accurate plasma half-lives of the two tracers. However, log transforms of the plasma clearance curves (Figure 28) show that in the first 60 minutes after injection, both [^{125}I]CNS 1261 and [^{125}I]MK801 clearance can be described by bioexponential kinetics. Log transforms of the plasma clearance curves also show that [^{125}I]CNS 1261 is metabolised much more rapidly than [^{125}I]MK801. The rapid metabolism of [^{125}I]CNS 1261 suggests that compared to [^{125}I]MK801, this tracer will reach steady-state concentrations within the brain more quickly and non-specifically bound ligand will be washed out down its concentration gradient at a faster rate. These properties may improve the quality of images and decrease imaging time. [^{125}I]CNS 1261 is thus metabolised in such a way as to confer significant advantages over [^{125}I]MK801 as an *in vivo* imaging agent.

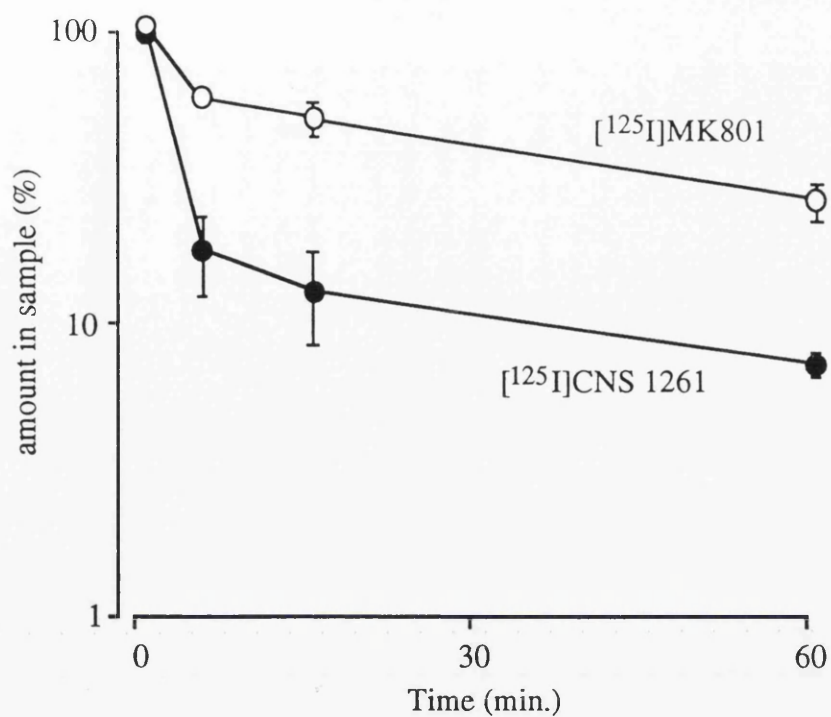


FIGURE 28 : Comparison of plasma clearance of $[^{125}\text{I}]\text{CNS 1261}$ and $[^{125}\text{I}]\text{MK801}$

Data are expressed as mean \pm S.E.M. (n=2-3). Log transforms of the plasma clearance of $[^{125}\text{I}]\text{CNS 1261}$ and $[^{125}\text{I}]\text{MK801}$ show both tracers display biexponential kinetics over the first 60 minutes following injection.

3.6 Effect of pharmacological doses of MK801 on the uptake and retention of [125 I]CNS 1261 in the normal rat brain

The effect of 2 doses of cold MK801 (0.4mg/kg + 6 μ g/kg/min. and 1.2mg/kg + 16 μ g/kg/min) were examined on the uptake and retention of [125 I]CNS 1261 in the normal rat brain.

3.6.1 General Observations

In these investigations [125 I]CNS 1261 was administered 30 minutes after initiation of the MK801 infusion and animals were killed 120 minutes thereafter. Physiological and respiratory variables were recorded prior to (t =0) and 60 minutes after the start of the infusion (Table 17). Administration of a bolus dose and infusion of MK801 (0.4mg/kg + 6 μ g/kg/min. or 1.2mg/kg + 16 μ g/kg/min.) induced an immediate, transient hypotension. Mean arterial blood pressure remained approximately 20mmHg lower than pre-infusion levels for the remainder of the experiment. Administration of MK801 had no effect on any of the parameters examined.

3.6.2. Authenticity of MK801

The batch of MK801 used in these experiments was subjected to nuclear magnetic resonance spectroscopy (NMRS) to determine the authenticity of the compound. NMRS data obtained for the batch of MK801 used (Figure 29) was compared to NMRS data for MK801 within the literature and confirmed that the compound analysed had an identical structure to MK801.

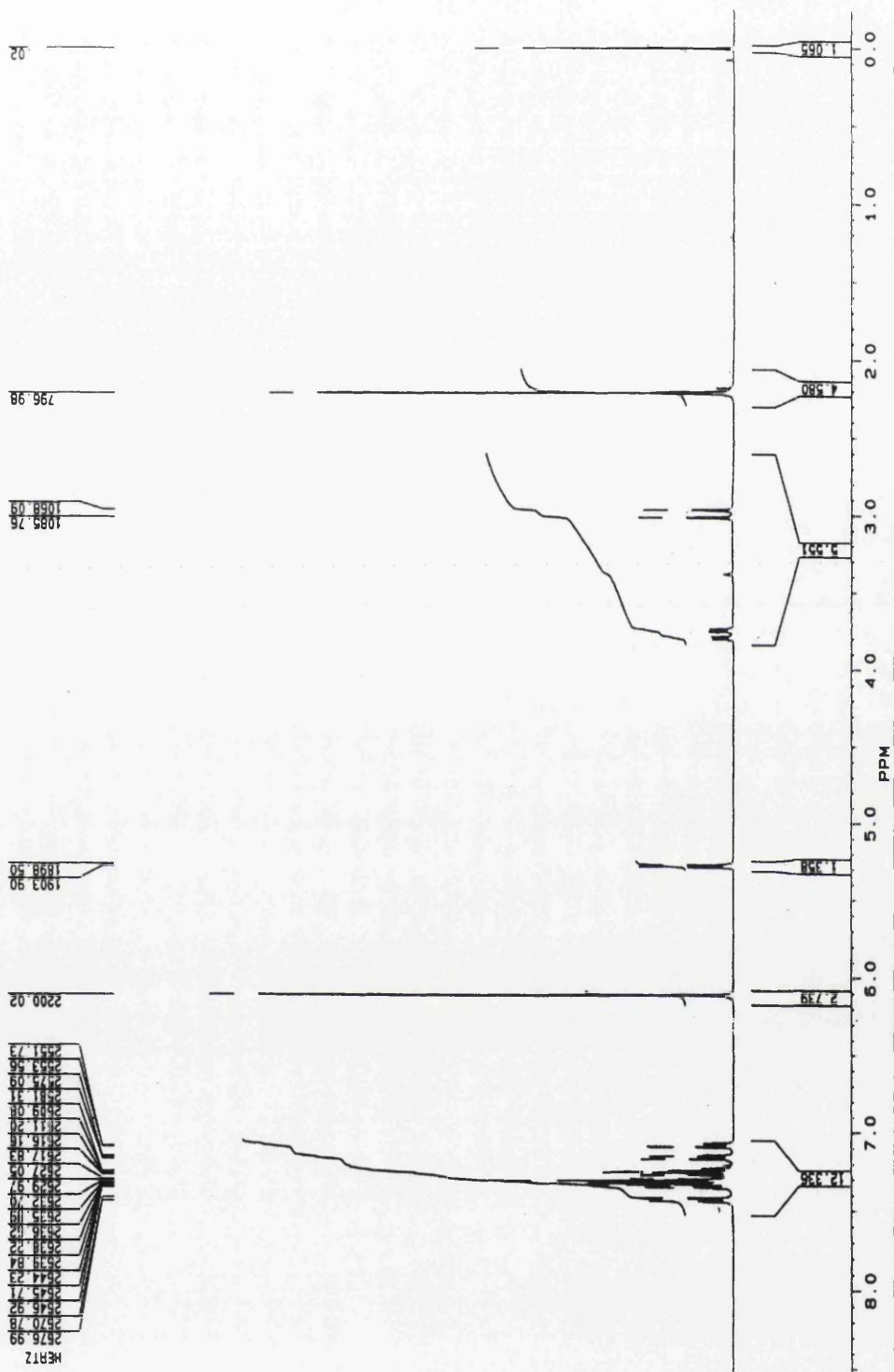
TABLE 17
Physiological variables before and 60 minutes after
initiation of MK801 infusion

Physiological variables	Sample time (min)	MK801 Infusion	
		0.4mg/kg + 6µg/kg/min.	1.2mg/kg + 16µg/kg/min.
p _a CO ₂ (mmHg)	0	40.5 ± 1.2	43.5 ± 3.7
	60	39.3 ± 3.1	40.5 ± 1.5
Arterial pH	0	7.44 ± 0.01	7.33 ± 0.05
	60	7.41 ± 0.01	7.41 ± 0.01
p _a O ₂ (mmHg)	0	154.3 ± 26.5	188.7 ± 13.1
	60	158.3 ± 18.1	192.5 ± 14.4
MABP (mmHg)	0	97 ± 7	85 ± 5
	60	79 ± 1	70 ± 5
temperature (°C)	0	37.2 ± 0.20	37.0 ± 0.03
	60	37.0 ± 0.20	36.9 ± 0.22

Samples were taken immediately prior to (t=0) injection of MK801 bolus dose and 60 minutes after initiation of infusion (t=60). [¹²⁵I]CNS 1261 was administered 30 min. after the start of the infusion and animals were killed 120 minutes later. Administration of MK801 caused a sustained decrease in MABP at both doses examined. Administration of MK801 did not affect any of the other parameters examined (One-way ANOVA). Data are presented as mean ± S.E.M (n=3-4).

FIGURE 29 : NMRS trace from a sample of MK801 used in displacement studies

Nuclear magnetic resonance spectroscopy was used to examine the the batch of MK801 used in displacement experiments. The trace was interpreted by A. Tebbutt and compared to MK801 NMRS traces from the literature. It was confirmed that the compound analysed was authentic MK801.



3.6.3 Uptake and retention of [125 I]CNS 1261

The general pattern of uptake in all autoradiograms reflected NMDA receptor distribution with high levels observed within hippocampal structures and low levels in the hypothalamus and cerebellum (Figure 30). [125 I]CNS 1261 uptake in each region of interest was expressed relative to the amount of [125 I]CNS 1261 bound within the cerebellum (Table 18).

In both groups of animals receiving MK801, isotope levels within hippocampal regions were the highest of all structures examined (approximately 150-200% above that observed in the cerebellum). Uptake in cortical regions and hypothalamus were 60 and 20% greater than cerebellar levels respectively.

The region of interest/cerebellar ratios of MK801 treated animals were compared to the corresponding ratios from previous experiments examining [125 I]CNS 1261 uptake at 120 minutes (see section 3.3.2). There was no significant difference in total [125 I]CNS 1261 binding between the control group and both groups treated with MK801 in any of the regions examined (Figure 31, see also Table 18).

FIGURE 30 : Effect of MK801 on [125 I]CNS 1261 uptake in normal rat brain

Representative autoradiograms of [125 I]CNS 1261 uptake in normal rat brain at the level of the dorsal hippocampus and cerebellum. Administration of pharmacologically active doses of MK801 ($0.4 \pm 6\mu\text{g/ml/min.}$ or $1.2 \pm 16\mu\text{g/ml/min.}$) had no effect of [125 I]CNS 1261 uptake within any region examined. Autoradiograms were compared to images obtained in a previous experiment investigating [125 I]CNS 1261 uptake in the normal brain at 120 minutes.

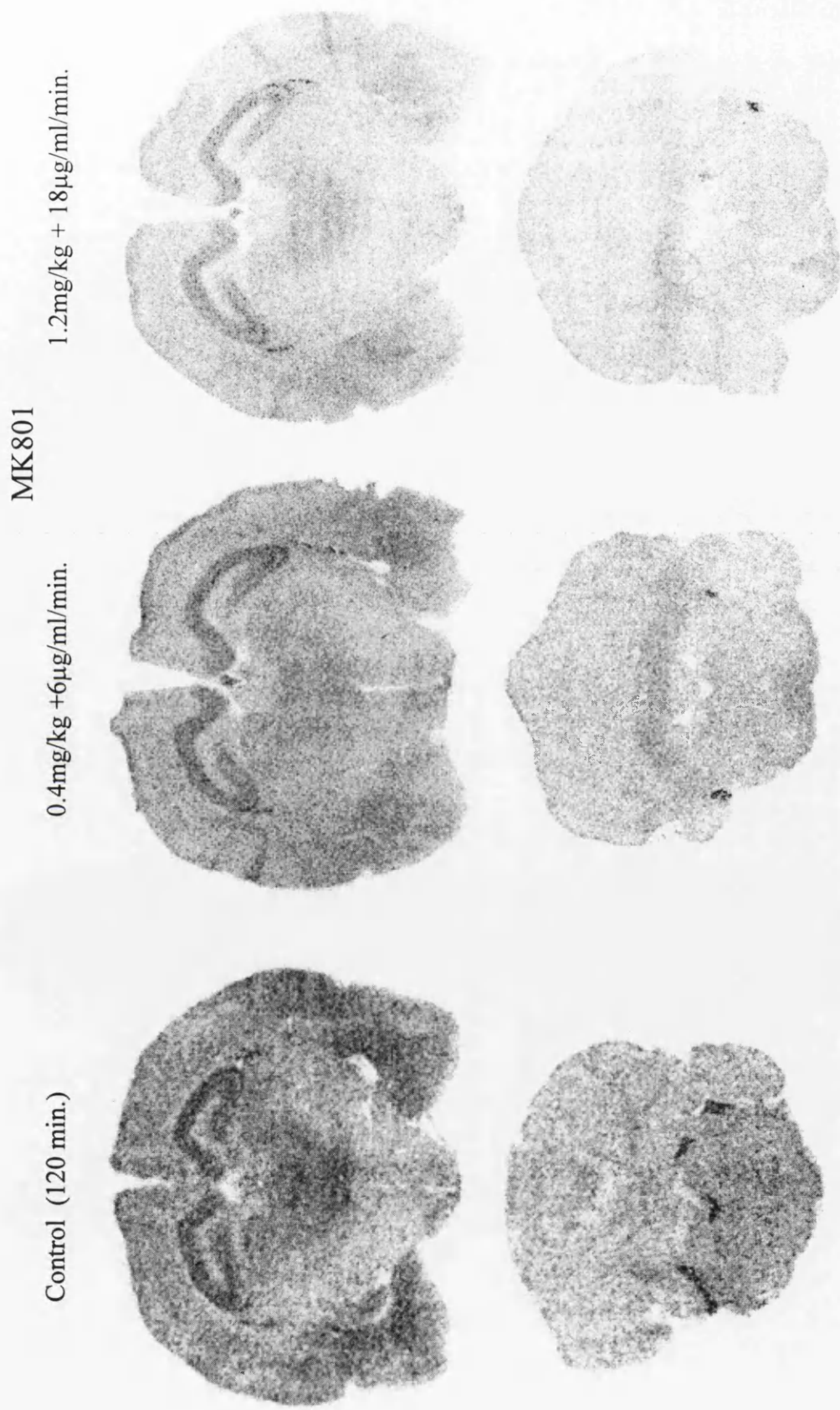


FIGURE 30 : Administration of MK801 had no effect on [¹²⁵I]CNS 1261 uptake in the normal brain

TABLE 18
Effect of MK801 on [125 I]CNS 1261 uptake

STRUCTURE	[125 I]CNS 1261 uptake (120 min.)	MK 801	
		0.4mg/kg + 6 μ g/kg/min	1.2mg/kg + 16 μ g/kg/min
anterior cingulate cortex	1.69 \pm 0.10	1.79 \pm 0.11	1.63 \pm 0.13
genu	1.42 \pm 0.16	1.44 \pm 0.06	1.44 \pm 0.08
caudate nucleus	1.38 \pm 0.05	1.30 \pm 0.05	1.36 \pm 0.04
sensory-motor cortex			
layers I-II	1.40 \pm 0.05	1.29 \pm 0.08	1.42 \pm 0.07
IV	1.39 \pm 0.07	1.48 \pm 0.09	1.52 \pm 0.05
V-VI	1.51 \pm 0.09	1.45 \pm 0.07	1.54 \pm 0.08
corpus callosum	1.47 \pm 0.08	1.43 \pm 0.05	1.51 \pm 0.08
anterior thalamus	1.58 \pm 0.04	1.68 \pm 0.10	1.56 \pm 0.06
hippocampus CA1	2.44 \pm 0.21	2.58 \pm 0.05	2.45 \pm 0.14
hippocampus CA3	2.43 \pm 0.19	2.64 \pm 0.13	2.58 \pm 0.15
lateral habenular nucleus	1.20 \pm 0.03	1.24 \pm 0.02	1.26 \pm 0.10
mediodorsal thalamus	1.61 \pm 0.09	1.64 \pm 0.07	1.68 \pm 0.06
ventrolateral thalamus	1.56 \pm 0.09	1.44 \pm 0.04	1.49 \pm 0.10
internal capsule	1.11 \pm 0.04	1.23 \pm 0.02	1.28 \pm 0.07
parietal cortex			
layers I-III	1.55 \pm 0.08	1.52 \pm 0.04	1.48 \pm 0.11
IV	1.49 \pm 0.05	1.60 \pm 0.04	1.63 \pm 0.09
V-VI	1.68 \pm 0.10	1.59 \pm 0.04	1.66 \pm 0.11
hypothalamus	1.05 \pm 0.04	1.22 \pm 0.01	1.27 \pm 0.06
posterior cingulate cortex	1.51 \pm 0.06	1.49 \pm 0.02	1.52 \pm 0.07
hippocampus molecular layer	2.91 \pm 0.22	2.94 \pm 0.10	2.89 \pm 0.90
dentate gyrus	2.50 \pm 0.15	2.64 \pm 0.08	2.58 \pm 0.15
auditory cortex			
layers I-III	1.63 \pm 0.06	1.60 \pm 0.02	1.65 \pm 0.14
IV	1.64 \pm 0.05	1.63 \pm 0.07	1.67 \pm 0.09
V-VI	1.77 \pm 0.05	1.79 \pm 0.08	1.82 \pm 0.11
substantia nigra pars compacta	1.24 \pm 0.04	1.24 \pm 0.00	1.30 \pm 0.05
substantia nigra pars reticulata	1.17 \pm 0.05	1.16 \pm 0.00	1.22 \pm 0.05
medial geniculate body	1.49 \pm 0.05	1.47 \pm 0.05	1.54 \pm 0.09
visual cortex			
layers I-III	1.73 \pm 0.09	1.81 \pm 0.04	1.81 \pm 0.11
IV	1.64 \pm 0.09	1.78 \pm 0.07	1.70 \pm 0.12
V-VI	1.67 \pm 0.04	1.77 \pm 0.08	1.76 \pm 0.12
entorhinal cortex	1.91 \pm 0.11	1.81 \pm 0.06	1.81 \pm 0.12
inferior colliculus	1.08 \pm 0.01	1.14 \pm 0.01	1.20 \pm 0.04
pons	1.31 \pm 0.06	1.38 \pm 0.01	1.34 \pm 0.07
cerebellar hemisphere	1.00 \pm 0.00	1.00 \pm 0.00	1.00 \pm 0.00
cerebellar white matter	1.25 \pm 0.14	1.43 \pm 0.04	1.33 \pm 0.08
superior olivary nucleus	1.19 \pm 0.07	1.24 \pm 0.07	1.17 \pm 0.05

[125 I]CNS 1261 uptake following treatment with MK801 (0.4mg/kg + 6 μ g/kg/min or 1.2mg/kg + 16 μ g/kg/min) were compared to [125 I]CNS 1261 uptake at 120 min. in a previous study (see section 3.3.2) using ANOVA. No significant differences in uptake were observed following treatment with MK801 at any of the doses examined.

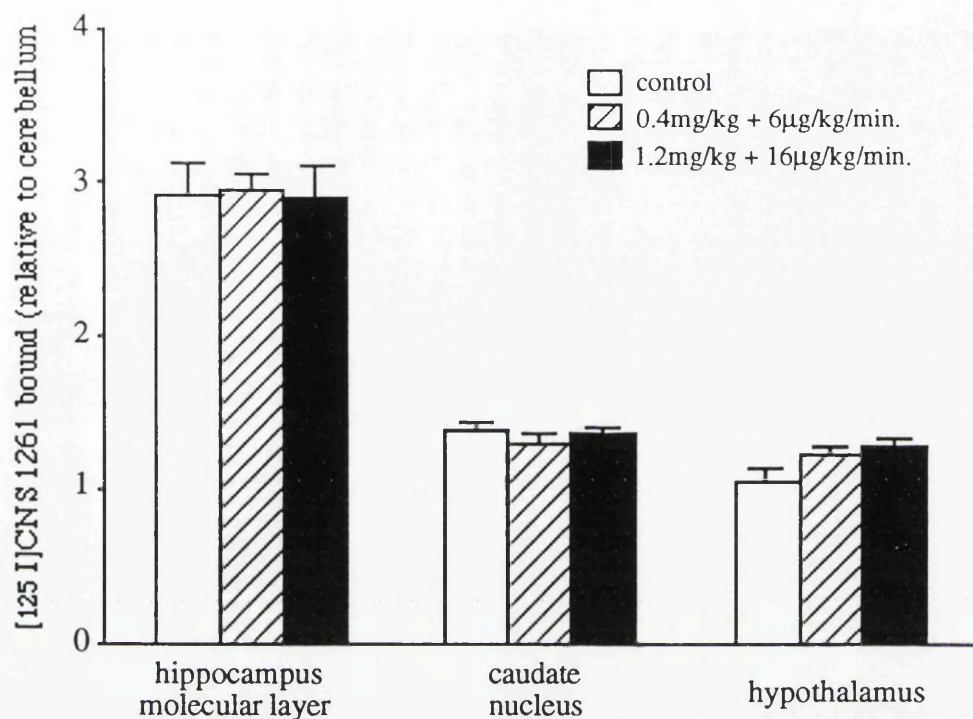


FIGURE 31 : MK801 does not displace $[^{125}\text{I}]\text{CNS 1261}$ binding in normal brain.

At the doses examined, MK801 had no effect on the level of $[^{125}\text{I}]\text{CNS 1261}$ binding in regions with high (hippocampus), intermediate (caudate nucleus) or low (hypothalamus) NMDA receptor density when compared to $[^{125}\text{I}]\text{CNS 1261}$ uptake at 120 minutes from a previous experiment (ANOVA). Data are presented as mean \pm S.E.M.(n=3-4).

3.7 [125I]MK801 and [125I]CNS 1261 uptake following changes in arterial CO₂ tension

This study consists of an initial short study to investigate the effect of changing arterial CO₂ tension (hypocapnia and hypercapnia) on [125I]MK801 uptake in the rat. This is followed by a more extensive investigation of the effect of hypercapnia only on [125I]CNS 1261 uptake in the rat brain

3.7.1 [125I]MK801 - general observations

Physiological variables were recorded before and 15 minutes after changes in CO₂ tension and are shown in Table 19. Prior to any manipulations (t = 0), physiological variables were deemed to be within normal limits and there were no significant differences between the three experimental groups.

Manipulation of respiratory status produced distinct changes in p_aCO₂, and consequently pH within the treatment groups. Hyperventilation produced a significant decrease in p_aCO₂ to approximately 22mmHg. The arterial pH of these hypocapnic animals was elevated from control values (pH 7.4) to pH 7.6. Increasing the concentration of CO₂ in inspired air to 20% increased p_aCO₂ to approximately 180mmHg. The arterial pH of these hypercapnic animals was decreased from pH 7.4 to pH 6.9. No differences were observed in any of the other parameters.

3.7.2 Analysis of [125I]MK801 autoradiograms

Before quantitative analysis, [125I]MK801 uptake in normocapnic animals was observed to be greatest within hippocampal structures (CA1, CA3). [125I]MK801 uptake was similar within the caudate nucleus, thalamus and cortical regions and no lamination could be detected within the cortex. Levels of [125I]MK801 uptake within the hypothalamus and cerebellum were decreased compared to cortical regions (Figure 32).

TABLE 19

Physiological variables following changes in arterial CO₂ tension

	sample time (min.)	NORMOCAPNIA (n = 8)	HYPOCAPNIA (n = 6)	HYPERCAPNIA n = 4
p _a CO ₂ (mmHg)	0	39 ± 1	41 ± 2	38 ± 1
	15	43 ± 1	22 ± 1 *	184 ± 5 *
Arterial pH	0	7.44 ± 0.07	7.41 ± 0.01	7.44 ± 0.01
	15	7.42 ± 0.01	7.61 ± 0.02 *	6.94 ± 0.01 *
p _a O ₂ (mmHg)	0	167 ± 11	145 ± 9	165 ± 8
	15	178 ± 10	196 ± 10	182 ± 10
MABP (mmHg)	0	85 ± 4	87 ± 3	90 ± 5
	15	86 ± 2	83 ± 1	88 ± 3
temperature (°C)	0	37.1 ± 0.1	37.0 ± 0.1	37.0 ± 0.3
	15	37.0 ± 0.1	37.1 ± 0.1	36.9 ± 0.1
glucose (mM)	-	10.4 ± 0.6	9.9 ± 0.4	9.8 ± 0.3
weight (g)	-	388 ± 11	398 ± 15	359 ± 14
n	-	8	6	4

Changes in CO₂ tension were induced 15 before tracer administration and maintained for the duration of the experiment. The data represents physiological variables measured before manipulations in CO₂ tension (t=0) and immediately prior to administration of [¹²⁵I]MK801 (t=15). * p < 0.05 for significant difference between treated and control animals (ANOVA, followed by Student's t-test).

Data are presented as mean ± S.E.M.

Normocapnia (pH 7.4)

Hypercapnia (pH 6.9)

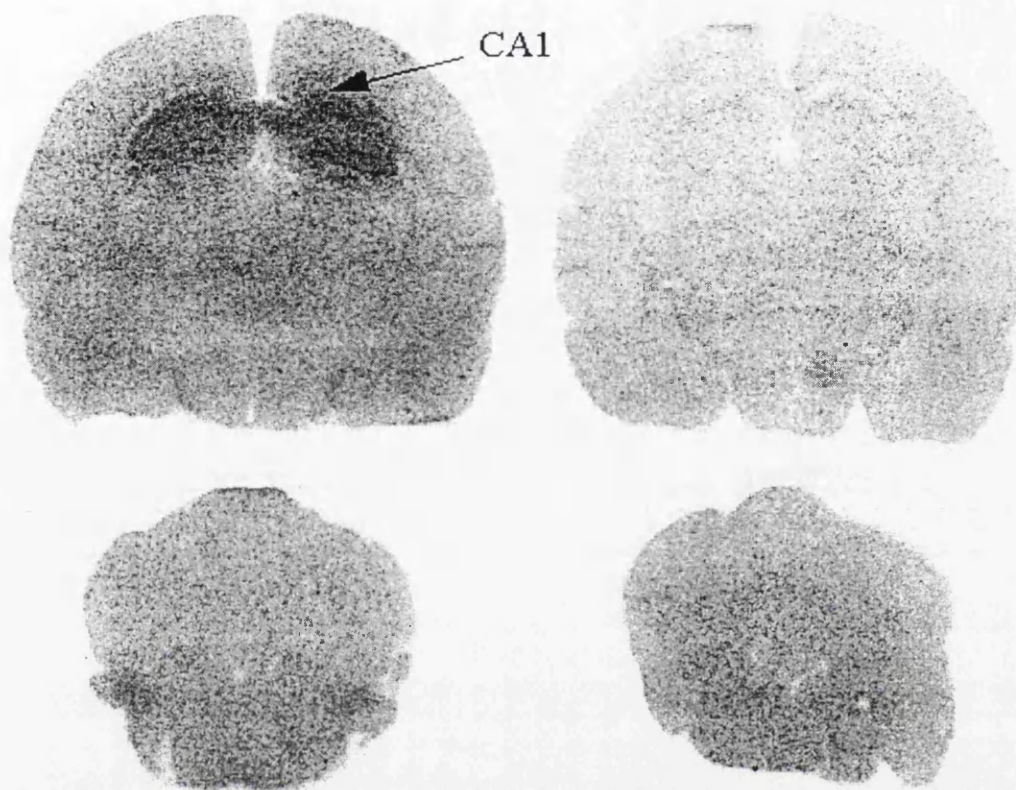


FIGURE 32 : Effect of hypercapnic acidosis on [125 I]MK801 uptake

Representative autoradiograms from the level of the dorsal hippocampus (upper) and cerebellum(lower) showing [125 I]MK801 uptake in normocapnic and hypercapnic animals. In normocapnic (control) animals highest levels of [125 I]MK801 were observed within the dorsal hippocampus (CA1) . Hypercapnia had a tendency to reduce [125 I]MK801 uptake within the hippocampus. (CA1 : hippocampus CA1).

The overall pattern of [^{125}I]MK801 uptake in autoradiograms from hypocapnic animals did not differ markedly from those of normocapnic animals. Autoradiograms from hypercapnic animals had a more homogeneous appearance with [^{125}I]MK801 uptake within the hippocampal formation only slightly above that within the cortex (Figure 32). Consistent with the other experimental groups, [^{125}I]MK801 uptake within the hypothalamus and cerebellum was decreased relative to cortical regions.

The uptake of [^{125}I]MK801 in 9 individual regions of interest was expressed as a ratio relative to [^{125}I]MK801 uptake within the cerebellum. [^{125}I]MK801 uptake ratios for normocapnic, hypocapnic and hypercapnic animals are shown in Table 20.

Quantitative analysis of autoradiograms from normocapnic animals confirmed that [^{125}I]MK801 uptake was relatively homogeneous in the majority of regions examined, approximately 10-20% greater than that observed within the cerebellum. [^{125}I]MK801 uptake within CA1 and CA3 of the hippocampus was slightly elevated and was approximately 30% above that observed within the cerebellum. [^{125}I]MK801 uptake within the hypothalamus was comparable to that within the cerebellum (Figure 32).

No significant differences in [^{125}I]MK801 uptake were observed between the hypocapnic group and control (normocapnic) animals in any of the regions examined.

Induction of hypercapnia ($p_a\text{CO}_2 = 180\text{mmHg}$, pH 6.9) was also found to have no significant effects on [^{125}I]MK801 uptake in any of the regions examined (Figure 33). There was a tendency however, for hypercapnic acidosis to reduce [^{125}I]MK801 uptake within the hippocampus (CA1, CA3), anterior cingulate cortex and sensory-motor cortex.

A Kolmogorov-Smirnov test (SigmaStat) performed on this data showed the values for [^{125}I]MK801 uptake in CA1 were not normally distributed. Since the outlying values were within 2 standard deviations of the mean and could not be excluded, all data was reanalysed using a Kruskal-Wallis test (SigmaStat). No statistical differences existed between the mean values of the treatment groups in any of the structures examined. These results support the original statistical analysis and suggest that [^{125}I]MK801 is an unsuitable agent to image potential changes in NMDA receptor activation in the normal rat brain.

TABLE 20
[¹²⁵I]MK801 uptake following changes in arterial CO₂ uptake

STRUCTURE	NORMOCAPNIA pH 7.4	HYPOCAPNIA pH 7.6	HYPERCAPNIA pH 6.9
Anterior cingulate cortex	1.12 ± 0.02	1.13 ± 0.02	1.07 ± 0.01
Sensory-motor cortex	1.11 ± 0.02	1.08 ± 0.02	1.03 ± 0.01
Caudate nucleus	1.08 ± 0.02	1.06 ± 0.02	1.06 ± 0.01
Hippocampus CA1	1.28 ± 0.05	1.35 ± 0.04	1.15 ± 0.03
Hippocampus CA3	1.22 ± 0.04	1.28 ± 0.03	1.15 ± 0.01
Hypothalamus	1.01 ± 0.02	1.01 ± 0.02	1.00 ± 0.03
Posterior cingulate cortex	1.10 ± 0.03	1.10 ± 0.04	1.09 ± 0.03
Thalamus	1.13 ± 0.03	1.19 ± 0.04	1.12 ± 0.03
Cerebellum	1	1	1

Uptake in individual regions of interest was expressed as a ratio relative to uptake within the cerebellar hemisphere. In all groups uptake was greatest in hippocampus CA1 and CA3. No significant differences in uptake were observed between hypo-or hypercapnic groups and control animals (ANOVA followed by Student's t-test with Bonferroni correction). Data are presented as mean ± SEM.

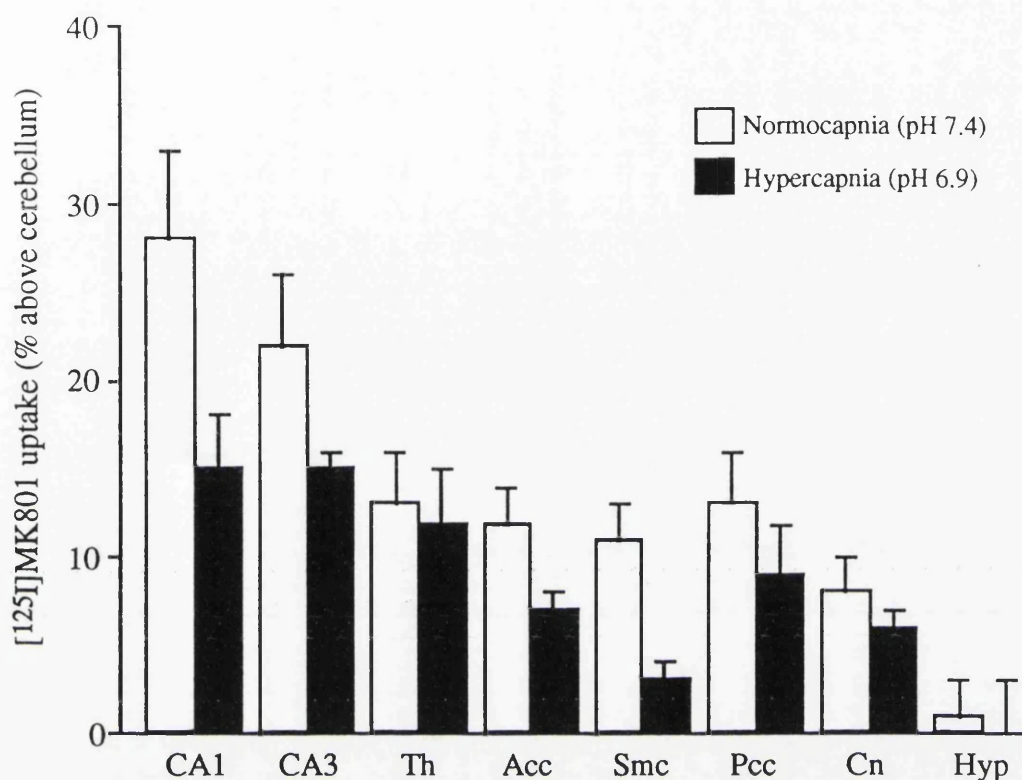


FIGURE 33 : The effect of hypercapnic acidosis on [^{125}I]MK801 uptake

Data is redrawn from Table 20 and represent levels of [^{125}I]MK801 uptake in 8 regions of interest. Highest levels of uptake in the normocapnic group were observed within the hippocampus (CA1 and CA3) and lowest levels were observed within the hypothalamus. [^{125}I]MK801 uptake was relatively homogeneous in the other regions examined. Hypercapnia had a tendency to reduce [^{125}I]MK801 uptake within the hippocampus, anterior cingulate cortex and sensory-motor cortex. Data are mean \pm S.E.M., $n=4-8$.

(CA1, CA3 =dorsal hippocampus, Th = thalamus, Acc = anterior cingulate cortex, Smc = sensory-motor cortex, Pcc = posterior cingulate cortex, Cn = caudate nucleus, Hyp = hypothalamus).

3.7.3 [^{125}I]CNS 1261 - general observations

Physiological variables were recorded before and 15 minutes after changes in arterial CO_2 tension and are shown in Table 21. Prior to any manipulations ($t = 0$), physiological variables were deemed to be within normal limits and there were no significant differences between the three experimental groups.

Manipulation of respiratory status produced distinct changes in p_aCO_2 , and consequently pH within the hypercapnic treatment group. Increasing the concentration of CO_2 in inspired air to 20% increased p_aCO_2 to approximately 170mmHg. The arterial pH of these hypercapnic animals was decreased from pH 7.4 to pH 6.9. The mean arterial blood pressure of hypercapnic animals was also significantly increased compared to control animals.

3.7.4 Analysis of [^{125}I]CNS 1261 autoradiograms

Before quantitative analysis, the highest levels of [^{125}I]CNS 1261 uptake were observed within the hippocampus (CA1, CA3, molecular layer) in all autoradiograms (Figure 34). The uptake of [^{125}I]CNS 1261 in 36 individual regions of interest was expressed as a ratio relative to [^{125}I]CNS 1261 uptake within the cerebellum. [^{125}I]CNS 1261 uptake ratios for normocapnic and hypercapnic animals are shown in Table 22.

Quantitative analysis of autoradiograms from normocapnic animals showed that [^{125}I]CNS 1261 uptake was relatively heterogeneous in the majority of regions examined. [^{125}I]CNS 1261 uptake was 60-90% above cerebellar values in cortical areas with the highest levels of uptake within deep layers (V-VI). Highest levels of [^{125}I]CNS 1261 uptake were observed within hippocampal regions (CA1, CA3 and molecular layer) where uptake was 2-300% greater than that observed within the cerebellum. Low levels of uptake were observed in cerebellar white matter and superior olives where uptake was approximately 30% greater than that observed within the cerebellum.

TABLE 21

Physiological variables following changes in arterial CO₂ tension

	sample time (min.)	NORMOCAPNIA	HYPERCAPNIA
paCO ₂ (mmHg)	0	42 ± 3	40 ± 1
	15	41 ± 2	166 ± 10**
Arterial pH	0	7.42 ± 0.01	7.44 ± 0.02
	15	7.40 ± 0.01	6.93 ± 0.01**
paO ₂ (mmHg)	0	161 ± 17	198 ± 10
	15	173 ± 33	208 ± 3
MABP (mmHg)	0	86 ± 3	80 ± 3
	15	80 ± 2	101 ± 2**
temperature (°C)	0	36.7 ± 0.32	37.1 ± 0.09
	15	36.8 ± 0.57	37.2 ± 0.19
weight (g)	-	334 ± 30	330 ± 25
n	-	3	3

Changes in CO₂ tension were induced 15 minutes before tracer administration and maintained for the duration of the experiment. The data represents physiological variables measured before manipulations in CO₂ tension (t=0) and immediately prior to administration of [¹²⁵I]CNS 1261 (t=15). **p< 0.01 for significant difference between hypercapnic and normocapnic animals (Student's unpaired t-test). Data are presented as mean ± S.E.M.

TABLE 22
[¹²⁵I]CNS 1261 uptake following changes in arterial CO₂ tension

STRUCTURE	Normocapnia pH 7.4	Hypercapnia pH 6.9
anterior cingulate cortex	2.01 ± 0.21	1.09 ± 0.13*
genu	1.75 ± 0.28	1.65 ± 0.15
sensory motor cortex		
layer I-III	1.64 ± 0.13	1.09 ± 0.07**
layer IV	1.73 ± 0.15	1.00 ± 0.04**
layers V-VI	1.86 ± 0.18	1.16 ± 0.04**
caudate nucleus	1.66 ± 0.13	1.39 ± 0.20
corpus callosum	1.82 ± 0.06	1.92 ± 0.31
anterior thalamus	2.03 ± 0.24	1.74 ± 0.25
hippocampus CA1	3.19 ± 0.19	2.22 ± 0.33
hippocampus CA3	3.42 ± 0.23	2.12 ± 0.26**
lateral habenular nucleus	1.40 ± 0.05	1.51 ± 0.30
mediodorsal thalamus	1.89 ± 0.20	1.33 ± 0.03*
ventrolateral thalamus	1.51 ± 0.14	1.30 ± 0.05
internal capsule	1.77 ± 0.30	1.45 ± 0.19
parietal cortex		
layers I-III	1.70 ± 0.14	1.09 ± 0.07**
layer IV	1.66 ± 0.08	1.15 ± 0.08**
layer V-VI	1.91 ± 0.19	1.40 ± 0.08
hypothalamus	1.33 ± 0.14	1.02 ± 0.05
posterior cingulate cortex	1.52 ± 0.21	1.31 ± 0.16
hippocampus molecular layer	4.13 ± 0.36	2.50 ± 0.35*
dentate gyrus	3.85 ± 0.25	2.31 ± 0.24*
auditory cortex		
layers I-III	1.84 ± 0.16	1.18 ± 0.04**
layer IV	1.93 ± 0.14	1.28 ± 0.08**
layer V-VI	2.39 ± 0.18	1.59 ± 0.20*
substantia nigra pars compacta	1.27 ± 0.25	1.30 ± 0.10
substantia nigra pars reticulata	1.13 ± 0.25	1.32 ± 0.05
medial geniculate body	1.50 ± 0.35	1.56 ± 0.25
visual cortex		
layers I-III	1.73 ± 0.20	1.30 ± 0.21
layer IV	1.80 ± 0.12	1.42 ± 0.23
layers V-VI	2.00 ± 0.19	1.46 ± 0.19
entorhinal cortex	2.31 ± 0.10	1.51 ± 0.28
inferior colliculus	1.00 ± 0.20	1.21 ± 0.11
pons	1.42 ± 0.29	1.44 ± 0.08
cerebellar cortex	1.00 ± 0.00	1.00 ± 0.00
cerebellar white matter	1.28 ± 0.26	1.25 ± 0.25
superior olives	1.22 ± 0.21	1.19 ± 0.01

Uptake of [¹²⁵I]CNS 1261 in individual regions of interest were expressed as a ratio relative to uptake within the cerebellum. Roman numerals (I-VI) indicate the cortical layer examined. [¹²⁵I]CNS 1261 uptake was greatest in the hippocampus in both groups. Data are presented as mean ± S.E.M., n = 3. *p<0.05. **p<0.01 (Students unpaired t-test).

Induction of hypercapnia had a tendency to reduce [^{125}I]CNS 1261 uptake in all of the regions examined. Hypercapnia had a marked effect in 13 of the 36 regions examined, significantly reducing [^{125}I]CNS 1261 uptake in anterior cingulate cortex, sensory motor cortex (layers I-VI), hippocampus CA3, mediodorsal thalamus, parietal cortex (layers I-IV), hippocampus molecular layer, dentate gyrus and auditory cortex (layers I-VI).

Following hypercapnia the highest levels of uptake were still observed within hippocampal regions, despite [^{125}I]CNS 1261 uptake being reduced by over 100%. This reduction in [^{125}I]CNS 1261 uptake within the hippocampus is clearly visible in the autoradiographic images (Figure 34). Reductions in [^{125}I]CNS 1261 uptake of 50-80% were observed in cortical regions. Reductions in [^{125}I]CNS 1261 uptake in regions with a lower density of NMDA receptors were of a smaller magnitude, typically $\leq 30\%$ and were not significant.

Relative [^{125}I]CNS 1261 uptake in the same 8 regions examined in section 3.7.2 were redrawn from Table 22 and are shown in Figure 35.

These results suggest that [^{125}I]CNS 1261 can image the heterogeneity in NMDA receptor activation within the normal brain and, is a suitable agent to image reductions in NMDA receptor activation induced by hypercapnic acidosis.

FIGURE 34 : Effect of hypercapnic acidosis on [^{125}I]CNS 1261 uptake

Autoradiograms from individual experiments of [^{125}I]CNS 1261 uptake at the level of the dorsal hippocampus. [^{125}I]CNS 1261 uptake in normocapnic animals (upper) was compared to that in hypercapnic animals (lower). Hypercapnic acidosis decreased the amount of [^{125}I]CNS 1261 uptake within CA1 and CA3 regions of the hippocampus in all animals.

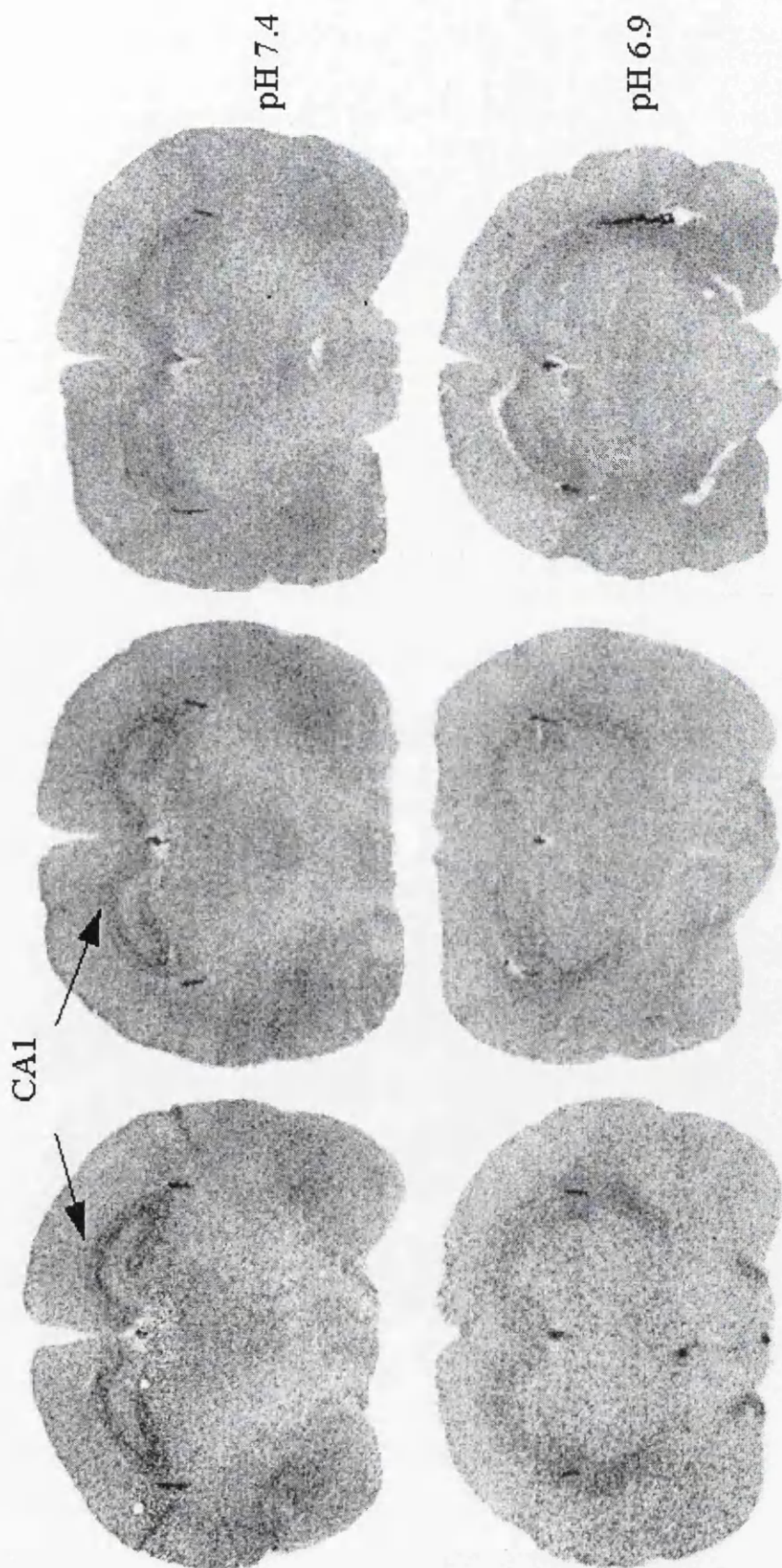


FIGURE 34 : Effect of hypercapnic acidosis on [¹²⁵I]CNS 1261 uptake

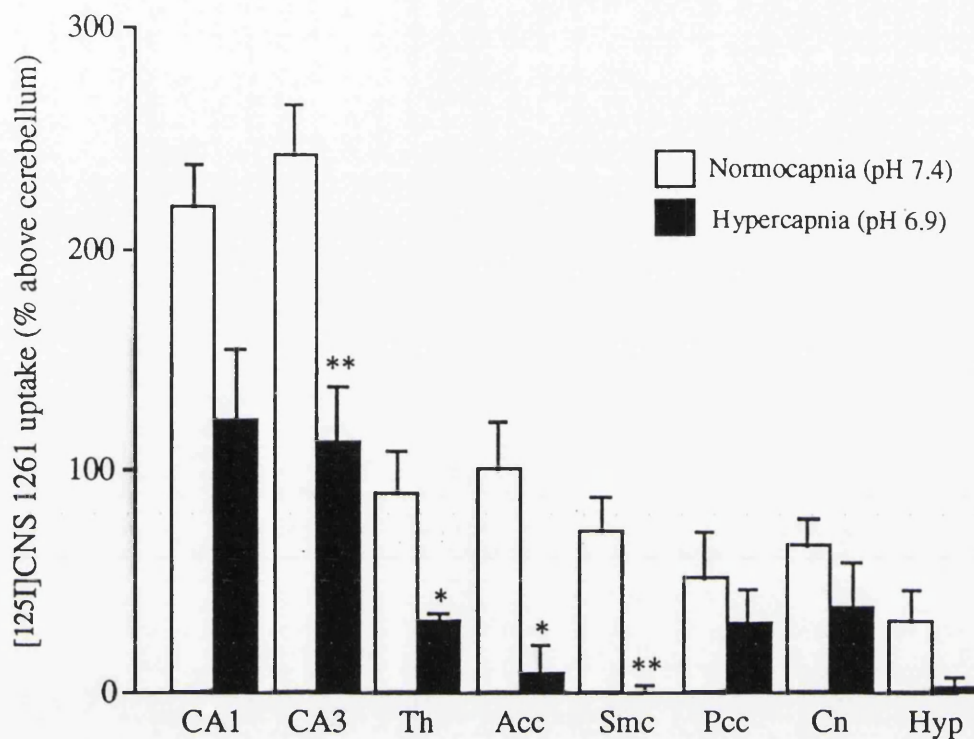


FIGURE 35 : Effect of hypercapnic acidosis on [^{125}I]CNS 1261 uptake

Data is redrawn from Table 22 and represent levels of [^{125}I]CNS 1261 uptake in 8 regions of interest. Highest levels of uptake in the normocapnic group were observed within the hippocampus (CA1 and CA3) and lowest levels were observed within the hypothalamus. Hypercapnia significantly reduced [^{125}I]CNS 1261 uptake within the hippocampus CA3, thalamus, anterior cingulate cortex and sensory-motor cortex.

** $p < 0.01$, * $p < 0.05$ (Student's unpaired t-test). Data are mean \pm S.E.M., $n=4-8$

(CA1, CA3 =dorsal hippocampus, Th = mediodorsal thalamus, Acc = anterior cingulate cortex, Smc = sensory-motor cortex (IV), Pcc = posterior cingulate cortex, Cn = caudate nucleus, Hyp = hypothalamus).

3.8. [¹²⁵I]CNS 1261 uptake following intracortical injection of NMDA or CSF

3.8.1. Verification of dose

Initial investigations examined the effect of injecting NMDA (9 μmoles) in a volume of 1 μl. The practical aspects of injecting such a small volume of fluid and the inability to locate the position of the injection site on autoradiograms prompted a change to the experimental protocol. The injection volume was increased to 3 μl, thus increasing the amount of NMDA injected to 27 μmoles.

The ability of this dose of NMDA to induce receptor activation was verified by [¹⁴C]2-deoxyglucose autoradiography. [¹⁴C]2-deoxyglucose (50 μCi) was administered 15 minutes after intrastriatal injection of NMDA. Brains were removed and processed for autoradiography 45 minutes after injection of tracer.

Following NMDA injection, increases in glucose utilisation were observed in all layers of the sensory motor cortex (Table 23). The general pattern of uptake at the site of NMDA injection showed a pale core region where glucose utilisation was reduced by 50% relative to the corresponding area of the contralateral cortex, surrounded by a rim of increased glucose utilisation (Figure 36). Glucose utilisation in this rim was approximately 2.5 times greater than in corresponding region of the contralateral hemisphere.

3.8.2. General Observations

In these investigations, [¹²⁵I]CNS 1261 was administered 15 minutes after intrastriatal injection of NMDA (or CSF) and the animals sacrificed at 5min., 60min. and 120min. thereafter. Physiological and respiratory variables were recorded prior to injection of NMDA or CSF (t=0 min.) and before intravenous administration of [¹²⁵I]CNS 1261 (t=15 min.) and are shown in Table 24.

TABLE 23

Changes in glucose utilisation following intracortical injection of NMDA

STRUCTURE	Glucose Use (μ moles/100g/min.			
	Animal 1		Animal 2	
	ipsi	contra	ipsi	contra
anterior cingulate cortex	82	82	74	75
genu	33	31	33	30
sensory motor cortex				
layers I-III	113	73	69	59
layer IV	92	62	73	63
layers V-VI	43	51	127	60
caudate nucleus	86	95	83	86
corpus callosum	32	35	43	38
anterior thalamus	84	86	52	48
hippocampus CA1	41	41	34	42
hippocampus CA3	77	82	64	79
lateral habenular nucleus	82	82	83	76
mediodorsal thalamus	53	56	48	43
ventrolateral thalamus	53	61	58	50
internal capsule	23	24	20	16
parietal cortex				
layers I-III	83	78	47	47
layer IV	63	64	44	45
layers V-VI	64	64	48	46
hypothalamus	41	42	42	47
posterior cingulate cortex	88	86	67	70
hippocampus molecular layer	45	50	55	51
dentate gyrus	97	100	95	85
auditory cortex				
layers I-III	76	98	65	63
layer IV	80	87	52	58
layers V-VI	66	81	54	59
substantia nigra pars compacta	77	81	88	88
substantia nigra pars reticulata	72	68	46	45
medial geniculate body	50	52	38	42
visual cortex				
layers I-III	62	73	51	56
layer IV	67	80	48	52
layers V-VI	58	62	47	47
entorhinal cortex	58	61	51	45
inferior colliculus	62	59	56	53
pons	37	38	45	41
cerebellar hemisphere	35	38	44	36
cerebellar white matter	23	21	24	22
superior olivary nucleus	44	49	53	50

Glucose utilisation was measured by [14 C]2-deoxyglucose autoradiography following injection of NMDA into the ipsilateral sensory-motor cortex. Data are individual values of glucose use within the ipsilateral and contralateral hemispheres of the 2 experimental animals investigated. Roman numerals indicate the cortical layer examined.

TABLE 24
Physiological variables before and after injection of CSF or NMDA

	sample time (min.)	Vehicle (CSF)			NMDA		
		5 min.	60 min.	120 min.	5 min.	60 min.	120 min.
P _a CO ₂ (mmHg)	0	39.0 ± 4.6	41.8 ± 1.5	43.9 ± 2.25	35.3 ± 3.8	41.1 ± 1.7	42.3 ± 3.3
	15	33.4 ± 6.3	42.7 ± 4.0	40.8 ± 0.95	38.0 ± 2.0	42.5 ± 0.5	41.1 ± 3.2
Arterial pH	0	7.39 ± 0.01	7.38 ± 0.04	7.42 ± 0.00	7.42 ± 0.01	7.45 ± 0.00	7.42 ± 0.02
	15	7.42 ± 0.06	7.40 ± 0.01	7.41 ± 0.02	7.41 ± 0.02	7.42 ± 0.03	7.38 ± 0.04
P _a O ₂ (mmHg)	0	175.9 ± 13.0	179.3 ± 20.9	182.4 ± 16.7	167.1 ± 17.2	138.0 ± 23.4	201.6 ± 20.4
	15	190.7 ± 44.8	170.1 ± 18.3	199.9 ± 8.8	173.9 ± 21.2	150.7 ± 32.7	195.2 ± 15.6
MABP (mmHg)	0	74 ± 16	81 ± 8	80 ± 3	85 ± 2	82 ± 5	88 ± 5
	15	73 ± 11	81 ± 4	73 ± 6	84 ± 1	83 ± 1	75 ± 2
temperature (°C)	0	36.8 ± 0.20	37.2 ± 0.12	37.5 ± 0.50	37.2 ± 0.35	36.5 ± 0.18	36.6 ± 0.35
	15	36.8 ± 0.20	37.1 ± 3.50	36.8 ± 0.10	36.5 ± 0.45	37.3 ± 0.45	37.1 ± 0.25

Physiological and respiratory variables were measured before injection of NMDA (27μmoles), or CSF (t = 0) and immediately prior to administration of [¹²⁵I]CNS 1261 (t = 15). Brains were processed for autoradiography 5, 60 or 120 minutes after tracer injection. Injection of CSF or NMDA had no effect on any of the parameters measured. There were also no differences observed between animals injected with vehicle or NMDA at any of the time points examined (ANOVA). Data are expressed as mean ± S.E.M., n=2-4.

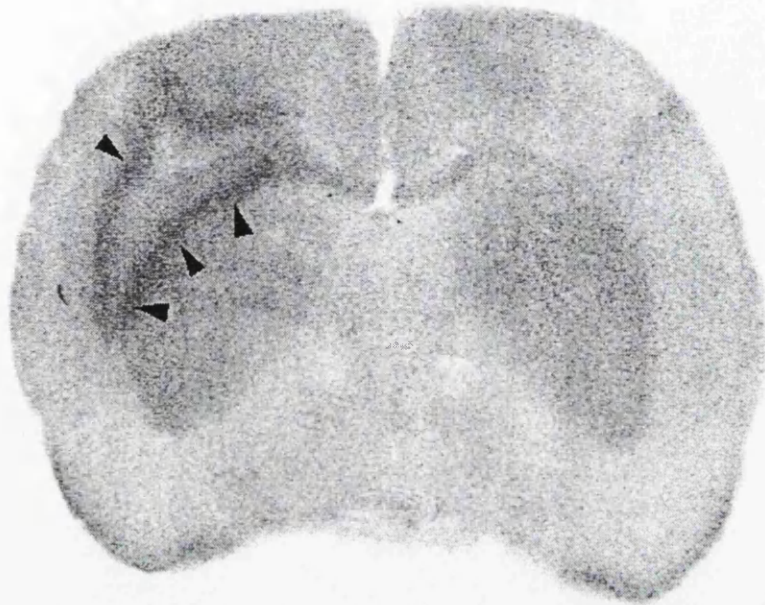


FIGURE 36 : Glucose use within the parietal cortex is increased following injection of NMDA

Representative autoradiogram illustrating glucose use after unilateral injection of NMDA into the parietal cortex (left hemisphere) at the level of the injection site. Increased glucose use is evident in the zone of tissue bordering the injection site (arrowheads). Glucose use in this border zone was 250% above that in corresponding regions of the contralateral hemisphere.

Injection of NMDA or CSF into the sensory-motor cortex had no effect on any of the parameters examined. The physiological variables of animals receiving an intracortical injection of NMDA were not different from animals receiving an injection of vehicle at any of the time points examined. No differences in physiological variables were observed within the experimental groups.

3.8.3. Histology

Additional brain sections from these animals were stained with haematoxylin and eosin (H & E). While fresh frozen brain sections do not preserve cell morphology as well as tissue fixed with formaldehyde, these sections gave an indication of the changes caused by intracortical injection of NMDA and CSF and confirmed the presence of an injection site. In all sections, an area of pallor was evident following staining which corresponded in shape and size to the pale zone surrounding the injection site on autoradiographic films (Figures 37-39). At all time points a boundary could be delineated between the area of pallor and surrounding histologically normal tissue however this was more defined following injection of NMDA (Figure 40).

At all time points examined, the area of pallor was larger following NMDA injection. In addition to the loss of stain within this area, neuronal cells had a shrunken appearance. At later time points there was evidence of shrunken neurons outwith the area of pallor. In all cases cells within the contralateral hemisphere were histologically normal (Figures 41-43).

3.8.4. Uptake and retention of [125 I]CNS 1261

The *in vivo* uptake and retention of [125 I]CNS 1261 was examined in 38 anatomically discrete regions 5, 60 and 120 minutes after intracortical injection of NMDA or CSF. [125 I]CNS 1261 uptake in individual regions of interest was expressed as a ratio relative to uptake within the cerebellar hemisphere. Ratios of [125 I]CNS 1261 uptake relative to cerebellar levels are shown in appendix 2.

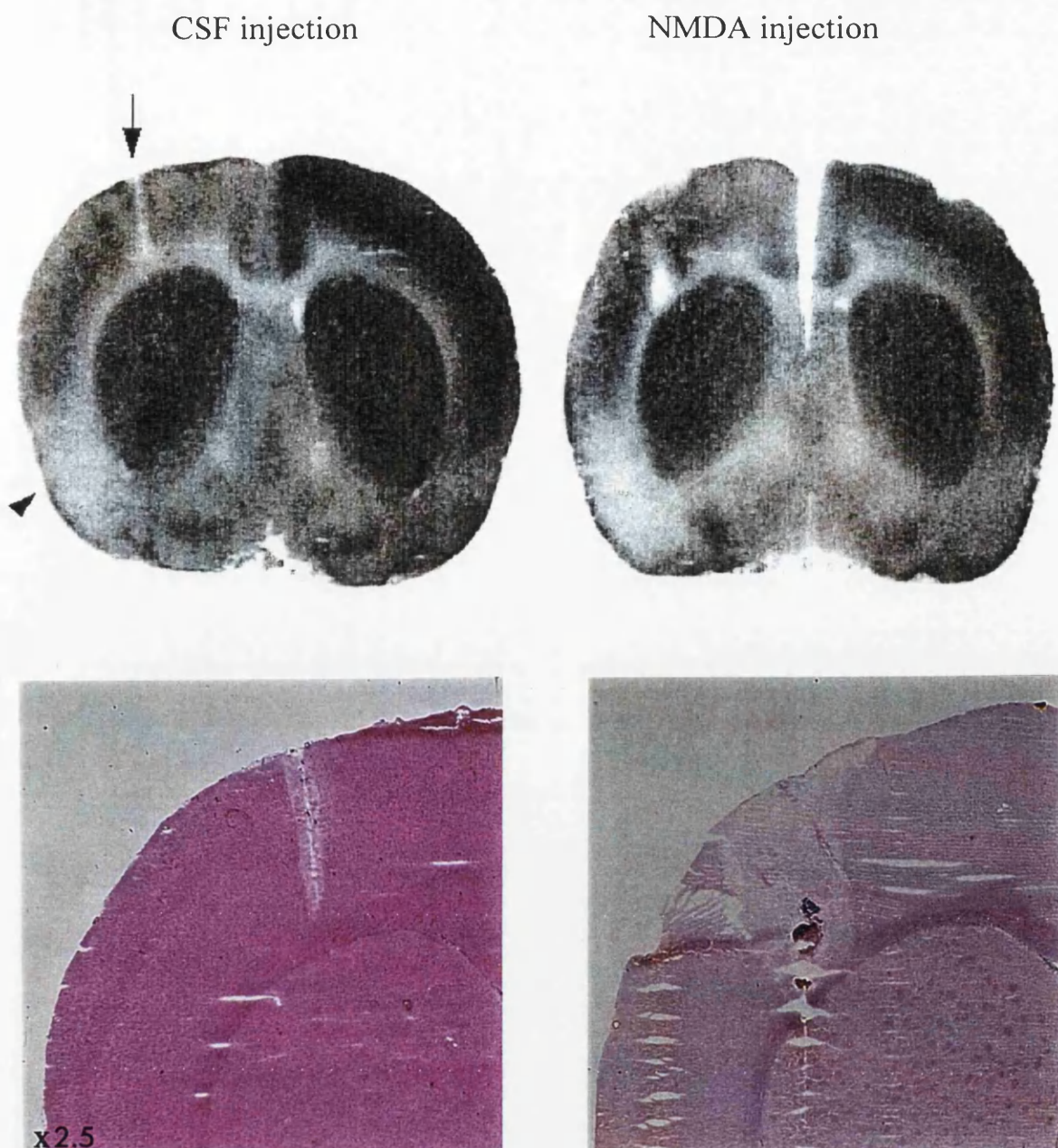


FIGURE 37 : Effect of NMDA (or CSF) injection on $[^{125}\text{I}]\text{CNS 1261}$ uptake 5 min. after administration

Representative autoradiograms (upper) showing $[^{125}\text{I}]\text{CNS 1261}$ uptake 5 min. after intracortical injection of CSF (left) or NMDA (right). Corresponding haematoxylin and eosin (H&E) stained sections (lower) show that the size and shape of the area of pallor in these sections is similar to that observed in autoradiograms. The site of the injection is marked with an arrow. Note the decrease in $[^{125}\text{I}]\text{CNS 1261}$ uptake within the insular cortex in both autoradiograms (arrowhead).

CSF injection

NMDA injection

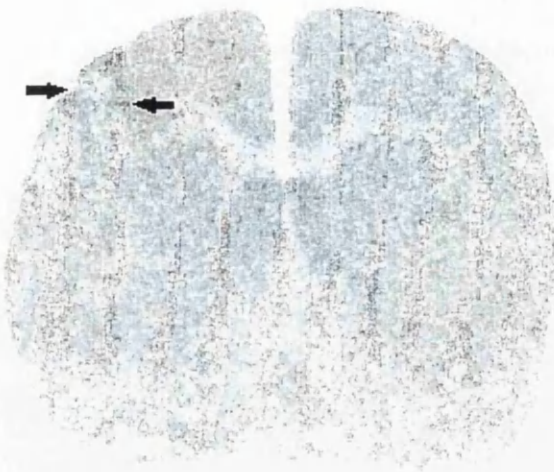


FIGURE 38 : Effect of NMDA (or CSF) injection on [125 I]CNS 1261 uptake 60 min. after administration

Representative autoradiograms (upper) showing [125 I]CNS 1261 uptake 60 min. after intracortical injection of CSF (left) or NMDA (right). Corresponding haematoxylin and eosin (H&E) stained sections (lower) show that the size and shape of the area of pallor in these sections is similar to that observed in autoradiograms. Note the rim of increased [125 I]CNS 1261 uptake surrounding the area of pallor in both autoradiograms (arrows).

CSF injection

NMDA injection

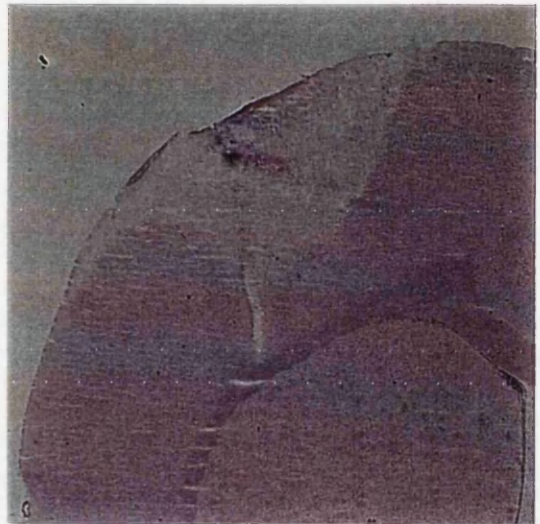
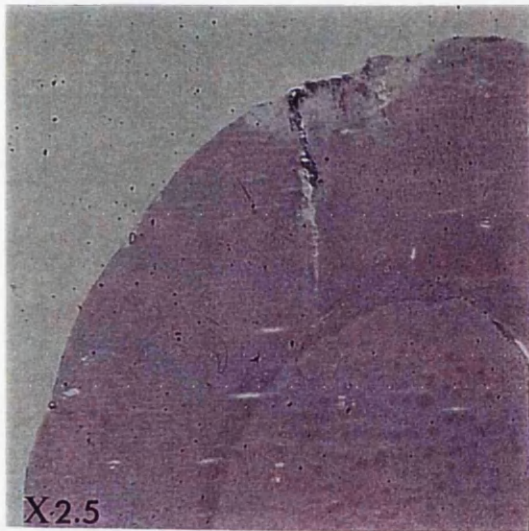


FIGURE 39 : Effect of NMDA (or CSF) injection on $[^{125}\text{I}]\text{CNS 1261}$ uptake 120 min. after administration

Representative autoradiograms (upper) showing $[^{125}\text{I}]\text{CNS 1261}$ uptake 120 min. after intracortical injection of CSF (left) or NMDA (right). Corresponding haematoxylin and eosin (H&E) stained sections (lower) show that the size and shape of the area of pallor in these sections is similar to that observed in autoradiograms. Note the rim of increased $[^{125}\text{I}]\text{CNS 1261}$ uptake surrounding the area of pallor in following NMDA injection (arrows).

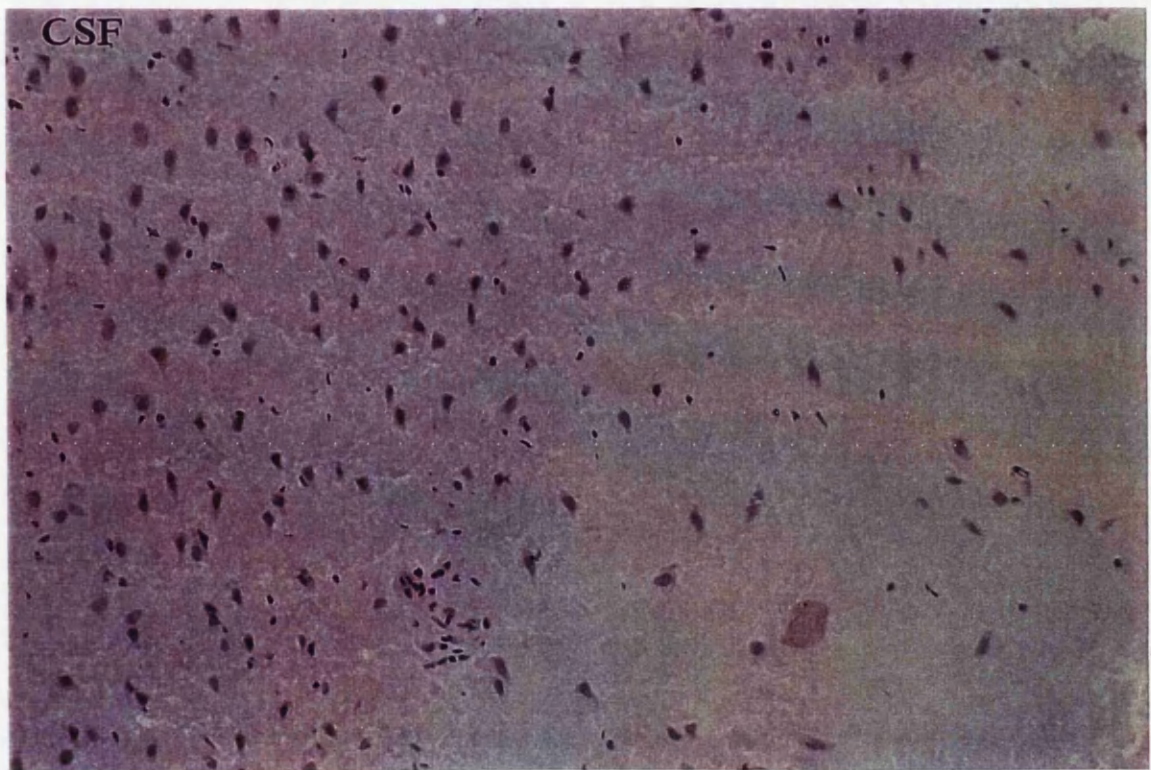
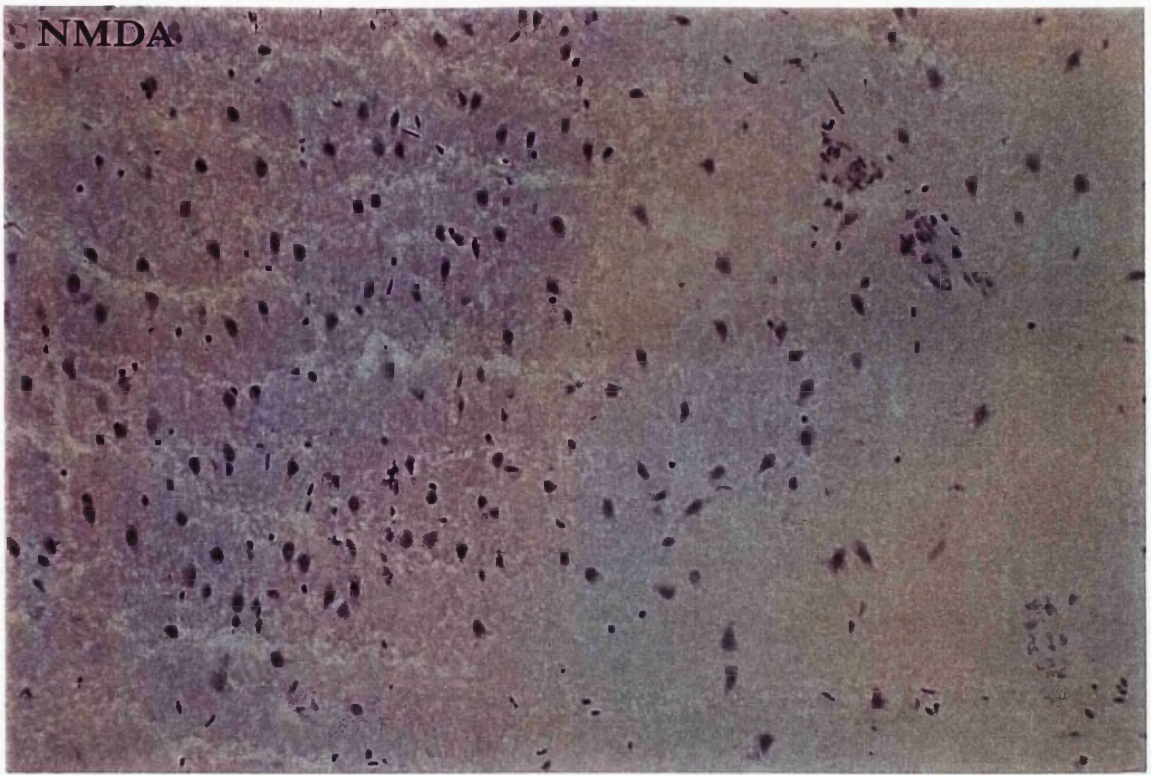


FIGURE 40 : Comparison of the boundary between the area of pallor and histologically normal tissue at 120 minutes

High power (x 50) photomicrographs taken from the boundary zone between the area of pallor and histologically normal tissue 120 minutes after intracortical injection of NMDA (upper) or CSF (lower) into the ipsilateral cortex. Note that the boundary was more defined following NMDA injection.

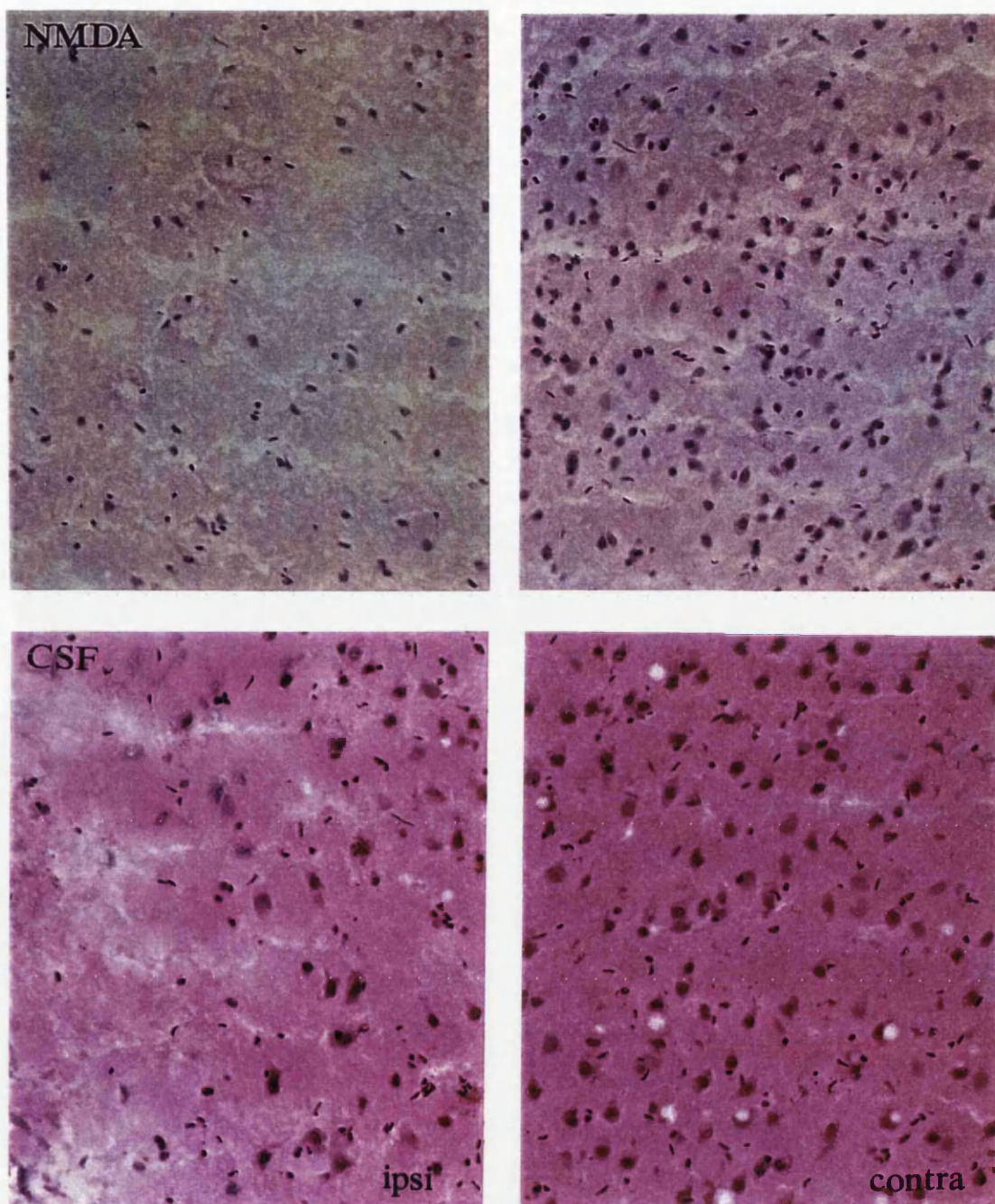


FIGURE 41 : High power photomicrographs from the ipsilateral and contralateral cortex 5 minutes after injection of NMDA or CSF

High power photomicrographs (x 50) were taken from the area of pallor (ipsilateral cortex) and from the corresponding area of the contralateral hemisphere 5 minutes after intracortical injection of NMDA (upper) or CSF (lower). Note the loss of staining within the ipsilateral cortex (left).

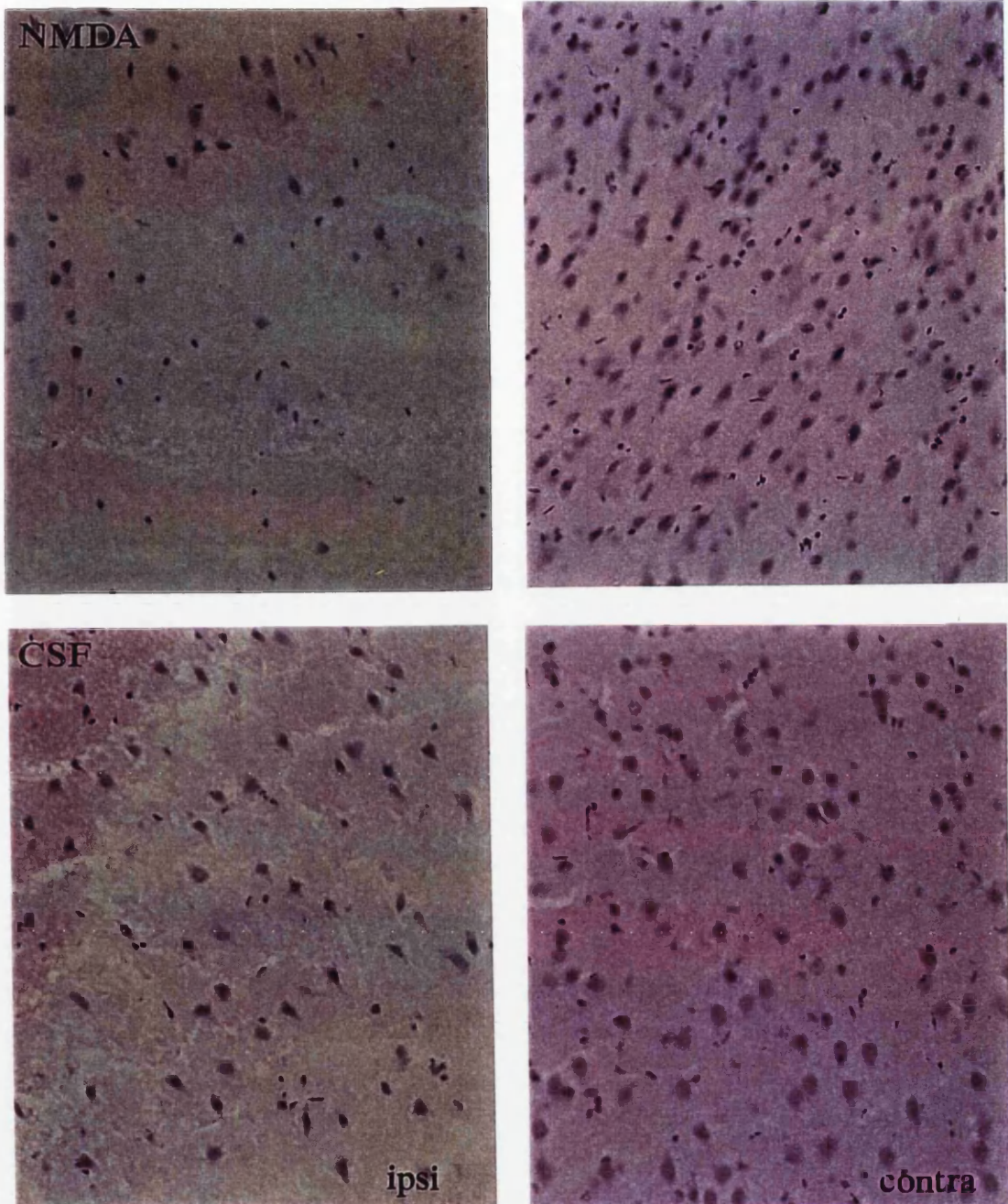


FIGURE 42 : High power photomicrographs from the ipsilateral and contralateral cortex 60 minutes after injection of NMDA or CSF

High power photomicrographs (x 50) were taken from the area of pallor (ipsilateral cortex) and from the corresponding area of the contralateral hemisphere 60 minutes after intracortical injection of NMDA (upper) or CSF (lower). Note the loss of staining within the ipsilateral cortex (left).

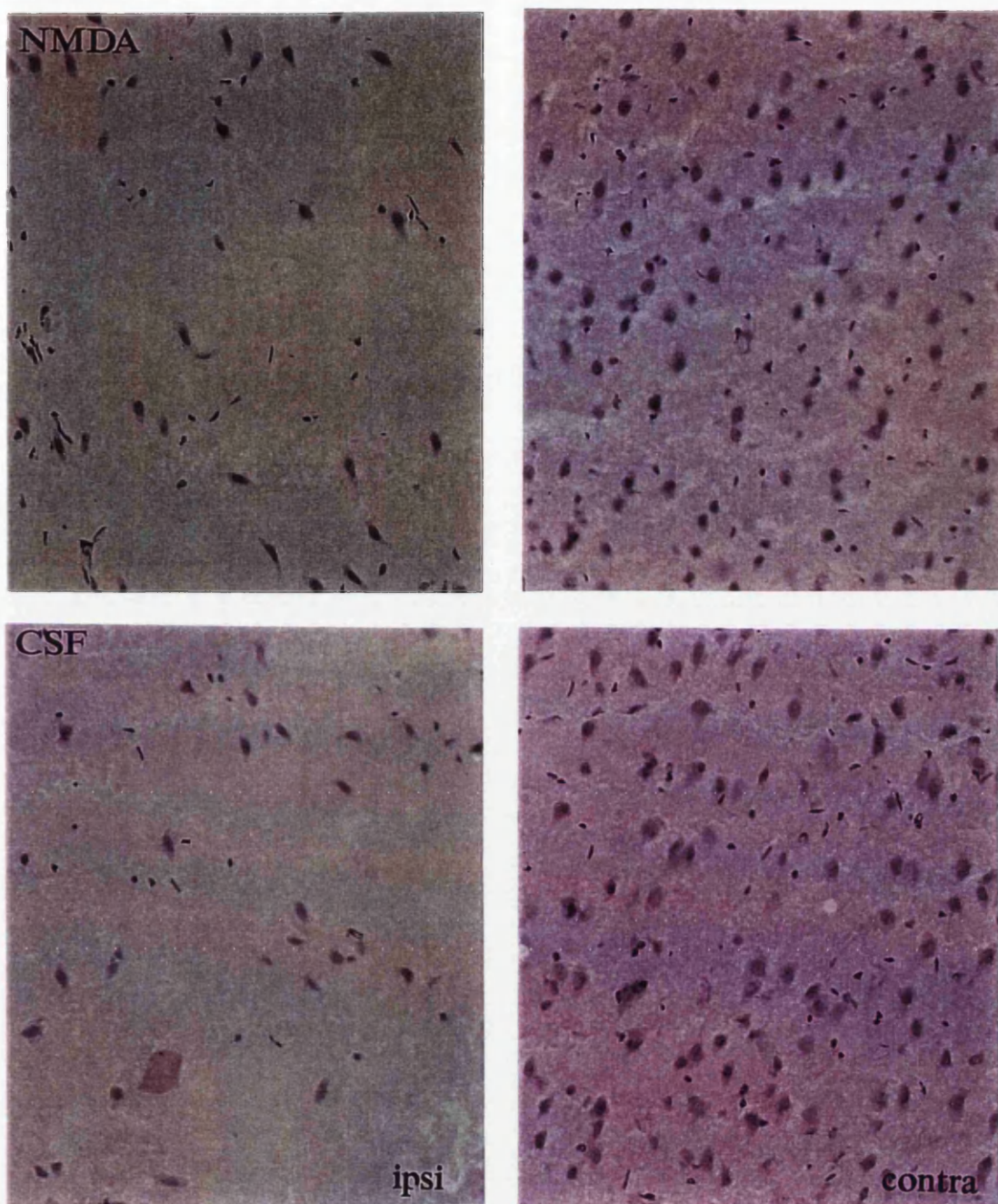


FIGURE 43 : High power photomicrographs from the ipsilateral and contralateral cortex 120 minutes after injection of NMDA or CSF

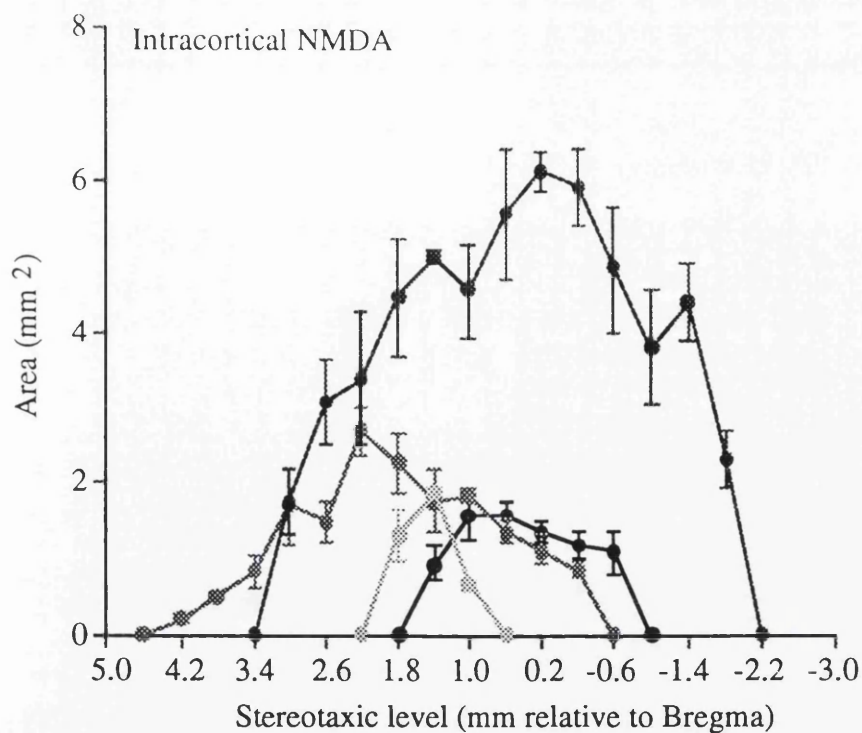
High power photomicrographs (x 50) were taken from the area of pallor (ipsilateral cortex) and from the corresponding area of the contralateral hemisphere 120 minutes after intracortical injection of NMDA (upper) or CSF (lower). Note the loss of staining within the ipsilateral cortex (left).

Five minutes after intravenous injection the distribution of [125 I]CNS 1261 in the contralateral hemisphere was highest within areas known to have high blood flow, such as the anterior thalamus and cortical areas (layers V-VI > layer IV > layers I-III, Figure 37). High levels of uptake were also observed within the supraoptic and paraventricular hypothalamic nuclei and mamillary body. Intermediate levels of uptake were observed in thalamus and lowest levels of uptake in the hippocampus and hypothalamus.

Intracortical injection of NMDA or CSF produced distinct alterations in [125 I]CNS 1261 uptake within the ipsilateral hemisphere. Intracortical injection of both NMDA and CSF produced a general decrease in [125 I]CNS 1261 uptake in the anterior cingulate, sensory motor, parietal, auditory, posterior cingulate, visual and entorhinal cortices. A reduction on [125 I]CNS 1261 uptake was also observed within the insular cortex (Figure 37). In addition, intracortical injection of NMDA produced an intensely 'white zone' on the autoradiograms which was localised around the injection site. This 'white zone' extended through all the cortical layers and for approximately 400 μ m on either side of the injection site. This 'white zone' was bounded by a narrow margin of increased [125 I]CNS 1261 uptake.

Intracortical injection of CSF produced a smaller and less intense 'white zone' at the injection site. A narrow boundary of increased uptake was less evident in these animals.

Sixty minutes after intravenous injection the highest levels of [125 I]CNS 1261 uptake were observed within the hippocampus (80% above that within the cerebellum). Injection of NMDA or CSF produced alterations in [125 I]CNS 1261 uptake within the ipsilateral cortex. NMDA injection produced a lesion with a pale core area surrounded by a narrow border of increased uptake, the size and extent of the lesion is detailed in Figure 44.



(b)

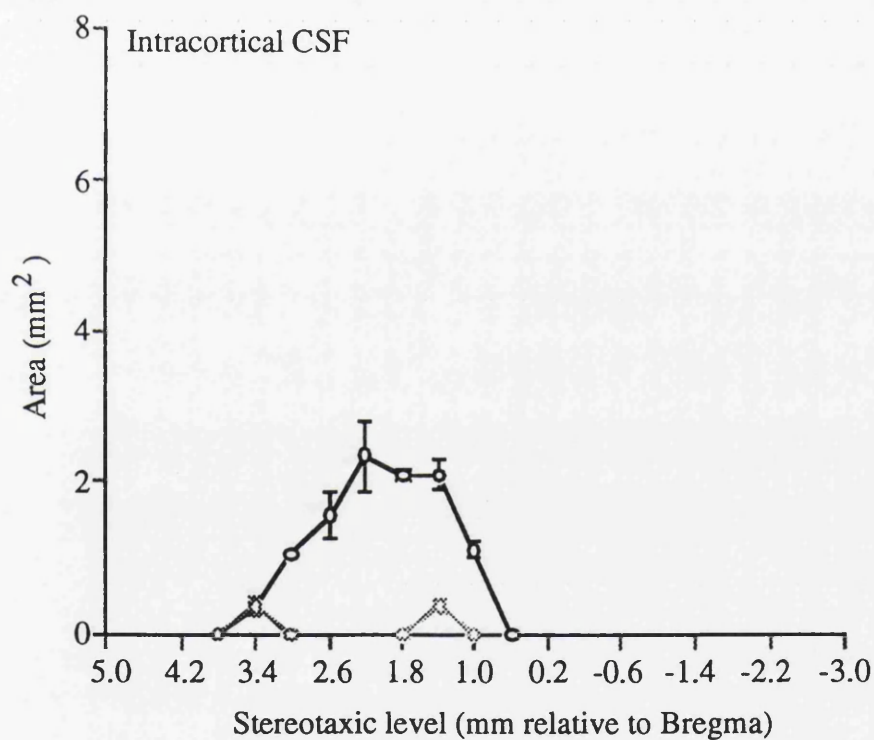


FIGURE 44 : Size and extent of lesions 60 minutes after injection of NMDA or CSF

The size of the lesions on individual [¹²⁵I]CNS 1261 autoradiograms 60 minutes after intracortical injection of NMDA (upper) and CSF (lower) were measured by area analysis and plotted against stereotaxic level. NMDA injection produced larger more extensive lesions than CSF injections.

At its maximum the pale core area measured between 2-6 mm² and extended approximately 6mm. [¹²⁵I]CNS 1261 uptake within the pale core area was approximately 50% lower than in the corresponding area of cortex on the contralateral hemisphere. [¹²⁵I]CNS 1261 uptake within the border zone was 40% above that in the darkest area of the contralateral hemisphere.

In contrast, CSF injection produced much smaller, more localised lesions (Figure 44). Extremely small (<1 mm²) lesions were measured in two animals and a slightly larger lesion (2mm²) in the third animal investigated. A rim of increased [¹²⁵I]CNS 1261 uptake was observed around the largest lesion (20% above contralateral hemisphere), however this was less evident than in NMDA-induced lesions.

120 minutes after intravenous injection, [¹²⁵I]CNS 1261 uptake was similar to that described in previous experiments at 60 minutes and reflected the classical pattern of NMDA receptor distribution, with highest levels within the hippocampus, intermediate levels in the thalamus and lowest levels within the hypothalamus and cerebellum. Both NMDA and CSF injection produced alterations in [¹²⁵I]CNS 1261 within the ipsilateral cortex. NMDA injection produced a large lesion, the size and extent of which is shown in Figure 45. The lesion could be characterised as an extensive area of pallor (40% lower than contralateral levels) extending from the cortical surface to immediately above the corpus callosum. At its maximum, the area of pallor measured between 4-8 mm² and extended approximately 6mm from the injection site. A narrow margin of increased [¹²⁵I]CNS 1261 uptake was observed surrounding this paler core area. [¹²⁵I]CNS 1261 uptake in this area was approximately 70% higher than in corresponding areas of the contralateral hemisphere. CSF injection produced a smaller, much more circumscribed lesion than NMDA injection (Figure 45). This lesion could still be described as an areal of pallor (< 1mm²) bounded by a rim of increased uptake (20% above contralateral values), however this was less evident than in NMDA-induced lesions.

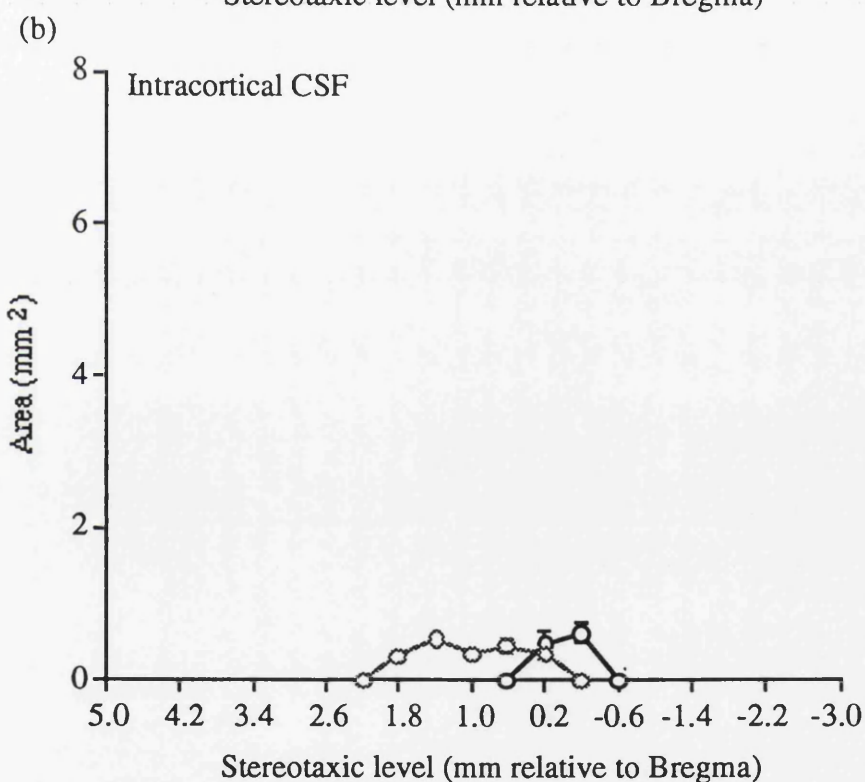
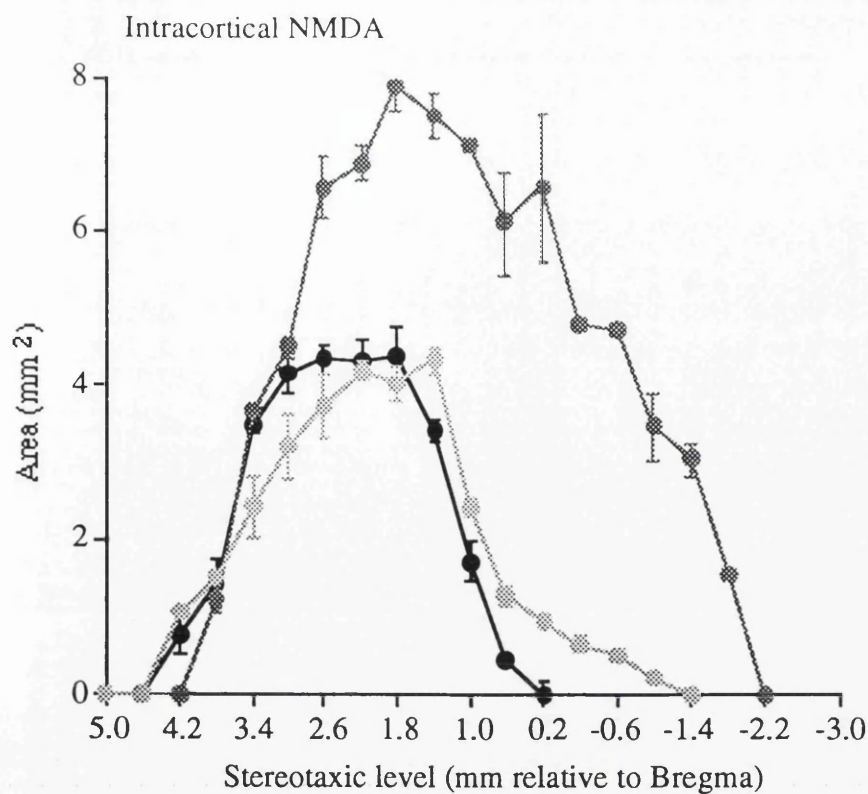


FIGURE 45 : Size and extent of lesions 120 minutes after injection of NMDA or CSF

The size of the lesions on individual [¹²⁵I]CNS 1261 autoradiograms 120 minutes after intracortical injection of NMDA (upper) and CSF (lower) were measured by area analysis and plotted against stereotaxic level. NMDA injection produced larger more extensive lesions than CSF injections.

In a single animal, [^{125}I]CNS 1261 uptake at 120 minutes after intracortical injection of CSF did not reflect the pattern described in previous experiments with the same procedure (Figure 46). Notes taken during this experiment state that some damage was caused to pial vessels during removal of the bone. Sub cortical blood was evident when the brain was cut and processed for autoradiography indicating inadvertant rupture of a blood vessel during injection. H & E staining showed an area of pallor extending beyond the subcortical white matter into the caudate nucleus. Disruption of white matter was evident within this area (Figure 46). This animal was excluded from the CSF injection group due to these observations. Examination of this autoradiogram showed fairly homogeneous low levels of [^{125}I]CNS 1261 uptake throughout the brain. However, areas of increased [^{125}I]CNS 1261 uptake (approximately 3 times greater than in corresponding contralateral areas) exist within the ipsilateral cortex and within the caudate nucleus.

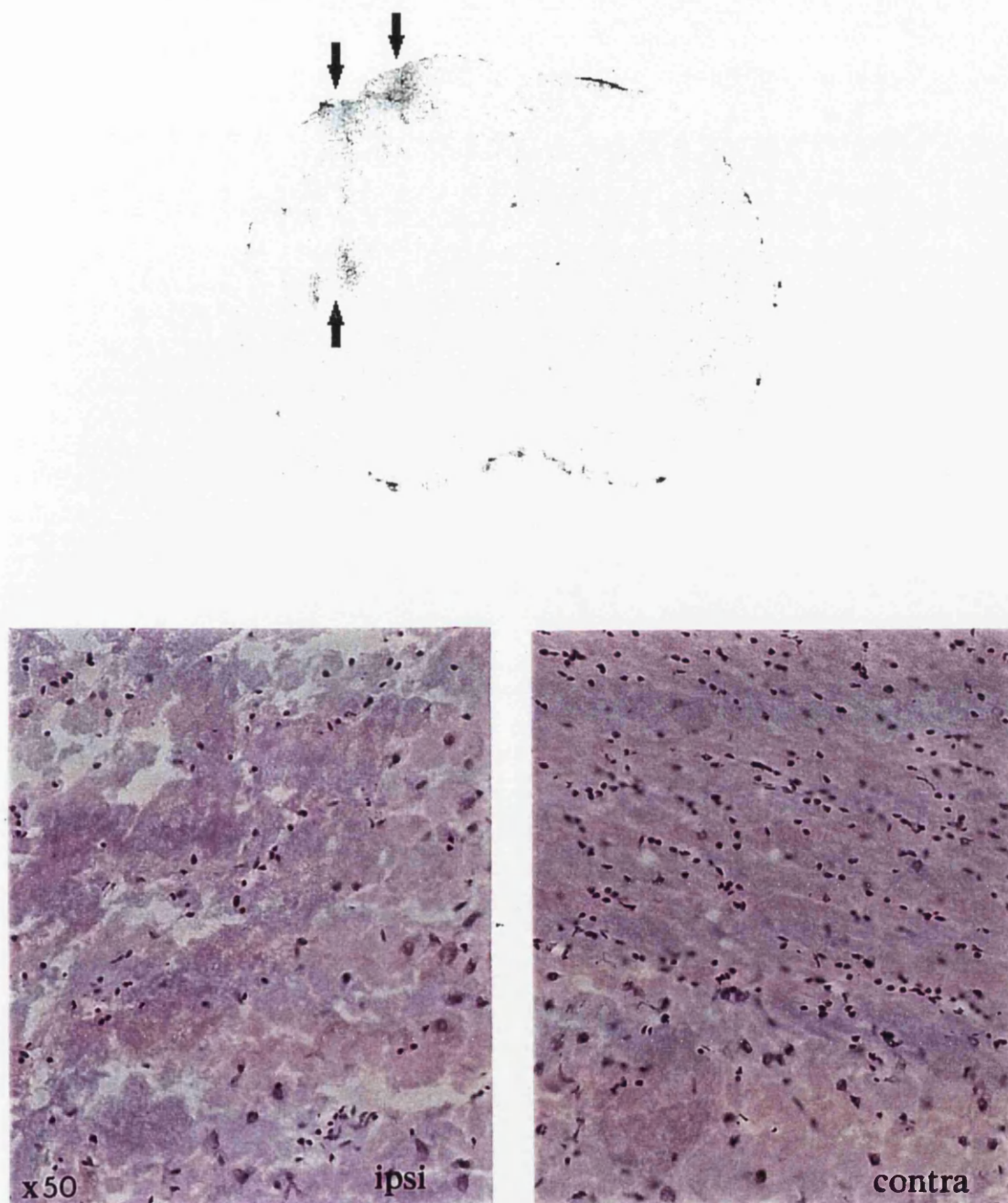


FIGURE 46 : $[^{125}\text{I}]\text{CNS 1261}$ uptake is increased in areas of damage

The upper figure shows a representative autoradiogram from an experiment with abnormal $[^{125}\text{I}]\text{CNS 1261}$ uptake following CSF injection. $[^{125}\text{I}]\text{CNS 1261}$ was increased at the injection site and in subcortical region within the ipsilateral hemisphere (arrows). High power photomicrographs (lower) show that there is damage within the subcortical white matter of the ipsilateral cortex (left). Contralateral subcortical white matter is shown on the right for comparison.

CHAPTER IV
DISCUSSION

4.1 CNS 1261 acts as a non-competitive NMDA receptor antagonist

Potential candidates for use as *in vivo* imaging agents must satisfy a number of criteria *in vitro*. Ligand binding must be pharmacologically selective, and of high affinity for the receptor target of interest.

Initial *in vitro* binding experiments showed that CNS 1261, an analogue of Cerestat (Aptiganel, CNS 1102) inhibited [^3H]MK801 binding to rat brain membranes with $K_i = 25\text{nM}$ in Tris buffer. Wong *et al* (1988) reported that MK801 displaced [^3H]MK801 binding to rat brain homogenates with $K_i = 3\text{nM}$, with similar results for the inhibition of [^3H]TCP binding. CNS 1261 is therefore approximately 10 times less potent than MK801 in inhibiting [^3H]MK801 binding. The association affinity constant (K_i) of CNS 1261 is comparable with the reported values for inhibition of [^3H]MK801 binding by known non-competitive NMDA receptor antagonists TCP and PCP (14nM and 42nM respectively). The dissociative anaesthetic ketamine inhibits [^3H]MK801 binding with $K_i = 1\mu\text{M}$ (Wong *et al*, 1988).

Results of the commercial screen show that at the doses examined, CNS 1261 caused a 99% inhibition of [^3H]MK801 binding. CNS 1261 showed little affinity for other subtypes of glutamate receptor, inhibiting [^3H]AMPA binding by only 3%. CNS 1261 also did not display affinity at the transmitter recognition site or the glycine site of the NMDA receptor complex.

Non-competitive antagonists can generally be classified into groups which exhibit more or less selectivity between MK801 and σ opioid sites (Wong *et al*, 1988). Modification of the structure of DTG (*N,N'*-di-*o*-tolylguanidine), a known selective σ receptor ligand, led to the synthesis of novel diarylguanidines which exhibit high selectivity for the NMDA receptor ion channel site and weak or negligible for σ receptors. Compounds having ortho or meta substituents on the phenyl rings, such as CNS 1102 (*N*-(1-naphthyl)-*N'*-(3-ethylphenyl)-*N'*-methylguanidine), show greater affinity for the NMDA receptor ion channel site (Reddy *et al*, 1994). CNS 1261, a structural analogue of CNS 1102, displays a clear selectivity for the NMDA receptor ion channel site and does not

display activity in the opiate receptor binding assay (5% inhibition of [³H]naloxone binding).

It was of interest that CNS 1261 was found to inhibit [³H]prazosin binding to the α 1 adrenoceptor by 33%. While 'activity' in a given assay was described as > 50% inhibition, this effect may be an indication of potential sympathomimetic effects of this compound.

Observations from *in vitro* binding experiments suggest that CNS 1261 displays both high affinity and selectivity for the MK801 binding site within the NMDA receptor channel.

The [¹⁴C]2-deoxyglucose autoradiographic technique allows an anatomically comprehensive assessment of function-related alterations in cerebral glucose use *in vivo*. The functional activity of any brain region is intrinsically linked with the energy consumption within that region. Local alterations in glucose use have been used to demonstrate the involvement of discrete brain areas during various physiological and pharmacological interventions. The systemic administration of NMDA channel blocking agents such as MK801 result in overt behavioural responses and marked alterations in glucose use within the central nervous system which can be distinguished from those produced by competitive NMDA antagonist (Kurumaji *et al*, 1989, Sharkey *et al*, 1994). CNS 1261 administration produced behavioural effects at all doses examined (1, 3, 10mg/kg) consisting of stereotypical side-to-side and cyclical head movements, sedation and a reduced response to external stimuli. These overt behavioural changes were similar to those described by others following administration of MK801 (Kurumaji *et al*, 1989, McCulloch and Iversen, 1990).

Administration of CNS 1261 (3mg/kg and 10mg/kg) to conscious animals produced a dose-dependent moderate hypertension (e.g. 20-40 mmHg increase in mean arterial pressure compared to pre-injection levels). A modest increase in p_aCO₂ was also observed following administration of CNS 1261 (10mg/kg). Studies investigating the effect of MK801 on glucose use reported comparable effects on cardiovascular and

respiratory parameters. Administration of competitive NMDA antagonists, such as CPP did not significantly alter arterial pressure (Kurumaji *et al*, 1989, Nehls *et al*, 1990., Sharkey *et al*, 1994). In ligand binding studies, CNS 1261 does not interact with dopamine, serotonin, muscarinic, GABA or benzodiazepine binding sites, however sympathomimetic effects are implied from its moderate activity at the α -1 adrenoceptor. The increase in mean arterial pressure after administration is consistent with such an effect. Baroreceptor reflexes activated by a rise in arterial pressure cause a reflex bradycardia and inhibition of respiration which may account for the observed increase in CO₂ tension following administration of the highest dose of CNS 1261

CNS 1261 administration (1-10mg/kg) resulted in statistically significant increases in glucose use within the hippocampus molecular layer, dentate gyrus, limbic system (posterior cingulate cortex, caudal entorhinal cortex mamillary body, anteroventral thalamus), retrosplenial cortex and the myelinated fiber tracts of the fornix. Glucose use within the neocortex and inferior colliculus was particularly sensitive to CNS 1261 administration. The overall pattern of alterations in glucose use produced by administration of CNS 1261 was extremely similar to that described for MK801 (Kurumaji *et al*, 1989, Nehls *et al*, 1990, for review see McCulloch and Iversen, 1991, Kurumaji *et al*, 1993). The regional changes in glucose utilisation following administration of CNS 1261 do not correlate simply with the NMDA receptor density (Jarvis *et al*, 1987, Wong *et al*, 1988). While glucose use was increased in areas such as the hippocampal molecular layer which possesses a high number of NMDA receptors, no changes in glucose use were observed within the CA1 region of the hippocampus which has one of the highest densities of NMDA receptors in the central nervous system

The magnitude of elevations in glucose use within limbic structures was generally in the region of 80%, however exceptionally large increases in glucose use (100-200%) were observed within entorhinal cortex (caudal) and within the mamillary body.

The dentate gyrus and hippocampus receive a major glutamatergic innervation from the entorhinal cortex via the perforant pathway (White *et al*, 1977). The activation and hypermetabolism observed in some limbic structures following administration of CNS

1261 is consistent with an increased firing in the perforant pathway in response to receptor blockade within the hippocampal formation. Agents producing a use-dependent, non-competitive blockade of the NMDA receptor increase firing in the perforant pathway, leading to a progressive intensification of the blockade and corresponding increase in glucose use not only within the hippocampus and entorhinal cortex, but throughout the entire Papez circuit (entorhinal cortex → hippocampus → mamillary body → anterior thalamus → cingulate cortex → entorhinal cortex). Lesions of the entorhinal complex remove the ability of MK801 to increase glucose use in the hippocampus molecular layer and dentate gyrus (Kurumaji and McCulloch, 1990)

The use of the f ranking function provides a means of incorporating all the information available from the dose-response relationships for each agent in each of the 36 regions investigated and provides a valuable approach for comparing and contrasting the anatomical patterns of glucose use alterations evoked by CNS 1261 and MK801 treatment. The utility of the f ranking function has previously been illustrated by its ability to separate the functional effects of the benzodiazepine diazepam, from those of the GABA agonists muscimol and THIP (Kelly *et al*, 1986). Despite the broad similarities in regional responsiveness to CNS 1261 and MK801, differences in f values were observed in a small number of regions indicating subtle differences in sensitivity in the effects of the two agents on glucose use in certain central nervous system regions. In the present study glucose use in the majority of regions examined was generally equipotent. The entorhinal cortex (caudal) was the most responsive region to both agents, however f values for CNS 1261 and MK801 were 3.45 and 1.85 respectively. In the same way, glucose use in the anteroventral thalamus, mamillary body, inferior colliculus and fornix was more sensitive to CNS 1261 than MK801. In contrast, the entorhinal cortex (rostral) was much less sensitive to CNS 1261 than to MK801 ($f = 0.024$ and 0.79 respectively). The clustering of f function data for both agents into a well accepted functional system suggests that the similarity of effects of the 2 agents are not random numerical artefacts. The precise mechanism underlying the subtle functional heterogeneity of the 2 agents is unknown. It is suggested that this does not reflect an action on other receptor

populations since both agents display high affinity and specificity for the NMDA channel binding site. The heterogeneity may imply preferential actions of the compounds on different subtypes of NMDA receptor in certain brain regions (Nakanishi, 1992).

The overall pharmacological effects of CNS 1261 on radioligand binding *in vitro* and on glucose use *in vivo* are consistent with the action of a non-competitive NMDA receptor antagonist. This is further confirmed by the action of CNS 1261 on electrically-induced cortical spreading depression (CSD) *in vivo*.

CSD is a transient suppression of electrical activity with associated membrane depolarisation which propagates across the cortex at a rate of 2-5mm/min. This phenomenon has been associated with the pathology of a number of neurological conditions, including stroke, epilepsy, and migraine with aura (McLachlan and Girvan, 1994). While the driving force for CSD propagation is high extracellular K^+ (>10 - 12 nM), a transient, localised release of glutamate and Ca^{2+} influx through the NMDA receptor are also essential (Nellgård and Wieloch, 1992, Obrenovitch, 1995). CSD is consistently observed in regions adjacent to the ischaemic core produced by middle cerebral artery occlusion, and has been implicated as a factor which ultimately determines infarct size (Nedergaard and Hansen, 1995). This short study was carried out at Pfizer Central Research, Sandwich. While this study was not central to ligand development, it provided a further insight into CNS 1261 pharmacology *in vivo* (protocol detailed in Appendix 1). CNS 1261 (1mg/kg) completely abolished initiation and propagation of CSD in all animals studies. Inhibition of responses occurred 14 ± 1 (n = 4) min. post-injection. Blockade of responses remained evident 90 minutes post-administration.

4.2 [125 I]CNS 1261 uptake in the normal rat brain

[125 I]MK801 has been employed to map the distribution of activated NMDA receptor complexes throughout the central nervous system (McCulloch *et al*, 1992, Wallace *et al*, 1992). The principle underlying this technique is that ligands acting at the NMDA receptor ion channel bind in a use-dependent manner, i.e. MK801 (and Iodo-MK801)

preferentially gain access to the binding site within the channel when the receptor has been activated (Huettnner and Bean, 1988, MacDonald and Nowak, 1990). MK801 and Iodo-MK801 are highly lipophilic molecules and readily cross the blood-brain barrier. Therefore, following intravenous injection of tracer levels of [^{125}I]MK801, the subsequent autoradiographic detection and measurement of [^{125}I] in discrete brain regions allows quantitative mapping of [^{125}I]MK801 binding. Within the normal brain, it is suggested that the level of NMDA receptor activation reflects the distribution of receptors such that uptake of radiolabelled tracers directed towards the NMDA ion-channel binding site is greatest in areas with a large population of receptors (hippocampus), lower in areas of intermediate density (cortex and thalamus) and least in areas with a paucity of receptors (hypothalamus and cerebellum, Monaghan and Cotman 1985).

In the present thesis a modification of the [^{125}I]MK801 *in vivo* binding technique described by McCulloch *et al* (1992) was used to investigate the *in vivo* uptake and retention of [^{125}I]CNS 1261, to elucidate whether this novel tracer can be used to map the distribution and hence the activation of the NMDA receptor-channel complex in the normal brain.

In order to take into account the degree of non-specific binding of tracers within the brain, densitometric measures of isotope levels in forebrain structures were compared with cerebellar isotope levels. It was suggested that tracer uptake within the cerebellum serves as a measure of non-specific binding due to the paucity of NMDA receptors in this region (McCulloch *et al*, 1992).

Quantitative autoradiographic studies using [^3H]MK801 describe a 5 fold greater receptor density within the CA1 region of the hippocampus than in the cerebellum (150 fmol/mg compared to 30 fmol/mg respectively, Bowery *et al*, 1988). This is supported by observations from studies using [^3H]TCP where receptor densities were 2-6 fold greater in CA1 than in the cerebellum (Sircar and Zukin, 1985, Hosford *et al*, 1990). In addition to these findings radioligand binding studies have demonstrated differences in the affinity

of ligands for NMDA receptors throughout the rat brain. The affinity of [^3H]TCP was 10 times higher for NMDA receptors within the cortex and hippocampus compared to the medulla oblongata and cerebellum, implying non-competitive NMDA receptor antagonists bind preferentially to sites within the forebrain (Vignon *et al*, 1986). Studies by Sakurai (1991) confirmed these observations however the differences in affinity were of a small magnitude (< 1 log unit). Other radioligand binding studies showed that cerebellar receptors were not labelled by low concentrations of [^3H]MK801 (Bowery *et al*, 1988). Studies by Nakanishi (1992) showed that the heterogeneity can be attributed to differential expression of subunits, the cerebellum expresses NR2C subunits which have been shown to possess a lower affinity for antagonists. Therefore, due to both the lower density of NMDA receptors and the observed lower affinity of non-competitive antagonists in this region, the cerebellum appears to be an appropriate measure of non-specific binding.

The initial uptake of lipophilic molecules that enter the central nervous system with no diffusion restriction should be dominated by their rate of delivery to the tissue (Rapoport *et al*, 1976). Five minutes after administration, both [^{125}I]CNS 1261 and [^{125}I]MK801 uptake was observed to be highest in areas known to have high blood flow, such as the anterior cingulate cortex and lateral habenulae (Table 25). Low levels of tracer were observed in areas with low blood flow. Despite similarities in the overall pattern of distribution of the two tracers, the appearance of the autoradiograms were markedly different.

TABLE 25

Tracer uptake appears to reflect cerebral blood flow (CBF) 5 minutes after administration

STRUCTURE	CBF (ml/100g/min.)	[¹²⁵ I]MK801 (μ Ci/g)	[¹²⁵ I]CNS 1261 (μ Ci/g)
Lateral habenular nucleus	146	152	62
Anterior cingulate cortex	119	120	61
Hippocampus	109	76	33
Corpus callosum	36	52	22

The absolute amount of [¹²⁵I]MK801 or [¹²⁵I]CNS 1261 uptake (μ Ci/g) within selected structures 5 minutes after administration was compared to cerebral blood flow values for these regions. Cerebral blood flow values (ml/100g/min.) were taken from a previous study carried out by Gotoh *et al*, 1990. It can be seen that the highest levels of tracer were observed within areas with high CBF values. Low levels of tracer were observed within white matter areas such as the corpus callosum which has correspondingly lower CBF values.

[¹²⁵I]MK801 uptake was diffuse and was reminiscent of autoradiograms produced by the blood flow tracer [^{99m}Tc]HMPAO (Gartshore, 1996).

In contrast a greater degree of resolution was observed in [¹²⁵I]CNS 1261 autoradiograms and increased uptake was observed in layer IV of the cerebral cortex and within the supraoptic and paraventricular hypothalamic nuclei. The increased uptake within these regions may be attributed to the high capillary density of these regions. The distribution of capillaries within the brain is heterogeneous (Zeman and Innes, 1963). The heterogeneity is structurally organised and correlates with the number of synapses within the region, the total length of the vessels in a unit volume of tissue is much greater in grey matter than in white matter. Capillary density also differs greatly within grey matter regions, with sensory and correlation centres more richly vascular than motor regions. Brain areas that possess a high density of capillaries also have high basal levels of glucose use and blood flow (Edvinsson *et al*, 1993). The paraventricular and supraoptic hypothalamic nuclei are the most richly vascular grey areas observed in the whole brain with approximately 2000mm of capillaries in 1mm³ of tissue. Within the cerebral cortex different laminae also differ in their vascularity, parietal cortex layer I possesses approximately 900mm of capillaries in 1mm³ of tissue while layer IV has 1300mm.

It appears therefore that the high levels of [¹²⁵I]CNS 1261 uptake within layer IV and within the hypothalamic nuclei can be accounted for by the large capillary surface area and hence the high cerebral blood flow of these regions. This relationship appears to extend to other brain areas with lower blood flow. Lower levels of [¹²⁵I]CNS 1261 uptake were observed within the cerebellum (800mm) and the ventromedial hypothalamus (500mm).

The precise reason underlying the observation that [¹²⁵I]MK801 uptake is not increased within layer IV of the cerebral cortex or the hypothalamic nuclei at early time points is unknown. However, it is suggested that even at very early time points the high lipophilicity of [¹²⁵I]MK801 causes this tracer to be distributed in a manner not solely dependent on blood flow.

At times beyond 30 minutes, the overall pattern of uptake of both [125 I]CNS 1261 and [125 I]MK801 appeared to reflected the known distribution of NMDA receptors (Bowery *et al*, 1988) with highest levels within the hippocampus and low levels in the hypothalamus and cerebellum. Closer inspection of the autoradiograms showed that NMDA receptor density did not determine tracer uptake in all regions examined. Isotope concentrations within the cerebral cortex 120 minutes after [125 I]MK801 administration were homogeneous, and did not reflect NMDA receptor density. In contrast 120 minutes after [125 I]CNS 1261 administration isotope levels did show some heterogeneity but this also did not reflect NMDA receptor density. [125 I]CNS 1261 uptake was increased within the deep layers of the cortex relative to the superficial layers and, it is well established that the greatest concentration of NMDA receptors is within the outer layers of the neocortex (Bowery *et al*, 1988, Maragos *et al*, 1988). Wallace *et al* (1992) also showed that the density of NMDA receptors *in vitro* did not determine the uptake of [3 H]MK801 *in vivo*. These observations suggest that factors other than receptor density (lipophilicity) determine local isotope uptake under conditions of basal NMDA receptor activation.

At 120 minutes the relative uptake of [125 I]CNS 1261 within hippocampal regions (CA1, CA3, molecular layer) was approximately twice as great as that of [125 I]MK801. It was proposed that a greater relative uptake of [125 I]CNS 1261 within the hippocampus (hippocampus/cerebellar ratio) could result from a faster washout of [125 I]CNS 1261 from the cerebellum compared to [125 I]MK801 rather than an increased uptake in the hippocampus. Therefore, the normalisation procedure was examined to determine if the increase in relative uptake could be attributed to differences in the rate of washout of the tracers from the cerebellum. The absolute amount of radioactivity (μ Ci/g) within a region of high, intermediate and low NMDA receptor density (hippocampus CA1, mediodorsal thalamus and hypothalamus respectively) was plotted against time over the last 60 minutes of the experiment for both [125 I]MK801 and [125 I]CNS 1261 along with the cerebellum (Figure 47).

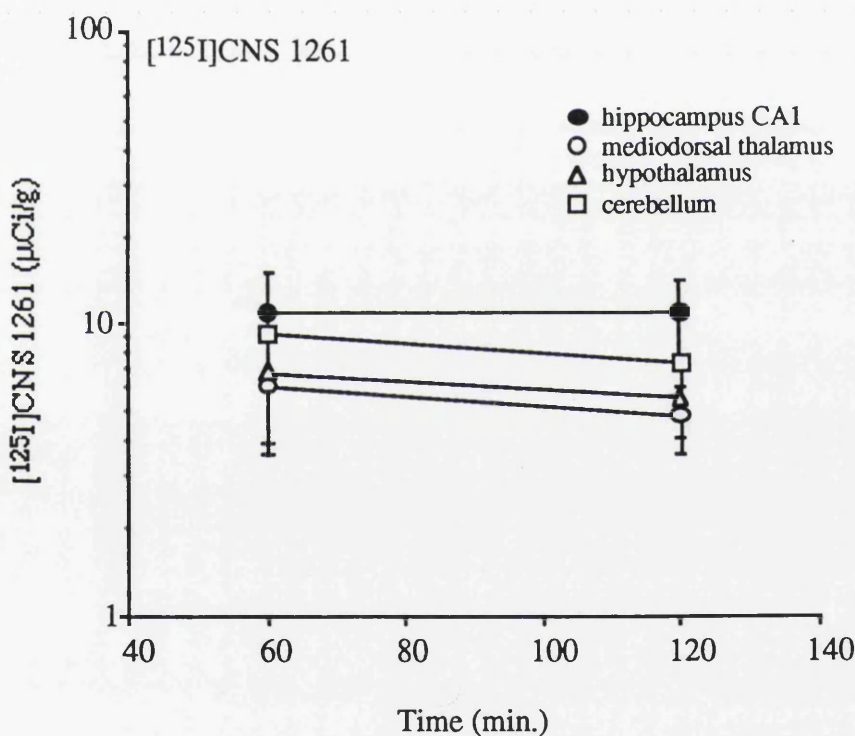
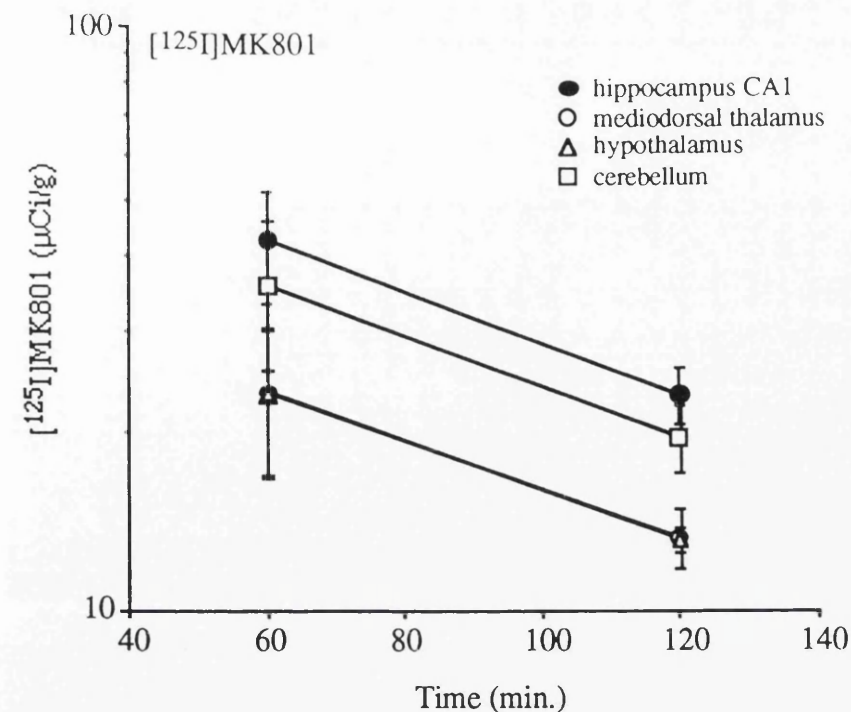


FIGURE 47 : Washout rates of [¹²⁵I]MK801 and [¹²⁵I]CNS 1261 from regions of interest

Over the final 60 minutes of the experimental period, [¹²⁵I]MK801 washed out of regions with high, intermediate and low NMDA receptor densities at the same rate. In contrast there was some degree of retention of [¹²⁵I]CNS 1261 within the hippocampus CA1. Data are mean \pm S.E.M.

For [^{125}I]MK801 the washout slope was the same for all regions examined. The washout rate was not affected by the NMDA receptor density. [^{125}I]MK801 was shown to wash out of the hippocampus at the same rate as from the cerebellum, therefore the relative uptake of [^{125}I]MK801 within the CA1 region changed little over the terminal 60 minutes of the experiment. This graph also shows that normalisation to the hypothalamus, another region with a paucity of NMDA receptor, would have given the same relative uptake values

Figure 47 shows that there is virtually no washout of [^{125}I]CNS 1261 from CA1 region over this time therefore the ratio of uptake in the CA1 region relative to the cerebellum increased over the same time period. In contrast, the rate of [^{125}I]CNS 1261 washout from other regions was approximately the same as that from the cerebellum. In this case, normalisation to the hypothalamus would also have given the same relative values of tracer uptake. Comparison of the tracer washout rates from the cerebellum over the remaining 60 minutes of the experimental period indicates that [^{125}I]MK801 washes out at a similar rate than [^{125}I]CNS 1261. It can be concluded therefore that the increased relative uptake of [^{125}I]CNS 1261 within the hippocampus 120 min after administration is not due to a faster washout of this tracer from the cerebellum compared to [^{125}I]MK801, but to retention of the tracer in regions with a high density of NMDA receptors.

4.3 [^{125}I]CNS 1261 produces superior images to [^{125}I]MK801 in the normal brain

Comparison of the uptake of [^{125}I]MK801 and [^{125}I]CNS 1261 in the normal brain at 120 minutes, showed that under identical experimental conditions the relative uptake of [^{125}I]CNS 1261 within hippocampal regions was greater than that of [^{125}I]MK801. A number of factors contribute to the amount of tracer within a brain region at a give time including cerebral blood flow, the concentration of tracer within the plasma and the lipophilicity of the tracer. It has been suggested that the most critical physical property for a high affinity radiotracer is lipophilicity (Audus *et al*, 1992) since hydrophilic ligands

do not cross the blood-brain-barrier and very lipophilic compounds display excessive non-receptor binding.

The blood-brain-barrier consists of a phospholipid bilayer which confers selective permeability to nonionised species. The solubility of unionised species can be measured conveniently as the octanol/water partition coefficient. LogD_{7.4} (octanol/buffer) values for CNS 1261 and IodoMK801 were 2.19 and 3.30 respectively, showing that while both compounds are extremely lipophilic, CNS 1261 is substantially less so than MK801. The presence and position of an iodine moiety in these structures appears to underlie this lipophilicity since the LogD values of the 'precursor' compounds, CNS 1102 and MK801, are similar (1.72 and 1.8 respectively).

The membrane permeability of a compound is also proportional to a partition parameter which represents the ability of the compound to partition between a lipid phase and aqueous solution (von Geldern *et al*, 1996). The 'brain/aqueous partition ratio' is generally considered to be a measure of lipophilicity (Rapoport, 1976) and represents the tendency of a compound to distribute into the brain (lipid) rather than the aqueous phase (plasma) and may be calculated from the non-specific binding of radioiodinated ligands to rat and human brain sections *in vitro*. The brain/aqueous partition ratios for both [¹²⁵I]CNS 1261 and [¹²⁵I]MK801 were high (15-35g/ml) confirming that these tracers are extremely lipophilic. In both rat and human brain sections, the brain/aqueous partition ratios for [¹²⁵I]CNS 1261 were 40% lower than those obtained for [¹²⁵I]MK801, implying [¹²⁵I]CNS 1261 may display a lower non-specific binding component *in vivo*.

Highly lipophilic compounds can bind tightly to serum proteins such that the free fraction of compound available to cross the blood-brain-barrier is reduced. It was of interest therefore to determine the extent of [¹²⁵I]MK801 and [¹²⁵I]CNS 1261 binding to protein in rat and human plasma. Results showed that both tracers were approximately 95% protein bound.

An essential property for a candidate SPECT ligand is that metabolism produces no lipophilic breakdown products. The low levels of activity found in rat plasma samples

after administration of a radiolabelled tracer were detected using an hplc flow monitor which markedly increase radio hplc detection sensitivity. Several methods of plasma sample preparation were investigated for use in this system. The preferred method was the precipitation of plasma proteins with an aqueous miscible organic solvent followed by centrifugation to leave a clear supernatant. The supernatant was then directly applied to the hplc column. This method has the advantage of allowing the direct measurement of both aqueous and organic soluble radiolabelled species in the sample. Using this method a measurement of the authenticity of the tracer within the brain at a given time point was also obtained. This method has been previously applied to small groups of rats to study [^{125}I]QNB, and to study [^{123}I]BZM metabolism in plasma in man. Hplc analysis of plasma samples was carried out by J. Owens at The West of Scotland Radionuclide Dispensary.

From the results of the hplc plasma analysis it appears that both tracers undergo deiodination on first pass metabolism. Two species were identified within the plasma of rats receiving [^{125}I]CNS 1251, authentic CNS 1261 and free iodine. A small amount of a third species, along with authentic MK801 and free iodide, was identified within the plasma of animals receiving [^{125}I]MK801. The identity of this species is unknown, but it may be a non-lipophilic metabolite of [^{125}I]MK801 since this species was not present within the brain. [^{125}I]CNS 1261 is metabolised much more rapidly than [^{125}I]MK801 and it is suggested that this rapid metabolism following administration of a bolus dose may confer advantages over a tracer with a slower metabolism.

4.3.1 Kinetic modelling

A 3 compartment model (Figure 48) was used to examine the hypothetical brain concentrations arising from tracers with an input function like that of [^{125}I]CNS 1261 where the tracer is rapidly cleared from the plasma (Figure 25). This was compared to hypothetical brain concentrations obtained following administration of a tracer with a slower input function like [^{125}I]MK801 (Figure 27).

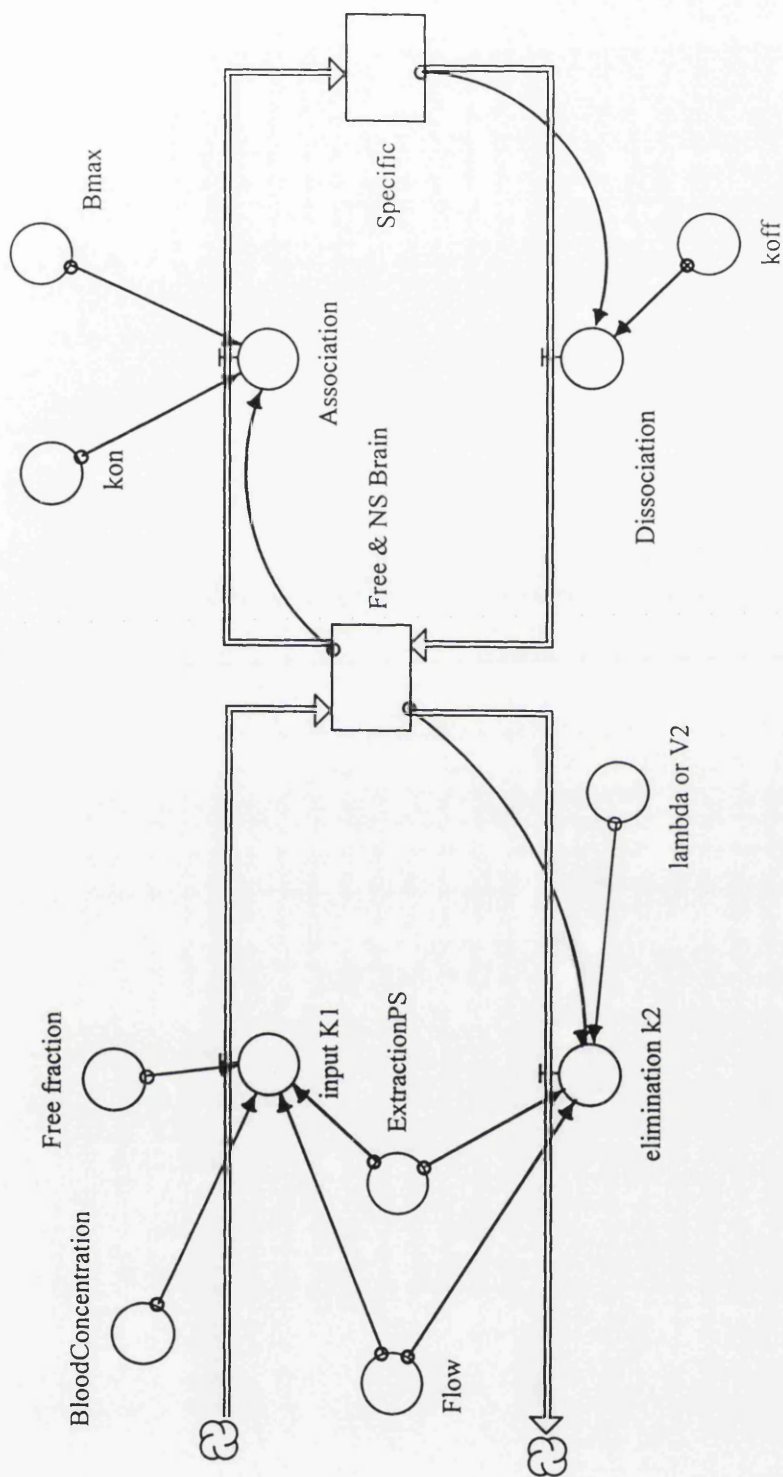
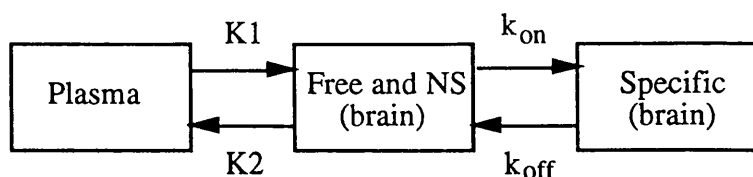


FIGURE 48 : 3 compartment model of tracer uptake into the brain

A three compartment model of tracer uptake into the brain was devised using the Stella II modelling program. The model is set up to reflect the situation where a tracer moves from the plasma into a second compartment within the brain which describes free and non-specifically bound tracer. An equilibrium exists between the 'free' brain pool and a third compartment describing tracer bound specifically to receptors within the brain. The factors influencing the movement of tracer between these three compartments are shown above. An explanation of terms is contained within the text.

A number of the specifications of this model require discussion. The model is set up to reflect the situation where a tracer compound moves from the plasma into a second compartment within the brain which describes free and non-specifically bound tracer.



A third compartment describes tracer bound specifically to receptors within the brain. The factors influencing the movement of tracer between these three compartments are described below.

1. The amount of tracer delivered to the brain is described by an input constant $K1$ which is determined by the plasma concentration of tracer, the free fraction within the plasma, cerebral blood flow, and the extraction fraction.

- Plasma concentration is described by a graph of percentage of authentic tracer within the plasma against time (see Figures 25 and 27).
- The free fraction was set at 0.03, a value obtained from the literature for iomazenil.
- Cerebral blood flow (ml/g/min.) was variable and values of 0.2, 0.4 and 0.8ml/g/min. were used to represent tracer uptake into white matter and grey matter with low and high flow respectively.
- The extraction fraction is dependent on the capillary surface area S , the capillary permeability P and perfusion (flow) F . The dependence on blood flow reflects the fact that at higher flows, the tracer spends less time within the capillary. The extraction fraction itself may vary as blood vessels dilate and constrict.

2. The elimination rate constant $K2$ describes the amount of tracer flowing out of the brain into the plasma. $K2$ can be expressed as $K1/(V2 \cdot f1)$ where $K1$ is the association rate constant, $V2$ is the volume of distribution of the free and non-specifically bound

compartment and f_1 is the free fraction of tracer within the blood. K_2 is dependent on the concentration of tracer within the brain, the partition coefficient of the tracer, the extraction fraction and cerebral blood flow.

The partition parameter or λ represents the lipophilicity of the tracer and was set at 20 for [^{125}I]CNS 1261 and 35 for [^{125}I]MK801 (see Table 15), this also represents the volume of distribution of the tracer.

3. Unbound ligand reversibly binds to receptors at a rate dependent on the concentration of the 2 reactants. The rate constant for this reaction is known as the association constant k_{on} . k_{on} was set at a value of 0.07. B_{max} equals the concentration of receptors available for binding. For tracer doses this is equal to the receptor density (unless investigating receptor blockade by an administered drug). B_{max} was set at 10 to represent an area with a high number of receptors.

4. The rate of dissociation of the tracer from the receptor is determined by the dissociation rate constant k_{off} and the concentration of tracer within the specifically bound compartment. k_{off} was set at 0.1.

Hypothetical brain concentrations arising from the two types of input function are shown in figure 49. The total brain concentrations of tracers with a rapid plasma clearance like [^{125}I]CNS 1261 reach steady-state more rapidly than tracers which are metabolised more slowly like [^{125}I]MK801. Non-specifically bound tracer is also observed to wash out down its concentration gradient at a faster rate.

Comparison of the actual washout rates of total [^{125}I]MK801 and [^{125}I]CNS 1261 uptake from the cerebellum, an area which represents non-specific binding, confirms the latter observation (Figure 50). It is proposed that the lower lipophilicity and rapid metabolism, leading to faster washout of non-specifically bound tracer may underlie the ability of [^{125}I]CNS 1261 to produce superior images to [^{125}I]MK801.

FIGURE 49 : Hypothetical brain uptake following administration of a tracer with rapid or slow plasma clearance

A three compartment model was used to model the hypothetical uptake and retention of a tracer with a rapid plasma clearance (like [^{125}I]CNS 1261) and one with a slow plasma clearance (like [^{125}I]MK801). Total brain uptake is shown in the upper figures and non-specific uptake in the lower figures. Hypothetical brain uptake and retention for the tracer with rapid clearance was modelled using the plasma input curve of [^{125}I]CNS 1261 and a lambda value of 20. Slow clearance was modelled using the [^{125}I]MK801 plasma input curve and a lambda value of 35. Numbered lines 1, 2 and 3 represent uptake and retention at cerebral blood flow values of 20, 40 and 80ml/100g/min respectively. All other factors influencing uptake and retention of tracers were the same for both tracers.

According to this model, tracers with rapid plasma metabolism reach steady state concentrations within the brain more rapidly and, non-specifically bound tracer washes out down its concentration gradient faster than tracers with slower metabolism.

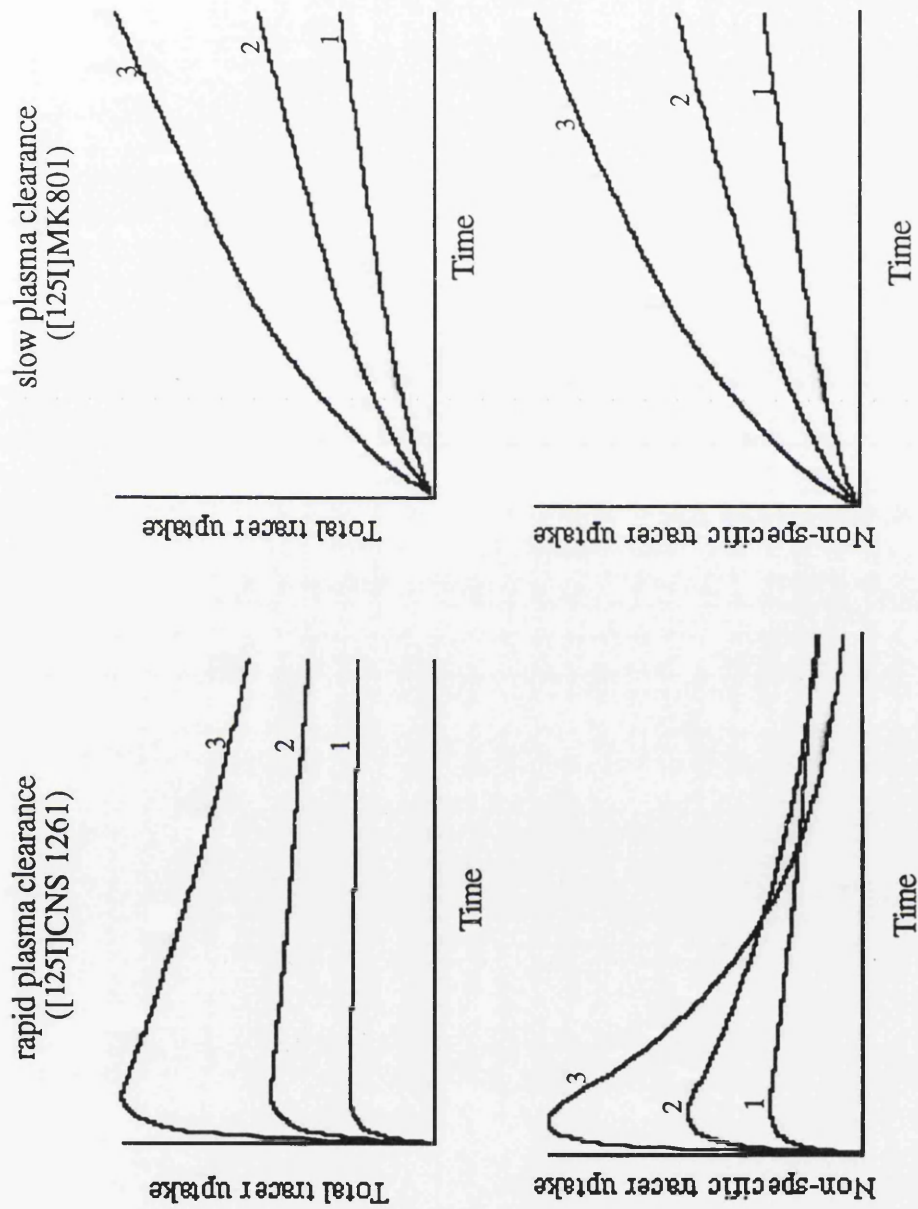


FIGURE 49 : Hypothetical brain uptake following administration of a tracer with rapid or slow plasma clearance

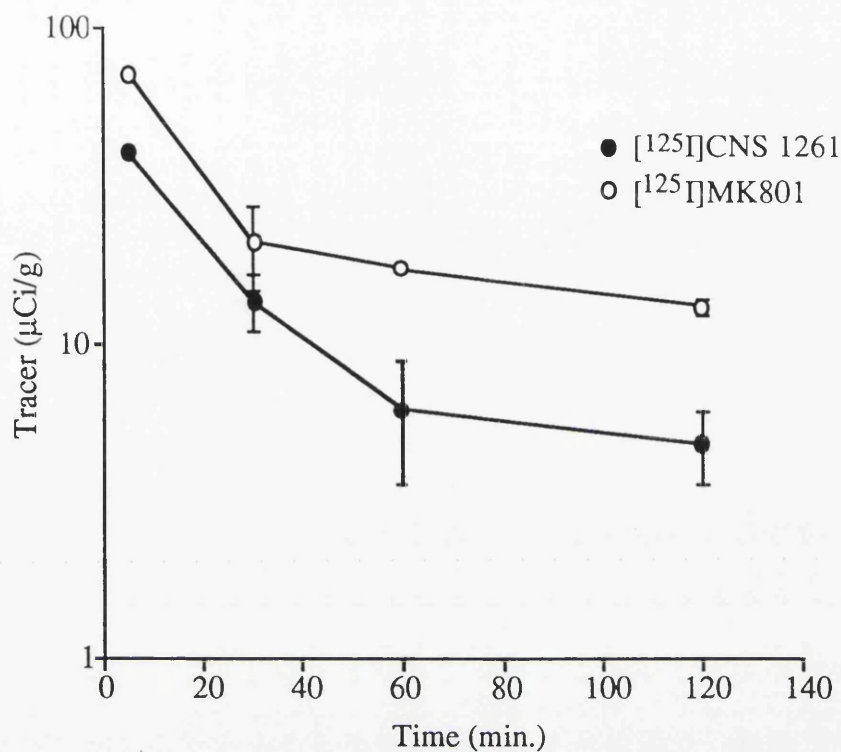


FIGURE 50 : Actual rates of tracer washout from the cerebellum

The actual rate of $[^{125}\text{I}]\text{MK801}$ washout from the rat cerebellum was compared to that of $[^{125}\text{I}]\text{CNS 1261}$. The less lipophilic tracer $[^{125}\text{I}]\text{CNS 1261}$ was shown to wash out of the cerebellum at a faster rate than $[^{125}\text{I}]\text{MK801}$. The cerebellum has a low density of NMDA receptors and serves as a within animal measure of non-specific binding.

4.4 Displacement of [125 I]CNS 1261 from normal rat brain

It has been established that 120 minutes post administration, [125 I]CNS 1261 uptake generally reflects the classical pattern of NMDA receptor distribution. It was postulated that a reduction in [125 I]CNS 1261 uptake by administration of unlabelled MK801 would confirm that enhanced uptake in areas of high receptor density such as the hippocampus, represents increased binding of this tracer to the NMDA receptor ion channel.

A preliminary experiment was performed to examine the effect of coinjection of MK801 (0.5mg/kg) and [125 I]CNS 1261 (200 μ Ci). It was apparent from the partition coefficients of the two compounds that [125 I]CNS 1261 would gain access to the brain more rapidly than cold MK801 (partition coefficients 25 and 4 respectively), however it was proposed that since the dose of MK801 administered was some 5000 times in excess of the tracer dose and the affinity for the NMDA receptor was approximately 12 times greater than that of [125 I]CNS 1261 that some displacement would occur.

[125 I]CNS 1261 uptake following coinjection of MK801 was comparable to the images obtained 120 minutes post-administration of [125 I]CNS 1261. Concomitant administration of cold MK801 did not cause displacement of [125 I]CNS 1261, indeed [125 I]CNS 1261 binding was greater in 34 of the 37 regions examined in the MK801 treated film. In hippocampus CA1, CA3 and molecular layer, [125 I]CNS 1261 binding was approximately 20% greater in MK801 treated animals, however further experiments were not carried out to substantiate this data. It is suggested that [125 I]CNS 1261 binding could be increased due to masking of a non-specific binding site by MK801, thus increasing the amount of tracer available for specific binding, but it is most likely due to the effect of MK801 on cerebral blood flow. Gibson *et al* (1992) reported that coinjection of unlabelled MK801 (4mg/kg) produced an increase in [125 I]MK801 uptake. MK801 has been shown to increase cerebral blood flow by as much as 2-fold (Nehls *et al*, 1990).

The receptor binding kinetics of [125 I]CNS 1261 may have an impact on the ease with which it can be displaced by MK801. It has been reported that lower affinity NMDA

antagonists such as memantine exhibit faster rates of block and unblock than compounds such as MK801 (Rogawski, 1993) and hence reach steady state more rapidly. While CNS 1261 displays nanomolar affinity for the NMDA receptor channel, it has a 10 fold lower affinity than MK801 and it is possible that as a result, the on/off rate at the receptor may be faster for CNS 1261. It was postulated that blockade of [125 I]CNS 1261 binding may therefore be easier to demonstrate than displacement.

Modification of the initial protocol resulted in the administration of MK801 as a bolus dose followed by an infusion ($0.4 + 6\mu\text{g/ml/min}$ or $1.2 + 16\mu\text{g/ml/min}$). Administration of MK801 produced an immediate hypotension (20mmHg decrease relative to preinjection values) that persisted throughout the experimental period. This was consistent with the observations of Kurumaji and McCulloch (1989) that administration of MK801 to halothane anaesthetised rats effected a decrease in mean arterial blood pressure.

The doses of MK801 were chosen to produce steady state plasma and brain concentrations of MK801 prior to administration of [125 I]CNS 1261 (30 min. after initiation of the infusion) and throughout the experimental period. A study by Willis *et al* (1991) using the same dosing regimen showed that initial peak levels of MK801 (in plasma and CSF) following the bolus dose reached equilibrium within 10 minutes. The lowest dose chosen gives a mean plasma concentration of 113.2ng/ml which has been shown to produce a significant reduction in the volume of ischaemic brain damage (Gill *et al*, 1991).

There was no significant difference in the levels of [125 I]CNS 1261 uptake between the control group and both groups treated with MK801 in any of the region examined.

The results presented above show that we have been unable to demonstrate displacement or blockade of [125 I]CNS 1261 binding in normal non-pathologic tissue by pharmacologically active doses of MK801. Since the batch of MK801 used in these studies was subjected to nuclear magnetic resonance spectroscopy and confirmed to be authentic, this lack of blockade may be due in part to differences in lipophilicity and/or kinetics of the two compounds. A second proposal is that under conditions where the

basal level of NMDA receptor activation is low, [^{125}I]CNS 1261 may not be sensitive enough tracer to image the putative changes in NMDA receptor activation caused by MK801. This suggestion is supported by the observation that a reduction in [^{125}I]MK801 uptake in normal brain was not observed 1 hour after coadministration of MK801. However, a 40% blockade of [^{125}I]MK801 uptake was observed 4 hours after coinjection, a sufficient time to permit washout of non-specifically bound ligand (Gibson *et al*, 1992).

4.5 Application of [^{125}I]CNS 1261

The consensus view is that highly lipophilic agents like MK801 are unsuitable *in vivo* ligands in the normal central nervous system. Non-specific binding is high and displacement has not been reliably demonstrated. In the present thesis the data obtained in normal non-pathological tissue confirms this view. Despite the inability to demonstrate displacement of [^{125}I]CNS 1261 from the normal brain, the lower lipophilicity, rapid plasma clearance and hence lower non-specific binding of this novel tracer confer significant advantages over [^{125}I]MK801, producing superior images under identical experimental conditions. [^{125}I]CNS 1261 is therefore a more suitable candidate for *in vivo* imaging within the normal central nervous system.

The ability to image changes in NMDA receptor activation *in vivo* must be demonstrated for a tracer to be of any value in man. McCulloch demonstrated a marked elevation in levels of [^{125}I]MK801 uptake in ischaemic areas (neocortex and striatum) following middle cerebral artery occlusion. These areas are generally accepted to be areas of excessive NMDA receptor activation.

There is accumulating evidence that external proton concentration is an important determinant of neuronal responses mediated by NMDA receptors. Acidosis is effective in reducing inward currents induced by NMDA in cultured neurons (Traynelis and Cull-Candy, 1990, Tang *et al*, 1990) and is protective against neuronal injury induced by

glutamate. Yoneda *et al* (1994) demonstrated a negative modulation by protons of [^3H]MK801 binding to the NMDA receptor channel in rat brain synaptic membranes. This observation was supported by the observation that decreasing the pH of the environment of cultured forebrain neurons slowed the association and dissociation rates of [^{125}I]MK801, by decreasing the amount of time that the channel spends in the open state (Rajdev and Reynolds, 1993). Varying the pH of the extracellular fluid therefore provides a mechanism of controlling the level of NMDA receptor activation without affecting agonist concentrations.

The brain extracellular fluid is not buffered against changes in arterial CO_2 tension, therefore increasing the percentage of CO_2 in inspired air was a convenient mechanism of producing hypercapnic acidosis in experimental animals. Changes in CO_2 tension induce a decrease in arterial pH and a parallel decrease in extracellular fluid pH (Figure 51). Arterial pH therefore gives a reasonable indication of the pH of the extracellular fluid and intracerebral electrodes were not implemented in these investigations.

NMDA-induced currents were reduced by approximately 70% in cerebellar neurones when the bath pH was reduced to 6.8 (Traynelis and Cull-Candy, 1990). Increasing the CO_2 in inspired air to 20% increased arterial pCO_2 to 180mmHg and decreased pH to 6.9. It was proposed that this change in pH would be sufficient to decrease the activation of NMDA receptors within the brain. In the same way, NMDA receptors are not fully activated at physiological pH therefore increasing the arterial pH to 7.6 should relieve the proton blockade and increase NMDA receptor activation.

In addition to the reported changes in arterial pCO_2 and pH, induction of hypercapnia caused an immediate transient hypotension followed by a recovery to levels slightly above pre-induction values.

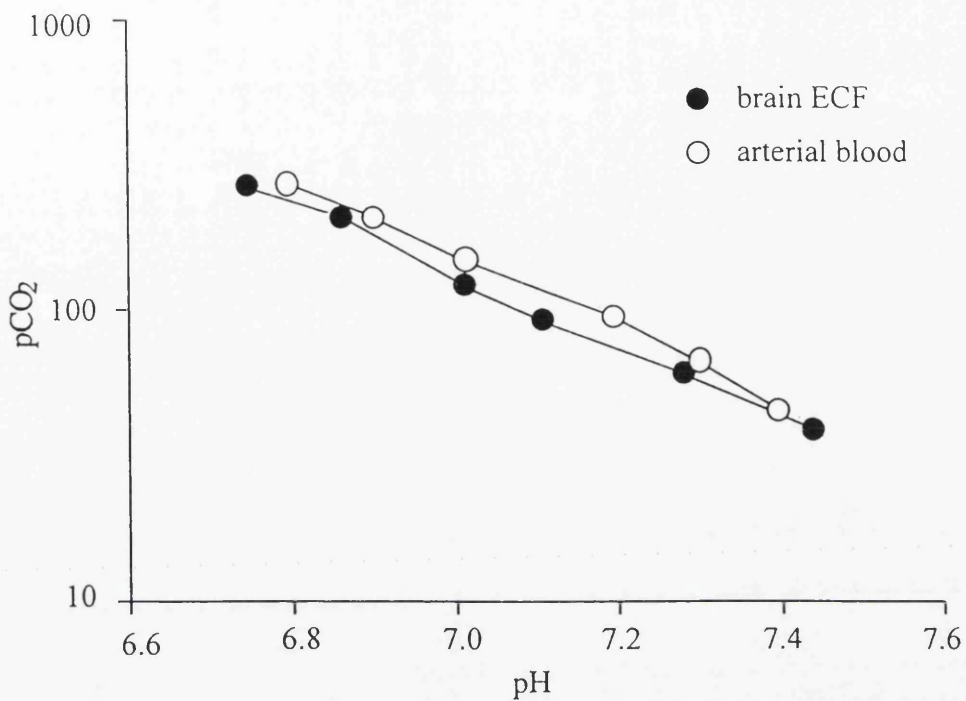


FIGURE 51 : Relationship between pCO₂ and pH in plasma and brain

Data redrawn from Siesjo (1972). Increasing CO₂ tension through hypercapnic ventilation induces a decrease in arterial pH and in the pH of the extracellular fluid (ECF) of the brain. For a given pCO₂ the pH within the ecf was slightly lower than that within the plasma

Cerebral blood flow has been shown to respond considerably to alterations in CO₂ tension, with an average increase of 4.9ml/100g/min. for every mmHg change in arterial pCO₂ (Hernandez *et al*, 1978).

[¹²⁵I]MK801 uptake in hypercapnic animals was not different from that in normocapnic animals and it is thought that the increase in pH from 7.4 to 7.6 was not a strong enough stimulus to increase NMDA receptor activation. This is supported by the pH dependence of the NMDA current measured in hippocampal neuron following application of NMDA (Tang *et al*, 1990). The data was fitted to a sigmoidal curve with a pK_a of 6.9. pH 7.4 was near the upper plateau of the curve therefore, a change of 0.2 pH units produced little increase in NMDA activated current and hence NMDA receptor activation. There was no significant difference in the relative levels of [¹²⁵I]MK801 within the dorsal hippocampus of normocapnic and hypercapnic animals despite the observed decrease in total [¹²⁵I]MK801 uptake within this region on the autoradiograms of hypercapnic animals. The failure to obtain a significant decrease in [¹²⁵I]MK801 uptake following hypercapnia may be attributed to the poor signal to noise ratio of this tracer due to high levels of non-specific binding in the cerebellum, [¹²⁵I]MK801 uptake in the hippocampus was 30% above that in the cerebellum and 20% greater than cerebellar levels in other regions.

In contrast to the results obtained with [¹²⁵I]MK801, an identical level of acidosis produced a significant decrease in the relative uptake of [¹²⁵I]CNS 1261 *in vivo* compared to normocapnic values. Hypercapnic acidosis (pH 6.9) also reduced [¹²⁵I]CNS 1261 uptake in other areas with a fairly high density of NMDA receptors. [¹²⁵I]CNS 1261 uptake within the hippocampus was 2-300% above that observed within the cerebellum and 60-90% above cerebellar levels in the majority of other regions examined. It appears from these results that [¹²⁵I]CNS 1261 is a better tracer to image the putative decrease in NMDA receptor activation induced by hypercapnic acidosis due to the higher relative uptake of this tracer in normocapnic animals.

The utility of [125 I]CNS 1261 in measuring changes in NMDA receptor activation was further examined by measuring [125 I]CNS 1261 uptake at different time points after intracortical injection of NMDA. Injection of 0.009M NMDA into the nucleus basalis magnocellularis (NBM) produced significant alterations in glucose use in cortical regions innervated by the NBM efferents (Browne, 1993) and is therefore sufficient to cause increased neuronal activity. Injection of 0.009M NMDA into the parietal cortex produced a lesion with a core area of decreased glucose use surrounded by a zone of increased glucose utilisation. The increase in glucose use appears to map the diffusion front of the injection and it is suggested that the pale area within the boundary represents an area where receptors have received a lethal dose of NMDA and are no longer functional.

It has been described previously that the initial uptake of [125 I]CNS 1261 reflects cerebral blood flow. Five minutes after injection of NMDA or CSF tracer uptake was decreased within the ipsilateral hemisphere, particularly in the insular cortex. Although the total volume injected was extremely small, it was injected into a medium with no capacity for expansion. It is possible that the increase pressure arising from the increase in volume partially occludes blood vessels thus hindering the delivery of tracer to the ipsilateral hemisphere. The decreased tracer uptake within the insular cortex is similar to that obtained in [14 C]iodoantipyrine autoradiograms from models of subdural haematoma (Miller *et al*, 1990). The additional volume added within the rigid confines of the skull causes compression of the base of the ventral surface of the brain restricting tracer uptake. Injection of NMDA produces localised increases in cerebral blood flow which are reflected in the markedly increased uptake of [125]CNS 1261 surrounding the injection site.

At times beyond 5 minutes, NMDA injection results in a sizeable lesion which extends in anterior and posterior directions and is characterised by an area of pallor as shown by H&E. The histopathological features of the lesion included loss of staining and shrinkage of neurons. The lesion was similar to that described following glutamate perfusion (Fujisawa *et al*, 1993), in that a sharp boundary between the lesion and histologically normal tissue could be readily detected, however there was no evidence of triangulated

neurons. In comparison, injection of CSF produced a much smaller, less well defined lesion.

120 minutes after injection of NMDA autoradiograms showed an area of decreased [125 I]CNS 1261 uptake immediately adjacent to the injection site surrounded by a rim of increased uptake. [125 I]CNS 1261 uptake in the contralateral hemisphere was similar to that observed in the normal brain at 120 minutes. CSF injections produced a smaller area of pallor on autoradiograms and the rim of increased [125 I]CNS 1261 uptake was less evident. The pattern of tracer uptake is consistent with the hypothesis that receptors within the core area are no longer functional due to excitotoxic damage and, receptors within the boundary of the lesion are being activated by NMDA. It has been established that the association rate of ligand binding to the NMDA receptor is dependent on the activation state of the receptor (Rajdev and Reynolds, 1993). Kinetic modelling (see Figure 48) was used to investigate the impact of changes in association rate and hence in receptor activation on tracer uptake. The rate of association of [125 I]CNS 1261 under conditions of normal receptor activation was set at 0.07, a value of 0.01 was used to represent the association rate within the core region where receptors were proposed to be relatively non-functional and, a value of 1 was used to represent the association rate within the boundary region where receptors are putatively abnormally activated. The hypothetical brain uptake obtained using the 3 compartment model confirms that very little washout of tracer occurs from 'activated' receptors over the course of the experimental period and at 120 min. tracer uptake in this area (representing the rim) is increased compared to areas of normal activation (Figure 52). In contrast, tracer uptake washes out of the 'core' area where receptors are closed much faster and low levels of uptake are present at the end of the experiment. The decreased binding of [125 I]CNS 1261 within areas representing the core in this model indirectly demonstrates displacement of the tracer.

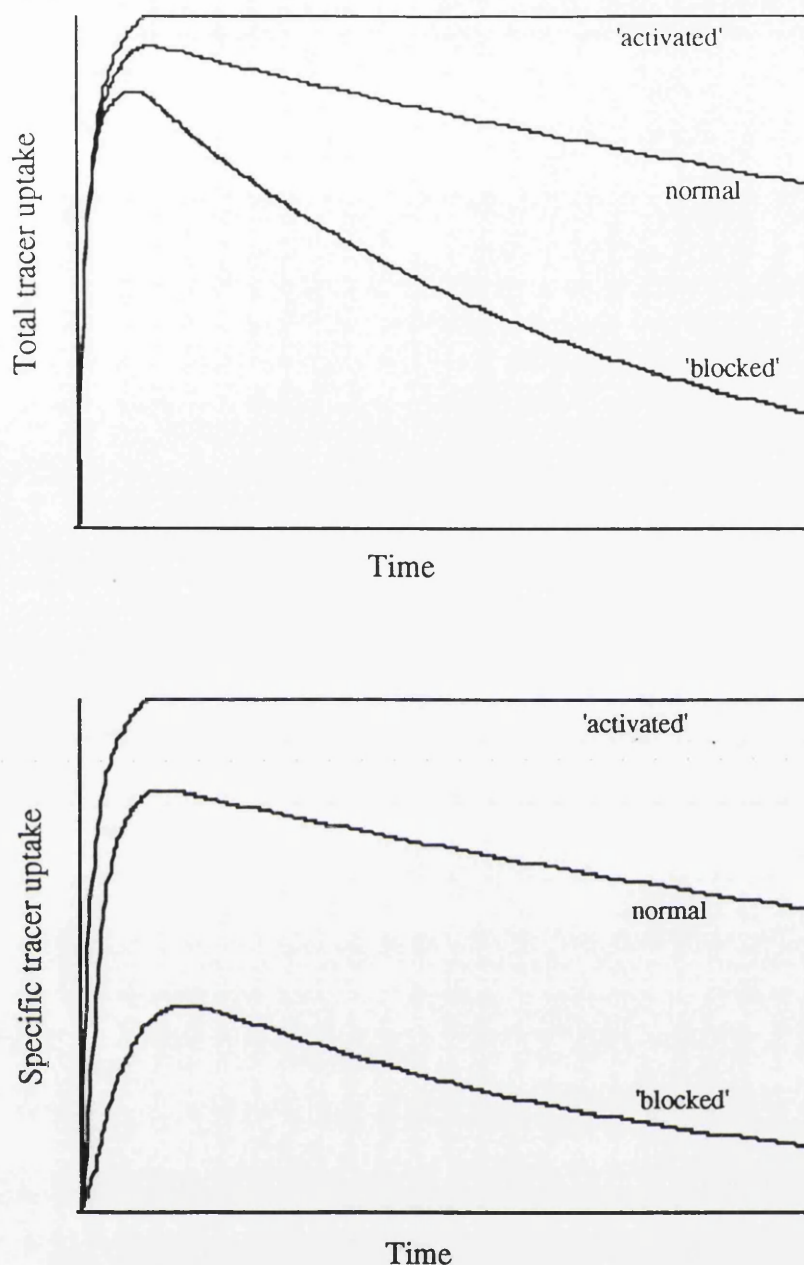


FIGURE 52 : Effect of varying association rate on the hypothetical uptake and retention of a tracer with rapid plasma clearance

Kinetic modelling (see Figure 48) was used to investigate the impact of changes in association rate (k_{on}) and hence receptor activation on tracer uptake. In this model the rate of association of a tracer ($[^{125}\text{I}]\text{CNS 1261}$) under conditions of normal receptor activation, was set at an arbitrary value of 0.07. Therefore, a value of 0.01 was used to represent the association rate within a region where receptors were relatively non-functional ('blocked') and, a value of 1 was used to represent the association rate to activated receptors. The hypothetical brain uptake obtained using the 3 compartment model confirms that very little washout of tracer occurs from 'activated' receptors at the end of the experimental period (120 min.) and tracer uptake in this area is increased compared to areas of normal activation. In contrast, tracer uptake washes out of areas where receptors are closed much more quickly.

[¹²⁵I]CNS 1261 uptake 60 minutes after injection of NMDA also showed an area of decreased tracer at the site of injection surrounded by an area of increased uptake. Imaging at an earlier time point did not demonstrate a larger area of elevated [¹²⁵I]CNS 1261 uptake within the rim on the autoradiograms. Post-mortem washing of sections from control experiments showed that [¹²⁵I]CNS 1261 binding within the hippocampus was reduced by 50% at around 30 minutes therefore, 60 minutes appears to be too late a time point to capture any increase in binding that may have been present. Sixty minutes after injection of CSF, small lesions (1mm²) were observed in 2 animals while the third animal possessed a much larger lesion (2mm²). The mechanism underlying the development of this larger lesion is unknown since there was no evidence of blood in or around the injection site.

These results suggest that the increased [¹²⁵I]CNS 1261 uptake within the boundary zone of the lesion reflects increased binding to NMDA receptors. This is supported by the difficulty in defining a zone of increased [¹²⁵I]CNS 1261 uptake following CSF injection. The observation that areas of increased [¹²⁵I]CNS 1261 uptake in subcortical areas corresponds to areas of damage in histological sections adds further weight to this hypothesis. Tissue damage causes glutamate release and subsequent NMDA receptor activation. [¹²⁵I]CNS 1261 was also able to map the evolution of the lesion as the pale core region of decreased uptake increased in size between 60 and 120 minutes. This implies that areas of increased uptake within the boundary zone at 60 minutes eventually become incorporated into the core area observed at 120 min. as the NMDA diffuses away from the injection site over time. These observations reinforce the view that [¹²⁵I]CNS 1261 is mapping a dynamic process.

The use of [¹²⁵I]CNS 1261 in man with SPECT imaging therefore provides a potential strategy for defining areas of NMDA receptor activation.

4.6 SPECT imaging in man with [^{123}I]CNS 1261

The initial clinical assessment of [^{123}I]CNS 1261 and its potential to provide SPECT images *in vivo* of NMDA receptor activation during cerebral ischaemia has been investigated. The study was approved by the Local Research Ethics Committee of the Institute of Neurological Sciences and by the Administration of Radioactive Substances Advisory Committee. Three patients were studied with clinical indications of possible ischaemia. Patient A presented with a large right frontal infarct and SPECT was carried out 24 hours after onset. Patient B presented with a left middle cerebral artery infarct and SPECT was performed 6 hours after stroke onset. Patient C had evidence of multiple small infarcts and SPECT was carried out 18 hours after onset. Three normal volunteers (2 males and 1 female, 58-88 years) were recruited as control subjects. SPECT imaging was carried out on a Strichman SME 810 dedicated neuro-scanner. [^{123}I]CNS 1261 (80-180MBq) was administered intravenously and images of the brain captured at regular time points post-injection. The patients lay unrestrained, except for a cushioned head support, during scanning. Multiple timed samples of venous blood were taken and the presence of authentic CNS 1261 and any metabolites determined by hplc. The objective of the imaging experiments was to investigate the kinetics of [^{123}I]CNS 1261 and not the regional distribution therefore, the scanning protocol involved acquisition of images from a single slice at the level of the occipital cortex at 25 timepoints over 90 minutes (2 minutes per slice).

Images from a control subject show that at early time points after administration [^{123}I]CNS 1261 uptake was greatest in areas with high cerebral blood flow, such as the cortex and cerebellum (Figure 53). At later time points high levels of uptake were present in the occipital cortex. There was no accumulation of [^{123}I]CNS 1261 in white matter at 40 minutes. The initial distribution of [^{123}I]MK801 in the brain also reflected cerebral blood flow with greatest radioactivity in the cerebellum and other cortical grey structures. However, there was a progressive loss of contrast between grey and white matter over the course of the experimental period and eventually no distinction could be made

FIGURE 53 : [^{123}I]CNS 1261 uptake and retention in a normal volunteer

Axial SPECT images show the distribution of radioactivity in the brain of a normal human control subject starting 2 minutes after the administration of [^{123}I]CNS 1261 with the final image in the series showing distribution 42 minutes after tracer injection. All images were captured at the level of the the occipital cortex. 'Hot' colours represent areas with high tracer uptake and 'cold' colours represent areas with low uptake. Early images show typical blood flow distribution with highest radioactivity observed within cortical areas. Late images show that the tracer does not accumulate in areas of white matter.

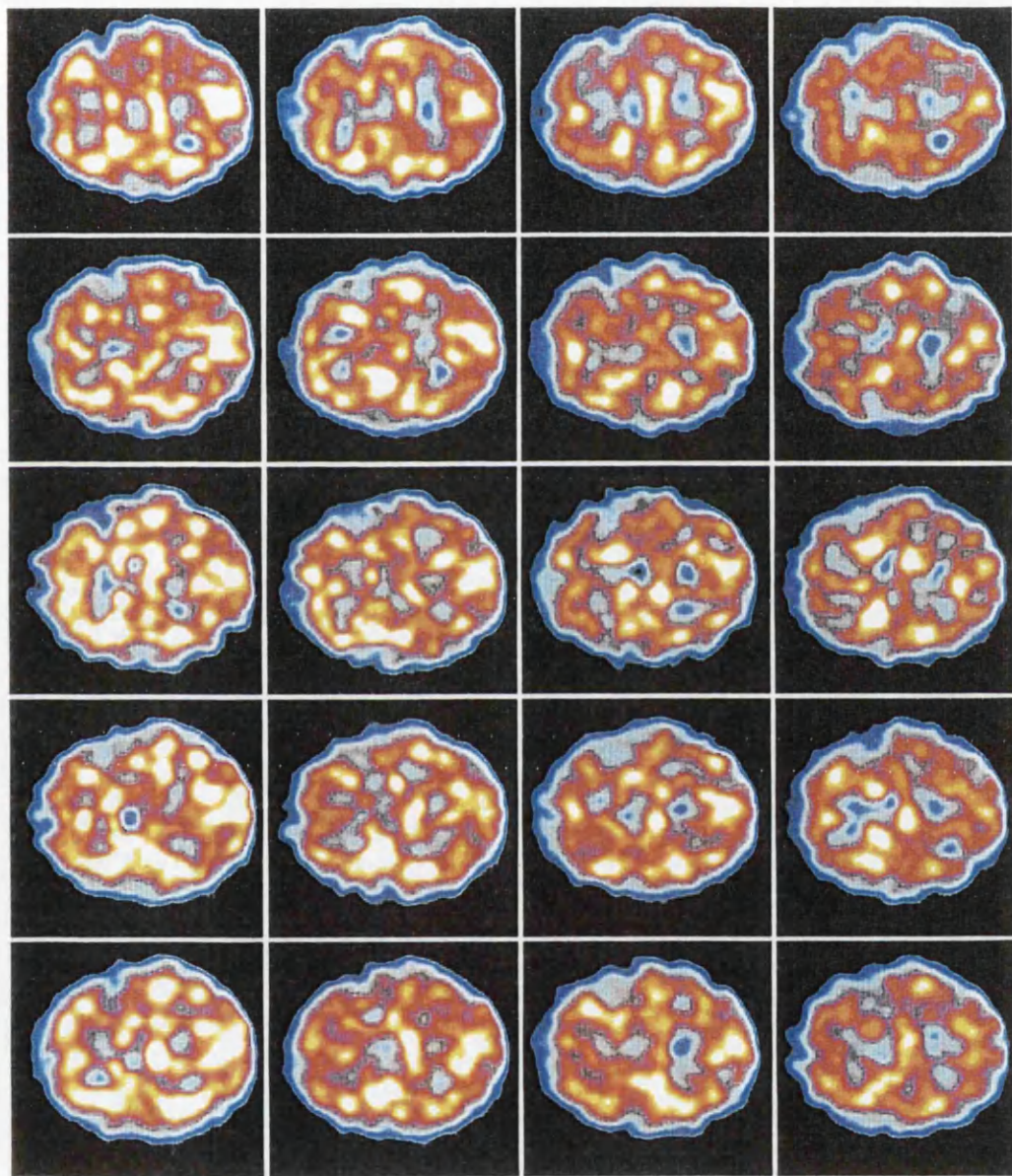


FIGURE 53 : [^{123}I]CNS 1261 uptake and retention in a normal volunteer

between these tissues on the images. Quantitative data showed that radioactivity in grey matter decreased over the experimental period while radioactivity in white matter was minimally altered (Owens *et al*, 1997).

Plasma clearance of [^{123}I]CNS 1261 was extremely rapid and was reminiscent of the situation in rat plasma (Figure 54). Brain clearance of the tracer was somewhat slower than expected from the plasma trace and indicates some form of trapping. This trapping has been attributed to plasma protein binding.

The *in vivo* uptake and retention of [^{125}I]CNS 1261 following permanent proximal occlusion of the middle cerebral artery in the rat was similar to that previously described for [^{125}I]MK801 (McCulloch *et al*, 1992). 120 minutes after injection, binding was significantly decreased in the dorsolateral caudate nucleus and insular cortex. Tracer uptake was markedly increased within the striatum, where uptake in the ipsilateral caudate nucleus was approximately 2-fold higher than that in the equivalent area of the contralateral hemisphere (Figure 55). These regions are generally accepted to be areas of increased NMDA receptor activation.

Results of the clinical assessment of [^{123}I]MK801 uptake in man showed relatively increased tracer retention at late time points (60-120 minutes) after tracer administration in cortical areas adjacent to the site of the haemorrhage in 2 of the 5 patients. This uptake was consistent with presence of activated NMDA receptors (Owens *et al*, 1997). While it may be possible to image NMDA receptor activation during an ischaemic episode in the living patient with [^{123}I]MK801, the utility of this tracer is ultimately limited by its lipophilicity (and consequent high non-specific binding).

[^{123}I]CNS 1261 SPECT images showed that 6 hours after onset of an ischaemic episode, the earliest time point examined in man, there was no evidence of increased uptake in peri-ischaemic areas where NMDA receptor activation is proposed to occur. The rate of washout in peri-ischaemic areas is similar to that observed in occipital cortex, an area removed from ischaemia (Figure 56). The overall uptake and washout in this patient did not look different from that in normal volunteers.

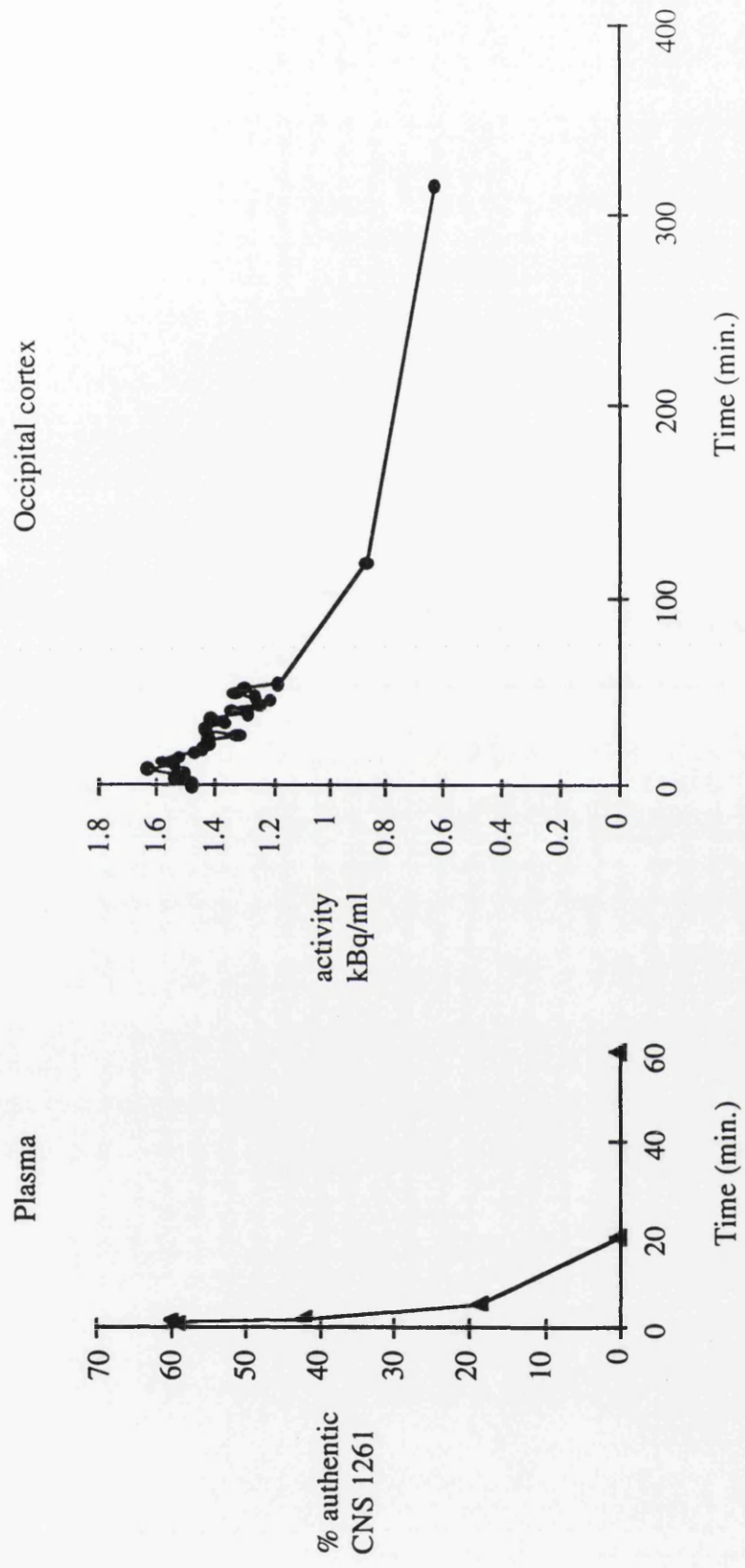


FIGURE 54 : Timecourse of [^{123}I]CNS 1261 clearance from plasma and occipital cortex in a normal volunteer

[^{123}I]CNS 1261 was rapidly cleared from the plasma of normal human subjects. Brain clearance was slower than that within the plasma.



FIGURE 55 : [125 I]CNS 1261 uptake is increased in ischaemic areas

Illustrative autoradiogram of [125 I]CNS 1261 uptake after permanent middle cerebral artery occlusion. The isotope was administered 15 minutes after occlusion and the animals sacrificed 120 minutes thereafter. The occluded hemisphere is on the left, areas of increased uptake are indicated by arrow.

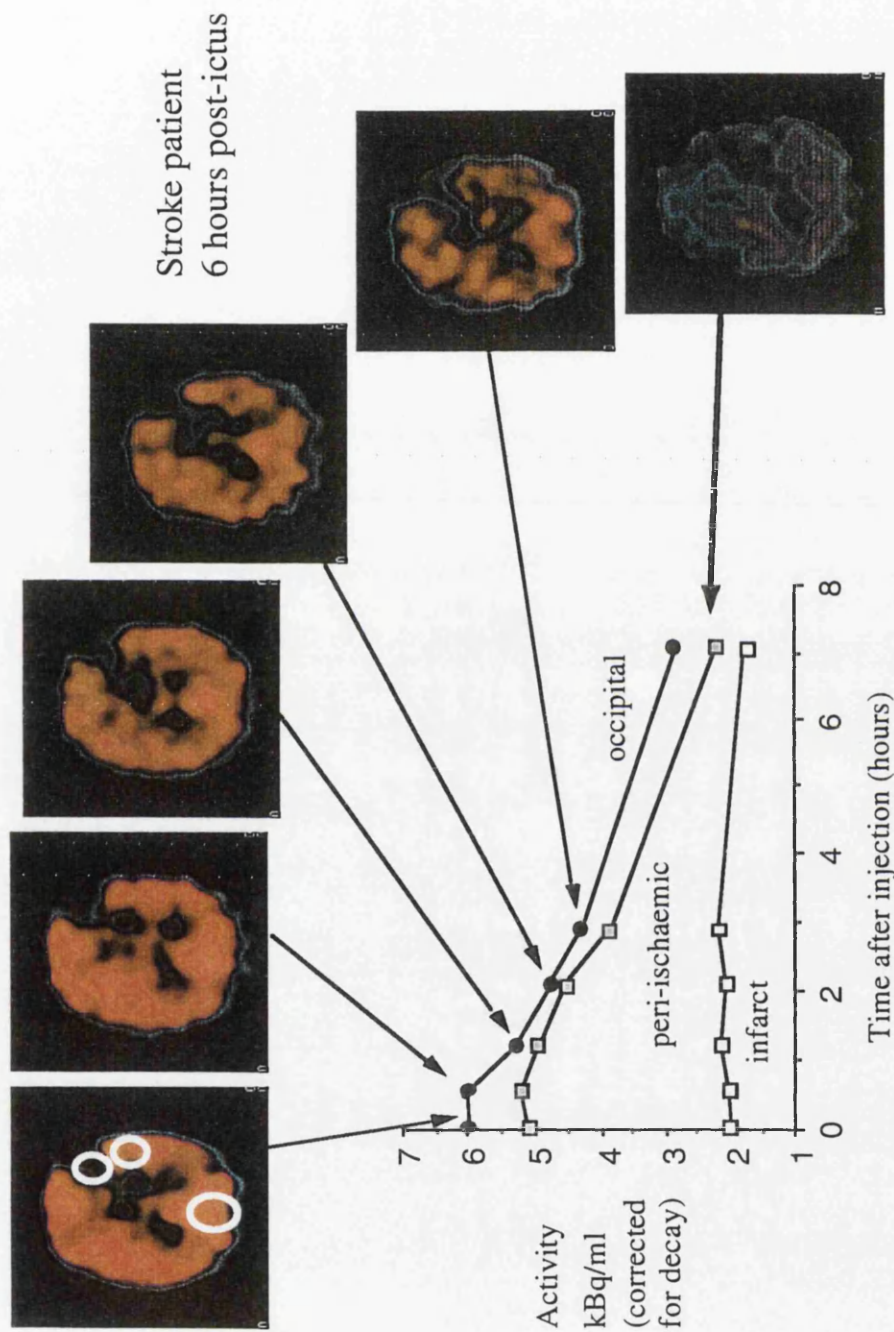


FIGURE 56 : Time course of radioactivity in a stroke patient 6 hours after onset

The data have been corrected for decay of ^{123}I and show uptake in the occipital cortex, area of infarct and peri-ischaemic zone (highlighted in 1st SPECT image) at various times after administration of ^{123}I CNS 1261. Representative SPECT images are also shown.

A number of factors may underlie the inability to observe increased [^{123}I]CNS 1261 retention in stroke patients. Both [^{125}I]CNS 1261 and [^{125}I]MK801 uptake was increased in ischaemic areas when administered 15 min. after middle cerebral artery occlusion in the rat. The uptake of [^{125}I]MK801 was shown to diminish as the time from occlusion increased (McCulloch *et al*, 1992). In the most acute stroke patient recruited, [^{123}I]CNS 1261 was administered 6 hours after onset of the ischaemic ictus. Assuming that a similar situation of diminished uptake over time occurs in humans, six hours after onset may be too late to capture NMDA receptor activation.

No increased tracer retention was observed in either of the stroke patients images at 18 or 24 hours. Baron *et al* (1996) have produced clinical evidence of heterogeneity between stroke patients in that some lacked a peri-ischaemic area. It is possible that the patient imaged 6 hours after onset of stroke represents the group of patients with no penumbral zone of NMDA receptor activation. It must be noted that the timing of imaging in humans is extremely difficult. Within the brain of a stroke patient it is assumed that there are areas of normal grey matter, ischaemic grey and white matter. Images must be captured at a time when radioactivity in normal grey matter is low enough to see any superimposed increases or, tracer accumulation in white matter is not so high that the phenomenon is masked. The background level of radioactive uptake cannot be 'faded out' and each event captured by imaging is superimposed on this level. If background (non-specific) levels of radioactivity are high, significant events will not be observed.

The initial results of the clinical evaluation of [^{123}I]CNS 1261 are encouraging. [^{123}I]CNS 1261 shows no accumulation in white matter and it is suggested that this tracer will be less limited by lipophilicity than [^{123}I]MK801. Further acute stroke patients recruited to this study may confirm the existence of areas of increased NMDA receptor activation following cerebral ischaemia.

A proposed future strategy to further evaluate [^{123}I]CNS 1261 is to recruit patients with chronic epilepsy, into the study. It is assumed that the mechanism underlying epilepsy and ischaemia are related and glutamate release during seizures will increase NMDA receptor activation. In summary, the use of [^{123}I]CNS 1261 in man with SPECT remains a potential strategy for defining the location of areas of NMDA receptor activation in pathological conditions where glutamate concentrations are elevated.

REFERENCES

- Aizenmann, E. and Harnett, K.A. (1992) The action of CGS-19755 on the redox enhancement of NMDA toxicity in rat cortical neurons *in vitro*. *Brain Research* 585:28-34.
- Assaf, S.Y. and Chung, S. (1984) Release of endogenous Zn^{2+} from brain tissue during activity. *Nature* 308:734-736.
- Astrup, J., Siesjo, B.K. and Symon, L. (1981) Thresholds in cerebral ischaemia - the ischaemic penumbra. *Stroke* 12 (6):723-725.
- Astrup, J., Symon, L., Branston, N.M. and Lassen, N.A. (1977) Cortical evoked potential and extracellular K^+ and H^+ at critical levels of brain ischaemia. *Stroke* 8:51-57.
- Audus, K.L., Chikhale, P.J., Miller, D.W., Thompson, S.E. and Borchardt, R.T. (1992) Brain Uptake of drugs: The influence of chemical and biological factors. *Advances in Drug Research* 23:1-64.
- Ault, B., Miller, M.S., Kelly, M.D., Hildebrand, L.M., Earley, W.G., Luttinger, D., Mallamo, J.P. and Ward, S.J. (1995) WIN 63480, a hydrophilic TCP-site ligand, has reduced agonist-independent NMDA ion channel access compared to MK801 and phencyclidine. *Neuropharmacology* 34 (12):1597-1606.
- Bartus, R.T., Elliott, P.J., Hayward, N.J., Dean, R.L., Harbeson, S., Straub, J.A., Li, Z. and Powers, J.C. (1995) Calpain as a novel target for treating acute neurodegenerative disorders. *Neurological Research* 17:249-258
- Baron, J.C., Comar, D., Zarifian, E., Agid, Y., Crouzel, C., Loo, H., Deniker, P and Kellershohn, C. (1985) Dopaminergic receptor sites in human brain : positron emission tomography. *Neurology* 35(1):16-24.
- Baron, J.C., Furlan, M., Marchal, G. (1996) The metabolic status of the ultimately noninfarcted ischaemic penumbra - a positron emission tomography study in humans. *Annals of Neurology* 40(3):M35

Ben-Ari, Y., Aniksztejn, L. and Bregestovski, P. (1992) Protein kinase C modulation of NMDA currents - an important link for LTP induction. *Trends in Neurosciences* **15**:333-339.

Benveniste, M. and Mayer, M.L. (1991) Structure-activity analysis of binding kinetics for NMDA receptor competitive antagonists : the influence of conformational restriction. *British Journal of Pharmacology* **104**:207-221.

Blin, J., Baron, J.C., Cambon, H., Bouret, A.M., Dubois, B., Loc'h, C., Maziere, B. and Agid, Y. (1989) Striatal dopamine D₂ receptors in tardive dyskinesia : PET study. *Journal of Neurology, Neurosurgery and Psychiatry* **52**(11):1248-1252.

Boundy, K.L., Barnden, I.R., Rowe, C.C., Reid, M., Kassiou, M., Katsifis, A.G. and Lambrecht, R.M. (1995) Human dosimetry and biodistribution of iodine-123-iododexetimide - a SPECT imaging agent for cholinergic muscarinic neuroreceptors. *Journal of Nuclear Medicine* **36**(7):1332-1338.

Bowery, N.G., Wong, E.H.F. and Hudson, A.L. (1988) Quantitative autoradiography of [³H]MK801 binding sites in mammalian brain. *British Journal of Pharmacology* **93**:944-954.

Bresink, I., Danysz, W., Parsons, C.G. and Mutschler, E. (1995) Different binding affinities of NMDA receptor channel blockers in various brain regions - indication of NMDA receptor heterogeneity. *Neuropharmacology* **34** (5):533-540.

Browne, S.E. (1993) Excitatory amino acid receptor-mediated events in the brain : quantitative autoradiography studies. A thesis submitted for the degree of Doctor of Philosophy to the Faculty of medicine, University of Glasgow.

Bruno, V., Battaglia, G., Copani, A., Giffard, R.G., Raciti, G., Raffaele, R., Shinozaki, H. and Nicoletti, F. (1995) Activation of Class II or III metabotropic glutamate receptors protects cultured cortical neurons against excitotoxic degeneration. *European Journal of Neuroscience* **7**:1906-1913.

Buchan, A., Li, H. and Pulsinelli, W.A. (1991) The N-methyl-D-aspartate antagonist, MK801, fails to protect against neuronal damage caused by transient, severe forebrain ischaemia in adult rats. *The Journal of Neuroscience* **11**(4):1049-1056.

Buchan, A.M., Lesiuk, H., Barnes, K.A., Li, H., Huang, Z.G., Smith, K.E. and Xue, D. (1993) AMPA antagonists : do they hold more promise for clinical stroke trials than NMDA antagonists? *Stroke* **24** [Suppl I]:I-148-I-152.

Buller, A.L., Larson, H.C., Schneider, B.E., Beaton, J.A., Morrisett, R.A. and Monaghan, D.T. (1994) The molecular basis of NMDA receptor subtypes : Native receptor diversity is predicted by subunit composition. *The Journal of Neuroscience* **14**(9):5471-5484.

Burke, S.P. and Nadler, J.V. (1988) Regulation of glutamate and aspartate release from slices of the hippocampal CA1 area : effects of adenosine and baclofen. *Journal of Neurochemistry* **51**:1541-1551.

Busatto, G.F., Pilowsky, L.S., Costa, D.C., Ell, P.J., Lingford-Hughes, A. and Kerwin, R.W. (1994) *In vivo* imaging of GABA_A receptors using sequential whole-volume iodine-123 iomazenil single-photon emission tomography. *European Journal of Nuclear Medicine* **22**(1):12-16.

Butcher, S.P., Bullock, R., Graham, D.I. and McCulloch, J. (1990) Correlation between amino acid release and neuropathologic outcome in the rat brain following middle cerebral artery occlusion. *Stroke* **21**:1727-1733.

Butcher, S.P., Sandberg, M., Hagberg, H. and Hamberger, A. (1987) Cellular origins of endogenous amino acids released into the extracellular fluid of the rat striatum during severe insulin-induced hypoglycaemia. *Journal of Neurochemistry* **48**:722-728.

Chen, H-S.V., Pellegrini, J.W., Aggarwal, S.K., Lei, S.Z., Warach, S., J
14392) Open-channel block of N-methyl-D-aspartate (NMDA) responses by memantine : Therapeutic advantage against NMDA receptor-mediated neurotoxicity. *The Journal of Neuroscience* **12**(11):4427-4436.

Chen, L., Gu, Y. and Huang, L.M. (1995) The mechanism of action for the block of NMDA receptor channels by the opioid peptide dynorphin. *The Journal of Neuroscience* **15**(6):4602-4611.

Cheng, L. and Huang, L. (1992) Protein kinase C reduces Mg²⁺ block of NMDA-receptor channels as a mechanism of modulation. *Nature* **356**:521-523.

- Chen, M.H., Bullock, R., Graham, D.I., Frey, P., Lowe, D. and McCulloch, J. (1991) Evaluation of a competitive NMDA antagonist (D-CPPene) in feline focal cerebral ischaemia. *Annals of Neurology* 30:62-70.
- Chen, N., Moshaver, A. and Raymond, L.A. (1997) Differential sensitivity of recombinant N-methyl-D-aspartate receptor subtypes to zinc inhibition. *Molecular Pharmacology* 51:1015-1023.
- Chesler, M. and Kaila, K. (1992) Modulation of pH by neuronal activity. *Trends in Neurological Sciences* 15(10):396-402.
- Chittajallu, R., Vignes, M., Dev, K.K., Barnes, J.M., Collingridge, G.L. and Henley, J.M. (1996) Regulation of glutamate release by presynaptic kainate receptors in the hippocampus. *Nature* 379:78-81.
- Choi, D. (1987) Ionic dependence of glutamate neurotoxicity. *The Journal of Neuroscience* 7(2):369-379.
- Cohen, R.A., Hasegawa, Y. and Fisher, M. (1994) Effects of a novel NMDA receptor antagonist on experimental stroke quantitatively assessed by spectral EEG and infarct volume. *Neurological Research* 16:443-448
- Cooper, J.R., Bloom, F.E. and Roth, R.H. (1996) Amino acid transmitters. In: *Biochemical basis of neuropharmacology*, New York : Oxford University Press p. 171-188.
- Curtis, D.R. and Watkins, J.C. (1960) The excitation and depression of spinal neurons by structurally related amino acids. *The Journal of Neuroscience* 6:117-141.
- Danysz, W., Parsons, C.G., Bresink, I. and Quack, G. (1995) Glutamate in CNS disorders. *DN and P* 8(5):261-176.
- del Cerro, S., Arai, A., Kessler, M., Bahr, B.A., Vanderklish, P., Rivera, S. and Lynch, G. (1994) Stimulation of NMDA receptors activates calpain in cultured hippocampal slices. *Neuroscience Letters* 167:149-152.
- Dettmers, C., Young, A., Rommel, T., Hartmann, A., Weingart, O. and Baron, J.C. (1993) CO₂ reactivity in the ischaemic core, penumbra, and normal tissue 6 hours after acute MCA-occlusion in primates. *Acta Neurochirurgica* 125:150-155.

Di, X. and Bullock, R. (1996) Effect of the novel high affinity glycine-site N-methyl-D-aspartate antagonist ACEA-1021 on ^{125}I -MK801 binding after subdural haematoma in the rat : an *in vivo* autoradiography study. *Journal of Neurosurgery* 85:655-661.

Drejer, J., Benveniste, H., Diemer, N.H. and Schousboe, A. (1985) Cellular origin of ischaemia-induced glutamate release from brain tissue *in vivo* and *in vitro*. *Journal of Neurochemistry*. 45:145-151, 1985.

Dzubay, J.A. and Jahr, C.E. (1996) Kinetics of NMDA channel opening. *The Journal of Neuroscience* 16(13):4129-4134.

Ebine, Y., Fujiwara, N. and Shimoji, K. (1994) Mild acidosis inhibits the rise in intracellular Ca^{2+} concentration in response to oxygen-glucose deprivation in rat hippocampal slices. *Neuroscience Letters* 168:155-158.

Eckelman, W.C. and Gibson, R.E. (1993) The design of site-directed radiopharmaceuticals for use in drug discovery. In: Nuclear imaging in drug discovery, development and approval. Edited by Burns, H.D., Gibson, R. and Dannals, R. Boston: Birkhauser p. 113-129.

Edvinsson, L., Mackenzie, E.T. and McCulloch, J. (1993) General and comparative anatomy of the cerebral circulation. In: Cerebral Blood Flow and metabolism. New York : Raven Press p 15-21.

Enomoto, R., Ogita, K., Han, D. and Yoneda, Y. (1992) Differential modulation by divalent cations of ^3H -MK801 binding in brain synaptic membranes. *Journal of Neurochemistry* 59:473-481.

Farde, L. (1996) The advantage of using positron emission tomography in drug research. *Trends in Neurosciences* 19(6):211-241.

Fahey, J.M., Pritchard, G.A. and Miller, L.G. (1993) Polyamine neurotoxicity is antagonised by dizocilpine in cultured chick cortical neurons. *Neuroscience Letters* 161:109-112.

Farooqui, A.A. and Horrocks, L.A. (1991) Excitatory amino acid receptors, neural membrane phospholipid metabolism and neurological disorders. *Brain Research Reviews* 16:171-191.

Fleck, M.W., Henze, D.A., Barrionuevo, G. and Palmer, A.M. (1993) Aspartate and glutamate mediate excitatory synaptic transmission in area CA1 of the hippocampus. *The Journal of Neuroscience* 13(9):3944-3955.

Fonnum, F. (1984) Glutamate: a neurotransmitter in mammalian brain. *Journal of Neurochemistry* 42(1):1-11.

Ford, I., Kelly, P.A.T. and McCulloch, J. (1985) Fingerprinting neuropharmacological profiles : A systematic approach to handling data from 2-deoxyglucose autoradiography. *Journal of Cerebral Blood Flow and Metabolism* 5[Suppl. 1]:S647-S648.

Forrest, D., Yuzaki, M., Soares, H.D., Ng, L., Luk, C., Sheng, M., Stewart, C.L., Morgan, J.I., Connor, J.A. and Curran, T. (1994) Targeted disruption of NMDA receptor gene abolishes NMDA response and results in neonatal death. *Neuron* 13:325-338.

Foster, A.C. and Fagg, G.E. (1987) Comparison of L-[³H]glutamate, D-[³H]aspartate, DL-[³H]AP5 and [³H]NMDA as ligands for NMDA receptors in crude postsynaptic densities from rat brain. *European Journal of Pharmacology* 133:291-300.

Foster, A.C., Gill, R. and Woodruff, G.N. (1988) Neuroprotective effects of MK801 *in vivo* : selectivity and evidence for delayed degeneration mediated by NMDA receptor activation. *The Journal of Neuroscience* 8(12):4745-4754.

Foster, A.C., Mena, E.E., Fagg, G.E. and Cotman, C.W. (1981) Glutamate and aspartate binding sites are enriched in synaptic junctions isolated from rat brain. *The Journal of Neuroscience* 1(6):620-625.

Foster, A.C. and Wong, E.H.F. (1987) The novel anticonvulsant MK801 binds to the activated state of the N-methyl-D-aspartate receptor in rat brain. *British Journal of Pharmacology* 91:403-409.

Franklin, P.H. and Murray, T.F. (1992) High affinity [³H]dextrorphan binding in rat brain is localised to a non-competitive antagonist site of the activated N-methyl-D-aspartate receptor cation channel. *Molecular Pharmacology* 41:134-146.

Fujisawa, H., Dawson, D., Browne, S.E., Mackay, K.B., Bullock, R and McCulloch, J. (1993) Pharmacological modification of glutamate neurotoxicity *in vivo*. *Brain Research* 629:73-78.

Garthwaite, G. and Garthwaite, J. (1986) Neurotoxicity of excitatory amino acid receptor agonists in rat cerebellar slices : dependence on calcium concentration. *Neuroscience Letters* 66:193-198.

Garthwaite, G. and Garthwaite, J. (1991) Mechanisms of AMPA neurotoxicity in rat-brain slices. *European Journal of Neuroscience* 3(8):729-736.

Gartshore, G. (1996) The consequences of reperfusion on cerebral ischaemic damage. A thesis submitted for the degree of Doctor of Philosophy to the Faculty of medicine, University of Glasgow.

Gibson, R.E., Burns, H.D., Thorpe, H.H., Eng, W., Ransom, R. and Solomon, H. (1992) *In vivo* binding and autoradiographic imaging of (+)-3-[¹²⁵I]Iodo-MK801 to the NMDA receptor-channel complex in rat brain. *Nuclear Medicine Biology* 19(3):319-326.

Gibson, R.E., Burns, H.D. and Eckelman, W.C. (1993) The potential uses of radiopharmaceuticals in the pharmaceutical industry. In: Nuclear imaging in drug discovery, development and approval. Edited by Burns, H.D., Gibson, R.E, Dannals, R.F. and Siegl, P. Boston:Birkhauser p 321-329.

Giffard, R.G., Monyer, H. and Choi, D.W. (1990) Selective vulnerability of cultured cortical glia to injury by extracellular acidosis. *Brain Research* 530:138-141.

Gill, R., Andine, P., Hillered, L., Persson, L. and Hagberg, H. (1992) The effect of MK801 on cortical spreading depression on the penumbral zone following focal cerebral ischaemia in the rat. *Journal of Cerebral Blood Flow and Metabolism* 12:371-379.

Gill, R., Brazell, C., Woodruff, G.N. and Kemp, J.A. (1991) The neuroprotective action of dizocilpine (MK801) in the rat middle cerebral artery occlusion model of focal ischaemia. *British Journal of Pharmacology* 103:2030-2036.

Gill, R., Foster, A.C. and Woodruff, G.N. (1987) Systemic administration of MK801 protects against ischaemia-induced hippocampal degeneration in the gerbil. *The Journal of Neuroscience* 7:3343-3349.

Gill, R. and Lodge, D. (1994) The neuroprotective effects of the decahydroisoquinoline, LY 215490 : a novel AMPA antagonist in focal ischaemia. *Neuropharmacology* 33 (12):1529-1536.

Goldberg, M.P. and Choi, D.W. (1993) Combined oxygen and glucose deprivation in cortical cell culture : calcium-dependent and calcium-independent mechanisms of neuronal injury. *The Journal of Neuroscience* 13(8):3510-3524.

Gotoh, O., Awni, A., McCulloch, J., Graham, D.I., Harper, A.M. and Teasdale, G.M. (1986) Nimodipine and the haemodynamic and histopathological consequences of middle cerebral artery occlusion in the rat. *Journal of Cerebral Blood Flow and Metabolism* 6:321-331.

Gozlan, H. and Ben-Ari, Y. (1995) NMDA receptor redox sites : are they targets for selective neuronal protection? *Trends in Pharmacological Sciences* 16:368-374.

Graham, S.H., Chen, J., Sharp, F.R. and Simon, R.P. (1993) Limiting ischemic injury by inhibition of excitatory amino acid release. *Journal of Cerebral Blood Flow and Metabolism* 13:88-97.

Greenamyre, J.T. (1986) The role of glutamate in neurotransmission and in neurological disease. *Archives of Neurology* 43:1058-1063.

Grimwood, S., Wilde, G.J.C. and Foster, A.C. (1993) Interactions between the glutamate and glycine recognition sites of the N-methyl-D-aspartate receptor from rat brain, as revealed from radioligand binding studies. *Journal of Neurochemistry* 60(5):1729-1738.

Grotta, J., Clark, W., Coull, B., Pettigrew, C., MacKay, B., Goldstein, L.B., Meissner, I., Murphy, D. and LaRue, L. (1995) Safety and tolerability of the glutamate antagonist CGS 19755 (Selfotel) in patients with acute ischaemic stroke. *Stroke* 26:602-605.

Hargreaves, R.J., Hill, R.G. and Iversen, L.L. (1994) Neuroprotective NMDA antagonists : the controversy over their potential for adverse effects on cortical neuronal morphology. *Acta Neurochirurgica* Suppl. 60:15-19.

Heiss, W. and Graf, R. (1994) The ischaemic penumbra. *Current Opinion in Neurology* 7:11-19.

Hernandez, M.J., Brennan, R.W., Bowman, G.S. (1978) Cerebral blood flow auto-regulation in the rat. *Stroke* 9(2):150-155.

Hosford, D.A., Bonhaus, D.W. and McNamara, J.O. (1990) A radiohistochemical measure of [³H]TCP binding to the activated NMDA-receptor gated ion channel in rat brain. *Brain Research* 516:192-200.

Howell, G.A., Welch, M.G. and Frederickson, C.J. (1984) Stimulation-induced uptake and release of zinc in hippocampal slices. *Nature* 308:736-738.

Huettner, J.E. and Bean, B.P. (1988) Block of the N-methyl-D-aspartate-activated current by the anticonvulsant MK801 : Selective binding to open channels. *Proclamations of the National Academy of Science s, USA* 85:1307-1311.

Iversen, L.L. (1993) Nuclear imaging in drug development - introduction. In: Nuclear imaging in drug discovery, development and approval, edited by Burns, H.D., Gibson, R., Dannals, R. and Siegl, P. Boston: Birkhauser p. 1-9.

Jacobson, W. and Cotrell, G.A. (1993) Rapid visualisation of NMDA receptors in the brain : characterisation of (+)-3-[¹²⁵I]-iodo-MK801 binding to thin sections of rat brain. *The Journal of Neuroscience Methods* 46:17-27.

Jansen, K.L.R., Dragunow, M., Faull, R.L.M. and Leslie, R.A. (1991) Autoradiographic visualisation of [³H]DTG binding to sigma receptors, [³H]TCP binding sites, and L-[³H]glutamate binding to NMDA receptors in human cerebellum. *Neuroscience Letters* 125:143-146.

Jarvis, M.F., Murphy, D.E. and Williams, M. (1987) Quantitative autoradiographic localisation of NMDA receptors in rat brain using [³H]CPP : comparison with [³H]TCP sites. *European Journal of Pharmacology* 141:149-152.

Javitt, D.C. and Zukin, S.R. (1989) Bioexponential kinetics of [³H]MK801 binding : evidence for access to closed and open N-methyl-D-aspartate receptor channels. *Molecular Pharmacology* 35:387-393.

Johnson, J.W. and Ascher, P. (1987) Glycine potentiates the NMDA response in cultures mouse brain neurons. *Nature* 325:529-533.

Johnson, J.W. and Ascher, P. (1990) Voltage-dependent block by intracellular Mg²⁺ of N-methyl-D-aspartate-activated channel. *Journal of Biophysics* 57:1085-1090.

- Johnson, T.J. (1996) Modulation of channel function by polyamines. *Trends in Pharmacological Sciences* 17:22-27.
- Jones, T.H., Morawetz, R.B., Crowell, R.M., Marcoux, F.W., Fitzgibbon, S.J., DeGirolami, U. and Ojemann, R.G. (1981) Thresholds of focal cerebral ischaemia in awake monkeys. *Journal of Neurosurgery* 54:773-782.
- Katsura, K., Kristian, T., Smith, M-L. and Siesjo, B.K. (1994) Acidosis induced by hypercapnia exaggerates ischaemic brain damage. *Journal of Cerebral Blood Flow and Metabolism* 14:243-250.
- Kelly, P.A.T., Ford, I. and McCulloch, J. (1986) The effect of diazepam upon local cerebral glucose use in the conscious rat. *Neuroscience* 19(1):257-265.
- Kemp, J.A. and Priestly, T. (1991) Effects of (+)-HA-966 and 7-chlorokynurenic acid on the kinetics of N-methyl-D-aspartate receptor agonist responses in rat cultured cortical neurons. *Molecular Pharmacology* 39:666-670.
- Kemp, J.A., Priestly, T. and Woodruff, G.N. (1986) MK801, a novel, orally active anticonvulsant, is a potent, non-competitive N-methyl-D-aspartate receptor antagonist. *British Journal of Pharmacology Proclamations* . Suppl.89:535P.
- Kew, J.N.C., Trube, G. and Kemp, J.A. (1996) A novel mechanism of activity-dependent NMDA receptor antagonism described the effect of ifenprodil in rat cultured cortical neurones. *Journal of Physiology* 497 (3):761-772.
- Kirino, T. (1982) Delayed neuronal death in the gerbil hippocampus following ischaemia. *Brain Research* 239:57-69.
- Kleckner, N.W. and Dingledine, R. (1988) Requirement for glycine in activation of N-methyl-D-aspartate receptors expressed in *Xenopus* oocytes. *Science* 241:835-837.
- Kodama, K., Okada, S., Hino, T., Takabayashi, K., Nawata, Y., Uchida, Y., Yamanouchi, N., Komatsu, N., Ikeda, T., Shinoda, N., Murakami, A., Sakamoto, T. and Sato, T. (1995) Single photon emission computed tomography in systemic lupus erythematosus with psychiatric symptoms. *Journal of Neurology, Neurosurgery, and Psychiatry* 58:307-311.

Kristian, T., Katsura, K., Gido, G. and Siesjo, B.K. (1994) The influence of pH on cellular calcium influx during ischaemia. *Brain Research* 641:295-302.

Kuhar, M.J. (1986) Quantitative receptor autoradiography : An overview. In : Quantitative Receptor Autoradiography. Edited by Boast, C.A., Snowhill, E.W. and Altar, C.A. New York : Alan R. Liss p 1-12.

Kuhar, M.J. and Unnerstall, J.R. (1985) Quantitative receptor mapping by autoradiography : some current technical problems. *Trends in Neurosciences* 8(2):49-53.

Kuner, T. and Schoepfer, R. (1996) Multiple structural elements determine subunit specificity of Mg^{2+} block in NMDA receptor channels. *The Journal of Neuroscience* 16 (11):3549-3558.

Kung, H.F. (1993) SPECT and PET ligands for CNS imaging. *Neurotransmission* 9 (4):1-5.

Kung, H.F., Alavi, A., Chang, W., Kung, M.P., Keyes J.W., Velchik, M.G., Billings, J., Pan, S. and Noto, R. (1990) *In vivo* SPECT imaging of CNS D₂ dopaminergic receptors : initial studies with iodine-123-IBZM in humans. *Journal of Nuclear Medicine* 31(5):573-579.

Kurumaji, A., Ikeda, M., Dewar, D., McCormack, A.G. and McCulloch, J. (1991) Effects of chronic administration of MK801 upon local cerebral glucose utilisation and ligand binding to the NMDA receptor complex. *Brain Research* 563:57-65.

Kurumaji, A. and McCulloch, J. (1989) Effects of MK801 on local cerebral glucose utilisation in conscious rats and rats anaesthetised with halothane. *Journal of Cerebral Blood Flow and Metabolism* 9:786-794.

Kurumaji, A. and McCulloch, J. (1990) Effects of MK801 upon local cerebral glucose utilisation in conscious rats following unilateral lesion of caudal entorhinal cortex. *Brain Research* 531:72-82.

Kurumaji, A., Nehls, D.G., Park, C.K. and McCulloch, J. (1989) Effects of the NMDA antagonists, MK801 and CPP, upon local cerebral glucose use. *Brain Research* 496:268-284,.

Kutsuwada, T., Masaki, H., Kumanishi, T., Arakawa, M and Mischina, M. (1992) Molecular diversity of the NMDA receptor channel. *Nature* 358:36-41.

Lehre, K.P., Levy, L.M., Ottersen, O.P., Storm-Mathisen, J. and Danbolt, N.C. (1995) Differential expression of two glial glutamate transporters in rat brain : quantitative and immunocytochemical observations. *The Journal of Neuroscience* 15:1835-1853.

Lei, S.Z., Pan, Z-H., Aggarwal, S.K., Chen, H-S.V. and Lipton, S.A. (1992) Effect of nitric oxide production on the redox modulatory site of the NMDA receptor channel complex. *Neuron* 8:1087-1099.

Lerma, J., Morales, M., Vicente, M.A. and Herreras, O. (1997) Glutamate receptors of the kainate type and synaptic transmission. *Trends in Neurological Sciences* 20(1):9-12.

Lester, R.A.J., Tong, G. and Jahr, C.E. (1993) Interactions between the glycine and glutamate binding sites of the NMDA receptor. *The Journal of Neuroscience* 13(3):1088-1096.

Lieberman, D.N. and Mody, I. (1994) Regulation of NMDA channel function by endogenous Ca^{2+} -dependent phosphatase. *Nature* 369:235-239.

Lodge, D. and Collingridge, G. (1990) Les agents provocateurs : a series on the pharmacology of excitatory amino acids. *Trends in Pharmacological Sciences* 11:22-24.

Lynch, D.R., Lawrence, J.L., Lenz, S., Anegawa, N.J., Dichter, M. and Pritchett, D.B. (1995) Pharmacological characterisation of heteromeric NMDA receptors composed of NR 1a and 2B subunits : differences with receptors formed from NR 1a and 2A. *Journal of Neurochemistry* 64(4):1462-1468.

MacDonald, J.F., Bartlett, M.C., Mody, I., Pahapill, P., Reynolds, J.N., Salter, M.W., Schneiderman, J.H. and Pennefather, P.S. (1991) Actions of ketamine, phencyclidine, and MK801 on NMDA receptor currents in cultured mouse hippocampal neurons. *Journal of Physiology* 432:483-508.

MacDonald, J.F. and Nowak, L.M. (1990) Mechanisms of blockade of excitatory amino acid receptor channels. *Trends in Pharmacological Sciences* 11:167-172.

- MacKay, K.B., Patel, T.R., Galbraith, S.L., Woodruff, G.N. and McCulloch, J. (1996) The relationship between glutamate release and cerebral blood flow after focal cerebral ischaemia in the cat : effect of pretreatment with enadoline (a kappa receptor agonist). *Brain Research* 712:329-334.
- Maragos, W.F., Chu, D.C.M., Greenamyre, J.T., Penney, J.B. and Young, A.B. (1986) High correlation between the localisation of [³H]TCP binding and NMDA receptors. *European Journal of Physiology* 123:173-174.
- Marti, T., Benke, D., Mertens, S., Heckendorn, R., Pozza, M., Allgeier, H., Angst, C., Laurie, D., Seeburg, P. and Mohler, H. (1993) Molecular distinction of three of the N-methyl-D-aspartate receptor subtypes *in situ* and developmental receptor maturation demonstrated with the photoaffinity ligand [¹²⁵I]-labelled CGP 55802A. *Proclamations of the National Academy of Sciences, USA*. 90:8434-8438.
- Martin, G., Nie, Z. and Siggins, G.R. (1997) mu Opioid receptors modulate NMDA receptor-mediated responses in nucleus accumbens neurons. *The Journal of Neuroscience* 17(1):11-22.
- Martin, R.L., Lloyd, H.G.E. and Cowan, A.I. (1994) The early events of oxygen and glucose deprivation : setting the scene for neuronal death? *Trends in Neurological Sciences* 17(6):251-257.
- Masdeu, J.C., Brass, L.M., Holman, B.L. and Kushner, M.J. (1994) Brain single-photon emission computed tomography. *Neurology* 44:1970-1977.
- Mayer, M.L., Westbrook, G.L. and Guthrie, P.B. (1984) Voltage-dependent block by Mg²⁺ of NMDA responses in spinal cord neurones. *Nature* 309:261-263.
- McBurney, R.N. (1997) Development of the NMDA ion-channel blocker, aptiganel hydrochloride, as a neuroprotective agent for acute CNS injury. In: Neuroprotective agents in cerebral ischaemia. Edited by Green, A.R. and Cross, A.J. San Diego : Academic Press Limited p. 173-195.
- McCulloch, J. (1992) Excitatory amino acid antagonists and their potential for the treatment of ischaemic brain damage. *British Journal of Pharmacology* 34:106-114.

McCulloch, J. (1994) Amelioration of ischaemic and haemorrhagic injury by pharmacological intervention. In: Brain Lesions in the Newborn, Alfred Benzon Symposium 37. Edited by Lou, H.C., Greisen, G. and Falk Larsen, J. Copenhagen: Munksgaard p 485-495.

McCulloch, J. (1994) Glutamate receptor antagonists in cerebral ischaemia. *Journal of Neural Transmission* Supplement 43:71-79.

McCulloch, J., Bullock, R. and Teasdale, G.M. (1991) Excitatory amino acid antagonists : opportunities for the treatment of ischaemic brain damage in man. In: Excitatory amino acid antagonists. Edited by Meldrum, B. Oxford : Blackwell Scientific Publications p 287-326.

McCulloch, J. and Iversen, L.L. (1991) Autoradiographic assessment of the effects of N-methyl-D-aspartate (NMDA) receptor antagonists *in vivo*. *Neurochemical Research* 16 (9):951-963.

McCulloch, J., Wallace, M.C, Laurie, D., Angerson, W.J., Burns, H.D. and Gibson, R.E. (1992) Imaging activation in the NMDA receptor complex with [¹²⁵I]MK801. In: Pharmacology of cerebral Ischaemia. Edited by Kriegstein, K. and Oberpichler-Schwenk, H. Stuttgart: Wissenschaftliche Verlagsgesellschaft p. 59-63.

McEntee, W.J. and Crook, T.H. (1993) Glutamate: its role in learning, memory and the aging brain. *Psychopharmacology* 3:391-401.

McLachlan, R.S. and Girvan, J.P. (1994) Spreading depression of Leao in rodent and human cortex. *Brain Research* 666:133-136.

Meldrum, B. (1985) Possible therapeutic applications of antagonists of excitatory amino acid neurotransmitters. *Clinical Science* 68:113-122.

Meldrum, B. and Garthwaite, J. (1990) Excitatory amino acid neurotoxicity and neurodegenerative disease. *Trends in Pharmacological Sciences* 11:379-387.

Mies, G., Ishimaru, S., Seo, K. and Hossmann, K.A. (1991) Ischemic thresholds of cerebral protein synthesis and energy state following middle cerebral artery occlusion. *Journal of Cerebral Blood Flow and Metabolism* 11:751-761.

Miller, J.D., Bullock, R., Graham, D.I., Chen, M.H., Teasdale, G.M. (1990) Ischaemic brain damage in a model of acute subdural haematoma. *Neurosurgery* 27(3):433-439.

Minematsu, K., Fisher, M., Li, L., Davis, M.A., Knapp, A.G., Cotter, R.E., McBurney, R.N. and Sotak, C.H. (1993) Effects of a novel NMDA antagonist on experimental stroke rapidly and quantitatively assessed by diffusion-weighted MRI. *Neurology* 43:397-403.

Minematsu, K., Fisher, M., Li, L. and Sotak, C.H. (1993) Diffusion and perfusion magnetic resonance imaging studies to evaluate a noncompetitive N-methyl-D-aspartate antagonist and reperfusion in experimental stroke in rats. *Stroke* 24(12):2074-2081.

Monaghan, D.T. and Cotman, C.W. (1985) Distribution of N-methyl-D-aspartate-sensitive L-[³H]glutamate-binding sites in rat brain. *The Journal of Neuroscience* 5 (11):2909-2919.

Monaghan, D.T. and Cotman, C.W. (1986) Identification and properties of N-methyl-D-aspartate receptors in rat brain synaptic plasma membranes. *Proclamations of the National Academy of Sciences USA* 83:7532-7536.

Monaghan, D.T., Olverman, H.J., Nguyen, L., Watkins, J.C. and Cotman, C.W. (1988) Two classes of N-methyl-D-aspartate recognition sites : differential distribution and differential regulation by glycine. *Proclamations of the National Academy of Sciences USA* 85:9836-9840.

Muir, K.W., Grosset, D.G., Gamzu, E. and Lees, K.R. (1994) Pharmacological effects of the non-competitive NMDA antagonist CNS 1102 in normal volunteers. *British Journal of Clinical Pharmacology* 38:33-38.

Muir, K.W. and Lees, K.R. (1995) Clinical experience with excitatory amino acid antagonist drugs. *Stroke* 26(3):503-513.

Munir, M., Subramaniam, S. and McGonigle, P. (1993) Polyamines modulate the neurotoxic effects of NMDA *in vivo*. *Brain Research* 616:163-170.

Murphy, T.H., Malouf, A.T., Sastre, A., Schnaar, R.L. and Coyle, J.T. (1988) Calcium-dependent glutamate cytotoxicity in a neuronal cell line. *Brain Research* 444:325-332.

Naito, S. and Ueda, T. (1993) Adenosine triphosphate-dependent uptake of glutamate into Protein 1-associated synaptic vesicles. *Journal of Biological Chemistry* 258(2):696-699.

Nakanishi, S. (1992) Molecular diversity of glutamate receptors and implications for brain function. *Science* 258:597-603.

Nedergaard, M. and Hansen, A.J. (1995) Characterisation of cortical depolarisation evoked in cerebral ischaemia. *Journal of Cerebral Blood Flow and Metabolism* 13:568-574.

Nehls, D.G., Park, C.K., MacCormack, A.G. and McCulloch, J. (1990) The effects of N-methyl-D-aspartate receptor blockade with MK801 upon the relationship between cerebral blood flow and glucose utilisation. *Brain Research* 511:271-279.

Nelgaard, B. and Wieloch, T. (1992) NMDA-receptor blockers but not NBQX, an AMPA-receptor antagonist, inhibit spreading depression in the rat brain. *Acta Physiologica Scandinavica* 146:497-503.

Nellgard, B. and Wieloch, T. (1992) Postischaemic blockade of AMPA but not NMDA receptors mitigates neuronal damage in the rat brain following transient severe cerebral ischaemia. *Journal of Cerebral Blood Flow and Metabolism* 12:2-11.

Nicholls, D. and Attwell, D. (1990) The release and uptake of excitatory amino acids. *Trends in Pharmacological Sciences* 11:462-468.

Nichols, R.A., Sirah, T.S., Czernik, A.J., Nairn, A.L. and Greenyard, P. (1990) Calcium calmodulin-dependent protein kinase II increases glutamate and noradrenaline release from synaptosomes. *Nature* 343:647-651.

Niethammer, M., Kim, E. and Sheng, M. (1996) Interactions between the C terminus of NMDA receptor subunits and multiple members of the PSD-95 family of membrane associated guanylate kinases. *The Journal of Neuroscience* 16(7):2157-2163.

Nishikawa, T., Kirsch, J.R., Koehler, R.C., Miyabe, M. and Traystman, R.J. (1994) Competitive N-methyl-D-aspartate receptor blockade reduces brain injury following transient focal ischaemia in cats. *Stroke* 25:2258-2264.

- Nowak, L., Bregestovski, P., Ascher, P., Herbet, A. and Prochiantz, A. (1984) Magnesium gates glutamate-activated channels in mouse central neurones. *Nature* **307**:462-465.
- O'Donnell, B.R. and Bickler, P.E. (1994) Influence of pH on calcium influx during hypoxia in rat cortical brain slices. *Stroke* **25**:171-177.
- Obrenovitch, T.P. (1995) The ischaemic penumbra : twenty years on. *Cerebrovascular and Brain Metabolism Reviews* **7**:297-323.
- Olney, J.W., Ho, O.L. and Rhee, V. (1971) Cytotoxic effects of acidic and sulphur containing amino acids on the infant mouse central nervous system. *Experimental Brain Research* **14**:61-76.
- Olney, J.W., Labruyere, J. and Price, M.T. (1989) Pathological changes in cerebrocortical neurons by phencyclidine and related drugs. *Brain Research* **244**:1360-1362.
- Orita, K., Maeda, M., Hashimoto, A., Nishikawa, T., Yugami, T. and Umezu, K. (1993) Synthesis and evaluation of 1-(1-[5-(2'-[¹⁸F]fluoroethyl)-2-thienyl] cyclohexyl)piperidine as a potential *in vivo* radioligand for the NMDA receptor-channel complex. *Nuclear Medicine Biology* **20**(7):865-873.
- Orrenius, S., McConkey, D.J., Bellomo, G. and Nicotera, P. (1989) Role of Ca²⁺ in toxic cell killing. *Trends in Pharmacological Sciences* **10**:281-285.
- Ouyang, X., Mukherjee, J. and Yang, Z.Y. (1996) Synthesis, radiosynthesis, and biological evaluation of fluorinated thientycyclohexyl piperidine as potential radiotracers for the NMDA receptor-linked calcium ionophore. *Nuclear Medicine Biology* **23**(3):315-324.
- Owens, J., Wyper, D.J., Patterson, J., Brown, D.R.P., Elliott, A.T., Teasdale, G.M. and McCulloch, J. (1997) First SPET images of glutamate (NMDA) receptor activation *in vivo* in cerebral ischaemia. *Nuclear Medicine Communications* **18**:149-158.
- Paoletti, P., Neyton, J. and Ascher, P. (1995) Glycine-independent and subunit-specific potentiation of NMDA responses by extracellular Mg²⁺. *Neuron* **15**:1109-1120.

Park, C.K., McCulloch, J., Kang, J.K. and Choi, C.R. (1994) Pretreatment with a competitive NMDA antagonist D-CPPene attenuates focal cerebral infarction and brain swelling in awake rats. *Acta Neurochirurgica* 127:220-226.

Park, C.K., Nehls, D.G., Graham, D.I., Teasdale, G.M. and McCulloch, J. (1988) The glutamate antagonist MK801 reduces focal ischaemic brain damage in the rat. *Annals of Neurology* 24:543-551.

Paxinos, G. and Watson, C. (1986) The rat brain in stereotaxic coordinates, Second Edition, Academic Press.

Pellegrini-Giampietro, D.E., Cherichi, G., Alesiani, M., Carla, V. and Moroni, F. (1990) Excitatory amino acid release and free radical formation may cooperate in the genesis of ischaemia-induced neuronal damage. *The Journal of Neuroscience* 10:1035-1041.

Perkins, M.N. and Stone, T.W. (1983) Pharmacology and regional variations of quinolinic-acid-evoked excitations in the rat central nervous system. *Journal of Pharmacology and Experimental Therapeutics* 226:551-557.

Petito, C.K. and Pulsinelli, W.A. (1984) Sequential development of reversible and irreversible neuronal damage following cerebral ischaemia. *Journal of Neuropathology and Experimental Neurology* 43 (2):141-153.

Pin, J. and Duvoisin, R. (1995) The metabotropic glutamate receptors : structure and functions. *Neuropharmacology* 34(1):1-26.

Plannells-Cases, R., Sun, W., Ferrer-Montiel, A.V. and Montal, M. (1993) Molecular cloning, functional expression, and pharmacological characterization of an N-methyl-D-aspartate receptor subunit from human brain. *Proclamations of the National Academy of Sciences USA* 90:5057-5061.

Porter, R.H.P. and Greenamyre, J.T. (1995) Regional variations in the pharmacology of NMDA receptor channel blockers : implications for therapeutic potential. *Journal of Neurochemistry* 64:614-623.

Premkumar, L.S. and Auerbach, A. (1996) Identification of a high affinity divalent cation binding site near the entrance of the NMDA receptor channel. *Neuron* 16:869-880.

Price, J.C., Waelsch, H. and Putnam, T.J. (1943) DL-glutamic acid hydrochloride in the treatment of petit mal and psychomotor seizures. *Journal of the American Medical Association* 122:1153-1156.

Raditsch, M., Ruppersberg, J.P., Kuner, T., Gunther, W., Schoepfer, R., Seeburg, P.H., Jahn, W. and Witzemann, V. (1993) Subunit-specific block of cloned NMDA receptors by argiotoxin 636. *FEBS Letters* 324 (1):63-66.

Rajdev, S. and Reynolds, I.J. (1992) Effects of monovalent and divalent cations on 3-(+)[¹²⁵I]Iododizocilpine binding to the N-methyl-D-aspartate receptor of rat brain membranes. *Journal of Neurochemistry* 58:1469-1476.

Rajdev, S. and Reynolds, I.J. (1993) Effects of pH on the actions of dizocilpine at the N-methyl-D-aspartate receptor complex. *British Journal of Pharmacology* 109:107-112.

Ransom, R.W. and Stec, N.L. (1988) Cooperative modulation of of [³H]MK801 binding to the N-methyl-D-aspartate receptor-ion channel complex by L-glutamate, glycine and polyamines. *Journal of Neurochemistry* 51:830-836.

Rapoport, S.I. (1976) Regulation of drug entry into the nervous system. In: The blood brain barrier in physiology and medicine. New York : Raven Press p 153-176.

Reddy, N.L., Hu, L-Y., Cotter, R.E., Fischer, J.B., Wong, W.J., McBurney, R.N., Weber, E., Holmes, D.L., Wong, S.T., Prasad, R. and Keana, J.F.W. (1994) Synthesis and structure-activity studies of N,N'-diarylguanidine derivatives. N-(1-naphthyl)-N'-(3-ethylphenyl)-N'-methylguanidine : A new selective non-competitive NMDA receptor antagonist. *Journal of Medicinal Chemistry* 37:260-267.

Reynolds, I.J., Murphy, S.N. and Miller, R.J. (1977) ³H-labeled MK801 binding to the excitatory amino acid receptor complex from rat brain is enhanced by glycine. *Proclamations of the National Academy of Sciences USA* 84:7744-7748.

Reynolds, I.J. and Rush, E.A. (1990) Role of lipid solubility in the interaction of drugs with the N-methyl-D-aspartate receptor. *Synapse* 5:71-76.

Rogawski, M.A. (1993) Therapeutic potential of excitatory amino acid antagonists : channel blockers and 2,3-benzodiazepines. *Trends in Pharmacological Sciences* 14:325-331.

Roth, J.E., Murray, T.F. and Franklin, P.H. (1996) Regional distribution and characterisation of [³H]dextrorphan binding sites in rat brain determined by quantitative autoradiography. *Journal of Pharmacology and Experimental Therapeutics* **227**(3): 1823-1836.

Rothman, S. (1985) Excitatory amino acid neurotoxicity is produced by passive chloride influx. *The Journal of Neuroscience* **6**:1884-1891.

Saatman, K.E., Murai, H., Bartus, R.T., Smith, D.H., Hayward, N.J., Perri, B.R., McIntosh, T.K. (1996) Calpain inhibitor AK295 attenuates motor and cognitive deficits following experimental brain injury in the rat. *Proceedings of the National Academy of Sciences USA* **93**:3428-3433.

Saido, T.C., Sorimachi, H., Suzuki, K. (1994) Calpain : new perspectives in molecular diversity and physiological-pathological involvement. *The FASEB Journal* **8**:814-822.

Saito, R., Graf, R., Rosner, G., Hubel, K. and Fujita, T. (1995) Halothane increases blood flow and reduces SD-like DC negativations and infarction in perifocal areas of focal ischaemia in cats. *Journal of Cerebral Blood Flow and Metabolism* **15** [Suppl 1]:S315.

Sakurai, W.Y., Cha, J-H., Penney, J.B. and Young, A.B. (1991) Regional distribution and properties of [³H]MK801 binding sites determined by quantitative autoradiography in rat brain. *Journal of Neurochemistry* **56**: 1731-1740

Schoepp, D.D. and Conn, P.J. (1993) Metabotropic glutamate receptors in brain function and pathology. *Trends in Pharmacological Sciences* **14**:13-20.

Scott, R.H., Sutton, K.G. and Dolphin, A.C. (1993) Interactions of polyamines with neuronal ion channels. *Trends in Neurological Sciences* **16**(4):153-160.

Seeburg, P. (1993) The molecular biology of mammalian glutamate receptor channels. *Trends in Neurological Sciences* **16**(9):359-365.

Sharkey, J., Ritchie, J.M., Butcher, S.P. and Kelly, J.S. (1994) Differential effects of competitive (CGS 19755) and non-competitive (MK801) NMDA receptor antagonists upon local cerebral blood flow and local cerebral glucose utilisation in the rat. *Brain Research* **651**:27-36.

Sheardown, M.J. (1993) The pharmacology of AMPA receptors and their antagonists. *Stroke* **24**:I-146-I-147.

Sheng, M., Cummings, J., Roldan, L.A., Jan, Y.N. and Jan, L.Y. (1994) Changing subunit composition of heteromeric NMDA receptors during development of rat cortex. *Nature* **368**:144-147.

Shibayama, Y., Sasaki, S., Tomita, U., Nishikawa, T. and Maeda, M. (1996) Synthesis and evaluation of new F-18 labeled thienylcyclohexylpiperidine (TCP) analogues as radioligands for the NMDA receptor channel complex. *Journal of Labelled Compounds and Radiopharmaceuticals* **38**(1):77-86.

Siesjo, B.K., Folbergrova, J., MacMillan, V. (1972) The effect of hypercapnia upon intracellular pH in the brain, elevated by the bicarbonate-carbonic acid method and from the creatine phosphokinase equilibrium. *Journal of Neurochemistry* **19**:2483-249.

Simon, R.P., Niir, M. and Gwinn, R. (1993) Brain acidosis induced by hypercarbic ventilation attenuates focal ischaemic injury. *Journal of Pharmacology and Experimental Therapeutics* **267**:1428-1431.

Sircar, R. and Zukin, S.R. (1985) Quantitative localization of [³H]TCP binding in rat brain by light microscopy autoradiography. *Brain Research* **334**(1):142-145.

Sokoloff, L., Reivich, M., Kennedy, C., Des Rosiers, M.H., Patlak, C.S., Pettigrew, K.D., Sakurada, O. and Shinohara, M. (1977) The [¹⁴C]deoxyglucose method for the measurement of local cerebral glucose utilisation: Theory, procedure, and normal values in the conscious and anaesthetised albino rat. *Journal of Neurochemistry* **28**:897-916.

Speliotis, E.K., Hartnett, K.A., Blitzblau, R.C., Aizenman, E. and Rosenberg, P.A. (1994) Comparison of the potency of competitive NMDA antagonists against the neurotoxicity of glutamate and NMDA. *Journal of Neurochemistry* **63** (3):879-885.

Sucher, N.J., Awobuluyi, M., Choi, Y. and Lipton, S.A. (1996) NMDA receptors: From genes to channels. *Trends in Pharmacological Sciences* **17**:348-355.

Swan, J.H., Evans, M.C. and Meldrum, B.S. (1988) Long term development of selected neuronal loss and the mechanism of protection by 2-amino-7-phosphonoheptanoate in a rat model of incomplete forebrain ischaemia. *Journal of Cerebral Blood Flow and Metabolism* **8**:64-78.

Swan, J.H. and Meldrum, B.S. (1990) Protection by NMDA antagonists against selective cell loss following transient ischaemia. *Journal of Cerebral Blood Flow and Metabolism* **10**(3):343-351.

Takadera, T., Shimada, Y. and Mohri, T. (1992) Extracellular pH modulates N-methyl-D-aspartate receptor-mediated neurotoxicity and calcium accumulation in rat cortical cultures. *Brain Research* **572**:126-131, .

Tang, C., Dichter, M. and Morad, M. (1990) Modulation of the N-methyl-D-aspartate channel by extracellular H⁺. *Proclamations of the National Academy of Sciences USA* **87**:6445-6449.

Terse, P.S. and Komiskey, H.L. (1997) Modulation of a competitive N-methyl-D-aspartate receptor antagonist binding by zinc oxide. *Brain Research* **744**:347-350.

Tombaugh, G.C. (1994) Mild acidosis delays hypoxic spreading depression and improves neuronal recovery in hippocampal slices. *The Journal of Neuroscience* **14** (9):5635-5643.

Torp, R., Danbolt, N.C., Babaie, E., Bjoras, M., Seeberg, E., Storm-Mathisen, J. and Ottersen, O.P. (1994) Differential expression of two glial glutamate transporters in the rat brain : an *in situ* hybridisation study. *European Journal of Neuroscience* **6**:936-942.

Traynelis, S.F. and Cull-Candy, S.G. (1990) Proton inhibition of N-methyl-D-aspartate receptors in cerebellar neurons. *Nature* **345**:347-350.

Traynelis, S.F., Hartley, M. and Heinemann, S.F. (1995) Control of proton sensitivity of the NMDA receptor by RNA splicing and polyamines. *Science* **268**:873-876.

Trotti, D., Rizzini, B.L., Rossi, D., Haugeto, O., Racagni, G., Danbolt, N.C. and Volterra, A. (1997) Neuronal and glial glutamate transporters possess an SH-based redox regulatory mechanism. *European Journal of Neuroscience* **9**:1236-1243.

Tymianski, M., Charlton, M.P., Carlen, P.L. and Tator, C.H. (1993) Source specificity of early calcium neurotoxicity in cultured embryonic spinal neurons. *The Journal of Neuroscience* **13**(5):2085-2104.

Urwyler, S., Campbell, E., Fricker, G., Jenner, P., Lemaire, M., McAllister, K.H., Neijt, H.C., Park, C.K., Perkins, M., Rudin, M., Sauter, A., Smith, L., Wiederhold, K.H. and Muller, W. (1996) Biphenyl-derivatives of 2-amino-7-phosphono-heptanoic acid, a novel class of potent competitive N-methyl-D-aspartate receptor antagonists - II. Pharmacological characterisation *in vivo*. *Neuropharmacology* 35(6):655-669.

Urwyler, S., Laurie, D., Lowe, D.A., Meier, C.L. and Muller, W. Biphenyl-derivatives of 2-amino-7-phosphonoheptanoic acid, a novel class of potent competitive N-methyl-D-aspartate receptor antagonists - 1. Pharmacological characterisation *in vitro*. *Neuropharmacology* 35(6):643-654.

Vallabhajosula, S., Hirschowitz, J. and Machac, J. (1997) Effect of haloperidol dose on iodine-123-IBZM brain SPECT imaging in schizophrenic patients. *Journal of Nuclear Medicine* 38(2):203-207.

Vignon, J., Privat, A., Chaudieu, K., Thierry, A., Kamenka, J.M. and Chicheportiche, R. (1986) [³H]Thienylphencyclidine ([³H]TCP) binds to two different sites in rat brain. Localisation by autoradiography and biochemical techniques. *Brain Research* 378:133-141.

Volterra, A., Trotti, D., Tromba, C., Floridi, S. and Racagni, G. (1994) Glutamate uptake inhibition by oxygen free radicals in rat cortical astrocytes. *The Journal of Neuroscience* 14 (5):2924-2932.

von Geldern, T.W., Hoffman, D.J., Kester, J.A. and Nellans, H.N. (1996) Arole endothelin antagonists 3. Using delta log P as a tool to improve absorption. *Journal of Medicinal Chemistry* 39:982-991.

Wahl, F., Obrenovitch, T.P., Hardy, A.M., Plotkine, M., Boulu, R. and Symon, L. (1994) Extracellular glutamate during focal cerebral ischaemia in rats : time course and calcium dependency. *Journal of Neurochemistry* 63:1003-1011.

Wallace, H.M. (1987) Polyamine catabolism in mammalian cells : excretion and acetylation. *Medical Science Research* 15:1437-1440.

Wallace, M.C., Teasdale, G.M. and McCulloch, J. (1992) Autoradiographic analysis of ³H-MK801 (dizocilpine) *in vivo* uptake and *in vitro* binding after focal cerebral ischaemia in the rat. *Journal of Neurosurgery* 76:127-133.

Wang, L.-Y. and MacDonald, J.F. (1995) Modulation by magnesium of the affinity of NMDA receptors for glycine in murine hippocampal neurones. *Journal of Physiology* **486**:83-95.

Wang, L., Orser, B., Brautigan, D.L. and MacDonald, J.F. (1994) Regulation of NMDA receptors in cultured hippocampal neurons by protein phosphatases 1 and 2A. *Nature* **369**:230-232.

Weiss, J.H., Hartley, D.M., Koh, J. and Choi, D.W. (1990) The calcium-channel blocker nifedipine attenuates slow excitatory amino-acid neurotoxicity. *Science* **247**:1474-1477.

Werns, S.W. and Lucchesi, B.R. (1990) Free radicals and ischaemic tissue injury. *Trends in Pharmacological Sciences* **11**:161-166.

Westbrook, G.L. and Mayer, M.L. (1987) Micromolar concentrations of zinc antagonise NMDA and GABA responses of hippocampal neurons. *Nature* **328**:640-643.

White, W.F., Nadler, J.V., Hamberger, A. and Cotman, C. (1977) Glutamate as a transmitter of hippocampal perforant path. *Nature* **270**:356-357.

Widdowson, P.S., Trainor, A. and Lock, E.A. (1995) NMDA receptors in rat cerebellum and forebrain : subtle differences in pharmacology and modulation. *Journal of Neurochemistry* **64**(2):651-661.

Williams, K. (1993) Ifenprodil discriminates subtypes of the N-methyl-D-aspartate receptor - selectivity and mechanisms in recombinant heteromeric receptors. *Molecular Pharmacology* **44**(4):851-859.

Willis, C.L., Brazell, C., Foster, A.C. (1991) Plasma and CSF levels of dizocilpine (MK801) required for neuroprotection in the quinolinate injected rat striatum. *European Journal of Pharmacology* **196**:285-290.

Wong, E.H.F., Knight, A.R. and Woodruff, G.N. (1988) [3 H]MK801 labels a site on the N-methyl-D-aspartate receptor channel complex in rat brain membranes. *Journal of Neurochemistry* **50**:274-281.

Xue, D., Slivka, A. and Buchan, A.M. (1992) Tirilizad reduces cortical infarction after transient but not permanent focal cerebral ischaemia in rats. *Stroke* **23**:894-899.

Yao, H., Markgraf, C.G., Dietrich, W.D., Prado, R., Watson, B.D. and Ginsberg, M.D. (1994) Glutamate antagonist MK801 attenuates incomplete but not complete infarction in thrombotic distal middle cerebral artery occlusion in Wistar rats. *Brain Research* **642**:117-122.

Yoneda, Y., Enomoto, R. and Ogita, K. (1994) Supporting evidence for negative modulation by protons of an ion channel associated with the N-methyl-D-aspartate receptor complex in rat brain using ligand binding techniques. *Brain Research* **636**:298-307.

Yoneda, Y. and Ogita, K. (1991) Heterogeneity of the N-methyl-D-aspartate receptor ionophore complex in rat brain, as revealed by ligand-binding techniques. *Journal of Pharmacology and Experimental Therapeutics* **259**(1):86-96.

Zangerle, L., Cuenod, M., Winterhalter, H.H. and Do, K.Q. (1992) Screening of thiol compounds - depolarisation-induced release of glutathione and cysteine from rat brain slices. *Journal of Neurochemistry* **59**:181-189.

Zeman, W. and Innes, J.R.M. (1963) The CNS and its topographical relation to the body. In: Craigie's Neuroanatomy of the Rat. New York : Academic Press p 11-41.

Zeevalk, G.D. and Nicklas, W.J. (1993) Hypothermia, metabolic stress, and NMDA-mediated excitotoxicity. *Journal of Neurochemistry* **61**(4):1445-1453.

Zhou, M., Peterson, C.L., Lu, Y. and Nadler, J.V. (1995) Release of glutamate and aspartate from CA1 synaptosomes : selective modulation of aspartate release by ionotropic glutamate receptor ligands. *Journal of Neurochemistry* **64**:1556-1566.

APPENDIX 1

1. Effect of CNS 1261 on cortical spreading depression

1.1 Surgical preparation of animals

Animals were anaesthetised with urethane (1500mg/kg i.p.) since halothane is known to inhibit CSD (Saito *et al*, 1995). A tracheotomy was performed and the animals connected to a small animal respirator (Ugo Basile, Linton Instruments) and ventilated with a mixture of 30% O₂ and 70% N₂O. The femoral vessels were exposed unilaterally by blunt dissection. Polyethylene catheters were inserted into the left femoral artery and vein and secured with silk thread. Animals were turned prone and the head fixed in a Kopf stereotaxic frame. A craniotomy (5x3mm) was drilled over the right parietal cortex and the bone and dura removed without damage to the underlying pial vessels. Two glass electrodes (tip diameter 10mm) were pulled from borosilicate glass capillaries (O.D. = 0.86mm, I.D. = 1.5mm, Clark Electromedical Instruments). The electrodes were filled with saline and positioned 1.5-2mm apart and 1mm deep into the cortex using a micromanipulator. All electrode manipulations were performed under low power magnification in order to avoid trauma to large pial vessels. Ag/AgCl wires were inserted into the electrodes to measure DC potential, the rostral electrode measured initiation and the caudal electrode propagation of CSD. In several preparations a second larger burr hole was drilled in the ipsilateral hemisphere and a laser doppler flow probe positioned touching the intact dura. Two saline-filled cannulae containing Ag/AgCl wire were inserted under the skin and served as reference electrodes. The preparation was allowed to stabilise for 15 minutes before any further manipulation were performed.

1.2 Induction of cortical spreading depression

CSD was electrically evoked using a bipolar stimulating electrode placed at 90° to the rostral recording electrode. The stimulating electrode was positioned so that it touched, but did not visibly depress the cortical surface. Electrocorical stimulation consisted of a

train of 5ms pulses at 40Hz for 2s at 10 minute intervals. The threshold for evoking CSD was determined by increasing the current gradually until a response was triggered. On determining the stimulation threshold (generally 0.1-0.2mA), the current was then increased by 10%. The cortex was stimulated 3 times in order to establish that responses were reproducible at both electrodes.

1.3 Drug treatment

CNS 1261 (1mg/kg) was administered intravenously following confirmation of reproducible responses. Responses were recorded for a further 120 minutes after administration

1.4 Data processing

All signals, including blood pressure, heart rate and DC potential were recorded using a Gras Model 7 polygraph and processed by an in-house DART computer using the program RATCSD. The rate of CSD propagation was calculated from the latency of the DC shift at the rostral and caudal electrodes and the distance between them.

APPENDIX 2

TABLE 1
[¹²⁵I]CNS 1261 uptake 5 minutes after intracortical injection of CSF or NMDA

STRUCTURE	VEHICLE (CSF)		NMDA (27μmoles)	
	ipsilateral	contralateral	ipsilateral	contralateral
anterior cingulate cortex	0.74 ± 0.08	1.37 ± 0.08	0.98 ± 0.06	1.23 ± 0.24
genu	0.23 ± 0.01	0.35 ± 0.02	0.40 ± 0.01	0.47 ± 0.07
sensory motor cortex				
layers I-III	0.63 ± 0.08	1.33 ± 0.07	1.65 ± 0.70	1.86 ± 0.10
layer IV	0.82 ± 0.07	1.51 ± 0.08	2.00 ± 0.87	1.89 ± 0.08
layers V-VI	0.92 ± 0.02	1.30 ± 0.03	2.03 ± 0.75	1.70 ± 0.05
caudate nucleus	1.18 ± 0.02	1.22 ± 0.01	1.42 ± 0.11	1.56 ± 0.13
corpus callosum	0.25 ± 0.03	0.40 ± 0.01	0.49 ± 0.23	0.50 ± 0.06
anterior thalamus	1.62 ± 0.03	1.61 ± 0.11	2.04 ± 0.11	2.06 ± 0.14
hippocampus CA1	0.62 ± 0.01	0.64 ± 0.01	0.77 ± 0.00	0.81 ± 0.05
hippocampus CA3	0.61 ± 0.00	0.71 ± 0.01	0.80 ± 0.01	0.84 ± 0.05
lateral habenular nucleus	1.77 ± 0.23	1.72 ± 0.15	2.07 ± 0.15	2.08 ± 0.04
mediodorsal thalamus	0.93 ± 0.04	1.01 ± 0.02	1.13 ± 0.13	1.20 ± 0.33
ventrolateral thalamus	1.07 ± 0.05	1.13 ± 0.10	1.48 ± 0.19	1.38 ± 0.25
internal capsule	0.34 ± 0.01	0.36 ± 0.00	0.46 ± 0.02	0.44 ± 0.01
parietal cortex				
layers I-III	0.61 ± 0.01	1.27 ± 0.11	1.12 ± 0.21	1.45 ± 0.47
layer IV	0.75 ± 0.02	1.43 ± 0.13	1.26 ± 0.02	1.69 ± 0.28
layers V-VI	0.82 ± 0.04	1.23 ± 0.10	1.30 ± 0.03	1.51 ± 0.26
hypothalamus	0.68 ± 0.09	0.66 ± 0.09	0.94 ± 0.11	0.93 ± 0.01
posterior cingulate cortex	1.48 ± 0.16	1.59 ± 0.21	1.58 ± 0.11	1.65 ± 0.30
hippocampus molecular layer	0.80 ± 0.03	0.85 ± 0.12	0.87 ± 0.12	0.99 ± 0.23
dentate gyrus	0.88 ± 0.04	1.03 ± 0.06	1.01 ± 0.09	1.03 ± 0.14
auditory cortex				
layers I-III	0.95 ± 0.28	1.38 ± 0.15	0.96 ± 0.13	1.53 ± 0.12
layer IV	1.18 ± 0.44	1.53 ± 0.07	1.18 ± 0.39	1.76 ± 0.13
layers V-VI	0.71 ± 0.01	1.22 ± 0.04	1.10 ± 0.21	1.55 ± 0.23
substantia nigra pars reticulata	1.01 ± 0.04	0.91 ± 0.11	1.20 ± 0.00	1.23 ± 0.10
substantia nigra pars compacta	0.79 ± 0.04	0.71 ± 0.03	1.05 ± 0.06	1.13 ± 0.15
medial geniculate body	1.18 ± 0.03	1.26 ± 0.01	1.42 ± 0.13	1.48 ± 0.15
auditory cortex				
layers I-III	0.70 ± 0.10	1.30 ± 0.10	0.91 ± 0.02	1.27 ± 0.01
layer IV	0.73 ± 0.10	1.55 ± 0.24	0.89 ± 0.14	1.45 ± 0.04
layer V-VI	0.74 ± 0.09	1.22 ± 0.05	0.86 ± 0.18	1.29 ± 0.08
entorhinal cortex	0.96 ± 0.14	1.19 ± 0.14	1.03 ± 0.38	1.15 ± 0.14
inferior colliculus	1.50 ± 0.06	1.47 ± 0.03	1.44 ± 0.22	1.42 ± 0.02
pons	0.77 ± 0.05	0.76 ± 0.04	0.74 ± 0.16	0.77 ± 0.13
cerebellar cortex	1.00 ± 0.00	1.00 ± 0.00	1.00 ± 0.00	1.00 ± 0.00
cerebellar white matter	0.38 ± 0.01	0.37 ± 0.02	0.39 ± 0.13	0.37 ± 0.11
superior olive	1.72 ± 0.23	1.76 ± 0.02	1.54 ± 0.22	1.56 ± 0.05

Data are presented as mean ± S.E.M., n=2. [¹²⁵I]CNS 1261 uptake was measured following injection of NMDA or vehicle (CSF) into the ipsilateral sensory-motor cortex. Uptake of [¹²⁵I]CNS 1261 in individual regions of interest was expressed as a ratio relative to uptake within the cerebellum. Roman numerals indicate the cortical layer examined.

TABLE 2
[¹²⁵I]CNS 1261 uptake 60 minutes after intracortical injection of CSF or NMDA

STRUCTURE	VEHICLE (CSF)		NMDA (27μmoles)	
	ipsilateral	contralateral	ipsilateral	contralateral
anterior cingulate cortex	1.46 ± 0.07	1.59 ± 0.09	1.69 ± 0.16	1.80 ± 0.14
genu	0.94 ± 0.06	1.14 ± 0.14	0.96 ± 0.09	1.04 ± 0.07
sensory motor cortex				
layers I-III	1.22 ± 0.08	1.30 ± 0.01	1.28 ± 0.14	1.49 ± 0.07
layer IV	1.30 ± 0.05	1.37 ± 0.07	1.43 ± 0.13	1.40 ± 0.05
layers V-VI	1.35 ± 0.04	1.39 ± 0.07	1.48 ± 0.09	1.45 ± 0.03
caudate nucleus	1.26 ± 0.05	1.25 ± 0.09	1.41 ± 0.05	1.39 ± 0.04
corpus callosum	1.06 ± 0.05	1.11 ± 0.07	1.07 ± 0.04	1.04 ± 0.05
anterior thalamus	1.53 ± 0.09	1.48 ± 0.07	1.65 ± 0.09	1.75 ± 0.18
hippocampus CA1	1.69 ± 0.08	1.71 ± 0.18	1.80 ± 0.25	1.77 ± 0.25
hippocampus CA3	1.76 ± 0.14	1.79 ± 0.20	1.88 ± 0.21	1.84 ± 0.27
lateral habenular nucleus	1.32 ± 0.14	1.21 ± 0.15	1.17 ± 0.10	1.15 ± 0.05
mediodorsal thalamus	1.48 ± 0.06	1.47 ± 0.13	1.62 ± 0.10	1.63 ± 0.14
ventrolateral thalamus	1.35 ± 0.10	1.32 ± 0.07	1.43 ± 0.05	1.42 ± 0.05
internal capsule	1.04 ± 0.05	1.02 ± 0.05	0.92 ± 0.10	0.91 ± 0.08
parietal cortex				
layers I-III	1.32 ± 0.11	1.44 ± 0.03	1.28 ± 0.08	1.36 ± 0.10
layer IV	1.34 ± 0.10	1.50 ± 0.10	1.36 ± 0.02	1.47 ± 0.06
layers V-VI	1.40 ± 0.07	1.52 ± 0.06	1.46 ± 0.07	1.48 ± 0.06
hypothalamus	1.16 ± 0.03	1.11 ± 0.04	1.14 ± 0.10	1.13 ± 0.11
posterior cingulate cortex	1.48 ± 0.06	1.42 ± 0.11	1.45 ± 0.18	1.43 ± 0.20
hippocampus molecular layer	1.95 ± 0.19	2.02 ± 0.36	1.97 ± 0.29	2.09 ± 0.38
dentate gyrus	1.93 ± 0.23	1.52 ± 0.02	2.09 ± 0.32	2.15 ± 0.40
auditory cortex				
layers I-III	1.43 ± 0.05	1.59 ± 0.12	1.48 ± 0.03	1.53 ± 0.05
layer IV	1.44 ± 0.03	1.51 ± 0.12	1.50 ± 0.08	1.53 ± 0.11
layers V-VI	1.52 ± 0.04	1.57 ± 0.10	1.59 ± 0.13	1.57 ± 0.09
substantia nigra pars compacta	1.28 ± 0.07	1.23 ± 0.08	1.17 ± 0.03	1.17 ± 0.07
substantia nigra pars reticulata	1.09 ± 0.04	1.06 ± 0.02	0.99 ± 0.08	1.08 ± 0.04
medial geniculate body	1.45 ± 0.08	1.38 ± 0.04	1.49 ± 0.09	1.50 ± 0.17
visual cortex				
layers I-III	1.41 ± 0.19	1.66 ± 0.14	1.72 ± 0.16	1.71 ± 0.16
layer IV	1.57 ± 0.06	1.59 ± 0.14	1.68 ± 0.16	1.60 ± 0.12
layers V-VI	1.58 ± 0.04	1.63 ± 0.14	1.65 ± 0.17	1.70 ± 0.14
entorhinal cortex	1.94 ± 0.18	1.90 ± 0.22	2.15 ± 0.41	2.03 ± 0.33
inferior colliculus	1.22 ± 0.05	1.16 ± 0.01	1.25 ± 0.06	1.24 ± 0.07
pons	1.25 ± 0.06	1.20 ± 0.02	1.32 ± 0.12	1.32 ± 0.17
cerebellar cortex	1.00 ± 0.00	1.00 ± 0.00	1.00 ± 0.00	1.00 ± 0.00
cerebellar white matter	0.88 ± 0.05	0.82 ± 0.05	0.86 ± 0.08	0.85 ± 0.08
superior olive	1.19 ± 0.05	1.19 ± 0.04	1.26 ± 0.11	1.31 ± 0.13

Data are presented as mean ± S.E.M., n=3-4. [¹²⁵I]CNS 1261 uptake was measured following injection of NMDA or vehicle (CSF) into the ipsilateral sensory-motor cortex. Uptake of [¹²⁵I]CNS 1261 in individual regions of interest was expressed as a ratio relative to uptake within the cerebellum. Roman numerals indicate the cortical layer examined.

TABLE 3
[¹²⁵I]CNS 1261 uptake 120 minutes after intracortical injection of CSF or NMDA

STRUCTURE	VEHICLE (CSF)		NMDA (27μmoles)	
	ipsilateral	contralateral	ipsilateral	contralateral
anterior cingulate cortex	1.87 ± 0.29	1.90 ± 0.27	1.67 ± 0.12	1.82 ± 0.13
genu	1.34 ± 0.22	1.50 ± 0.26	1.22 ± 0.06	1.29 ± 0.03
sensory motor cortex				
layers I-III	1.60 ± 0.31	1.76 ± 0.43	1.16 ± 0.08	1.34 ± 0.07
layer IV	1.68 ± 0.44	1.63 ± 0.35	1.16 ± 0.11	1.30 ± 0.09
layers V-VI	1.68 ± 0.36	1.64 ± 0.39	1.10 ± 0.09	1.44 ± 0.08
caudate nucleus	1.48 ± 0.28	1.51 ± 0.28	1.33 ± 0.10	1.35 ± 0.07
corpus callosum	1.58 ± 0.25	1.54 ± 0.25	1.24 ± 0.06	1.26 ± 0.10
anterior thalamus	1.61 ± 0.08	1.74 ± 0.12	1.47 ± 0.16	1.48 ± 0.10
hippocampus CA1	2.38 ± 0.43	2.38 ± 0.39	2.13 ± 0.22	2.20 ± 0.17
hippocampus CA3	2.42 ± 0.45	2.61 ± 0.48	2.23 ± 0.27	2.28 ± 0.14
lateral habenular nucleus	1.24 ± 0.17	1.23 ± 0.16	1.19 ± 0.11	1.17 ± 0.08
mediodorsal thalamus	1.64 ± 0.30	1.71 ± 0.33	1.58 ± 0.28	1.62 ± 0.12
ventrolateral thalamus	1.41 ± 0.26	1.44 ± 0.29	1.36 ± 0.19	1.37 ± 0.05
internal capsule	1.21 ± 0.32	1.17 ± 0.31	1.05 ± 0.10	1.10 ± 0.08
parietal cortex				
layers I-III	1.38 ± 0.16	1.44 ± 0.22	1.42 ± 0.19	1.58 ± 0.17
layer IV	1.41 ± 0.21	1.49 ± 0.29	1.48 ± 0.16	1.52 ± 0.13
layers V-VI	1.58 ± 0.23	1.58 ± 0.23	1.50 ± 0.16	1.52 ± 0.14
hypothalamus	1.08 ± 0.16	1.10 ± 0.18	1.10 ± 0.12	1.13 ± 0.12
posterior cingulate cortex	1.46 ± 0.31	1.45 ± 0.28	1.14 ± 0.18	1.13 ± 0.18
hippocampus molecular layer	2.50 ± 0.52	2.81 ± 0.58	2.40 ± 0.26	2.39 ± 0.13
dentate gyrus	2.49 ± 0.45	2.50 ± 0.45	2.20 ± 0.24	2.22 ± 0.06
auditory cortex				
layers I-III	1.65 ± 0.13	1.65 ± 0.13	1.49 ± 0.09	1.50 ± 0.06
layer IV	1.61 ± 0.18	1.64 ± 0.33	1.50 ± 0.13	1.45 ± 0.09
layers V-VI	1.69 ± 0.32	1.75 ± 0.30	1.59 ± 0.11	1.55 ± 0.09
substantia nigra pars compacta	1.29 ± 0.21	1.25 ± 0.25	1.08 ± 0.04	1.10 ± 0.02
substantia nigra pars reticulata	1.07 ± 0.03	1.14 ± 0.14	0.99 ± 0.03	1.02 ± 0.01
medial geniculate body	1.42 ± 0.17	1.43 ± 0.20	1.42 ± 0.11	1.44 ± 0.11
visual cortex				
layers I-III	1.55 ± 0.07	1.58 ± 0.22	1.78 ± 0.07	1.85 ± 0.10
layer IV	1.41 ± 0.07	1.55 ± 0.37	1.69 ± 0.08	1.75 ± 0.11
layers V-VI	1.50 ± 0.16	1.56 ± 0.38	1.74 ± 0.09	1.82 ± 0.11
entorhinal cortex	1.85 ± 0.13	1.71 ± 0.23	1.84 ± 0.09	1.92 ± 0.03
inferior colliculus	1.01 ± 0.07	1.01 ± 0.13	1.36 ± 0.14	1.38 ± 0.15
pons	1.18 ± 0.08	1.24 ± 0.15	1.47 ± 0.14	1.47 ± 0.15
cerebellar cortex	1.00 ± 0.00	1.00 ± 0.00	1.00 ± 0.00	1.00 ± 0.00
cerebellar white matter	0.97 ± 0.04	0.94 ± 0.08	0.97 ± 0.02	0.94 ± 0.05
superior olive	1.23 ± 0.04	1.22 ± 0.08	1.08 ± 0.01	1.14 ± 0.02

Data are presented as mean ± S.E.M., n=2-3. [¹²⁵I]CNS 1261 uptake was measured following injection of NMDA or vehicle (CSF) into the ipsilateral sensory-motor cortex. Uptake of [¹²⁵I]CNS 1261 in individual regions of interest was expressed as a ratio relative to uptake within the cerebellum. Roman numerals indicate the cortical layer examined.

PUBLISHED ABSTRACTS

Effect of extracellular acidosis on NMDA receptor activation *in vivo* (1995) McGregor, A.L., Owens, J. and McCulloch, J. *XVII International Symposium on Cerebral Blood Flow and Metabolism*, Cologne, Germany 15 Supplement 1 S414.

Imaging NMDA receptor activation *in vivo* with [125 I]CNS 1261 (1995) McGregor, A.L., Dawson, D., Owens, J., Kodama, K., McCulloch, J., Magar, S., Perlman, M., Zhang, L. and Knapp, A.G. *25th Annual Meeting for the Society for Neuroscience*, San Diego, California 21 250.12

Development of radiolabelled neuroligands to image glutamate (NMDA) receptor systems *in vivo*. (1996) Owens, J., Tebbutt, A., McGregor, A., Patterson, J., Wyper, D., Teasdale, G., Elliott, A., Durant, G., Magar, S. and McCulloch, J. *The First Easter School in Radiopharmaceutics* Liverpool.

Uptake and retention in human CNS of a new ion channel ligand. (1997) McCulloch, J., Muir, K., Owens, J. R., Hadley, D.M., Grossett, D., Durant, G.J., Magar, S., Knapp, A.G., Kodama, K., McGregor, A.L., Wyper, D.J., Tebbutt, A.A., Robbins, D.J. and Patterson, J. *XVIII International Symposium on Cerebral Blood Flow and Metabolism*, Baltimore, Maryland 17 (1997), Supplement 1, S132.

The pharmacology of CNS 1261 : an NMDA ion channel blocker. (1997) McGregor, A.L., Kodama, K., Knapp, A.G. and McCulloch, J. *XVIII International Symposium on Cerebral Blood Flow and Metabolism*, Baltimore, Maryland 17 , Supplement 1, S461

[125 I]CNS 1261 is a superior imaging agent to [125 I]MK801 in the normal brain. (1997) McGregor, A.L., Owens, J., Tebbutt, A., Kodama, K. and McCulloch, J. *XVIII International Symposium on Cerebral Blood Flow and Metabolism*, Baltimore, Maryland 17 , Supplement 1, S462.

Development of CNS 1261 a novel NMDA ligand. (1997) Tebbutt, A., Owens, J., McGregor, A. and McCulloch, J. *Accepted for European Association of Nuclear Medicine*, Glasgow.

